CATALYTICALLY ACTIVE ENZYME-BASED NANOPARTICLES FOR CELLULAR MODULATION

DISSERTATION

zur Erlangung des akademischen Grades
„Doktor der Naturwissenschaften“
im Promotionsfach Chemie
am Fachbereich Chemie, Pharmazie und Geowissenschaften
der Johannes Gutenberg-Universität Mainz

Eingereicht von
Lydia Radi, Dipl.-Chem.
geboren in Georgiewka / Kasachstan
Mainz, 2018

– D77 –

Mainzer Dissertation

Dekan:

Erstgutachter:

Zweitgutachter:

Tag der Einreichung: 10.04.2018

Tag der mündlichen Prüfung: 09.05.2018

EIDESSTATTLICHE ERKLÄRUNG

Die vorgelegte Dissertation wurde am Institut für Pharmazie und Biochemie der Johannes Gutenberg-Universität in Mainz zur Erlangung des Grades „Doktor der Naturwissenschaften“ angefertigt.

Erstgutachter:

Zweitgutachter:

Hiermit erkläre ich an Eides statt, dass ich die vorliegende Dissertation selbstständig und nur mit den angegebenen Hilfsmitteln angefertigt habe. Diese Dissertation wurde noch nicht als Prüfungsarbeit für eine andere Prüfung eingereicht. Zudem wurden bisher weder die gleiche, noch Teile der Abhandlung als Dissertation bei einer anderen Fakultät oder einem anderen Fachbereich eingereicht.

Mainz, …… ……

Lydia Radi

Look up at the stars and not down at your feet.
Try to make sense of what you see,
and wonder about what makes the universe exist.
Be curious.

Stephen Hawking

Für meine Eltern

~

Danke!

ACKNOWLEDGMENTS

ABSTRACT

Protein-based nanomedicine platforms are versatile application systems due to their biodegradability, biocompatibility and low toxicity. Especially the use of enzymes, which represent highly specific biocatalysts, is a promising challenge in therapeutic applications. These systems can offer the potential to intervene in cellular mechanisms and to manipulate them.

This PhD thesis presents a novel approach for the synthesis of catalytically active enzyme-based nanoparticles. The nanosystems consist solely of enzyme-polymer conjugates, where natural enzymes are covalently linked to the FDA-approved synthetic polymer polyethylene glycol. The preservation of the enzymatic activity was realized by mild PEGylation routes. For this, four different activated PEG chains were synthesized and used for the surface modification of lysozyme. Due to the design of a lipophilic biomaterial, an emulsion-based technique was used as particle preparation method, resulting in stable nanoparticles in a size range of 120–200 nm. This concept was applied to the development of peroxidase active nanoparticles for the modulation of reactive oxygen species (ROS). Three different peroxidases were used in their PEGylated form as active building blocks. It could be shown that the nanoparticle systems act both, extra- and intracellular as redox-active material, leading to the decrease of harmful ROS.

Furthermore, the design of an active dual-enzyme nanoparticle system was presented. The combination of two PEGylated enzymes in the emulsification evaporation method led to the creation of a cascade-performing particle system. The investigation of five various enzyme quantities within the particle system resulted in catalytically active nanoparticles with different substrate affinities and catalytic efficiencies.

This thesis provides, not only novel biomimetic approaches to study cellular processes but also offer the potential to produce next-generation delivery and manipulation platforms for innovative applications in biomedical research.

ZUSAMMENFASSUNG

In der Nanomedizin stellen Protein-basierte Nanosysteme aufgrund ihrer Bioabbaubarkeit, Biokompatibilität und geringen Toxizität, innovative Applikationssysteme dar. In diesem Zusammenhang, ist die Verwendung von Enzymen, die hoch spezifische Biokatalysatoren repräsentieren, ein vielversprechender therapeutischer Ansatz. Mit diesen Systemen kann ein Eingreifen in zelluläre Prozesse und deren Manipulation ermöglicht werden.

Die vorliegende Dissertation präsentiert einen neuen Ansatz zur Synthese von katalytisch aktiven Enzym-basierten nanopartikulären Systemen. Die Nanopartikel bestehen aus Enzym-Polymer Konjugaten, die, durch die kovalente Verknüpfung von natürlichen Enzymen mit dem Polymer Polyethylen Glykol, hergestellt wurden. Die Erhaltung der enzymatischen Aktivität konnte dabei durch die Verwendung von milden PEGylierungs-Routen gewährleistet werden. Hierfür wurden vier unterschiedlich aktivierte Polymerketten synthetisiert und für die Oberflächenmodifikation von Lysozym verwendet. Aufgrund der resultierenden Lipophilie des Biomaterials, konnte eine Emulsionstechnik für die Herstellung der Nanopartikel genutzt werden. Diese führt zur Bildung stabiler Nanosysteme von einer Größe zwischen 120–200 nm. Das Konzept konnte erfolgreich für die Herstellung von Peroxidase-aktiven Nanopartikeln verwendet werden. Hierfür wurden jeweils drei verschiedene Peroxidasen in ihrer PEGylierten Form als aktives Partikelmaterial eingesetzt. Es konnte gezeigt werden, dass die Nanopartikelsysteme als extra- und intrazelluläres Redox-aktives Material fungieren können und im Stande sind, vorhandene schädliche reaktive Sauerstoffspezies zu reduzieren.

Darüber hinaus konnte ein aktives binäres Nanosystem hergestellt werden. Die Verarbeitung von zwei Oberflächen-modifizierten Enzymen in dem Emulsionsverfahren, führte zur Herstellung eines Partikelsystems, das Kaskadenreaktionen durchführen kann. Die Untersuchung von fünf hergestellten partikulären Systemen, mit jeweils unterschiedlichen Enzymkonzentrationen, führte zur Bildung katalytisch aktiver Nanopartikel mit verschiedenen Substrataffinitäten und katalytischen Umsatzraten.

Diese Arbeit stellt, neben einem neuen Ansatz zur Entwicklung biologisch nachahmender Systeme, die zur Untersuchung von zellulären Prozessen herangezogen werden können, die Synthese neuartiger Transport- und Manipulationssysteme vor, die im biomedizinischen Forschungsbereich Anwendung finden können.

TABLE OF CONTENT

EIDESSTATTLICHE ERKLÄRUNG ..... **IV**

ACKNOWLEDGMENTS ..... **IX**

ABSTRACT ..... **XI**

ZUSAMMENFASSUNG ..... **XIII**

TABLE OF CONTENT ..... **XV**

1 INTRODUCTION **1**

1.1 Nanosystems for Biomedical Applications **2**

1.1.1 Nanosystems - Types and Preparation Methods 3

1.1.2 Biodistribution and Cellular Uptake of Nanoparticles 5

1.2 Protein-based Nanosystems **9**

1.2.1 Artificial Assemblies using Proteins as Structural Elements 9

1.2.2 Artificial Assemblies of Intact Proteins 11

1.2.3 Enzymes as Biomaterial for Nanosystems 17

1.3 General Aspects of Enzyme Kinetics and Assays **28**

2 AIM OF THE WORK **31**

3 RESULTS AND DISCUSSION **35**

3.1 Enzyme PEGylation under Activity Preservation **35**

3.1.1 Polyethylene Glycol Activation 35

3.1.2 PEGylation of Lysozyme 37

3.1.3 Lysozyme-based Nanoparticles 46

3.2 Design of Catalytically Active Enzyme Nanoparticles **55**

3.2.1 PEGylation of Peroxidases 55

3.2.2 Peroxidase-based Nanoparticles 62

3.2.3 Catalytic Activity of Peroxidase-based Nanoparticles 67

3.3 Cascade Reactions using Enzyme-based Nanoparticles **78**

3.3.1 PEGylation of Glucose Oxidase 79

3.3.2 Dual-Enzyme Nanoparticles 82

3.3.3 Kinetic Investigations of the Dual-Enzyme Cascade Reaction 92

3.3.4 Application of the Dual-Enzyme Nanoparticles 99

4 CONCLUSION AND OUTLOOK 103
4.1 Enzyme Surface PEGylation under Activity Preservation 103
4.2 Design of Catalytically Active Enzyme Nanoparticles 105
4.3 Cascade Reactions in Enzyme-based Nanoparticles 106
5 EXPERIMENTAL PART 108
5.1 Materials 108
5.1.1 Reagents and Solvents 108
5.1.2 Buffers and Media 110
5.1.3 Disposables 112
5.2 Equipment 113
5.3 Enzyme PEGylation 118
5.3.1 Activation of mPEG 118
5.3.2 Fluorescence Labeling of Cyt *c*, HRP and Cat 121
5.3.3 Enzyme PEGylation 122
5.3.4 Analysis of Protein-Polymer Conjugates 124
5.4 Nanoparticle Preparation 125
5.4.1 Single Emulsion-Based Nanoparticle Preparation 125
5.4.2 Nanoparticle Analysis 126
5.5 Enzyme Activity Assays 127
5.5.1 Enzymatic Activity of Lysozyme 127
5.5.2 Enzymatic Activity of PEGylated Peroxidases and Peroxidase-NPs 127
5.5.3 Enzymatic Activity of Dual-Enzyme NPs 130
5.6 Cell Toxicity of PEGylated Materials and NPs 131
5.6.1 Cell Viability 131
6 APPENDIX 133
6.1 List of Abbreviations 133
6.2 Literature 136
6.3 Supplemental Data 143
6.3.1 Data of the First Project 143
6.3.2 Data of the Second Project 150
6.3.3 Data of the Third Project 151
CURRICULUM VITAE 155
LIST OF PUBLICATIONS 156

1 INTRODUCTION

Diverse biochemical processes occur specifically and synergistically, ensuring a healthy life. Disruptions by certain substances or mechanisms can lead to an abnormal state, resulting in serious diseases. Investigations of pathophysiological states such as in cancer, neurological disorders and diabetes prove the dysfunctional involvement of proteins.[1] Viewed from a therapeutic perspective, proteins themselves represent very efficient drugs and play a significant role in medical applications. Major advantages of these biopolymers are their high specificity in certain processes and a resulting low potential for adverse side effects. As proteins have the most dynamic and diverse role of any biomacromolecules in living beings, the catalysis of biochemical reactions represents one important of them. Using enzymes in therapeutic approaches offer the potential to intervene in specific cellular processes and allows not only to alleviate an abnormal state but also to eliminate it.

Due to physicochemical and pharmacokinetic characteristics of these biopolymers such as instability, short elimination half-life and immunogenicity, many biological, chemical and technological strategies have been developed during the last decades in order to overcome the mentioned limitations. The most excellent development during the last 50 years, since Bangham[2] and co-workers discovered liposomes, are nanoparticles. These systems revolutionized the diagnosis and treatment of many diseases.[3] Main features such as unique properties, which include nanoscale size and a high surface-to-volume ratio, an improved cellular circulation and the potential to encapsulate drugs, thereby enhancing their pharmacokinetic and pharmacodynamic profile, make nanoparticles to remarkable application systems.

The combination of proteins, especially enzymes with nanoparticulate systems represents an innovative challenge with the potential to create extraordinary materials and to further the understanding of cellular functions. This thesis should build on this and presents a novel technique for the development of catalytically active enzyme-based nanosystems. The following chapters present the current state of research and give all relevant information to the used methods.

1.1 Nanosystems for Biomedical Applications

Nature provides a remarkable source of nano-sized architectures such as the DNA helix, viruses and proteins.[4] Inspired by these nanoscale constructs, an important medical research field, the nanomedicine, was developed in recent years.[5] Nanoparticle formulations have been successfully used in the diagnosis and therapy of numerous diseases like cancer,[6] neurological disorders[7] or diabetes.[8] Novel therapy areas and concepts such as multimodality, combination therapies and theranostics extend this research field.[9]

Nanoparticles represent remarkable delivery systems for therapeutic drugs, biological agents and imaging probes. The different cargos can either be entrapped in the interior of the particles,[10] incorporated within the material network[11] or attached to the exterior.[12] Especially for therapeutic approaches, nanosystems show several advantages over conventional medical agents. The entrapment of active but poorly water soluble pharmaceutical ingredients can be ensured, whereby high drug-loading capacities can be achieved. Encapsulated agents can be protected from degradation and acidic environments by the nanoparticle shell, e.g. in the stomach or in acidic cellular compartments. One of the most desired features is the targeted delivery of agents to organs, tissues and cells[13] and the related controlled release of encapsulated molecules at target areas.[14] Hence, by the use of nanoparticles, undesired side effects of free drugs, such as toxicity, low solubility and nonspecific biodistribution can be overcome.

Doxil®, a liposomal formulation, which encapsulates the anti-cancer drug doxorubicin, represents the first oncological nanotherapeutic and was approved by the FDA in 1995. Research advances including several types of nanocarriers were developed in recent years and are approved by the FDA.[15] In the next chapter, the most commonly used systems and their production will be presented.

1.1.1 Nanosystems - Types and Preparation Methods

Chemical compositions and physical properties such as size, shape and surface quality are decisive characteristics of a nanosystem. Looking at the chemical structure, various types of nanoparticles were designed, since the first pioneering works in 1960 (Figure 1).[3]

Lipid-based nanoparticles represent an important area of therapeutics and were the first class of nanosystems, which received clinical approval for cancer treatment.[16] These nanocarriers are generally built-up by phospholipids consist of one or several lipid bilayers with an aqueous interior, a lipophilic bilayer compartment and a hydrophilic exterior.[17] Based on this construction, lipid-based nanocarriers have the primary benefit to encapsulate hydrophilic materials, for example siRNA,[18] while lipophilic cargos can be included in the bilayer region.

Polymers, synthetic or natural origin, are further building blocks of nanosystems. The diversity of their composition such as in size, morphology and surface functionality, make them to suitable candidates. Especially the high flexibility of their chemical composition, using modern bioorganic synthesis routes, represents a promising approach in order to create a nanoparticle system with individual characteristics. Polymer-based nanomaterials such as micelles,[19] dendrimers,[20] polymersomes[21] and polymer-hybrid systems[22] are common examples.[23] In this context, the use of biodegradable polymers is an important approach. These macromolecules are able to respond to certain stimulus, ensuring degradation of the polymeric building blocks, providing control in drug release and facilitating excretion from organisms.[24]

Another commonly used system, to be mentioned in this context, are inorganic nanoparticles. They offer the advantage of being extremely stable, robust and highly resistant to enzymatic degradation.[25] However, toxicity[26] represents a major problem in the application of inorganic nanocarriers, which is why natural polymers play an increasingly important role in nanomedicine.

Biocompatible and biodegradable natural macromolecules such as polysaccharides,[27] nucleic acids[28] and proteins[11, 29] represent promising candidates for the development of nanoparticles in the nanomedicine.[30] In our group, a nanoparticle system, using the polysaccharide dextran, was established. Bamberger *et al.* developed a biomaterial-based particulate system by the processing of acetylated dextran by an emulsion technique.

The approximately 100 nm synthesized nanoparticles were successfully used for the delivery of siRNA.[27a] Due to their significance for this PhD work, proteins are described more in detail in Chapter 1.2.

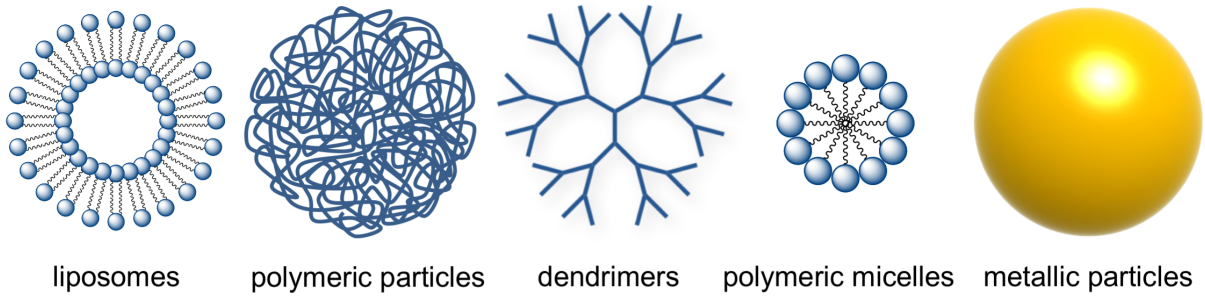

Figure 1. The most common nanocarrier systems, which are used in medicinal applications and research. Redrawn from Sun *et al.*[31]

With increasing demand, various technological and chemistry-based approaches have been developed for the preparation of nanosystems. Suitable methods including nanoprecipitation,[32] thermal gelation,[33] organic syntheses of dendrimers,[20] and colloidal nanochemistry, are described detailed in the literature. The following preparation methods focus on the design of particulate systems using biomaterials.

Self-assembly processes represent one of the first used techniques and should be considered in this context more in detail. The behavior is based on the organization of co-existing components into unique nanostructures, in order to reduce the system's free energy. Hydrophobic and hydrophilic moieties assemble to spherical constructs due to the increasing amount of one of the solvents, which represents the preferred environment of one of the components. This self-assembly process can be used for the encapsulation of various molecules, especially pharmaceutical ingredients. Based on this concept, Breitenbach *et al.* synthesized e.g. micelles made of amphiphilic sugar-based block copolymers for the delivery of hydrophobic drugs.[34]

The coacervation/desolvation method represents a thermodynamically driven self-assembly process and is commonly used to obtain protein-based nanoparticles. A desolvating agent (e.g. ethanol or acetone) is added to an aqueous solution, which contains the hydrophilic protein, leading to the denaturation of the biomacromolecule and the forming of the particle matrix by this material.[35]

To ensure the stabilization of the nanoparticles, the addition of crosslinking agents such as glutaraldehyde, formaldehyde or 2,3-butadione are necessary.[36] The toxicity of these compounds is the major disadvantage of this method.

Emulsion-based techniques can be considered as self-assembly processes and present highly suitable and common used approaches. Nanoemlusions can be prepared utilizing high-energy emulsification, including sonication and high-pressure homogenization. To prevent agglomeration and coalescence of the nanodroplets, synthetic and natural emulsifiers can be added to the systems.[37] Fréchet and co-workers presented an innovative development of biodegradable nanomaterials using acetal-derivatized dextran.[38] Using a double emulsion-based procedure, they were able to encapsulate hydrophilic payloads, whereby the use of a single emulsion technique leads to the entrapment of hydrophobic drugs. The major advantage of this method is the absence of toxic stabilizers. Inspired by this approach and its promising results, this technique was applied for the development of protein-based nanoparticles in this work.

In view of therapeutic approaches, the nanoparticle uptake by cells and their distribution in organisms have to be considered. In the next chapter, the most important current findings will be mentioned.

1.1.2 Biodistribution and Cellular Uptake of Nanoparticles

Tracking nanoparticles *in vivo* after the intravenous administration, opsonization of the particles represents the first process in the cellular environment. This is the adsorption of plasma proteins, especially serum albumins and apolipoproteins, resulting in the formation of a so-called protein corona around the nanoparticles.[39] This altered nanoparticle exterior represents the interface with the environment *in vivo* and determines the biology identity of the particulate system. The extent of the corona formation depends on nanoparticle factors like size, surface charge, hydrophobicity and surface chemistry.[40] Opsonization can be minimized using nanoparticle surface modifications. The most commonly used strategy is PEG coating, which due to the great steric demand of the hydrophilic polymer ('stealth effect'), results in an increased circulation half-life and a reduced uptake by the mononuclear phagocyte system.[41]

The foundation to apply nanosystems, especially in cancer therapy, is based on the passive accumulation of nanoparticles in solid tumors due to their increased capillary permeability. This transport phenomenon, known as the enhanced permeability and retention effect (EPR) was first described by Maeda and co-workers in 1986[42] and represents a passive targeting mechanism. In contrast to normal vasculatures, that possess tight interendothelial junctions and thus prevent particles larger than 2 nm from crossing, tumors have an abnormally dense and permeable vasculature that facilitates the penetration of entities from 10–500 nm in size. Investigations on nanoparticle sizes and shapes confirm that nanoscale constructs with a diameter of approximately 100 nm and a neutral and hydrophilic polymer-extended surface show the best results regarding prolonged blood circulation and thus an increased tumoral accumulation and anti-tumor activity.[43] Several experience reports confirm that the described passive accumulation of nanoparticles is strongly governed by the size and morphology of the drug carrier, and at the same time depends on the location and the microvascular network of the tumor.[44]

The endothelial wall and its limited pore size represents a biological barrier, which ensures a selective accumulation of nanoparticles in certain tissue areas. In general, tissues with leaky endothelial walls such as tumors and reticuloendothelial organs (for example liver and spleen), show an enhanced uptake of nanoparticles.[45] In this context, active targeting nanomedicine presents an appropriate approach. To minimize the enhanced accumulation of nanoparticles in liver and spleen, various antibodies, proteins or peptides, small molecules and aptamers can be used as suitable ligands for the surface modification of nanoparticles.[46]

In vitro investigations confirm that the endocytosis represents the major uptake pathway of nanoparticles (Figure 2, left). These processes can be initiated by either highly selective bindings between agents on the particle exterior and receptors on the cell membrane, or nonselective bindings based on hydrophobic and electrostatic interactions. Five major pathways were described for the internalization of nanoparticles by cells: the clathrin- and caveolin-mediated endocytosis as well as of these proteins independent uptake, the macropinocytosis and the phagocytosis. The clathrin- and caveolin-mediated endocytosis, which represents a receptor-mediated pathway, is used by many cells to internalize nanoscale materials, results in clathrin- or caveolin-coated pits with an approximate size of 100 nm in diameter. This endocytosis mechanism is especially important for the uptake of small and spherical particles.[47]

The macropinocytosis pathway, which can occur in all types of cells, involves the nonspecific internalization of biological fluids from the external cellular environment. This so-called 'cell drinking' is very important for the uptake of large particles.[48] Phagocytosis represents the active binding and internalization of materials larger than 250 nm in diameter by phagocytic cells such as macrophages, dendritic cells and neutrophils. Further, non-endocytic pathways are described in the literature (Figure 2, right),[49] where nanoparticles directly penetrate through the cells. In particular, tiny particles, cationic particulate systems, and nanoparticles equipped with cell-penetrating peptides are able to pass directly through cell membranes.

In conclusion, investigations on uptake mechanisms confirm that these processes are significantly influenced by the physicochemical properties of the particles as well as the type and physiological condition of cells.[50]

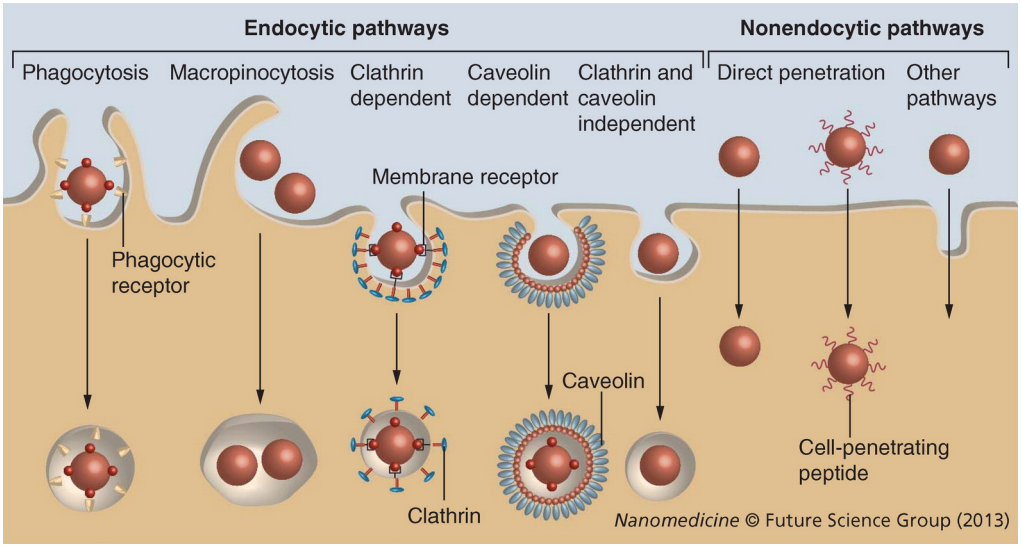

Figure 2: Cellular uptake of nanoparticles by endocytic pathways and non-endocytic mechanisms. The five endocytic uptakes include the phagocytosis, macropinocytosis, the clathrin- and caveolin-dependent and independent pathway. These mechanisms ensure the active internalization of spherical particles of different sizes. In contrast, tiny particles, cationic systems, and nanoparticles equipped with cell-penetrating peptides can pass cell membranes by non-endocytic pathways. Reprinted with permission from Qu *et al.*[49]

Intracellular, the engulfed nanoparticles undergo several processes along the endolysosomal network. To achieve a successful application of nanosystems, the escape from the endosomal pathway in order to reach various subcellular compartments such as the cytosol, the mitochondria and the nucleus is necessary.

This is important in order to avoid the transport through endomembrane compartments as well as the clearance and degradation under harsh lysosomal conditions. Saltzman and co-workers proposed an endocytosis-exocytosis pathway after their investigations of rhodamine-loaded PLGA nanoparticles in three different types of epithelial cells.[51] After internalization, the particles escape from endosomes and are transported to the Golgi apparatus. The intracellular transport in HeLa cells was investigated by Nie *et al.* using TAT-peptide-conjugated quantum dots.[52] Their results show that these systems were internalized through macropinocytosis and were entrapped in cytoplasmic organelles. Using nanomaterials, which are disassembled, for example by surrounding cellular conditions such as pH, temperature and redox, are another common approach to induce an endolysosomal escape.[53] In this context, acid-degradable nanoparticles represent one of the most promising carriers and had widely be explored by Frechét and co-workers. They developed a delivery system for protein-based vaccines by an emulsion-based encapsulation, using acrylamide as the monomer and an acidic degradable crosslinker containing a hydrophilic triglyme moiety. These carrier systems degrade in an acidic environment of endosomes and ensure the release of the encapsulated protein.[54] Lee *et al.* reported another successful delivery strategy, using core-shell structured polyionic complex micelles.[55] The 50 nm particles were formed by electrostatic interactions, using charge-inverted cytochrome *c* and the cationic block copolymer PEG-pAsp-(DET). To achieve an anionic protein material, the cationic enzyme cytochrome *c* was modified with citraconic amides or *cis*-aconitic amides. The micelles dissociated rapidly at the endosomal pH value of 5.5 based on the charge conversion of the used amides from negative to positive. This leads to an efficient cytochrome *c* endosomal escape and a subsequent diffusion to the cytosol. They assumed that the released block copolymer could come into direct contact with the endosomal membrane to induce the efficient escape of the enzyme. Furthermore, the group found out that a higher pH sensitivity of the micelle system, consequently the faster dissociation of the particles in the endosome, could lead to a faster endosomal escape and diffusion into the cytosol. In general, these examples illustrate that a particle system, which disassembles within the endosome, enables a better endosomal escape of the encapsulated molecules.

1.2 Protein-based Nanosystems

Nature's toolbox provides a variety of biopolymers such as polysaccharides, polynucleotides and proteins. These biomaterials are readily accessible and can be produced in high quantity with modern biotechnological techniques.[56]

Since only proteins were used in this work, this versatile and fascinating group of biopolymers will be considered in more detail. Proteins are structurally well-defined, natural polymers with unique physical, chemical and biological properties, and undertake diverse vital roles in living organisms. In cells, they act as a structural material, are anchored in cellular membranes and perform important signaling functions. Proteins transport molecules, react to external stimuli and can sense their surroundings. In particular enzymes, a very important class of proteins, represent dynamic and multifunctional materials, performing highly efficient catalytic reactions. These biomacromolecules show several advantages over synthetic polymers, including biodegradability, biocompatibility, non-antigenicity and low toxicity.[57] With the toolkit of bioorganic chemistry, proteins can be easily modified and represent a promising material source for biotechnological and therapeutic applications.

In the following section, previously described protein- and enzyme-containing nanosystems will be presented, whereas a distinction will be made between denatured and intact protein materials.

1.2.1 Artificial Assemblies using Proteins as Structural Elements

Considering nanomaterials, proteins can be applied as a material scaffold to create systems with individual properties in size, shape and functionality.[58] Nature offers many structural proteins such as silk,[59] collagen,[60] gelatin[61] and elastin,[62] which can be used as building blocks for the assembly of nanosystems. Intrinsic properties like high flexibility, specific morphology, great mechanical strength and self-assembling behavior make these biopolymers as suitable starting materials for the development of protein-based nanoparticles.[63] Apart from structural biomacromolecules, globular proteins can be used. The spherical arrangement of polypeptides in these proteins makes them particularly attractive for the use in biotechnological applications.[64]

In the compact globular conformation, most of the hydrophobic amino acids are located in the interior, whereby the hydrophilic ones are on the exterior of the protein. By denaturation, non-polar and sulfur-containing amino acids point outwards and show a greater tendency to aggregate. In general, the denaturation of the native protein structure represents the requirement for these approaches. Using techniques such as desolvation,[35, 65] emulsification,[37] and thermal gelation[66] the resulting protein material can be utilized as a building block for the creation of nanosystems.[56a] For the preparation of albumin-based nanoparticles, which represents an important protein class in this context,[33] the desolvation technique is a frequently used method. Here, an organic solvent, like acetone or ethanol, is added dropwise to an aqueous buffered protein solution. Based on a resulting reduction of the protein solubility, this leads to an aggregation of the formed hydrophobic material. Additionally, poorly water-soluble drugs can be encapsulated by this method.[65a] Furthermore, the thermal gelation represents an alternative method to obtain albumin nanoparticles. This technique includes a heat treatment, which causes the denaturation of the protein and resulting in the assembly into particles via hydrophobic interactions.[67] The mentioned methods often include a crosslinking step to stabilize the resulting particles. Common crosslinkers are 2,4-toluene diisocynate, which reacts with hydroxyl and amine groups,[68] glutaraldehyde, which crosslinks amines,[64] and formaldehyde.[56a] Disadvantages of these agents are their partial toxicity, highly chemical reactivity and the resulting reduced amount of chemically active groups for further conjugations.

To create new functional nanomaterials, protein backbones can be combined with synthetic polymers using modern biochemical techniques (Figure 3).[69] The proteins function as essential components of the nanoparticle systems without maintaining their intact natural structure. By adding chemically synthesized polymers, nanosystems for biological and chemical applications can be designed.[70] For example, the Weil group utilized the polypeptide backbone of BSA in different approaches to formulate nanoreactors[71] and drug delivery systems.[72]

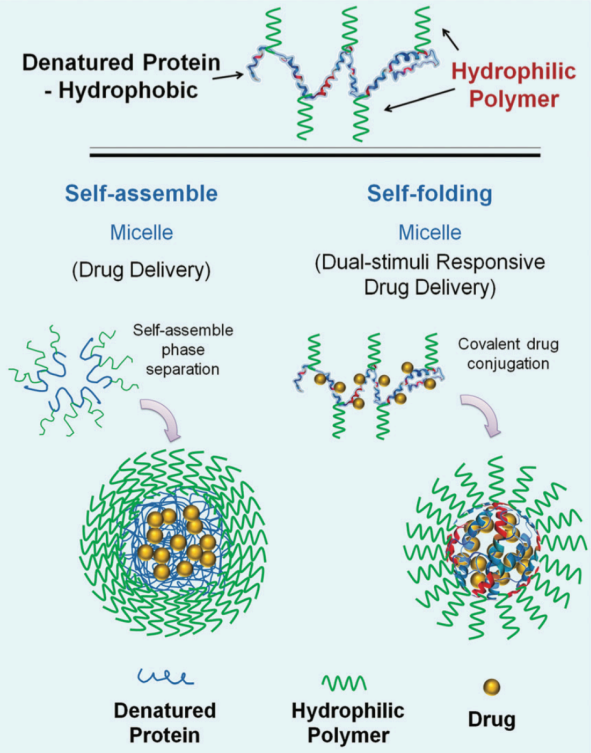

Figure 3: Schematic illustration of nanoparticles formed by self-assembly and self-folding of protein-polymer hybrids. Conjugates of denatured proteins with synthetic polymers represent the building blocks. Utilizing this method, higher structured systems such as micelles can be developed. Additionally, these constructs could be used as drug carrier. Reprinted with permission from Wu *et al.*[70a]

1.2.2 Artificial Assemblies of Intact Proteins

The maintaining of the native protein structure and activity offers the possibility to use the protein itself as an active compound. In the best case, natural processes can be imitated, allowing the proteins to fulfill their natural functions.

Based on the structure, charge and hydrophobic properties of different natural proteins, supramolecular complexes can be obtained, retaining the native structure of the biopolymer. The most important example in this context is Abraxane® (approved in 2005 by the FDA).[73] Albumin acts as a natural carrier for endogenous hydrophobic molecules like vitamins and hormones, that are bound in a reversible non-covalent manner to the protein.

These protein complexes are internalized by a caveolin-mediated endocytosis, which is triggered by the binding to the cell-surface albumin receptor gp60. The extracellular matrix glycoprotein osteonectin, known as secreted protein acid rich in cysteine (SPARC), has been shown to bind albumin too, because of a sequence homology with gp60. This explains the accumulation of albumin in some tumors since SPARC are often present in neoplasms. Exploiting this pathway, albumin-bound hydrophobic anti-cancer drugs can directly be transported to tumors. Binding the hydrophobic agent paclitaxel to albumin by a solvent-free method (*nab*™ technology) results in 130 nm nanocomplexes. The colloidal suspension is derived from the lyophilized formulation of paclitaxel and human serum albumin diluted in saline solution (0.9% NaCl). The nanocomplexes are internalized by the natural mentioned albumin pathway and show an increased anti-tumor activity. Furthermore, based on electrostatic interactions, natural proteins can form complexes with various other synthetic polymers[74], biopolymers[75] or even nanoparticles.[76]

To extend the functionality of proteins and overcome the already mentioned limitations such as instability and short half-lives within the body, the synthesis of protein-polymer conjugates represents an opportunity in the development of new multifunctional systems. This provides the advantage to combine chemical properties of a synthetic polymer with biological characteristics of a biomacromolecule. The most common method is the attachment of synthetic polymers to the exterior of proteins using their functional groups on the surface.[77]

Protein-polymer conjugates can be obtained using three major approaches, the 'grafting to', the 'grafting from' or the 'grafting through' method (Figure 4). The grafting to method represents the most common and straightforward approach and is based on the covalent attachment of end-functionalized polymers to the protein.[78] The major advantage of this method is that the polymer can be synthesized separately in non-aqueous solutions without considering the protein characteristics and preferences. Both other approaches belong to 'living polymerization' techniques and focus on controlled polymerizations, such as atom transfer radical polymerization (ATRP) and reversible-addition fragmentation transfer (RAFT). The 'grafting from' strategy starts with the functionalization of the protein with a polymerization initiator, such as azide-containing initiators, dithiophenol maleimide-functionalized or biotin-functionalized ones.[79] The *in situ* polymerization is then induced from this initiating site of the protein and affords controlled growth of the polymer chain.

The 'grafting to' and 'grafting from' methods allow the conjugation of several polymers onto one protein core, whereby the 'grafting through' strategy facilitates the attachment of several proteins onto one polymer chain. A multivalent polymer can be synthesized using the ATRP and RAFT technique, followed by the protein linkage along the polymer chain.

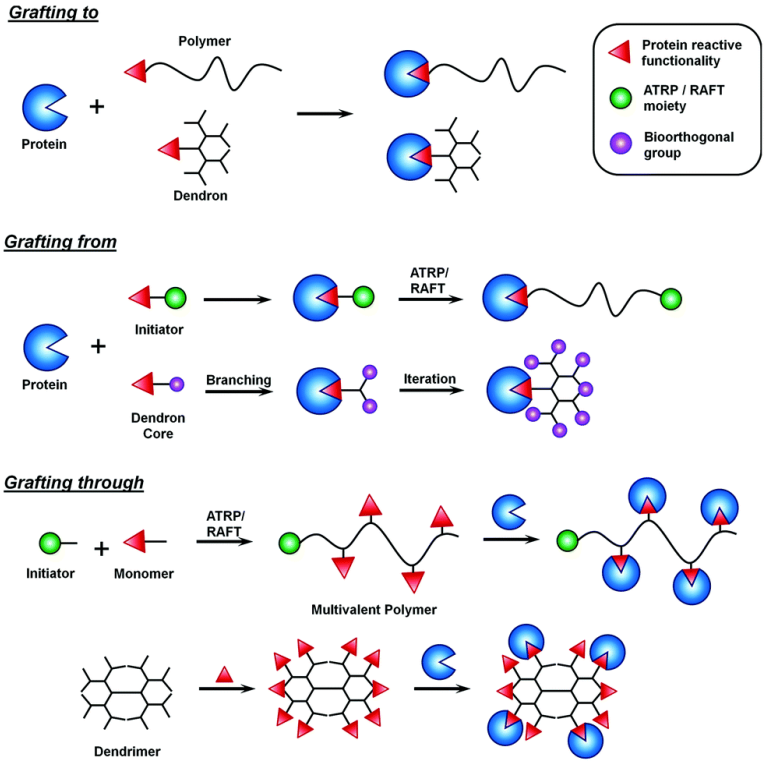

Figure 4: Three common approaches for the development of protein-polymer conjugates. The 'grafting to' method based on the covalent attachment of end-functionalized polymers to the protein. With the 'grafting from' technique, which includes the 'living polymerization' a controlled growth of the polymer chain can be achieved by using atom transfer radical polymerization (ATRP) and reversible-addition fragmentation transfer (RAFT). The 'grafting through' strategy represents again a 'living polymerization' technique and facilitates the attachment of several proteins onto one polymer chain. Reprinted with permission from Weil *et al.*[70a]

Different synthetic polymers are used in this context,[80] whereby polyethylene glycol (PEG) represents the standard for such conjugations.[81] This FDA-approved polymer has a high biocompatibility and shows an array of useful chemical and biological features.[82] One chemical advantage is its solubility in both, organic and aqueous media. Thus, a sufficiently high surface modification of a hydrophilic protein material results in a lipophilic protein-polymer conjugate and enables solubility in organic solvents.

Biological properties of protein-PEG conjugates include increased protein stability, enhanced pharmacokinetics, low intrinsic toxicity and immunogenicity.[83] The PEGylation of proteins can be divided into site-specific and randomly surface conjugations. The major advantage of the site-specific modification, using only a single or defined number of polymer chains, is that it can take place remotely from the catalytic center of a protein. This minimizes its influence on the protein activity.[84] The site-specific PEGylation, using the 'grafting to' strategy, can be achieved by addressing chemoselective anchor groups, e.g. cysteines,[85] disulfides[86] or the N-terminal amine group.

Multiple attachments of polyethylene glycol to protein surfaces represent the first generation of PEGylation since Davis and co-workers presented their first promising results in the late 1970s.[87] The covalent non-selective PEGylation targets nucleophilic amino acids including lysines, serines, tyrosines and histidines, and resulting in core-shell protein-polymer architectures. The macromolecular protection of the inner protein leads to nanometer-sized constructs with desirable pharmacokinetic characteristics such as reduced renal clearance and immune cell activation. [88] This method is used for all protein PEGylations in this work, ensuring a highly surface modification, which leads to the solution in organic solvents.

The use of degradable linkages between the PEG and the protein represents another exciting alternative to existing PEGylation strategies. For this, synthetic polymers that are cleavable in target tissues were designed.[89] Biodegradable linkers that are redox-sensitive, degradable at physiological pH and temperatures or acid-labile are potential variants.[80] PegIntron® (see Table 1) represents a cleavable protein-polymer conjugate, which is approved since 2000 and is applied in the treatment of hepatitis C.[90]

The applicability of the presented intact protein-polymer conjugates in medical approaches is underlined by the already FDA-approved protein therapeutics, listed in Table 1.[91]

Table 1: PEG-modified protein therapeutics approved by the FDA. Modified from Dozier *et al.*[84a]

drug	protein	PEG/ kDa	site-specific	year of approval	use
Andagen®	Adenosine deaminase	5	no	1990	Severe combined immunodeficiency diseases
Oncaspar®	Asparaginase	5	no	1994	Leukemia
PegIntron®	Interferon-α-2b	12	no, but 47.8% one isomer	2000	Hepatitis C
Pegasys®	Interferon-α-2b	40	no	2001	Hepatitis C
Neulasta®	Granulocyte colony-stimulating factor (G-CSF)	20	yes	2002	Neutropenia
Somavert®	Human growth hormone (hGH)	5	no	2003	Acromegaly
Mircera®	Erythropoietin	40	no	2007	Anemia
Cimzia®	Anti-tumor necrosis factor (TNF) α Fab'	40	yes	2008	Rheumatoid arthritis, Crohn diseases, psoriatic arthritis
Krystexxa®	Urate oxidase	10	no	2010	Gout
Omontys®	Synthetic, dimeric peptide (Erythropoiesis stimulating agent)	40 (2 20 kDa chains)	yes	2012 (recalled 2014)	Anemia in chronic kidney disease

All mentioned conjugation approaches can result in suitable materials for the creation of higher ordered supramolecular architectures.[64] Due to the general benefits of nanosystems, also protein-based materials can function as drug carrier.[92] They show the incredible advantage to be fully biocompatible and biodegradable.

For example, the group of Stephen Mann presented the development of protein-based micro-compartments, so-called proteinosomes. Intact BSA-polymer conjugates represent the building block of this system and are processed by an emulsion technique. These proteinosomes represent biomimetic protocells with characteristics such as guest molecule encapsulation, selective permeability, gene-directed protein synthesis and membrane-gated internalized enzyme catalysis (Figure 5).[93]

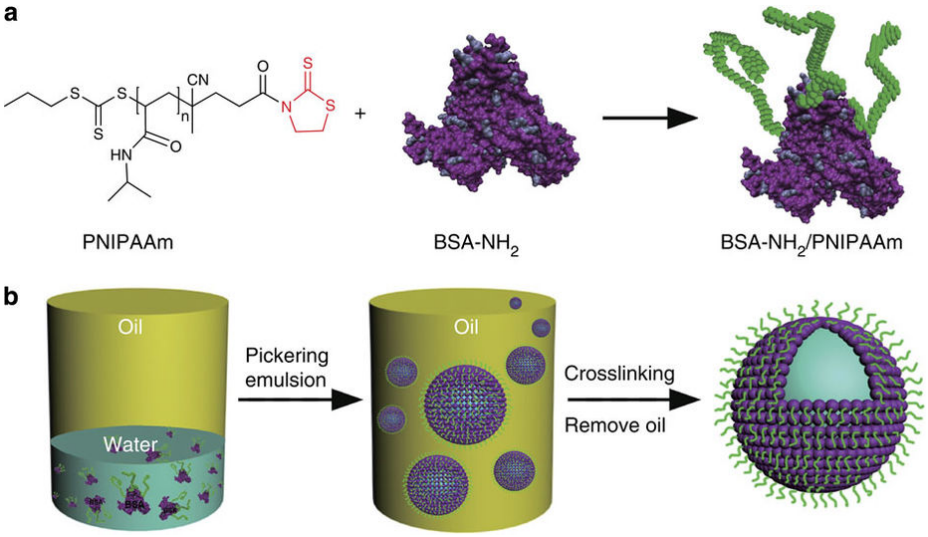

Figure 5: Preparation of proteinosomes. Protein-polymer conjugates based on BSA and PNIPAAm polymer chains represent the building blocks (**a**). The spontaneous assembly of the BSA-polymer conjugates leads to the formation of micro-compartments in oil. An additional crosslinking step stabilizes the constructs (**b**). Reprinted with permission from Mann *et al.*[93]

De Geest and co-workers developed transiently responsive BSA-polymer conjugates that are self-assembled into nanoparticles at physiological temperature and pH and simultaneously contain an immuno-modulator. An acid triggered hydrolysis of the attached units render the conjugates fully soluble in water and lead to a disassembly of the micelles.[94] An alternative approach for the development of protein-based nanoparticles was successfully presented in our working group.[11, 29] Intact protein-PEG conjugates were used as building blocks and assembled into stable particles utilizing a nanoemulsion-based technique (Figure 6). This method makes the application of crosslinkers and stabilizers redundant. The approach was presented in detail for the model protein lysozyme and transferred to β-lactoglobulin (BLG), OVA and HSA. Furthermore, the anti-cancer drug doxorubicin was encapsulated successfully in the particle matrix. The drug release was achieved in presence of proteases and under reductive conditions and *in vitro* applications confirm the cell toxicity.[11]

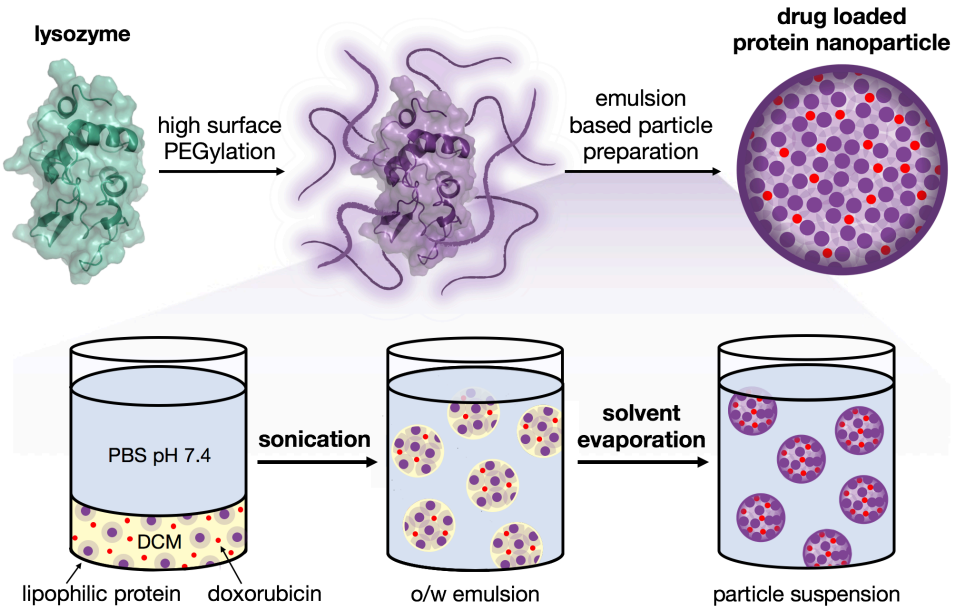

Figure 6: Protein-based nanoparticles for drug delivery. In the first step, a high surface PEGylation of lysozyme was performed, using activated PEG chains. Solely these protein-polymer conjugates represent the building blocks of the particle system, which was prepared by an emulsion-based technique. The lipophilic protein-polymer conjugates were dissolved in an organic phase together with a hydrophobic drug, in this case doxorubicin, covered with an aqueous phase and were sonicated. After the solvent evaporation, a stable particle suspension was received. Reprinted with permission from Fach *et al.*[11]

1.2.3 Enzymes as Biomaterial for Nanosystems

In order to create functional protein-based systems, enzymes can be used as biocatalytic materials for the modulation of biochemical reactions. Due to characteristics, such as high substrate selectivity, fast substrate kinetics and low side effects, these proteins can act themselves as perfect natural active drugs. Viewed from a therapeutic point, the performance of catalysis in cells with fully active enzyme-based systems offers the potential to intervene directly in abnormal mechanisms. This can lead to the alleviation or even more, the cure of a disease.

According to the catalyzed type of reaction, enzymes are classified into six main functional categories: oxidoreductases, transferases, hydrolases, lyases, isomerases and ligases. Further, classification is based on the chemical nature of the enzyme, for example bearing a prosthetic group (hemeproteins), a cofactor (flavoproteins) or metal ions (metalloenzymes).

In this context, two enzyme classes which were used in this work are considered and described more in detail.

Oxidoreductases catalyze oxidation and reduction reactions by transferring electrons with the help of cofactors such as nicotinamide adenine dinucleotide phosphate (NADP) or flavin adenine dinucleotide (FAD). Glucose oxidase (GOx) obtained from *Aspergillus niger*, is a dimeric ellipsoidal glycoprotein and consists of two identical subunits. Each monomer has a molecular weight of around 80 kDa (pI = 4.2) and contains a flavin adenine dinucleotide (FAD) as a redox cofactor and a key conserved active site for substrates. This enzyme oxidizes the conversion of *β*-D-glucose to D-glucono-*δ*-lactone, whereby the FAD cofactor is reduced to $FADH_2$. In a second step, the enzyme is oxidized by oxygen to the resting state of GOx, yielding hydrogen peroxide as a side product (Figure 7). In a further side reaction, D-glucono-*δ*-lactone is hydrolyzed to D-gluconic acid.[95] GOx is highly specific for the *β*-anomer of glucose and shows only slight catalysis of other sugars.[96] Based on this quality, GOx is widely used as a glucose biosensor.[97] The H_2O_2 formation confers GOx an anticancer effect[98] which can be used in cancer-starving and oxidation therapy.[99] This enzyme has gained remarkable commercial importance in the last few years due to its versatile application in the chemical and biotechnological field,[100] as food preservative[101] and in the textile industry.[102]

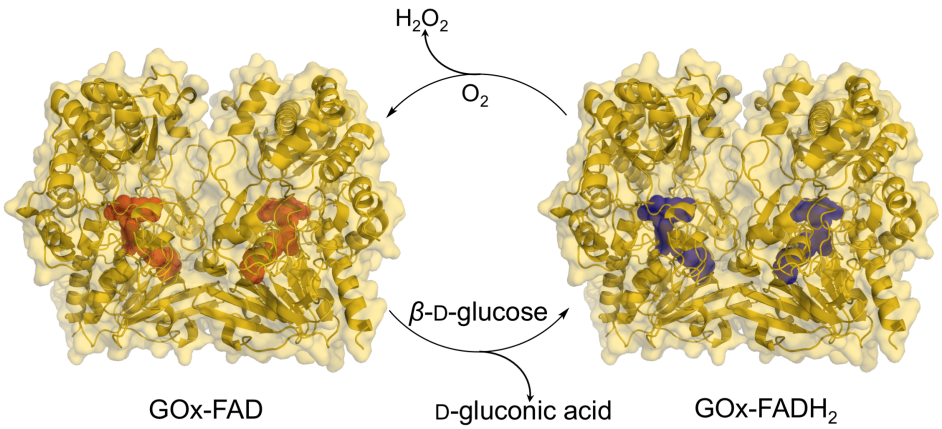

Figure 7: Schematic illustration of the catalyzed reaction by glucose oxidase. The substrate *β*-D-glucose is oxidized by the enzyme to D-glucono-*δ*-lactone, which reacts with water to D-gluconic acid. The FAD (red, left enzyme) acts as a redox cofactor and is reduced to $FADH_2$ (blue, right enzyme). In a second step, the enzyme reacts with molecular oxygen in order to form the resting state, producing hydrogen peroxide.

Peroxidases represent an additional subgroup of oxidoreductases. In general, they act as antioxidants and protect cells, tissues and organs against toxic peroxides. Most of them bear a heme group, which represents the catalytic center.

This prosthetic group catalyzes the oxidation of several organic and inorganic compounds by hydrogen peroxide, organic hydroperoxides, peracids or inorganic oxides.[103] The general peroxide-dependent reaction is shown in the following:

$$ROOH + 2\,AH_2 \xrightarrow{\text{Peroxidase}} ROH + H_2O + 2\,AH^{\bullet}$$

The heme group is responsible for many vital reactions, like electron transfer, redox catalysis, gas sensing, signaling and transport.[103-104] In nature, four main classes of hemes are known, of which the most frequently occurring is the heme *b* and heme *c* (Figure 8). All natural hemes contain a tetrapyrrole macrocycle as a chromophore. They chemical structure is differentiating from its peripheral *β*-pyrrolic-substituents. Heme *b*, also called iron (II) protoporphyrin IX, is the most common ferrous complex of all tetrapyrrole macrocycles. This heme structure serves as a template for the synthesis of heme *c*. Thereby, the heme *b* vinyl groups are replaced by thioether groups, which enable the covalent attachment of the prosthetic group to a protein backbone. Heme *c* groups most commonly contain a CXXCH motif, where C the cysteine residues, H the coordinated histidine residue and X can be any amino acid.

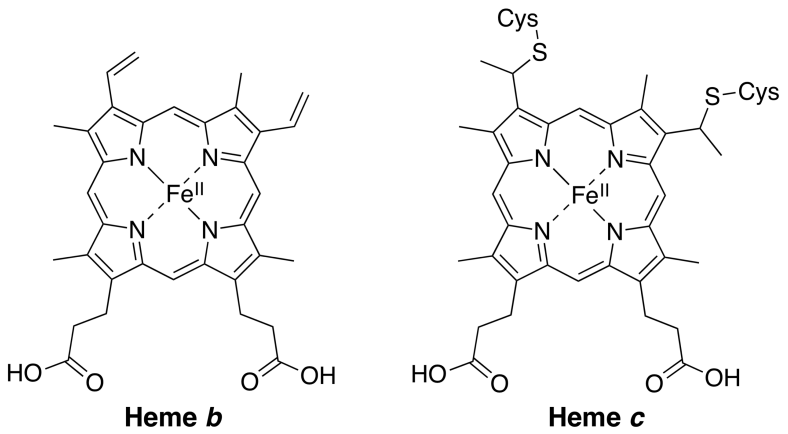

Figure 8: Chemical structure of heme *b* and heme *c*.

To understand the catalytic reaction of peroxidases, a look at the core of the porphyrin ring is essential. Many researchers investigated the ongoing processes and it has been generally stated that four consecutive reactions are present in the catalytic cycle.

The peroxidase mechanism was extensively studied at HRP, which can be used as a representative reaction sequence for many other peroxidase enzymes. Figure 9 shows the four main states of the ongoing reactions and the corresponding states of the heme iron.

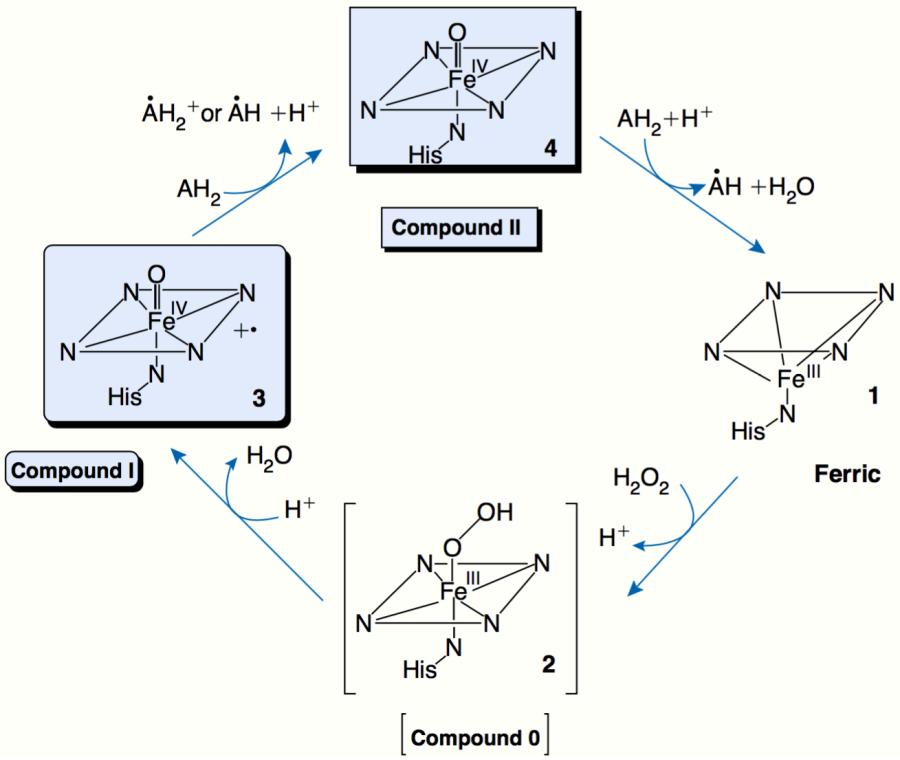

Figure 9: Peroxidase cycle of heme *b*. The tetrapyrrole macrocycle of the heme group is represented by a parallelogram (from Issac *et al.* [105]).

In the resting state (structure 1), the Fe^{3+} ion is penta-coordinated, whereby a conserved proximal histidine occupies the axial coordinate position. Starting from the resting state (structure 1), this ferric compound reacts with hydrogen peroxide to generate a transient hydroperoxide adduct, compound 0 (structure 2). This reaction takes place on the distal side of the heme, whereby a histidine residue acts as a base. This unstable ferric-hydroperoxide complex dissociates rapidly into an oxoferryl porphyrin π-cation radical, compound I (structure 3). Compound I represents the first intermediate state of the enzyme and is directly involved in the enzymatic mechanism. In the next step, an electron-rich substrate (AH_2) is oxidized by compound I, which generates the second intermediate state of the enzyme, compound II (structure 4). Thereby, a cation radical of the substrate is formed ($AH^{\bullet}$).

The second intermediate state of the enzyme contains Fe(IV) and two unpaired electrons. In the following reaction, a second AH_2 reduces compound II, which leads to the formation of the ferric resting state (structure 1), another $AH^{\bullet}$ and water.[105-106]

The described prosthetic group allows the horseradish peroxidase (HRP), isolated from the perennial plant horseradish, to oxidize a wide variety of organic and inorganic compounds in the presence of hydrogen peroxide. HRP is a globular biomacromolecule with a molecular weight of 44 kDa (pI = 3–9, isoenzyme range, at least seven exist). It contains a blocked N-terminal residue (by pyroglutamate), four disulfide bridges, a salt bridge between Asp99 and Arg123, and nine potential N-glycosylation sites, of which eight are occupied. The heme *b* group represents the catalytic center of this peroxidase and is linked to HRP by a proximal histidine residue (His170). The distal side of the heme plane is unoccupied in the resting state and accessible for hydrogen peroxide (structure 1, Figure 9). The structural integrity of the catalytic center into the protein scaffold is ensured on the one hand by hydrophobic interactions between surrounding amino acids and the tetrapyrrole macrocycle and on the other hand by additional polar interactions with the propionic acids. HRP bears two calcium ions, which are located distal and proximal to the heme plane and stabilize the secondary and tertiary structure of this enzyme.[107] The heme-binding region and both calcium binding sites are coordinated by a network of hydrogen bonds. Heme and calcium ions are essential for the functional and structural integrity of HRP.[106a, 108] In recent years, HRP has gained importance in clinical applications, molecular diagnostics and immunoassays.[109] In combination with prodrugs, especially indole-3-acetic acid, this enzyme can be used in cancer therapy.[110]

Looking at heme *c* peroxidases, especially cytochrome *c* (Cyt *c*), the covalent attachment of the prosthetic group to the polypeptide backbone plays an important biological role. It shows electrochemical effects on the electron transfer thermodynamics and kinetics, which are vital as Cyt *c* plays a major part in the respiratory chain.

The second functional role is based on the significant structural and conformational change of mitochondrial Cyt *c* in response to an apoptotic signal, which induces the turn of Cyt *c* into a peroxidase. Cytochrome *c*, a globular, highly-conserved and positively charged hemeprotein (12.4 kDa, 3.4 nm in diameter, pI = 10.5), is found in the inner membrane space of all mitochondria. This enzyme is involved in two vital processes (Figure 10).

Firstly, it plays an important role in the apoptosis, where it is released into the cell cytosol upon stimuli. Cyt *c* acts as an apoptotic cell death mediator by binding to the apoptotic protease-activating factor-1 (Apaf-1), which builds up the apoptosome by the assembly of seven Apaf-1 molecules.[111]

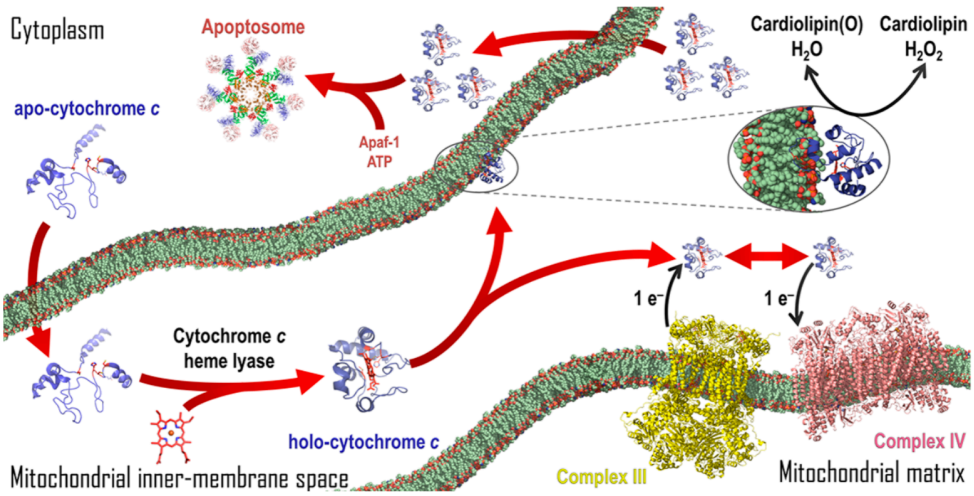

Figure 10: Schematic illustration of the locations and biological roles of Cyt *c* within the cell. The red arrows give information about the translocations and modifications of the enzyme associated with its function. Located in the mitochondrial inner-membrane space, Cyt *c* participates in the respiratory chain and shuttles electrons from Complex III to Complex IV. In apoptosis triggering, Cyt *c* undergoes a structural alteration and catalyzes the H_2O_2-dependent oxidation of cardiolipin. After the release of the enzyme into the cytoplasm, it associates with Apaf-1, forming the apoptosome, which leads to cell death (from Kleingardner *et al.*[112]).

Under healthy conditions, Cyt *c* resides in the mitochondrial inner membrane and participates in the respiratory chain, where it catalyzes the transfer of electrons between complex III (cytochrome *c* reductase) and complex IV (cytochrome *c* oxidase). This reaction is carried out by heme *c*. Like already mentioned, two cysteine residues (Cys-14/17) are covalently link the porphyrin macrocycle to the protein scaffold via two thioether bonds. Cyt *c* is a six-coordinate heme protein, where a histidine (His-18) and a methionine (Met-80) serve as axial ligands to the encapsulated iron.[104, 113] The enzyme is capable to undergo oxidation and reduction reactions and is involved in vital processes including the mentioned electron transfer, inhibition of reactive oxygen species (ROS) formation and prevention of oxidative stress.[114] Cytochrome *c* is widely used as a model enzyme in several biotechnological applications, in particular, because of its peroxidase activity.[115]

Catalases represent a special type of peroxidases and catalyze the dismutation of hydrogen peroxide into molecular oxygen and water in a two-stage reaction.[116] The catalase (Cat) represents one of the most important antioxidant enzymes and is found in all aerobic organisms. This heme-containing biopolymer is the most efficient natural catalysts with one of the highest turnover rates of all enzymes.[116] The used bovine liver catalase is a homotetrameric enzyme containing four identical 60 kDa subunits (pI = 5.4). Each monomer contains a heme *b* group, as a catalytic center and one NADPH molecule as a cofactor, which prevents the inactivation of the enzyme.[116-117] In general, catalases show a highly conserved β-barrel core structure. Substrates and products can reach the active site through one of the three accesses channels. Catalases show remarkable resistance over a wide pH range, high thermostability and are resistant to proteolysis. Based on these characteristics, catalases gained in importance for clinical and biological applications.[118]

The enzyme lysozyme (LYZ) represents another protein that was used in this work and belongs to the class of hydrolases. This glycoside hydrolase is an antibacterial enzyme and part of the innate immune system. It is widely distributed in nature and found in mammalian tissues and fluids such as milk, saliva, mucus, blood and tears. Lysozyme lyses cell walls of Gram-positive bacteria by cleaving the 1,4-β-glycosidic linkage between *N*-acteylmuramic acid and *N*-acteylglycosamine, which are building blocks of the peptidoglycan in bacterial cell walls. It is a small globular protein (3.5 nm in diameter, pI = 10.7) with a molecular weight of 14.3 kDa. Lysozyme is used in various therapeutic applications[11] and serves as a food preservative.[119]

Figure 11 summarizes the five used enzymes in this work and gives an overview of their molecular weight, spherical structure and compares the relative sizes to each other.

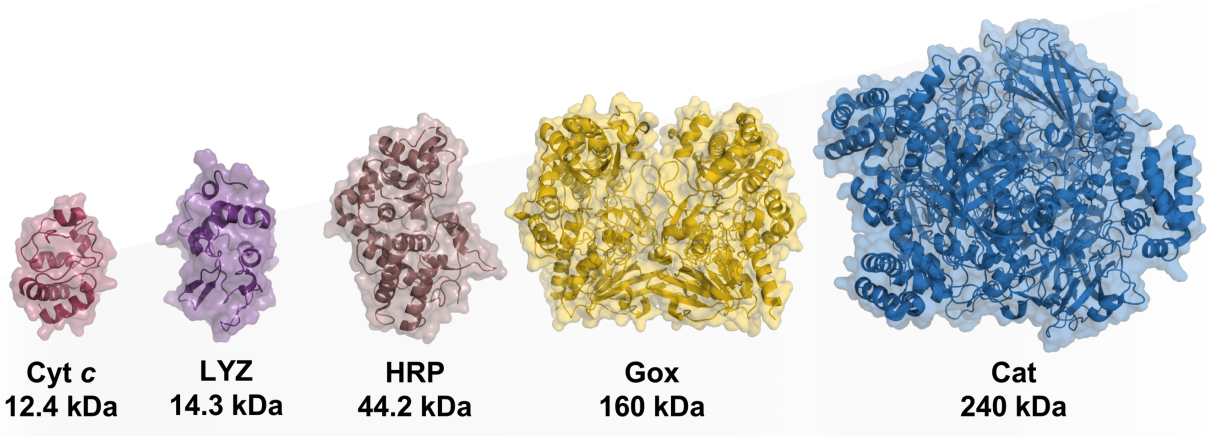

Figure 11: Used enzymes in this work. Cytochrome *c* from horse heart (Cyt *c*, red, PDB: 1hrc), lysozyme from hen egg (LYZ, purple, PDB: 1lyz), horseradish peroxidase (HRP, brown, PDB: 1hch), glucose oxidase from *Aspergillus niger* (GOx, yellow, PDB: 1gpe) and catalase from bovine liver (Cat, blue, PDB: 1tgu).

Reactive Oxygen Species and Natural Antioxidant Defense Mechanisms

The selected enzymes Cyt *c*, HRP and Cat represent, like already mentioned, important natural antioxidant biomacromolecules, which protect cells among other things from harmful reactive oxygen species (ROS). The formation of these highly reactive molecules and the participation of the chosen enzymes are presented in the following section in order to understand the attractiveness of the application of these biopolymers.

Metabolic processes in cells such as the respiration and enzyme complexes like the NADPH oxidases, lead to the production of reactive oxygen species (ROS), which can be defined as reduced metabolites of oxygen with strong oxidizing capabilities. The mitochondrial oxygen metabolism represents a major source of the superoxide anion (O_2^-), resulting from the inchoate coupling of electrons in the electron transport chain. Next to O_2^-, hydrogen peroxide (H_2O_2), the hydroxyl radical ($OH^\bullet$) and the superoxide anion radical ($O_2^{-\bullet}$) are classified as reactive oxygen species.[120] Physiological low concentrations of these species are vital due to their function as signaling molecules and their involvement in many processes, especially cell differentiation, proliferation, growth, apoptosis and in immune responses.

These comprehensive tasks demonstrate the significance of these species. However, an excessive production of ROS results in potentially cytotoxic oxidative stress which induces cell damages and inflammations. The irreversible destruction of vital biomolecules, especially proteins, lipids and the DNA makes them in particular harmful.[121] Pathological findings of various diseases show evidence for ROS involvement. Looking at the central nervous system (CNS), where low ROS concentrations are required for brain functions, high levels of these species cause in perilous neurodegenerative diseases like Alzheimer's and Parkinson's disease.[122] In the case of the Alzheimer's disease, soluble forms of amyloid are able to initiate the activation of microglia, leading to a long-lasting ROS generation which contributes to neuronal inflammations and dementia.[123] The involvement of ROS is also observed in cancer.[124] The DNA damages caused by these species contribute to the initiation and progression of this disease.

Natural non-enzymatic and enzymatic detoxification processes prevent the accumulations of ROS and protect cells against them. Endogenous enzymes, like superoxide dismutase (SOD), catalase (Cat) and glutathione (GSH) peroxidase are classified as ROS scavengers. Distinct superoxide dismutases rapidly convert O_2^- into the less reactive hydrogen peroxide. This molecule diffuses free or receptor-mediated across biological membranes and is implicated in signaling pathways including proliferation, cell growth and survival.[125] However, H_2O_2 can act as an oxidant and can be converted into the highly reactive hydroxyl radical ($OH^\bullet$) by iron-containing enzymes in a Fenton reaction. This species is considered as the most harmful ROS compound and causes massive cellular damages, which can only be restricted due to its short half-life. Another important enzyme, the glutathione peroxidase interferes here and converts hydrogen peroxide into water. This enzyme plays a central role in the maintaining of the redox homeostasis. Catalase is involved in these defense mechanisms and represents the most efficient protective antioxidant enzyme in this context. By decomposing hydrogen peroxide into oxygen and water, no further free radicals are produced by this enzyme.[117, 126] Looking at mitochondrial cytochrome *c*,[104a] Xu and co-workers could show that this enzyme acts as an antioxidant and is involved in the detoxification of ROS.[104a, 114b] Additionally, Pereverzev and co-workers confirmed these results and showed that cytochrome *c* oxidizes superoxide back to molecular oxygen.[127]

Furthermore, repair processes, non-enzymatic members such as glutathione, uric acid and lipoic acid, and exogenous antioxidant molecules like vitamin E (tocopherol), C (ascorbic acid) and carotenoids, represent other important antioxidant systems of cells.[120-121, 128] Since these are not important for the presented work, references are merely made to the literature.

To prevent an overproduction or accumulation of the mentioned reactive species, the delivery of enzymes using particulate systems becomes increasingly important. This approach can allow to protect cells from oxidative stress and prevent the occurrence of a disease. Some developed enzyme-based nanosystems will be presented in the next section.

Enzyme-based Nanosystems

The delivery of enzymes represents due to the mentioned characteristics of these biopolymers a promising approach in the nanomedicine. Multifunctional nanosystems can be created by exploiting intrinsic enzymatic characteristics. The application of enzymes can trigger, change or prevent a specific physiological response and lead to the modulation of metabolic processes.[129]

Away from higher ordered nanostructures, enzyme-polymer conjugates are already used in the medical field and should be mentioned in this context. The PEGylation step leads to the stabilization of the enzymes and results in nano-sized constructs. Oncaspar®, PEGylated L-asparaginase,[130] and Krystexxa®, PEGylated uricase [131] are important examples and demonstrate the effectiveness of enzymes in the administration as a drug (see Table 1).

Like already mentioned, diverse nanoscale constructs such as liposomes, micelles and polymer nanoparticles have been used for the delivery of proteins and enzymes.[132] The enzymes are either encapsulated inside the particles[133] or are attached to the exterior.[134] Mesoporous silica particles represent suitable matrices for the immobilization of enzymes.[135] Zhao *et al.* encapsulated lipase in mesoporous silica yolk-shell spheres in order to increase the thermal stability of the enzyme and protect them from degradation by proteases.[136] Qu and co-workers used poly(acryl acid)-modified nanospherical silica to immobilize bienzymes, in that case, glucose oxidase and horseradish peroxidase, to perform enzymatic cascade reactions.[97b] The encapsulation of enzymes into polymeric scaffolds represents another approach.[133a, 137]

Batrakova and co-workers investigated inflammatory diseases of the central nervous system, especially the Parkinson's disease and developed enzyme-based delivery systems. In one approach, they designed a macrophage-nanozyme system in order to deliver the redox-enzyme catalase to Parkinson affected brain areas.[118b] With this system, it was possible to reduce the hydrogen peroxide level, which is increased in Parkinson's disease. Additionally, they confirmed their first results in murine models and demonstrated the feasibility of cell-mediated catalase delivery systems for Parkinson's disease therapies.[138] Inspired by the cell organization and the separation of vital biochemical processes in defined compartments, the working group of J. van Hest developed several nanoreactors[139] and cages[140] using various proteins and enzymes as essential building blocks.[141] They demonstrated the synthesis of so-called lyophilisomes using elastin as a building block, which can be used for the development of bioactive capsules.[142]

As stable alternatives to natural enzymes, fully artificial, enzyme-like materials have been designed and established in recent years.[143] Metal oxide-based materials form a huge area in this field. So-called nanoceria, cerium oxide-based nanomaterials are able to scavenge reactive oxygen intermediates[144] and exhibit superoxide dismutase- (SOD),[145], catalase,[146]- oxidase[147] and phosphatase[148]-like activities. Magnetic iron oxide-based nanomaterials, which regarded to be chemically and biologically inert, also exhibit an intrinsic peroxidase-like activity.[149] Yan and co-workers provided the first pioneering studies and established a new area of research in this context.[150] Other metal-based nanosystems have also been explored, especially investigations of gold nanoparticles have been made.[151] Lin and co-workers demonstrated the peroxidase-like and GOx-like activity of cysteamine- and citrate-capped AuNP encapsulated in mesoporous silica.[152] However, *in vitro* experiments demonstrated therapeutic potentials of the mentioned nanomaterials, their use for *in vivo* applications is often limited due to cytotoxic effects.[153] Additionally, looking at the specificity and efficiency, natural enzymes are well ahead of these engineered nanosystems. The delivery of native active enzymes to specific cells and organs is more efficient. One reason is the much higher conversion rate of biochemical reactions by natural biomacromolecules compared to the artificial one. Moreover, the therapeutic application of native biomaterials presents a lower healthy risk.

1.3 General Aspects of Enzyme Kinetics and Assays

In order to investigate and understand the enzymatic activity, kinetic mechanisms must be considered. Enzyme-catalyzed reactions follow the Michaelis-Menten model and can be described with corresponding kinetic parameters. Simplified, this theory can be applied to an enzymatically catalyzed reaction with two reaction steps:

$$\mathrm{E} + \mathrm{S} \underset{k_r}{\overset{k_f}{\rightleftharpoons}} \mathrm{ES} \xrightarrow{k_{cat}} \mathrm{P} + \mathrm{E}$$

where the enzyme (E) forms an enzyme-substrate complex (ES) in the first step, which subsequently decomposes into the product of the reaction (P) and the enzyme. k_f (forward rate), k_r (reverse rate) and k_{cat} (catalytic rate) represent the rate constants of the corresponding steps.

The Michaelis-Menten equation is based on the assumption that a rapid equilibrium between reactants and the enzyme-substrate complex is achieved, and represents the basic equation of enzyme kinetics:

$$v_0 = \frac{V_{max}\,[S]}{K_\mathrm{M} + [S]} = \frac{k_{cat}\,[E]_0\,[S]}{K_\mathrm{M} + [S]}$$

V_{max} is the maximum rate of the system at saturating substrate concentrations and can be defined as $V_{max} = k_{cat}[E]_0$ at higher substrate concentrations with $[S] \gg K_\mathrm{M}$. The turnover rate k_{cat} indicates the maximum number of substrate molecules converted to the product by one enzyme per second. Thus, higher turnover rates imply a more efficient conversion of the substrate per second. The Michaelis constant K_M represents the substrate concentration at which the reaction rate is at half-maximum and is an inverse information about the substrate's affinity for the enzyme. Smaller K_M values indicate high substrate affinity based on the attainment of V_{max} with lower substrate concentrations. To be able to classify the efficiency of enzymes, the catalytic parameters K_M and k_{cat} have to be considered. The quotient of these variables results in the specificity constant (k_{cat}/K_M), which indicates how efficient an enzyme converts its substrates into the products (named as 'catalytic efficiency' in this work). Higher values represent more efficient enzymes.

In the laboratory scale, kinetic investigations can be carried out with the aid of absorption- and fluorescent-based assays. In general, the formation of a product or the consumption of a substrate over time are measured. The following descriptions focus on the three used assays in this work, the ABTS assay, the Amplex Red assay and the enzyme-specific H_2O_2 assay for catalase. The selected procedures represent enzyme assays where all participants, such as enzymes, substrates and chromogens are in solution and the relevant readout takes place in microtiter plates.

The ABTS assay represents a well-known colorimetric method and is based on a peroxidase-catalyzed one-electron oxidation of 2,2'-azinobis-(2-ethylbenzthiazoline-6-sulfonate) (ABTS) into the corresponding radical cation $ABTS^{\bullet+}$ (Figure 12). The oxidation of this compound and related molecules were already investigated in the middle 1960s by Hünig and co-workers.[154] Even in the following years, ABTS was established as a chromogen for hydrogen peroxide assays using peroxidases as catalysts.[155] The formation of the radical anion is analyzed spectroscopically and measured between 405 and 420 nm over a short time, in most cases less than 10 minutes. This method enables an easy quantification of the initial rates of enzymatic reactions. Peroxidases and peroxidase containing materials can be assayed using this chromogen.

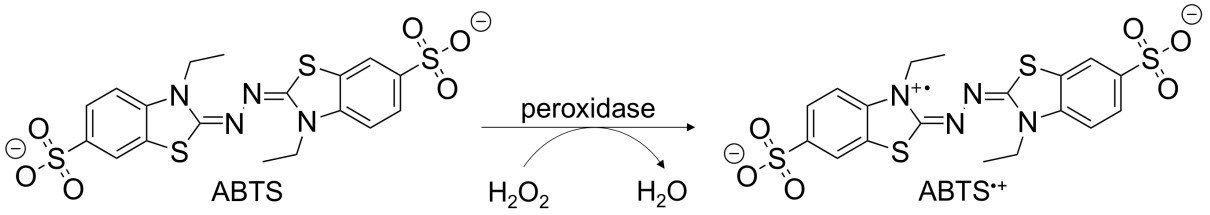

Figure 12: Reaction of ABTS with a peroxidase and hydrogen peroxide to the corresponding $ABTS^{\bullet+}$ radical cation, a green product (absorption at 405 nm).

A common procedure of this assay is to vary the substrate concentration, in this case hydrogen peroxide, and keeping the amount of ABTS and the enzyme concentration stable. At slightly acidic or neutral conditions (pH 6–7), the formation of $ABTS^{\bullet+}$ is measured spectroscopically in the presence of different H_2O_2 concentrations. As already mentioned in Chapter 1.2.3, the generation of a hydroperoxide adduct, formed by the iron of the heme group and hydrogen peroxide, represents the first step. This unstable ferric-hydroperoxide complex dissociates rapidly into an oxoferryl porphyrin π-cation radical, forming compound I (Figure 9).

At this point, the electron-rich substrate ABTS reduces compound I to compound II, whereby a green-colored cation radical is formed ($ABTS^{\bullet+}$). Possible side reactions are the conversion of $ABTS^{\bullet+}$ into ABTS or an over-oxidation of ABTS, which occurs in the presence of H_2O_2 excess, leading to the formation of the azodication $ABTS^{2+}$.[156]

The Amplex Red assay is based on the same principle and differs only in the use of a fluorescent dye (Figure 13). Hydrogen peroxide represents the substrate and initiates the reaction, whereby Amplex Red acts as the electron-rich compound. The reaction leads to the formation of the red-colored and highly fluorescent compound resorufin (ex: 563 nm / em: 587 nm). Fluorescent probes provide convenient and sensitive dyes for the detecting of certain substances and processes, especially in cells and tissues. This assay is commonly used for the measurement of extracellular hydrogen peroxide and, at the same time, for the peroxidase activity of developed enzyme containing materials.[157]

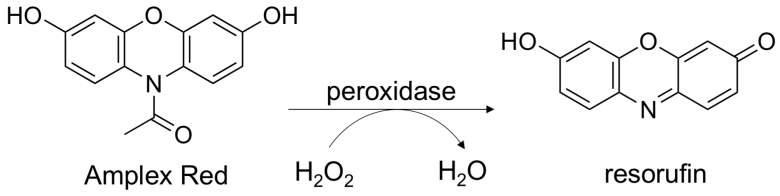

Figure 13: Reaction of Amplex Red with a peroxidase and hydrogen peroxide to the highly fluorescent dye resorufin.

For the investigation of the peroxidase activity of catalase, an enzyme-specific assay was used. The consumption of hydrogen peroxide by catalase and the following disappearance of H_2O_2 at 240 nm was measured spectroscopically. This assay can be monitored continuously at 240 nm containing a constant amount of enzyme and different hydrogen peroxide concentrations at an appropriate time interval.[158]

Modern evaluation programs like GraFit® (Erithacus Software Limited) enable the analysis and comprehensive fitting of all received data to determine K_M and V_{max} in order to calculate the important kinetic parameters k_{cat} and the specificity constant (k_{cat}/K_M).

2 AIM OF THE WORK

Protein-based nanoparticle systems represent innovative nanomaterials due to their biodegradability, their structural and chemical diversity and their potential to act as bioactive molecules. In this context, the development of catalytic active nanosystems utilizing enzymes as functional building blocks represents a challenging approach and offers the potential to modulate cellular processes.

In order to use enzymes in biochemical approaches, the enhancement of their physicochemical properties is unavoidable. For this, the surface modification with the FDA-approved synthetic polymer polyethylene glycol (PEG) represents a common approach. Based on the amphiphilic behavior of this synthetic polymer, a high surface PEGylation results in a lipophilic material and allows a solubility in organic solvents. Previously, this approach was utilized in our working group to formulate a stable protein-based nanoparticle system. Lysozyme was used as a model enzyme and was modified with TsT-activated polyethylene glycol. Trichlorotriazine (TsT) is an established activation agent for PEG since Abuchowski and co-workers published their initial results of protein PEGylation in the early 1980s. The TsT group represents a highly reactive electrophilic linker for the unselective modification of protein surfaces. This reactivity can lead to the crosslinking of protein molecules, resulting in undesired high molecular weight conjugates. Over the years, TsT has been supplanted by several other more controllable activation linkers for PEG.

Build on the applied PEGylation strategy in our working group, in the first project of this thesis other electrophilic agents should be investigated for PEG activation (Figure 14). For this, it was planned to select four different electrophilic groups, which distinguish themselves by their chemical functionality and their reactivity towards nucleophilic amino acids on the protein surface. Subsequently, LYZ should be modified with these activated PEGs to achieve a lipophilic biomaterial. The main goal of this first project was to find a highly reactive and in particular mild PEGylation method, which ensures the preservation of the enzymatic activity. Furthermore, it was the idea to prepare protein-based nanoparticles with the synthesized protein-polymer conjugates. For this, an emulsification method which was established in our group after the first promising results of Fach *et al.* should be used.

It was planned to investigate the effect of the different used LYZ-PEG conjugates on the resulting protein nanoparticles regarding size, morphology and stability.

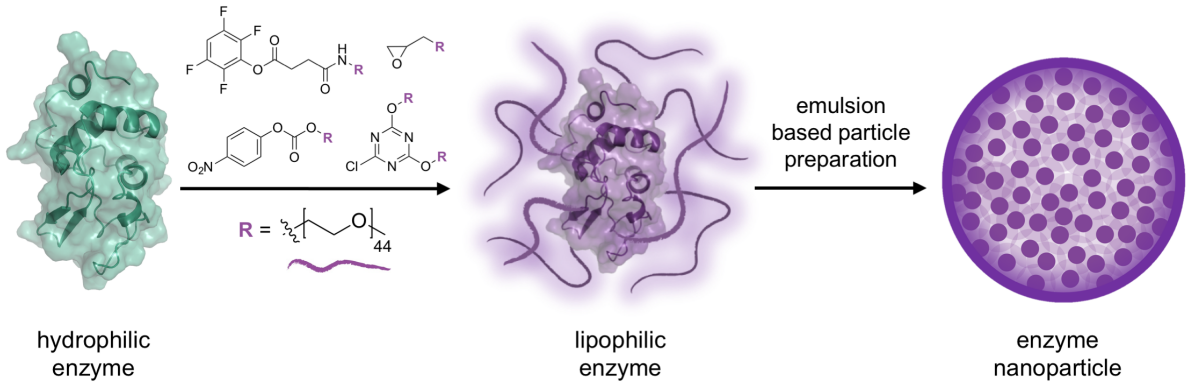

Figure 14: The first project of this thesis focused on the PEGylation of a protein, using four different activated PEG chains. It was the aim to achieve a lipophilic protein material, which can be processed by an emulsion-based technique to prepare a solely enzyme-based nanoparticle system. In the first step, it was the idea to find a highly reactive and in particular mild PEGylation method, which ensures the preservation of the enzymatic activity. In the second step, it was planned to investigate the effect of the different used LYZ-PEG conjugates on the resulting nanoparticles regarding size, morphology and stability.

Enzyme-based materials offer the potential to intervene in specific cellular mechanisms and to correct defective processes in a therapeutic approach. For this, the combination of synthesized materials with natural enzymes represents a promising approach in the design of biomimetic systems. Several nanomaterials, consisting of synthetic or natural compounds and containing natural enzymes as biocatalysts, have been reported in the literature, previously. The common feature of all these systems is that the enzymes are either encapsulated within the particle system, attached on their surface or incorporated within the matrix. Thus, additional carrier materials are necessary, which have to be biocompatible and non-toxic for therapeutic applications.

The second project of this PhD thesis focused on the development of a catalytically active nanomaterial (Figure 15). The idea was to exploit the intrinsic enzymatic activity of the used biomacromolecules in order to create catalytically functional nanoparticles. In contrast to the mentioned nanomaterials, it was planned to develop a system consisting solely of surface-PEGylated enzymes using the emulsion-based technique. This would make the use of additional carrier materials and stabilization agents redundant. The PEG polymer should merely be used as aiding component in order to achieve a lipophilic biomaterial.

Three peroxidases, Cyt *c*, HRP and Cat, which differ in size, morphology and catalytic efficiency should be used as an active biomaterial. It was planned to investigate the designed enzyme-based nanosystems regarding catalytic activity and integrity, and to compare them to each other. If the developed biocatalysts retained their enzymatic activity, it was the idea to examine the catalytic performance of the nanoparticles in a cellular environment, using HeLa cells as a model system. The focus should be on the design of functional nanomachines that can intervene in cellular processes and manipulate them within the biological environment.

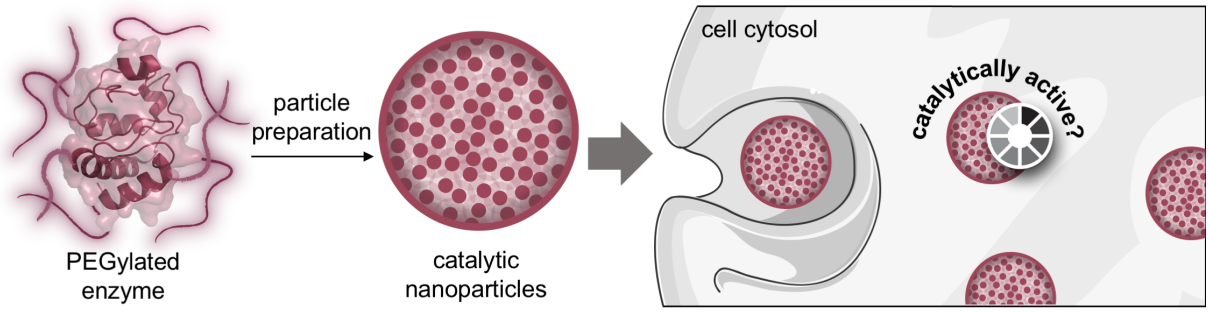

Figure 15: The idea of the second project was to create catalytically active enzyme-based nanoparticles, which are able to modulate cellular processes. In the first step, PEGylated enzymes should act as active building blocks due to develop catalytic nanoparticles, using the established emulsion technique. In the second step, it was planned to investigate the catalytic potential of the created systems within a cellular environment.

In recent years, renowned researchers such as Stephen Mann and Jan C. M. van Hest presented the design of bio-inspired nanoreactors. The imitation of compartmentalization such as in living cells and thus the temporal and positional occurrence of vital reactions within these nanocages represents an innovative challenge in fundamental and applied science.

In the third project of this work, it was the idea to develop a catalytically active dual-enzyme nanoparticle system which can perform cascade reactions (Figure 16). It was planned to investigate whether it is possible to co-embed two different enzymes in their active form within one particle system using the established single emulsion particle preparation technique. For this, the two well-known enzymes glucose oxidase (GOx) and horseradish peroxidase (HRP) should be utilized in their PEGylated variant in order to achieve a lipophilic biomaterial.

For the subsequent nanoparticle preparation, we planned to utilize different concentration ratios of both enzyme and to investigate the effect on the resulting dual-enzyme systems regarding substrate sensitivity and catalytic efficiency.

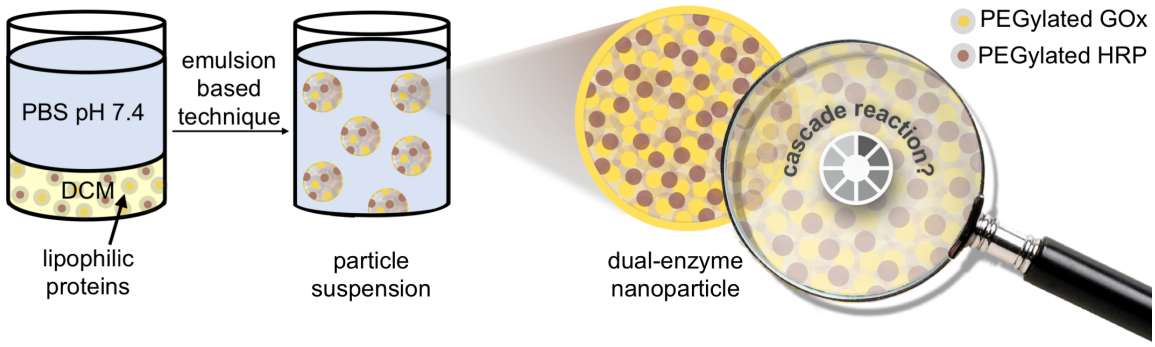

Figure 16: In the third project of this PhD work, a nanoparticle system which can perform cascade reactions should be developed. The idea was to create a catalytically active particle system based on two PEGylated enzymes. For this, it was planned to use the established single emulsion technique and co-embed PEGylated glucose oxidase and horseradish peroxidase within one nanoparticle system. The enzymatic activity should be investigated with chromogenic molecules.

3 RESULTS AND DISCUSSION

3.1 Enzyme PEGylation under Activity Preservation

In the first study, different linkers for the electrophilic PEG activation should be investigated with the aim to find a highly reactive and at the same time mild PEGylation method for enzymes. The focus was on the preservation of the native structure and the catalytic activity of the used enzyme. These surface modifications were carried out with the aim to build up a protein-based nanoparticle system using a mild nanoemulsion technique.

The majority of the data in this section has already been published in *Medical Chemical Communications* (*MedChemComm*), the *Journal of the Royal Society of Chemistry* (Radi *et al.*[29]) and is discussed in this work more in detail.

3.1.1 Polyethylene Glycol Activation

Methoxypolyethylene glycol (mPEG) with a molecular weight of 2 kDa was used as a basic building block and was functionalized with four different electrophilic linkers. Due to the low reactivity of the terminal alcohol group of mPEG, an activation is necessary for the reaction with nucleophilic groups on protein surfaces. Accessible amino acids in particular are lysine, cysteine, serine, threonine, arginine and tyrosine. Among them, lysine represents the most abundant amino acid in protein sequences and its *ε*-amino group is a common target for conjugations.[159]

Active esters of PEG carboxylic acids are appropriate acylating agents for protein modification. The reactive electrophilic group reacts with primary amines under physiological conditions forming stable amides. *N*-hydroxysuccinimidyl active esters (NHS esters) represent one suitable variant and are used widely for protein PEGylation[89] In this first project, the mentioned NHS active esters were not used because of the following reasons. These agents show a high hydrolysis tendency in aqueous solution, which is why high amounts are necessary for a sufficient protein surface PEGylation.

Furthermore, high costs of the commercial available NHS-mPEG limit their use in this approach. Fluorinated phenyl esters of PEG carboxylic acid (TFP-mPEG) are further commonly used alternatives. One primary advantage of this electrophilic group compared to the NHS ester is the better stability towards hydrolysis in aqueous solution, exhibiting a 10-fold increased half-life under slightly basic buffered conditions.[160] In an esterification reaction, *α*-methoxy-*ω*-carboxy PEG was modified with the electrophilic tetrafluorophenyl group using tetrafluorophenol and *N*,*N'*-dicyclohexylcarbodiimide (DCC) as a dehydrating agent.[161] The white solid was isolated in 61% yield.

Cyclic ethers, especially epoxides are potent electrophiles and can be used for the activation of mPEG. This functional group is highly reactive towards primary amines, hydroxyl, imidazole and thiol groups on the protein surface. The hydroxyl-functionalized mPEG was activated using epichlorohydrin and sodium hydride as a strong base in order to functionalize the polymer with a glycidyl end group in an epoxidation reaction (epoxy-mPEG).[162] The yellow solid was isolated in good yield (92%) and was stable in aqueous solution for 48 h.

Another acylating chemistry is based on the activation of the terminal PEG hydroxyl group with chloroformates. The resulting carbonate ester of mPEG represents another electrophilic group for the reaction with nucleophiles. The activated polymer was synthesized under alkaline conditions using *p*-nitrophenyl chloroformate (yield 70%, carbonate-mPEG).[163] One disadvantage of this compound is the relatively low stability towards hydrolysis.

As a fourth activating agent, trichlorotriazine (TsT) was used. According to the initial work of Abuchowski,[87a, 87b] the conjugation of TsT with one polymer chain results in a highly reactive conjugate which can react with multiple functional groups on the protein surface, forming a secondary amine. It is known in the literature that the remaining chloride shows a sufficient reactivity, which can lead to the crosslinking of protein molecules. In order to circumvent this side reaction a triazine functionalized with two PEG chains was synthesized according to Inada.[164] Using this bi-functionalized PEGylation agent for the protein surface modification, the lipophilicity of the resulting biomaterial can be increased rapidly, based on the introduction of simultaneously two polymer chains per amine modification. Under mild alkaline conditions, the attachment of two polymer chains to TsT takes place in a nucleophilic aromatic substitution (S_NAr).

Despite the activating agent is toxic, the resulting materials show minimal toxicity and have proven to be successful in various *in vitro* and *in vivo* therapeutic applications.[11, 59b] According to size-exclusion chromatography and elementary analysis, 88% of cyanuric chloride was functionalized with two mPEG chains, leaving the rest mono-functionalized (TsT-mPEG).

3.1.2 PEGylation of Lysozyme

The antimicrobial enzyme lysozyme (LYZ, 14.3 kDa) was used in this first study as a model protein for PEGylation. In order to achieve a high surface modification and to facilitate a solubility of the protein-polymer conjugate in organic solvents, the reactivity of the synthesized PEGs (as described in Chapter 3.1.1) was investigated. The study compares the four different LYZ-PEG conjugates and focuses on their structural integrity and their remaining enzymatic activity (Figure 17). The globular enzyme LYZ offers ten nucleophilic groups on their surface. With the N-terminal amine and overall six accessible lysines, the primary ε-amino groups (pK_a 10.5) represent the main target for PEGylation. Other three hydroxyl groups of tyrosine (pK_a 10.9) are available and can react with the activated polymers in a nucleophilic substitution reaction. In general, the SH-group of cysteines is another target anchor.

All conjugations were performed in alkaline buffered aqueous solutions (pH 8–10) with a 3- to 20-fold excess of activated mPEG per amine. The modification of LYZ with TFP-mPEG, epoxy-mPEG and carbonate-mPEG take place at room temperature for 48 h, using the polymer in a threefold excess. Utilizing TsT-mPEG as PEGylating agent, a mild heating (40 °C) of the sample was necessary for two hours. To substitute the third chlorine of TsT an increased temperature are required (third chlorine: 70–100 °C).[165] Higher temperatures, in order to ensure the substitution of the third chlorine, are not possible, as it would be lead to the denaturation of the protein. In combination with slightly increased reaction temperatures and a high amount of TsT-mPEG (20-fold), a LYZ surface modification using this PEGylating agent was carried out.

All resulting protein-polymer conjugates were purified by dialysis or centrifugal devices. After freeze-drying, a colorless solid was obtained in all four cases.

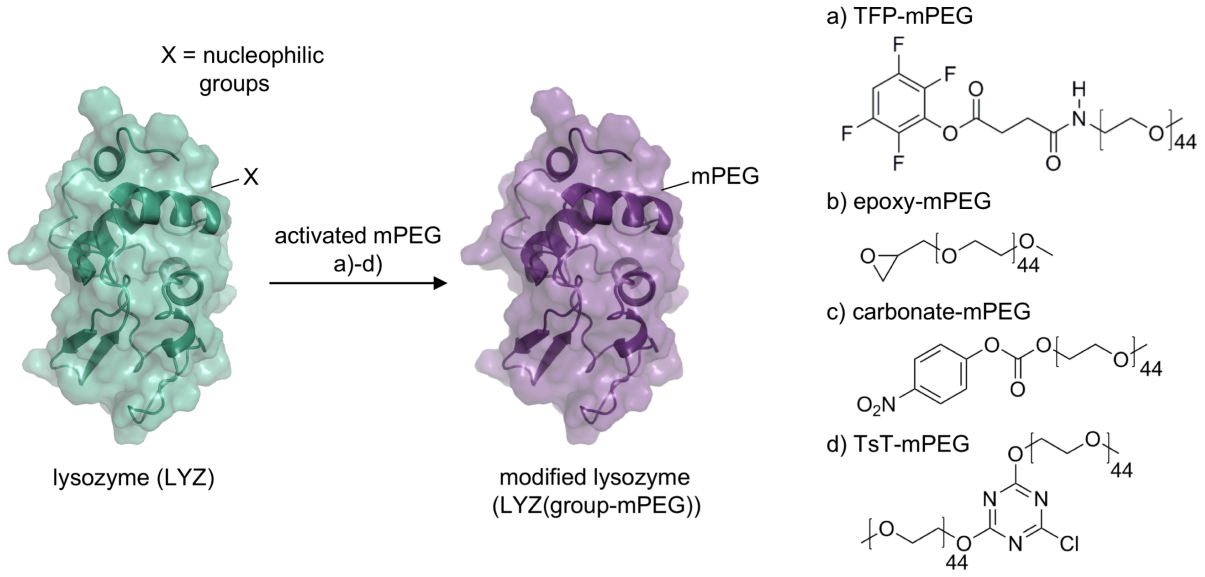

Figure 17: Surface modification of lysozyme with methoxypolyethylene glycol (2 kDa). Four different activated mPEG chains (a–d) were synthesized and used for the PEGylation of LYZ. The X represents the ten accessible nucleophilic groups of lysozyme such as the amine or the hydroxyl group.

Molecular Weight Analysis of LYZ-PEG Conjugates

To investigate the resulting molecular weights of the protein-polymer conjugates, two common methods were used. The sodium dodecyl sulfate polyacrylamide gel electrophoresis (SDS-PAGE) is widely used for the determination of molecular weights of proteins. Denaturized protein samples form negatively charged complexes with sodium dodecyl sulfate (SDS), which can move through a defined-sized porous polyacrylamide gel in an applied electric field. Lower molecular weight samples move faster through the polymer matrix than larger one. The second used method was the matrix-assisted laser desorption/ionization time of flight mass spectrometry (MALDI-ToF MS), which represents a mild and ideal method for the molecular weight determination of biopolymers.

Figure 18 shows the PEGylated proteins (lane 1–4) in comparison to the native lysozyme (lane 0 and 5, sharp protein band below 15 kDa). Looking at the resulting lysozyme-polymer materials, different molecular weights are presented. These findings indicate that the reactivity of each mPEG varies towards the protein surface.

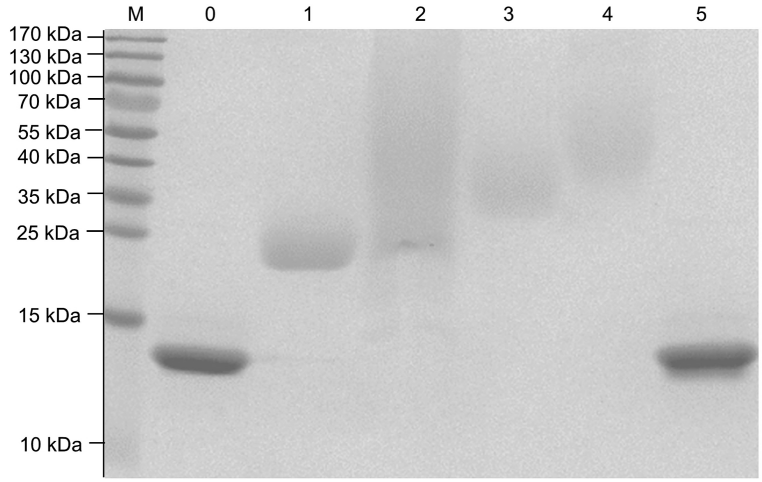

Figure 18: SDS-PAGE (15%) of native lysozyme (lanes 0 and 5) and PEGylated proteins (lanes 1-4). PEGylation was performed with TFP-mPEG (lane 1), epoxy-mPEG (lane 2), carbonate-mPEG (lane 3) and TsT-mPEG (lane 4). (The used marker (M) is a PageRuler pre-stained protein ladder. Each lane was loaded with 20 μL of the material. The gel was stained with Coomassie brilliant blue G) (from Radi *et al.*[29]).

The protein modification with TFP-mPEG leads to a defined protein band in the SDS-PAGE at around 20–25 kDa (Figure 18, lane 1). This result can be confirmed by MALDI-ToF MS (22.89 kDa, Figure 19A), indicates that four mPEG chains were attached to the protein surface.

In contrast, the LYZ(epoxy-mPEG) conjugate shows a broad distributed protein band in the SDS-PAGE (Figure 18, lane 2). The resulting biomaterial seems to have a higher molecular weight between 30 kDa up to the detection limit of 170 kDa. By MALDI-ToF MS the exact weight of 32.44 kDa (Figure 19B) was determined, leading to around 9 mPEG chains on the lysozyme surface. The smearing behavior of PEGylated proteins in the gel electrophoresis is known in the literature and is attributed to the formation of complexes between PEG and SDS. This results in a different migration behavior of PEGylated proteins compared to native ones and complicates a correct molecular weight information of the product.[166]

The use of carbonate-mPEG as PEGylating agent leads to narrowly defined products, similar to the TFP-mPEG modification, but with slightly higher molecular weights of around 26–30 kDa (Figure 18, lane 3).

The MALDI-ToF MS measurement (28.36 kDa, Figure 19C) confirms the result of the SDS-PAGE and indicates that around 7 mPEG chains were introduced per protein.

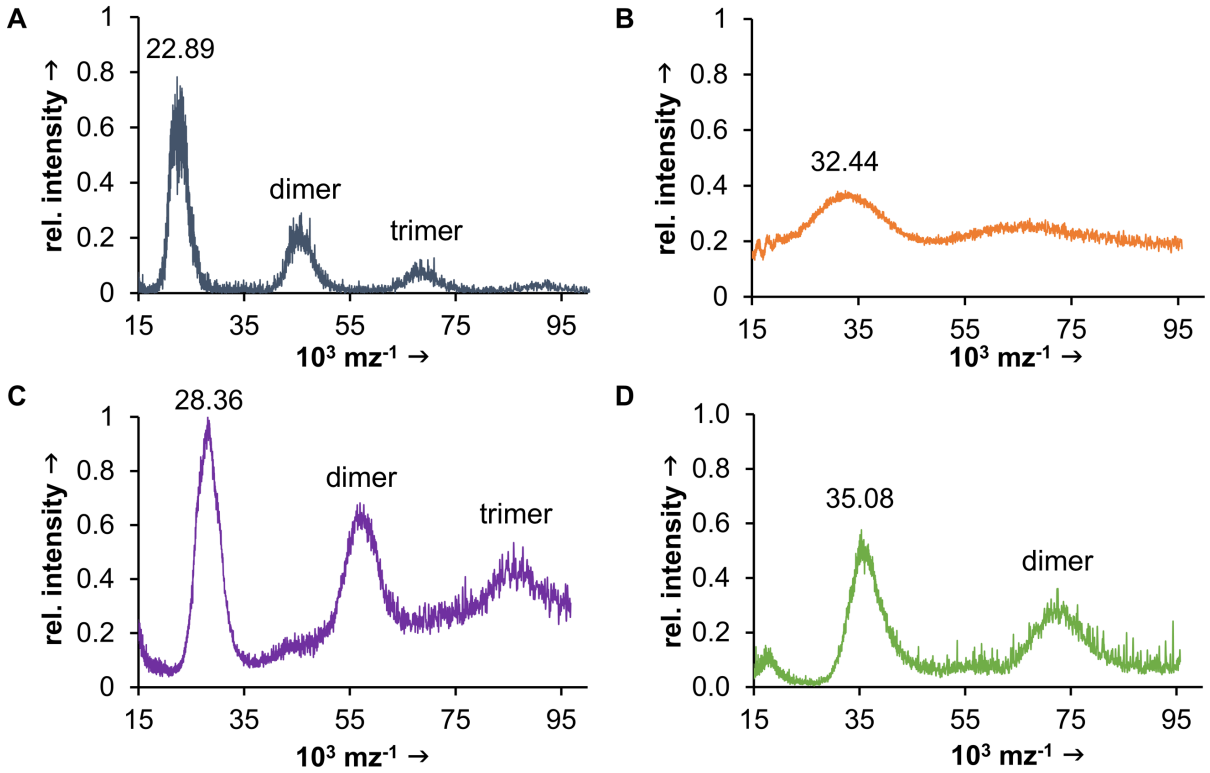

Figure 19: MALDI-ToF MS of modified lysozyme with TFP-mPEG (**A**), epoxy-mPEG (**B**), carbonate-mPEG (**C**) and TsT-mPEG (**D**). All diagrams indicate an increase in the molecular weight and confirm the absence of unmodified enzyme.

The reaction with TsT-mPEG yields products with a molecular weight of 40–70 kDa (Figure 18, lane 4) in the electrophoresis gel. MALDI-ToF MS examination of LYZ(TsT-mPEG) conjugates confirms a molecular weight of 35.08 kDa (Figure 19D). Since one TsT molecule carries two mPEG chains, 5–6 TsT molecules were attached to the protein surface, leading to around 10–12 polymer chains overall. This PEGylation method represents the highest surface modification of lysozyme compared to the other used electrophilic activated mPEGs.

All samples do not show any traces of native protein in the SDS-PAGE indicating a complete conversion to highly PEGylated conjugates. After PEGylation, all protein samples were soluble in organic solvents and could be used for the preparation of nanoparticles via an emulsion-based technique (see Chapter 3.1.3).

Determination of Primary Amines on the LYZ Surface

To determine the remaining primary amines on the lysozyme surface after PEGylation a fluorescamine assay was performed. The non-fluorescent substance fluorescamine, a spirane, reacts with primary amines to form a highly fluorescent product.

In comparison to the native protein, which bears seven free amines on their surface, the modification with TFP-mPEG leads to the detection of one free primary amine. This result disagrees with the determined amount of polymer chains via SDS and MALDI-ToF MS. One possible explanation could be, that the attached PEG chains shield off another available amines on the protein surface, which results in a falsified modification efficiency. The investigation of lysozyme which was modified with epoxy-mPEG yields one remaining amine. In this case, six primary *ε*-amino groups of lysine could be PEGylated together with three OH-groups of the available tyrosines, resulting in one free amine and overall 9 polymer chains. This result corresponds to the SDS and the MALDI-ToF MS investigations. For LYZ(carbonate-mPEG) no free amines were detected on the protein surface, which is in accordance with the other investigations of this sample. The determination of LYZ(TsT-mPEG) indicates that no free amines are available. Since 5–6 polymer chains were introduced two or one remaining primary amine should be detected by this assay. Again, this result demonstrates the shielding effect of PEG, which can lead to a falsified determination by this method. Nevertheless, this assay provides information about the reactivity of the used activated mPEG chains and can be used as an additional method of analysis.

Structural Integrity of PEGylated LYZ Analyzed by CD

The initial aim was to perform a mild surface modification without harming the native structure of lysozyme. Therefore, circular dichroism (CD) spectroscopy was performed to analyze the protein conformation after PEGylation. The CD spectroscopy is suitable for the rapid evaluation of structural elements of proteins.[167] This analysis refers to the differential absorption of right-handed and left-handed circularly polarized light.

When any types of optically active molecules interact with that light in a different way, the difference in absorbance between left and right circularly polarized light will be measured by CD spectropolarimeters. Looking at proteins, the chromophores of interest are the peptide bond (absorption between 190 nm to 240 nm), aromatic amino acid side chains (absorption in the range from 240 nm to 320 nm) and non-protein cofactors such as flavins (300–500 nm) or the heme group (Soret band, strongly absorption around 410 nm). A CD spectrum is characteristic for every protein and provides an insight into their structural nature.

In the first study, we compared the secondary structure of the PEGylated proteins with that of the native lysozyme (Figure 20) by investigation of the far-UV area. All measurements were carried out at 20 °C. The spectra of all four different modified samples are very similar to that of the native enzyme. This result indicates that the most secondary structure elements were preserved.

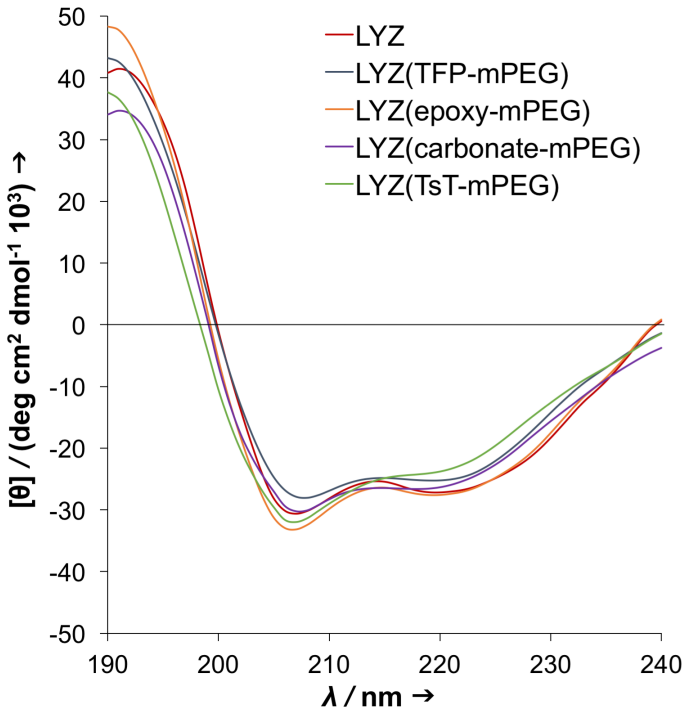

Figure 20: CD spectra of all PEGylated protein samples and native LYZ (red line). This investigation indicates no or minimal loss of secondary structure elements after the protein modification with different electrophilic activated mPEGs (from Radi *et al.*[29]).

In order to make a precise and detailed assertion about the number of *α*-helices, *β*-sheets, turns and unordered formations, a calculation of the secondary structure elements have been implemented by using DICHROWEB (Table 2). Native LYZ shows a relative high amount of *α*-helices and unordered structures (30–40%). The *β*-sheets and turns are present up to 15%. The PEGylation leads to no general tendency regarding the increase or decrease of the individual structural components. LYZ(TsT-mPEG) shows the highest structural discrepancy compared to the native enzyme and the other modification routes. This result can be explained by the high surface PEGylation (10–12 mPEG chains), which can lead to a higher structural alteration. Although the LYZ(epoxy-mPEG) and LYZ(carbonate-mPEG) samples bear 7–9 mPEG chains, the structural preservation is more intact. This indicates clearly, that the PEGylation with epoxy-mPEG and carbonate-mPEG are milder than with the TsT-mPEG. The use of TFP-mPEG results in similar structural deviations like utilizing epoxy-mPEG and carbonate-mPEG. This demonstrates a harsher conjugation route compared to the first-mentioned methods, because only four mPEG chains were introduced. In conclusion, the CD analysis shows only minimal variations within the used modification strategies, which indicates the suitability of these four linkers for mild protein surface PEGylations.

Table 2: Calculated amounts of secondary structure elements of LYZ and the modified samples (in %); Results calculated with DICROWEB using the CONTIN-LL method (reference Set 7) (from Radi *et al.*[29]).

	LYZ	**LYZ(TFP-mPEG)**	**LYZ(epoxy-mPEG)**	**LYZ(carbonate-mPEG)**	**LYZ(TsT-mPEG)**
α-helix	32.54	30.6	33.5	26.6	22.3
β-sheet	15.2	12.7	12.9	15.1	22.1
turns	13.4	13.1	13	13.6	15.4
unordered	38.86	43.6	40.6	44.7	40.2

Enzymatic Activity of PEGylated LYZ

Although the preservation of the secondary structure was confirmed of all PEGylated samples, surface alterations can lead to a decline in the enzymatic activity. Therefore, a fluorescence assay was performed with the synthetic lysozyme substrate 4-methylumbelliferyl-*β*-D-*N*,*N'*,*N"* triacetylchitotrioside in order to investigate the catalytic activity of the PEGylated lysozymes compared to the native one (Figure 21).

The catalytic activity of LYZ based on the cleavage of 1,4-β-glycosidic linkage of mureins, which represent important building blocks of bacterial cell walls. A large cleft on one side of the oval-shaped protein represents the active site of this enzyme. Thereby the two amino acid residues Glu35 (glutamic acid) and Asp52 (aspartic acid) play an essential role in the cleavage of the murein peptidoglycan. Looking at the PEGylation step, the ε-amino group of the Lys33 shows, together with Lys97, the highest accessibility for modification. But these lysines are very close to the enzymatic center.[159a] The Tyr51 residue is another modification target and is located close to the active site, too. PEGylations near to the catalytic center could have a greater impact on the resulting enzymatic activity.

Based on the cleavage of the synthetic substrate by native lysozyme and the four different LYZ-PEG conjugates, the amount of resulting fluorescent molecules (4-metylumbelliferone) was quantified spectrometrically (ex: 380 nm / em: 460 nm), whereby the fluorophore concentration is correlated with the enzyme activity. With the resulting slope of the fluorescence signal over time, an assertion about the enzymatic activity can be made.

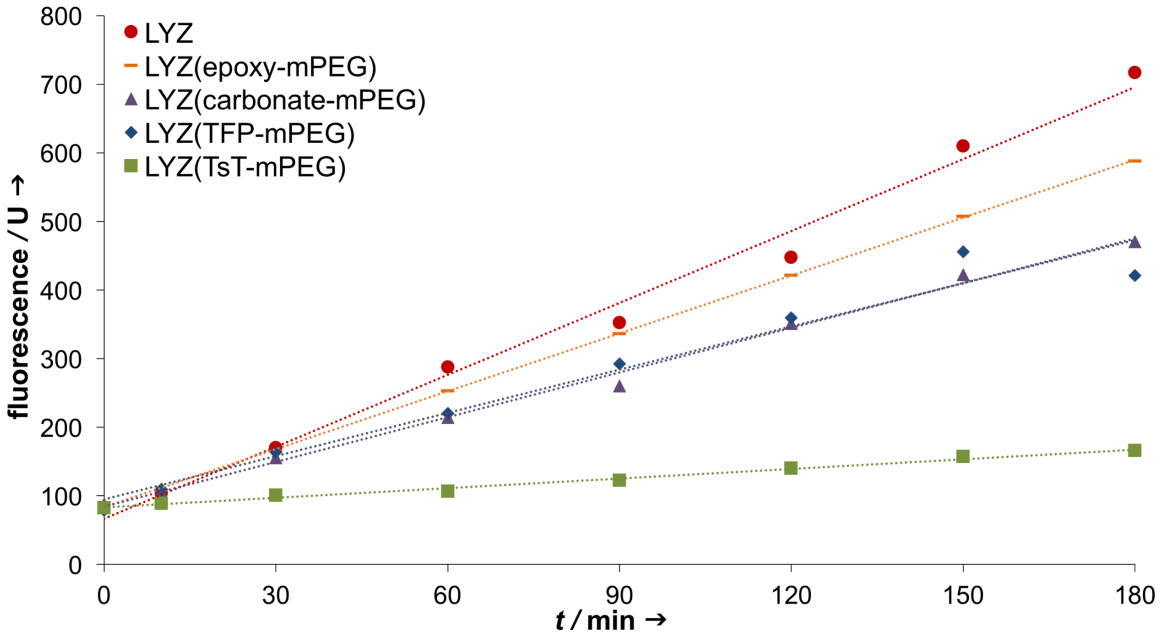

Figure 21: Activity assay of LYZ and PEGylated samples. The LYZ(epoxy-mPEG) conjugate shows the highest remaining activity (80%) compared to LYZ(TFP-mPEG) and LYZ(carbonate-mPEG) (around 60%). The LYZ(TsT-mPEG) conjugate shows the lowest remaining enzymatic activity (13%) (from Radi *et al.*[29]).

Epoxy-mPEG modified lysozyme shows the highest remaining enzymatic activity of 80%, followed by LYZ(carbonate-mPEG) and LYZ(TFP-mPEG) with a remaining activity of 60–62% compared to the native enzyme. Apparently, the protein active site is not significantly affected by the introduction of 9 mPEG chains using epoxy-mPEG. The use of carbonate-mPEG and TFP-mPEG leads to similar remaining catalytic activities, although a difference of three introduced polymer chains exists (LYZ(TFP-mPEG) = 4 mPEG chains; LYZ(carbonate-mPEG) = 7 mPEG chains). When we assume, that the polymer introduction occurs near to the active site when using TFP-mPEG, the impact on the catalytic activity is more distinct, than when using carbonate-mPEG and assuming a better distribution of seven mPEGs on the overall protein surface. In comparison, the modification with TsT-mPEG leads to a significant loss of activity (13%). The reduced activity can be attributed to the shielding effect of the introduced polymer chains, restricting the access of the substrate to the active site (see SDS and MALDI-ToF MS experiments, Chapter 3.1.2, page 38). Furthermore, it can be traced back to the structural shift seen in the CD spectrum (Chapter 3.1.2, Page 41). In general, the conformational flexibility of the protein after the surface modification is another important aspect, which closely correlates with the enzymatic activity.

With the different activated mPEG chains, it was possible to produce lipophilic biomaterials which differ in the PEGylation efficiency, structure and protein activity. Table 3 summarizes the results of these four materials. In conclusion, LYZ(epoxy-mPEG) shows the highest preservation of the enzyme activity after the introduction of 9 mPEG chains. It represents in comparison to the other materials the mildest and the most non-destructive PEGylation agent.

Table 3: Resulting protein properties after PEGylation (SDS-PAGE in kDa; MALDI-ToF MS in 10^3 mz^{-1}); fluorescamine assay for free surface amines; remaining protein activity in %; approx. amount of introduced 2 kDa mPEG chains) (from Radi *et al.*[29]).

sample	**molecular weight /kDa**		**remaining amines**	**protein activity /%**	**mPEG chains**
	SDS	MALDI			
LYZ(TFP-mPEG)	21–24	20–24	1.17	60	4
LYZ(epoxy-mPEG)	23–130	30–34	1.32	80	9
LYZ(carbonate-mPEG)	26–36	26–30	0.47	62	7
LYZ(TsT-mPEG)	36–55	33–40	0.04	13	10–12

3.1.3 Lysozyme-based Nanoparticles

Single Emulsion-Based Particle Preparation

An ultrasonic emulsification method was used for the preparation of protein-based nanoparticles which solely consist of protein-polymer conjugates. This technique is suitable for the encapsulation of hydrophobic materials and was established in our group for the entrapment of the anti-cancer drug doxorubicin.[11] In this study, it was the aim to examine, if the different used activated PEGs have an effect on the resulting nanoparticles. For this, the four different particle systems were investigated regarding particle size, shape and stability.

The surface PEGylation renders the protein fully soluble in organic solvents. This allows the use of an emulsion-based oil-in-water (o/w) method to formulate nanoparticles. The different PEGylated proteins were dissolved in dichloromethane (DCM) and the organic phase was covered with ice-cold PBS buffer (pH 7.4). This biphasic system was sonicated, resulting in an oil-in-water nanoemulsion. After the evaporation of the volatile organic solvent, a nanoparticle suspension was received (Figure 22). In the presented method, the use of additional crosslinking agents or stabilizers is waived for the resulting nanoparticle suspension.

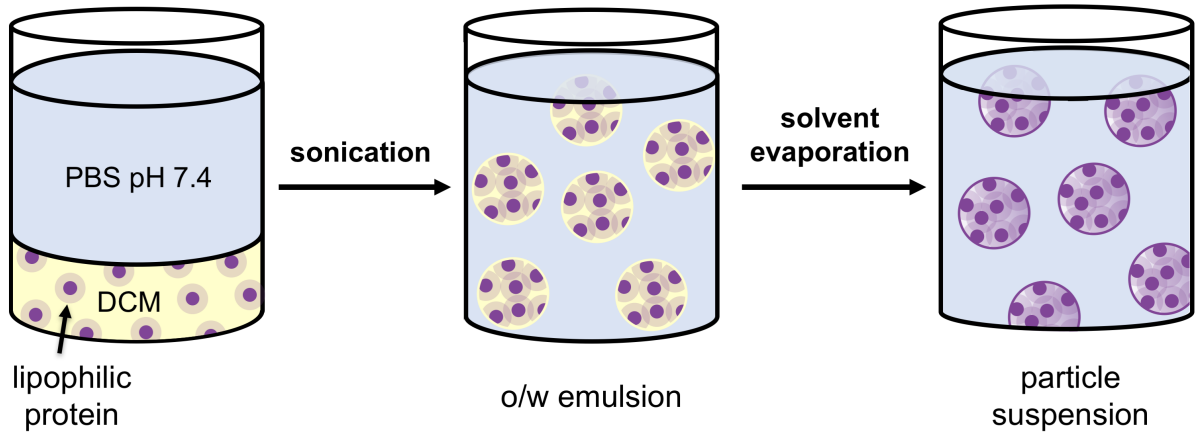

Figure 22: Single emulsion-based nanoparticle preparation method. The lipophilic proteins were dissolved in dichloromethane (DCM) and covered with an aqueous phase (PBS pH 7.4). The sonication of this biphasic system leads to an o/w emulsion. The following solvent evaporation results in a particle suspension. Redrawn from Fach *et al.*[11]

Nanoparticle Size Determination

For the size characterization of all prepared protein-based nanoparticles, the Nanoparticle Tracking Analysis (NTA) was used. This innovative method was first commercialized in 2006 and represents an excellent technique for sizing soft matter particles from about 30 to 1000 nm. This analysis combines the laser light scattering microscopy with a charge-coupled device camera (CCD), which visualize and record nanoparticles in solution. The Brownian motion of the individual nanoparticles is identified and is tracked by the NTA software, which relates the movement to a particle size according to the formula derived from the Stokes-Einstein equation.[168] The particle suspensions were diluted in PBS to a final concentration of 10 μg/mL and were injected into the sample chamber with syringes. All measurements were performed at room temperature in five individual runs over a time of 30 seconds.

NTA results of all synthesized samples indicate the formation of protein particles with a diameter of around 100–150 nm (Figure 23, Table 4). Utilizing the (LYZ)epoxy-mPEG and (LYZ)TFP-mPEG material for the nanoparticle preparation, systems with a diameter of around 108–112 nm are received. In contrast, the use of (LYZ)carbonate-mPEG and (LYZ)TsT-mPEG result in larger particles (130–150 nm). While the individual LYZ(epoxy-mPEG) samples bear 9 mPEG chains, the assembly of these protein-polymer conjugates yields tighter particles (see Figure 23B) in comparison to LYZ(TsT-mPEG) (see Figure 23D) and LYZ(carbonate-mPEG) (see Figure 23A), which were conjugated with two more or less polymer chains. Probably, two interactions have an impact on the particle size. On the one hand, the interaction between the protein surface and the directly covalent linked polymer chains, and on the other, the interaction between the individual modified proteins within the particle system.

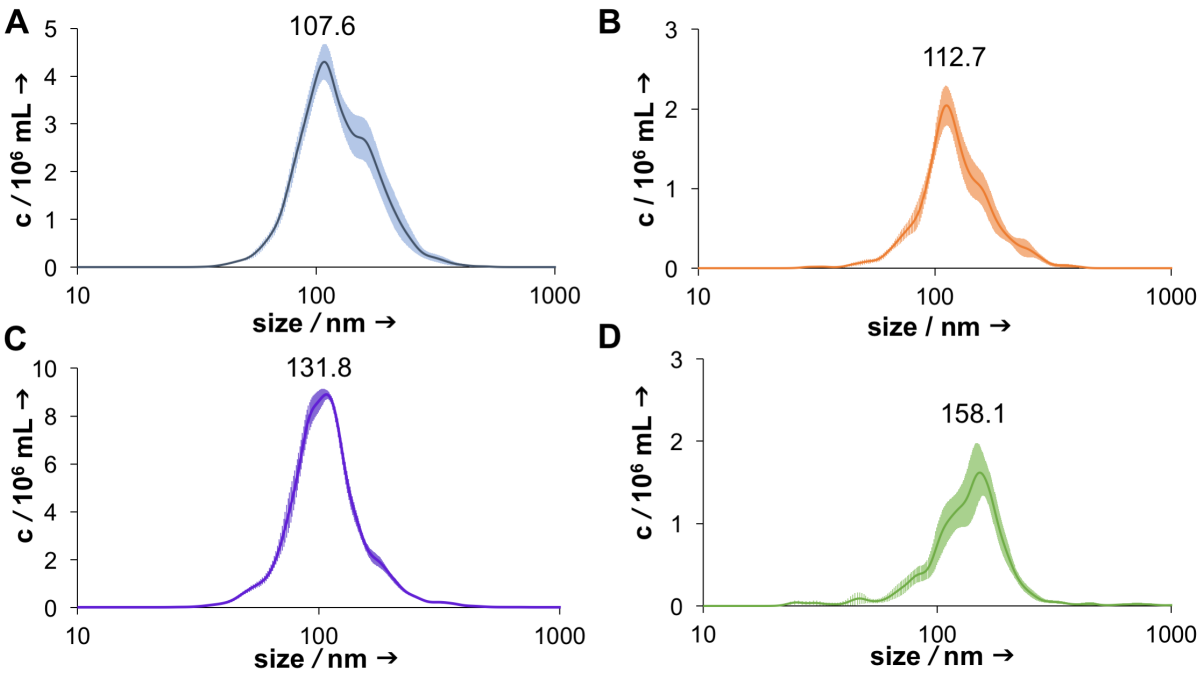

Figure 23: NTA diagrams of LYZ(TFP-mPEG) (**A**), LYZ(epoxy-mPEG) (**B**), LYZ(carbonate-mPEG) (**C**) and LYZ(TsT-mPEG) (**D**).

Table 4: Detailed size values obtained by NTA measurements of the LYZ nanoparticles. Particle size (diameter) was determined with five individual measurements per sample (from Radi *et al.*[29]).

particle	mean / nm	mode / nm	SD / nm
LYZ(TFP-mPEG)-NP	149.4 ± 5.8	107.6 ± 1.6	61.5 ± 4.4
LYZ(epoxy-mPEG)-NP	147.0 ± 6.0	112.7 ± 2.7	57.2 ± 5.6
LYZ(carbonate-mPEG)-NP	164.0 ± 5.9	131.8 ± 3.3	66.7 ± 6.3
LYZ(TsT-mPEG)-NP	199.6 ± 7.0	158.1 ± 15.9	76.0 ±7.12

Mean size and SD (standard deviation) correspond to the arithmetic calculated values based on the sizes of all particles detected in the NTA measurement. Mode values describe the average size of the main particle population.

Transmission Electron Microscopy

Transmission Electron Microscopy (TEM) was performed to visualize the protein nanoparticles. The dehydration of the protein solution was chosen as the TEM sample preparation method. For this, the nanoparticle suspension (1 mg mL^{-1}) was drop-casted (5 μL) on a mesh copper carbon grid. To remove the solvent, a wipe was positioned at one side of the grid and absorbed the aqueous solution.

Drying is the most frequently applied method to study soft materials but includes at the same time some disadvantages. The resulting images present the samples in a dried state, thus are not representative of the nanoparticle behavior in solution. For a correct TEM interpretation, the additional investigation of the particulate system in solution, for example by NTA (see Chapter 3.1.3, Page 47) is unavoidable. Furthermore, dissolved salts of the aqueous particle solution can be precipitate upon decreasing the solvent content, which can cause in drying patterns. Moreover, the particles themselves need to be stable. Looking at the interactions within the particulate system, they need to be able to compete with interactions that occur with the carbon surface layer.[169] Alternatives to the described method are staining and cryo-TEM. To enhance the contrast of an image, the negative staining method with uranyl acetate and phosphotungstic acid is suitable. The stain does not penetrate through the object but only cover their surface, which results in a foot-print like appearance. Nevertheless, there are some disadvantages. For example, the presence of uranyl acetate crystals can lead to a misinterpretation of the resulting images. To represent a soft matter system in its most native state, the cryo-TEM is by far the most informative technique. In this case, a drop of the particle solution is given on a grid, and the sample is cooling rapidly to achieve the vitrification of the water. Since this step is very fast, the sample is physically fixed in its current state. Disadvantages of this method are the use of additional preparation tools and the more complex sample preparation.

We performed TEM measurements with the NP sample that showed a good nanoparticle size distribution and provided the best results regarding modification, structural integrity and enzymatic activity, in our case the LYZ(epoxy-mPEG)-NPs. The images of this sample confirm a spherical particulate nanosystem with a diameter of around 100 nm. The examined grid showed a representative nanoparticle system with no other patterns (Figure 24).

A closer look reveals a density difference within the nanoparticles (Figure 24C). The proteins seem to appear darker, thus represent the high-density material, and the polymer chains appear brighter as a low-density substance. The images should be considered with caution because the interpretation of TEM data is often incorrect and is greatly dependent on the used sample preparation method.

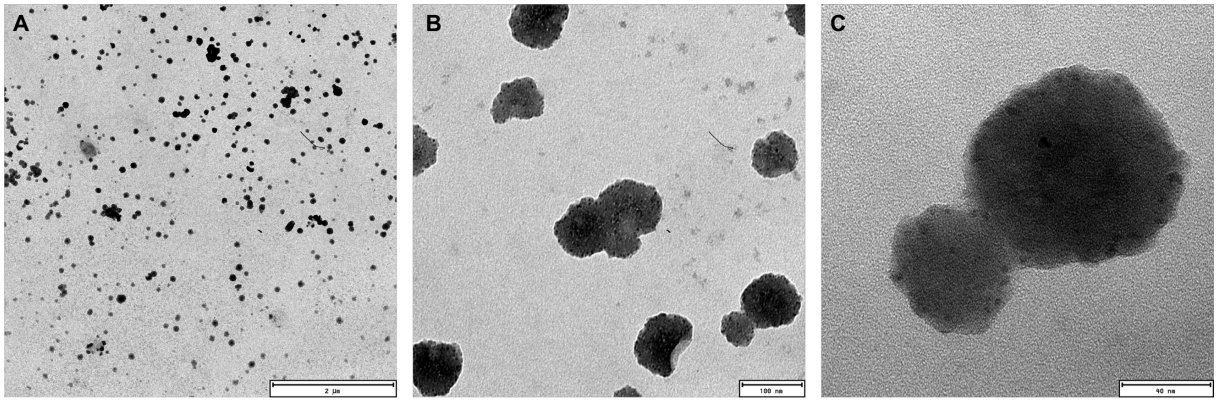

Figure 24: TEM images of LYZ(epoxy-mPEG) nanoparticles. The drying method was used as sample preparation method. The images show a spherical particulate system with a diameter of around 100 nm (**A**–**C**).

Unfortunately, only the described LYZ(epoxy-mPEG)-NPs lead to representative TEM images. All other NP samples showed no recognizable pattern, crystals or other structures (Figure 25). Typical artifacts, which are known in the literature, are found on the grids.[169]

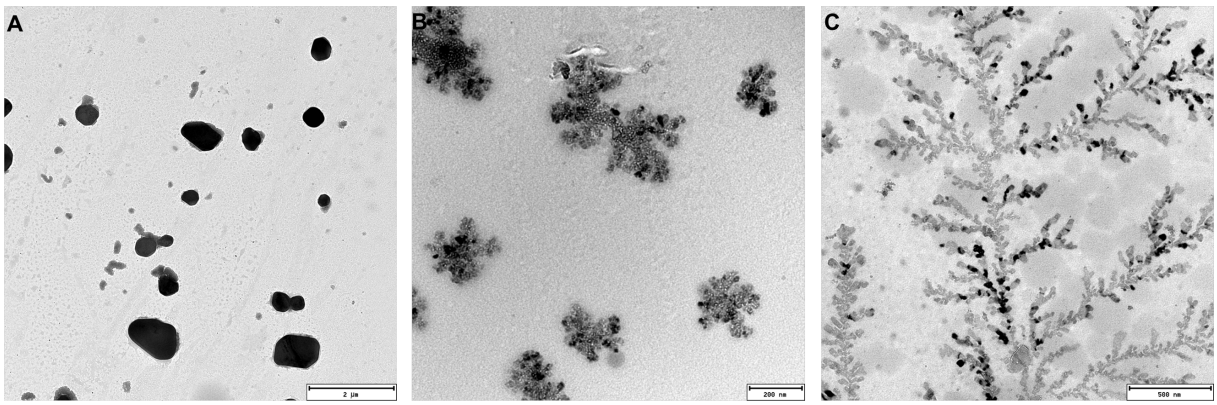

Figure 25: TEM images of LYZ-NP samples, which show no representative particle system. Seen are black spots, which can be attributed to dried PEG (**A**), and crystal structures which probably result from salts that are precipitate during the removal of the solvent (**B, C**).

Figure 25A shows round black spots with a diameter of around 500 nm up to 1 μm which can be attributed to dried polymers, in our case mPEG. The crystal structures seen in Figure 25B can result from the crystallization of dissolved materials. Buffer salts lead to typical patterns, that remind on crystal branches (Figure 25C). The discussed TEM images can be traced back to the sample preparation method but generate the problem that no representative visualization is available of the LYZ(TFP-mPEG), LYZ(carbonate-mPEG) and LYZ(TsT-mPEG) nanoparticles. In the future, the already mentioned cryo-TEM technique should be used for the imaging of the protein-based materials in order to avoid possible mistakes and over-interpretation.

Stability of LYZ Nanoparticles

The overall surface charge of a nanoparticle can be exploited to predict their stability. The ζ-potential is the potential difference between the solvent and the stationary layer attached to the dispersed particle, and can be used as an indicator of the suspension stability. Generally, high values, positive or negative, indicate a stable dispersion, based on the electric repulsion of the highly charged particles. In the case of low ζ-potential values, the suspension tends to coagulate or flocculate.[170]

Table 5: ζ-potential of native lysozyme, the PEG-modified proteins and the prepared nanoparticles (abbreviated with NP) (from Radi *et al.*[29]).

protein/particle	**ζ-potential/mV**
lysozyme	+5.46
LYZ(TFP-mPEG)	–3.21
LYZ(epoxy-mPEG)	–1.71
LYZ(carbonate-mPEG)	–3.27
LYZ(TsT-mPEG)	–9.09
LYZ(TFP-mPEG)-NP	–15.47
LYZ(epoxy-mPEG)-NP	–13.33
LYZ(carbonate-mPEG)-NP	–19.67
LYZ(TsT-mPEG)-NP	–11.80

Therefore, the ζ-potential of all four nanoparticle suspensions (1 mg mL^{-1}) was investigated in PBS. To compare the resulting values of the four nanoparticle systems, the individual used materials and the native enzyme were investigated in the same manner. The particulate systems show ζ-potentials in the range of –12 to –19 mV (see Table 5). This result is beneficial for a stable particle suspension since it prevents aggregation and unwanted nonspecific interactions, for example with blood proteins. Lysozyme has a positive ζ-potential, whereas the PEGylated samples have slightly negative values due to the functionalization of the positively charged amino acids on the protein surface.

In Vitro Effects of LYZ-based Materials

To investigate the biocompatibility of the prepared LYZ-PEG conjugates and the corresponding NPs, the cell viability of HeLa cells, a cervical carcinoma cell line, was investigated using the MTT method. The reduction of the water-soluble salt MTT (3-(4,5-dimethylthiazol-2-yl)-2,5-diphenyltetrazolium bromide) by cellular oxidoreductases leads to the formation of the insoluble purple molecule formazan. This compound can be quantified spectroscopically at 570 nm. Thereby, the reduced amount of MTT correlates with the number of living cells.

After 48 h, the synthesized LYZ-polymer conjugates cause no toxicity on HeLa cells in material concentrations up to 200 μg mL^{-1} (the given concentrations refer to the used nanoparticle amount in mg mL^{-1}) (Figure 26).

Looking know at the four corresponding nanoparticle systems, two of them show an unexpected result in the considering concentration ratio (Figure 27). Whereas the LYZ(TFP-mPEG)-NPs and the LYZ(epoxy-mPEG)-NPs are non-toxic on HeLa cells, the LYZ(carbonate-mPEG)-NPs and the LYZ(TsT-mPEG)-NPs show toxicity at high particle concentrations. After the treatment with LYZ(carbonate-mPEG)-NPs and LYZ(TsT-mPEG)-NPs, a remaining cell viability of 10% and 40% is given at a particle concentration of 0.2 mg mL^{-1}, respectively. This result was surprising for the LYZ(TsT-mPEG)-NPs since the non-toxic behavior of this system was shown in the literature.[11]

A possible explanation can be provided by the synthesis route of the activated carbonate-mPEG and TsT-mPEG. Toxic educts (*p*-nitrophenyl chloroformate, trichlorotriazine) and harmful solvents (benzene, THF) were used for this mPEG activation. An incomplete consumption of the applied molecules or an insufficient purification (precipitation, recrystallization), could result in residues of the initially used molecules, which are toxic to cells.

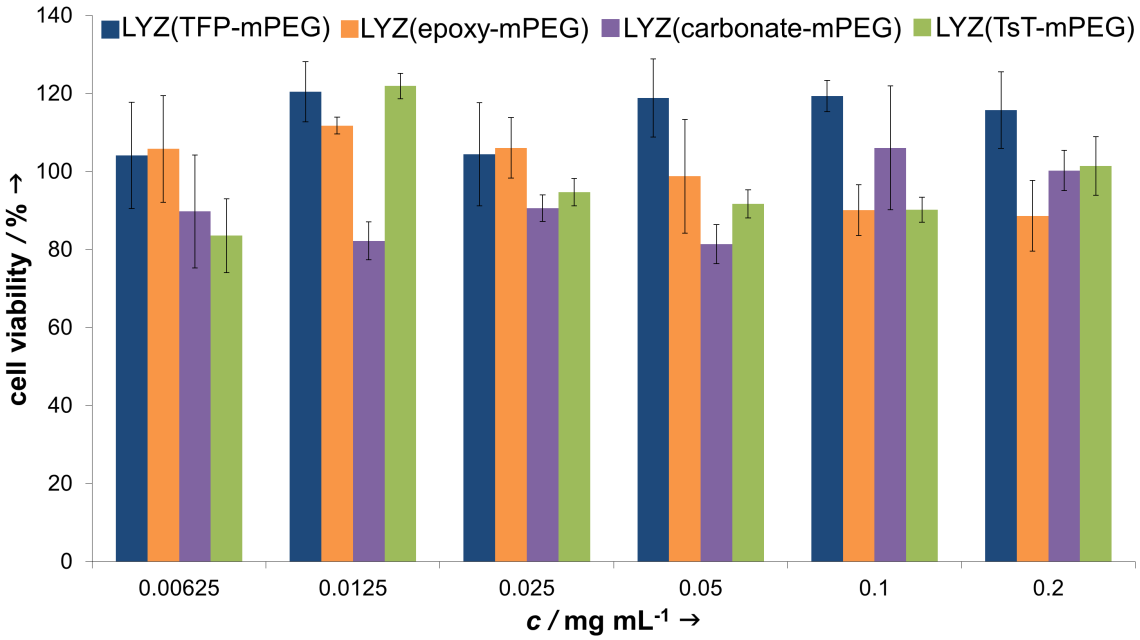

Figure 26: MTT assay for LYZ conjugates. All used LYZ-polymer conjugates are non-toxic on HeLa cells in a concentration up to 200 μg mL^{-1}. The given concentration refers to the used nanoparticle amount in mg mL^{-1}.

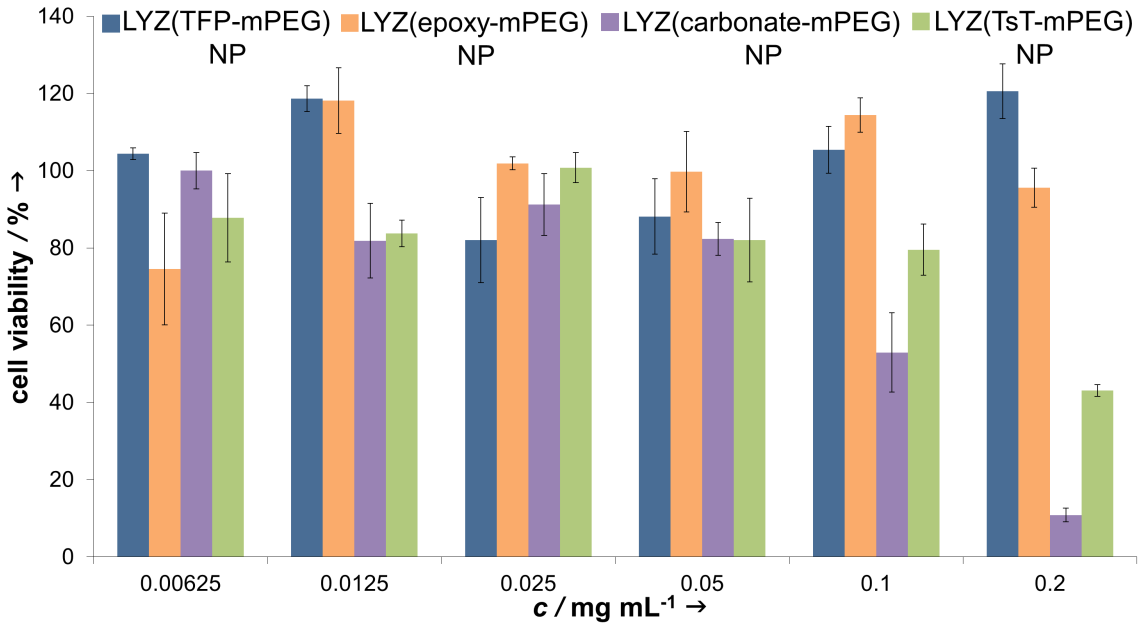

Figure 27: MTT assay for LYZ-NPs. The LYZ(TFP-mPEG)-NPs and LYZ(epoxy-mPEG)-NPs show no toxicity on HeLa cells in the considered concentration range. LYZ(carbonate-mPEG)-NPs and LYZ(TsT-mPEG)-NPs are toxic at a particle concentration of 0.2 mg mL^{-1}. Whereby LYZ(carbonate-mPEG)-NPs already show a cell viability of only 60% at a particle concentration of 0.1 mg mL^{-1}. The given concentration refers to the used nanoparticle amount in mg mL^{-1}.

In this first study, protein-based nanoparticles (100–130 nm) were successfully developed using the four different LYZ-PEG conjugates, respectively. All synthetized protein-polymer materials showed an intact structure and a remaining enzymatic activity. While all PEGylated lysozyme samples maintained their secondary structure elements, their resulting catalytic activity varied significantly among the different used PEGylation agents. The LYZ(epoxy-mPEG) material showed the highest remaining activity (80%), followed by LYZ(carbonate-mPEG) and LYZ(TFP-mPEG) (60-62%). The LYZ(TsT-mPEG) conjugates showed only an activity retention of 13%. Looking at the individual enzyme PEGylations, the efficiency and the extent of the surface modifications are significantly varied among the different synthesized compounds (4–12 mPEG chains). The use of epoxy-mPEG led to the introduction of 9 polymer chains. In comparison to the other protein conjugates, this material shows the best results regarding lipophilicity, structural integrity and catalytic activity. Furthermore, the processing of this conjugate in the emulsion-based technique results in the smallest nanoparticles (107.6 nm).

3.2 Design of Catalytically Active Enzyme Nanoparticles

Enzymes are macromolecular biological catalysts in living beings that accelerate vital biochemical reactions with high precision. The idea was to exploit the natural catalytic efficiency of these biomacromolecules in order to create enzymatically active nanoparticles. Based on the results of the first project, it was planned to use the synthesized PEGylation agents for the surface modification of three different peroxidases. Subsequently, nanoparticles should be synthesized by the emulsion technique. The aim was to modulate cellular processes and involve in intracellular mechanisms with these particle systems, for the reduction of harmful reactive oxygen species (ROS).

All shown data for the peroxidase cytochrome *c* (Cyt *c*) has already been submitted and is discussed here more in detail.

3.2.1 PEGylation of Peroxidases

To achieve a lipophilic protein material which is fully soluble in organic solvents, the surface of three different peroxidases were modified with polyethylene glycol. The selected enzymes differ in molecular weight, structure and catalytic efficiency.

The horseradish peroxidase (HRP), a heme-containing enzyme represents one of the most used peroxidases in science, research and medicine, especially for molecular and clinical diagnostics. With a molecular weight of 44.17 kDa, six lysine residues on their surface and a high intrinsic peroxidase activity, this enzyme was chosen as a building block for the formulation of enzymatic active nanoparticles. Furthermore, cytochrome *c* (Cyt *c*), a globular 12.4 kDa small enzyme was selected. This biomacromolecule has a high amount of basic amino acids (19 *ε*-amino groups of lysine) on the surface but compared to HRP, a lower peroxidase activity. As a third peroxidase, we chose the catalase (Cat), a very efficient catalyst with one of the highest turnover rates for hydrogen peroxide. This tetrameric enzyme has an overall molecular weight of 240 kDa and bears 25 lysines per monomer, thereof 14 are readily accessible.

Based on the results of the first study, two PEGylation agents were selected for the modification of these enzymes. First, epoxy-mPEG (2 kDa) as a highly reactive compound and in addition TFP-mPEG (2 kDa), which leads to size defined conjugates.

The PEGylation of HRP, using these activated mPEGs, led to an undesired outcome. A polymer excess of three equivalents per amino group, resulted in an uncomplete HRP PEGylation. Unmodified HRP was still remaining. The variations of other conditions such as reaction time (3 h, 24 h and 48 h) temperature (4 °C and room temperature) and the increase of the polymer amount (6 eq. per NH2 group), led to no improvement of this enzyme modification. Additionally, an incomplete solubility behavior was determined in organic solvents. To achieve a more lipophilic protein-polymer conjugate, epoxy-mPEG with a molecular weight of 5 kDa was synthesized and used for the protein modification. The conjugation led to a solubility switch, but the SDS-PAGE indicated remaining native HRP. Therefore, different purification methods, like centrifugation, dialysis and column chromatography were applied but leading not to the desired result. Based on these outcomes, another PEGylation agent was evaluated to achieve a lipophilic enzyme material. Functionalized polyethylene glycol with a *N*-hydroxysuccinimidyl active ester (NHS-mPEG) is used widely for protein PEGylation and represents a suitable alternative to the already mentioned PEGylation compounds.[89] In general, the high reactivity of the NHS functional group enables a random protein surface modification. Unfortunately, the hydrolysis of the NHS ester group goes along with relevant reaction conditions for the protein PEGylation. A successful protein PEGylation takes place at alkaline conditions due to the reactivity of amines of the lysine residues. However, under these conditions, the hydrolysis of the NHS ester is increased. Thus, a compromise between PEGylation efficiency and hydrolysis of the functionalized PEG have to be chosen. A mild alkaline buffer with a pH of 8.5 was used to achieve a sufficient surface modification with NHS activated PEG. Commercial obtained NHS-mPEG with a molecular weight of 5 kDa was used in an excess of five equivalents per amino group. The modification results in a protein material mix with one or two mPEG chains. However, native HRP was still present. To circumvent this, an increased excess of the 5 kDa polymer up to 20 equivalents per NH_2 group was used. SDS-PAGE analysis shows a defined protein band at 55 kDa, indicating that two polymer chains were introduced on the protein surface (Figure 28B, lane 4). MALDI-ToF MS measurement shows more precisely that partially one or two mPEG chains were introduced.

However, a small amount of unmodified protein was detected (Figure 29B). Nevertheless, the synthesized protein material was fully soluble in organic solvents and can be used for further applications.

Based on the good results of the HRP modification with NHS-activated polyethylene glycol, this compound was also used for the surface PEGylation of Cyt *c*. In this case, a low molecular weight PEG (2 kDa) was selected. Based on the high amount of lysine residues on the Cyt *c* surface, shorter polymer chains should be sufficient to achieve a lipophilic enzyme material. The surface modification using NHS-mPEG with five equivalents per amino group (calculated for 10 lysine residues) led to a protein material with a molecular weight of 36.35 kDa, which indicates that eleven polymer chains were attached on the surface. To investigate if a lower amount of PEG was sufficient to achieve a lipophilic Cyt *c*-PEG conjugate, a decreased equivalent amount of the polymer up to 1.5 equivalents per NH_2 group (calculated for 10 lysine residues again) was selected. After purification by column chromatography, a defined enzyme-polymer material was received with a molecular weight of 28 kDa. This material was fully soluble in organic solvents (Figure 28A, lane 2). Therefore, according to SDS gel electrophoresis and MADLI-ToF MS (Figure 29A), eight polymer chains were introduced onto the surface of Cyt *c*.

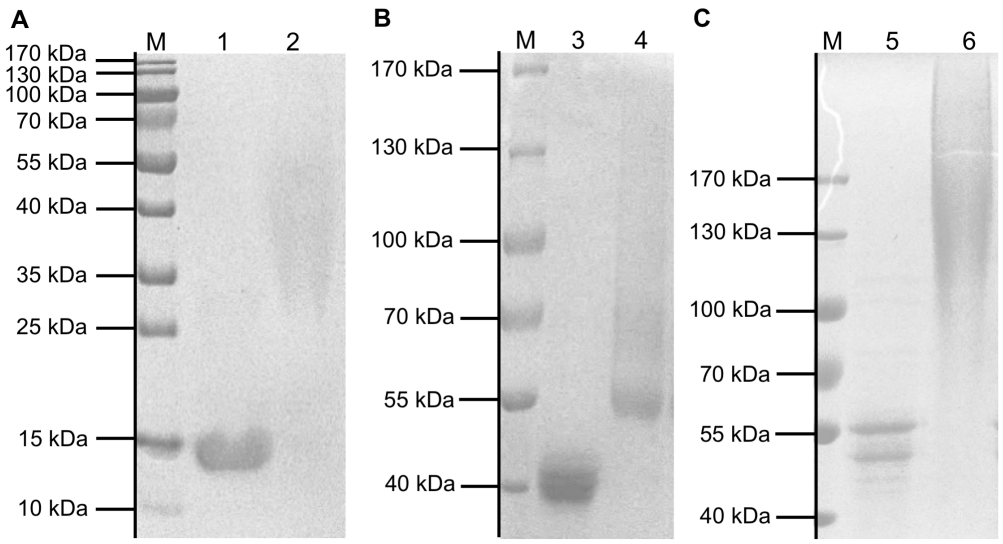

Figure 28: SDS-PAGES of successful PEGylated enzymes. Cyt *c* (lane 1) and the modified variant (lane 2) using NHS-$mPEG_{2k}$; 15% SDS-PAGE (**A**), native HRP (lane 3) and PEGylated HRP (lane 4) using NHS-$mPEG_{5k}$; 8% SDS-PAGE (**B**), catalase (lane 5) and surface-modified Cat (lane 6) using NHS-$mPEG_{5k}$; 8% SDS-PAGE (**C**).

The modification of Cyt *c* with the PEGylation agents epoxy-mPEG and TFP-mPEG (both 2 kDa) proceeded in a complicated manner. Although the PEGylation led to higher molecular weight protein materials, a mixture of different sized protein-polymer conjugates was obtained and the native enzyme was partially present.

Moreover, the PEGylation with epoxy-mPEG led to a heavy structural alteration of Cyt *c*, investigated by CD. Based on these results, the NHS-mPEG (2 kDa) was solely used for further Cyt *c* modifications.

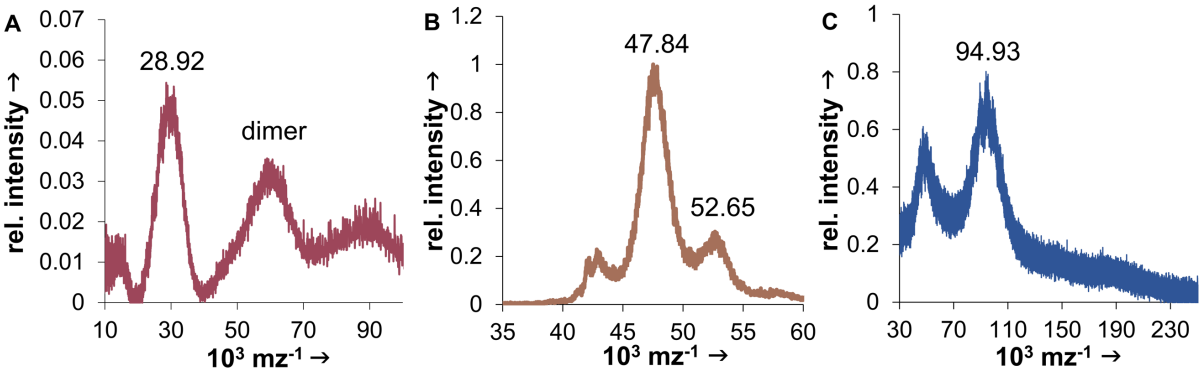

Figure 29: Size determination of PEGylated Cyt *c* (**A**), modified HRP (**B**) and PEGylated catalase (**C**) via MALDI-ToF MS.

For the surface modification of the large catalase, the longer NHS-mPEG chain (5 kDa) was applied. The use of a tenfold polymer excess per amino group, calculated for 56 amines, results in an enzyme material with a molecular weight range of 100 kDa up to the detection limit of 170 kDa (Figure 28C, lane 6). A typically broad distributed protein band was seen in the SDS gel, which impeded the exact size determination. The MALDI-ToF MS spectrum gives an exactly molecular weight for the PEGylated material per monomer of 94.93 kDa (Figure 29C). This result indicates that approximately eight polymer chains were attached to the surface per monomer, resulting in an overall molecular weight of 379.72 kDa for a possible tetramer. At this point, it is not able to confirm the presence of a tetramer. It is known in the literature, that a PEGylation could destabilize the structural arrangement of catalase.[87a, 171] In order to obtain further information about the protein structure, CD measurements were performed and discussed in the following section (see Page 60).

All prepared materials were soluble in organic solvents and were used for the formulation of enzyme-based nanoparticles.

Fluorescence Labeling of Peroxidases for *In Vitro* Applications

All three native enzymes were labeled with a fluorescent dye for further *in vitro* applications. A water-soluble sulfo-cyanin 5 NHS ester was chosen as a fluorophore (ex: 646 nm /em: 662 nm). This dye is suitable for the mild protein labelling in aqueous solutions and is compatible with the other used dye PY1 (see Chapter 3.2.3, Page 74). Primary amines on the protein surface react under slightly alkaline conditions with the NHS ester-activated dyes to yield stable amid bonds (Figure 30). The reaction took place at room temperature for one hour with a dye molecule equivalent of one per protein. The modified enzymes were purified subsequently via column chromatography. The number of fluorophores per protein was quantified by measuring the fluorescence of the modified proteins in comparison to free Cy5. To achieve differentiated excitation and emission signals, contrary to the information supplied by the manufacturer, the excitation had to be set to 605 nm and the emission to 675 nm.

The labeled enzymes differ in the number of attached fluorophores. Every 59th Cyt *c* enzyme was modified with one dye, whereas every 5th HRP enzyme and every 3rd Cat enzyme bears one fluorophore. The calculated amount for the Cyt *c* sample was very low compared to the other enzymes. It was assumed that Cyt *c* quenches the fluorescence of the used dye. This was confirmed by measuring the fluorescence of a Cy5 containing solution (solution 1) and a further one, containing the same amount of the fluorophore and additionally Cyt *c* (solution 2). Solution 2 showed a decreased fluorescence signal up to 13%.

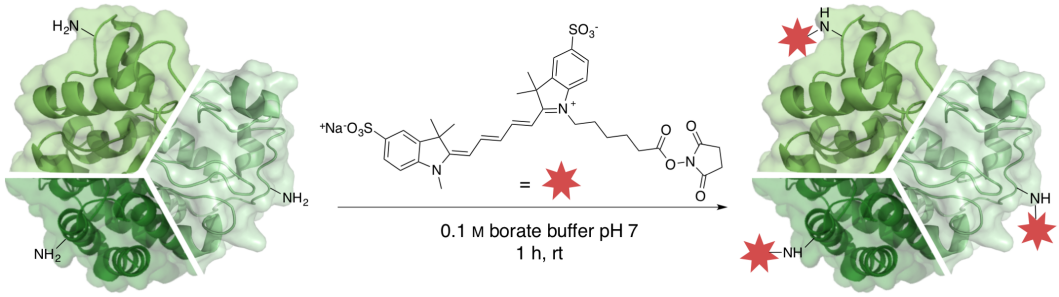

Figure 30: Fluorescence labeling of Cyt *c*, HRP and Cat with sulfo-cyanin 5 NHS ester. The reaction takes place at room temperature for one hour. The dye molecule was used with an equivalent of one per protein.

Subsequently, all three labeled enzymes were PEGylated in the already mentioned manner (see Chapter 3.2.1) and used for the preparation of enzyme-based nanoparticles. The fluorescent-labeled nanoparticle samples (Cy5_Cyt-NP, Cy5_HRP-NP, Cy5_Cat-NP) were investigated in flow cytometry experiments (see Chapter 3.2.3).

Structural Integrity of PEGylated Peroxidases Analyzed by CD

Circular dichroism (CD) investigations in the far-UV area show no or only slight alterations of the secondary structure elements of all three peroxidases (Figure 31, Table 6). The PEGylation of Cyt *c* results in the largest shift compared to the both other enzymes. In contrast to the native enzyme, the modification leads to a 24.5% reduction of *α*-helices and a definite increase of *β*-sheets. Comparing the calculated amounts of the secondary elements of Cat and their PEGylated variant, the modification results in a significant increase of *β*-sheets and a reduction of unordered elements. Looking at the number of introduced polymer chains, a dependence between the enzyme size and the structure alteration can be made. The attachment of eight polymer chains to the small Cyt *c* surface leads to a greater structure alteration compared to the same amount of PEGs introduced to the huge surface of catalase monomers. The PEGylated HRP sample shows no significant change in the secondary structure. It is assumed that this result can be traced back to the introduction of only one or two polymer chains. But overall, in all three cases, the surface modifications lead to no total loss of the secondary structure elements.

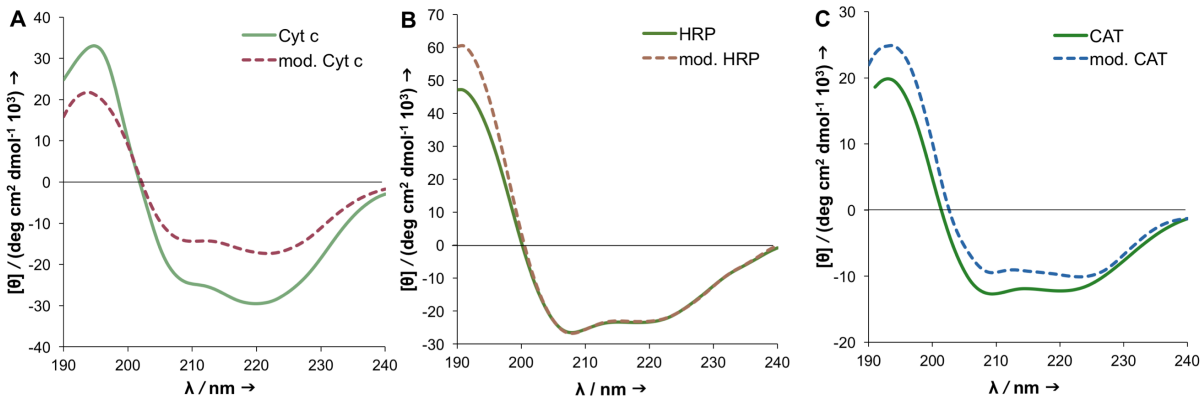

Figure 31: Far-UV CD spectra of Cyt *c* samples(**A**), HRP samples (**B**) and Cat samples (**C**).

Table 6: Calculated amounts of secondary structure elements for Cyt *c*, HRP, Cat and their PEGylated variant (in %); Results calculated with DICROWEB using the CONTIN-LL method (reference Set 7).

	Cyt *c*	**Cyt(mPEG)**	**HRP**	**HRP(mPEG)**	**Cat**	**Cat(mPEG)**
α-helix	65.8	41.3	61.5	65.5	36.6	31.6
β-sheet	0.1	7.7	3	3	13.4	33
turns	10.8	10.4	15.6	16	15.7	18.9
unordered	23.3	40.6	19.6	15.2	34.3	16.5

Near-UV CD spectra (260–320 nm) provide information about the overall tertiary structure of enzymes. The signals are due to the absorption, dipole orientation and the nature of the surrounding environment of aromatic amino acids. Tryptophan (Trp; peak close to 290 nm), tyrosine (Tyr; peak between 275 and 282 nm), and phenylalanine (Phe; weaker peak between 255 and 270 nm) tend to show characteristic signals in this area. The pronounced magnitude of the spectrum depends on the amount of each amino acid, their mobility and their environment within the protein. Unlike in the already mentioned far-UV CD, the near-UV CD spectra cannot be assigned to any three-dimensional structure. In our case, the investigation of this area can be used to compare the three-dimensional structure of the native enzyme with the PEGylated variant.[172] The CD spectra of all three investigated peroxidases show that the PEGylation results in no significant spatial change, indicating no disruption of the tertiary structure (Figure 32). Only Cyt *c* shows a characteristic spectrum of the individual aromatic amino acids Trp, Tyr and Phe. HRP and Cat show in this area only a signal around 280 nm, which can be assigned to tyrosine and the amide bond of all containing amino acids.

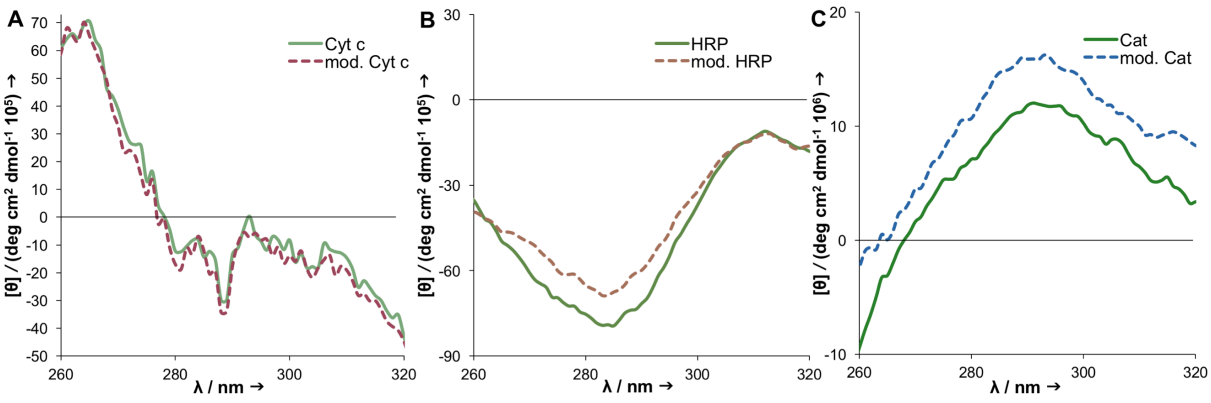

Figure 32: Near-UV CD spectra of Cyt *c* samples (**A**), HRP samples (**B**) and Cat samples (**C**).

All three enzymes have a heme group as catalytic center. The structural environment of this prosthetic group can be investigated at the Soret region (350–450 nm). Alterations in this area are an indicator for the integrity of the heme binding site (Figure 33). The PEGylated variants of Cyt *c* and HRP show no change in this area of the protein. Upon modification, the Soret band at 410 nm is visible in these spectra, indicating the remaining ferriporphyrin environment.[173] Looking at the CD spectrum of Cyt *c*, the very pronounced negative signal at 420 nm represents the heme-polypeptide interaction. The modification of Cat results in a signal shift at 400 nm, indicating an alteration of the structural arrangement around the heme group. The containing heme *b* coordinates with the surrounding amino acids, especially His54 and Asn127 assist in the reaction with hydrogen peroxide. A close PEGylation to this active site results in an increased hydrophobicity which can lead to a changed heme environment. Since a high alteration of the structural arrangement could be excluded around the active site of the peroxidases, the enzymatic activity of the synthesized materials was investigated in the following (see Chapter 3.2.3).

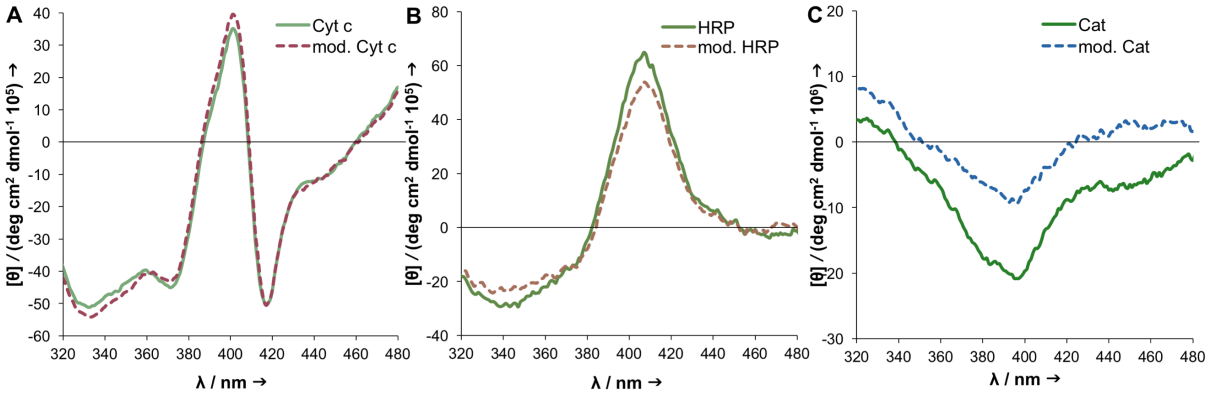

Figure 33: CD spectra of the Soret region of the Cyt *c* samples (**A**), HRP samples (**B**) and Cat samples (**C**).

3.2.2 Peroxidase-based Nanoparticles

The surface PEGylation of the three peroxidases leads to a solubility in organic solvents. This property permits the use of the already mentioned emulsion-based technique for the preparation of peroxidase-based nanoparticles.

For this, 2.5 mg of PEGylated peroxidase material was dissolved in dichloromethane, covered with an aqueous phase followed by sonication. After the evaporation of the organic solvent, a stable nanoparticle suspension was received.

Size determinations of the particles using NTA, result in materials with an average diameter of 115 nm for modified Cyt *c* (Cyt-NP, Figure 34A). The higher molecular weight PEGylated enzyme materials lead to larger nanoparticles with an average diameter of 125 nm for HRP (HRP-NP, Figure 34B) and 145 nm for Cat (Cat-NP, Figure 34C). In general, a slight dependence between enzyme size and the resulting nanoparticle size is present (Table 7).

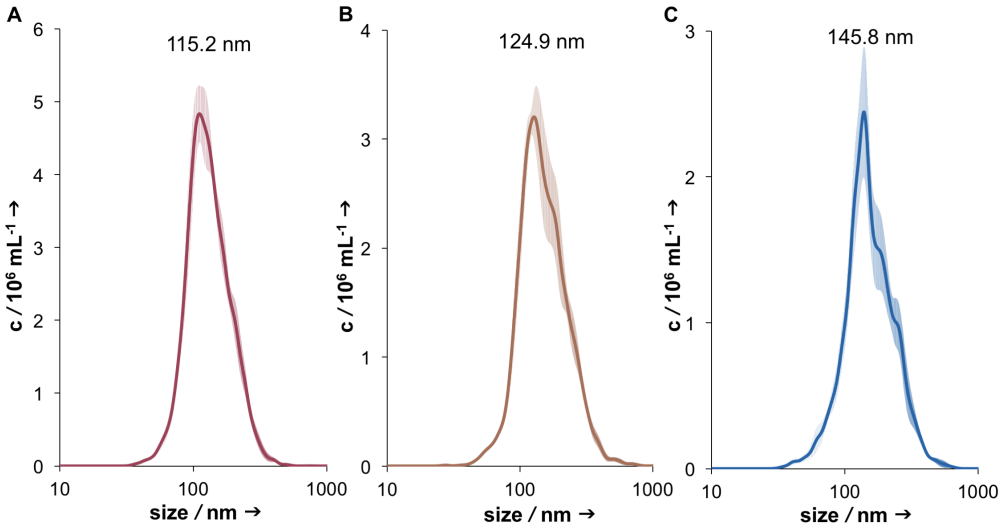

Figure 34: NTA data of Cyt *c* nanoparticles (**A**), HRP particles (**B**) and the Cat nanoparticles (**C**).

Table 7: Detailed size values obtained by NTA measurements of the peroxidase nanoparticles. Particle size (diameter) was determined with five individual measurements per sample.

particle	mean / nm	mode / nm	SD / nm
Cyt-NP	162.7 ± 4.9	115.2 ± 5.2	67.5 ± 3.5
HRP-NP	198.6 ± 5.5	124.9 ± 5.8	103.8 ± 10.1
Cat-NP	199.3 ± 10.2	145.8 ± 7.4	88.5 ± 5.5

Mean size and SD (standard deviation) correspond to the arithmetic calculated values based on the sizes of all particles detected in the NTA measurement. Mode values describe the average size of the main particle population.

TEM images of all three peroxidase samples confirm the formation of nanoparticles and show a similar size distributions as determined by NTA (Figure 35).

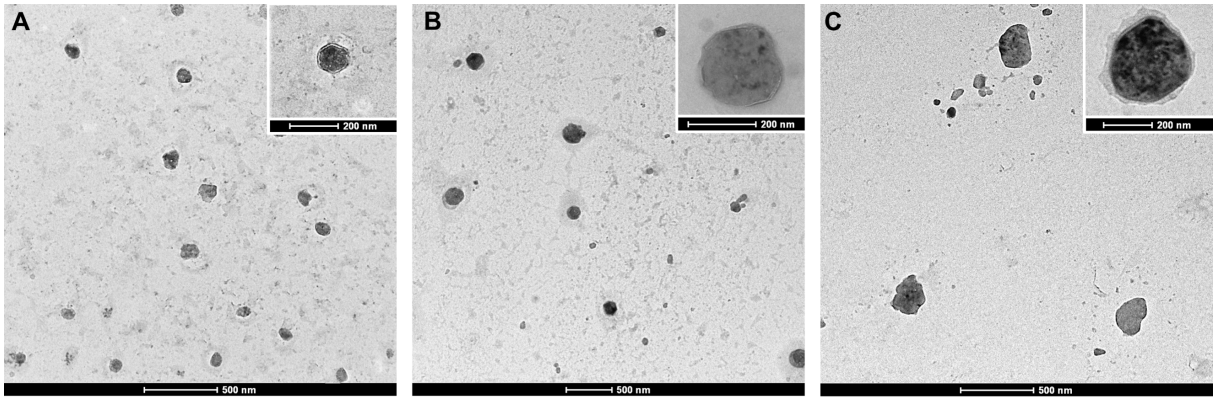

Figure 35: TEM images of Cyt-NP (**A**), HRP-NP (**B**) and Cat-NP (**C**).

To find out more about the three-dimensional arrangement of the prepared nanoparticles, atomic force microscopy (AFM) investigations were performed. Exemplary, only the Cyt-NPs were used for this measurement (Figure 36). This microscopy method is an ideal characterization tool for nanoscale structures and the determination of their shape and size distribution. One major advantage of this technique is the visualization of the particles in three dimensions.[174] The images confirm the presence of globular nanoparticles in a size range of 120 to 150 nm and support the already obtained results via NTA and TEM.

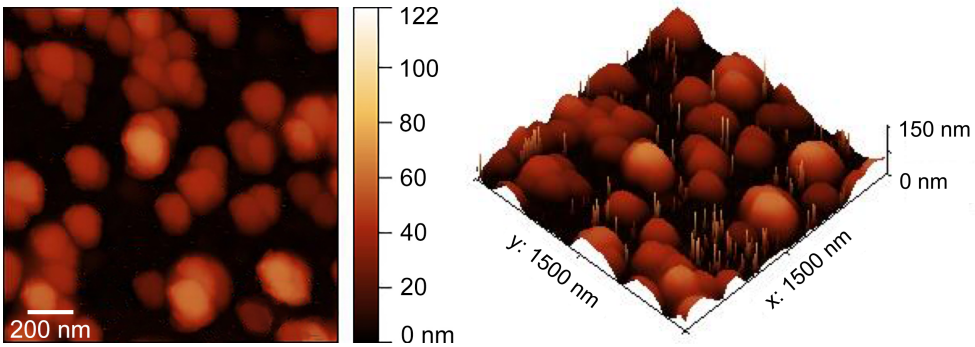

Figure 36: AFM images of Cyt-NPs. The images confirm the presence of spherical nanoparticles in a size range of 120 to 150 nm.

Cell Toxicity of Peroxidase-based Nanoparticles

The toxicity of all PEGylated peroxidases and their corresponding nanoparticles was investigated using the MTT method. After 48 h, native Cyt *c* and the PEGylated variant cause no toxicity in HeLa cells in high material concentrations up to 500 μg mL^{-1} (corresponding to a native Cyt *c* concentration of 13.16 nM) (Figure 37). The non-toxicity of native Cyt *c* was expected, because the enzyme itself can't pass the cytoplasmic membrane.[135, 175] Cyt-NPs show a slight inhibition of cell growth at high concentrations with viability values around 88%. Although Cyt *c* is an apoptotic cell death mediator and some toxicity could be expected, the surface modification of the individual enzymes most likely inhibits the binding to Apaf-1 and thus minimizes the formation of a cytotoxic apoptosome.[111]

All HRP samples show also no toxicity in HeLa cells after an incubation time of 48 h and a particle concentration up to 500 μg mL^{-1} (corresponding to a native HRP concentration of 18.18 nM) (Figure 38). As the non-toxicity of the native enzyme was expected, the PEGylation and NP preparation result in the maintaining effect on HeLa cells.

The MTT assay of the catalase samples shows different results (Figure 39). At an enzyme concentration of 0.37 nM (corresponding to a particle concentration of 500 μg mL^{-1}) a toxicity of around 30 to 36% is produced by the native enzyme and the PEGylated variant. The nanoparticles are non-toxic at this concentration. The toxicity decrease, in dependence on the reduced enzyme concentration, up to a not significant impairment of the cell viability. But the tendency, that the native enzyme is more toxic than the PEGylated samples, is given for all investigated concentrations.

In conclusion, all prepared peroxidase-based nanoparticles show no significant toxicity on HeLa cells and represent promising biomaterials for further cell treatments.

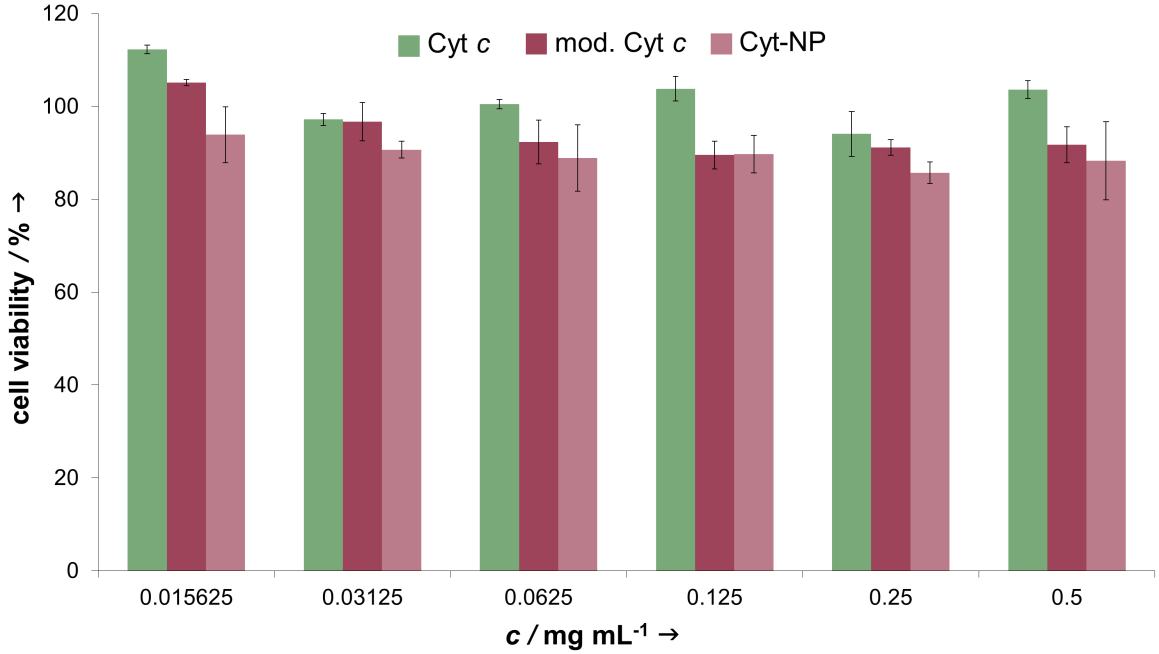

Figure 37: MTT result of Cyt *c* samples. The given concentrations refer to the number of nanoparticles in mg mL^{-1}. The highest material concentration of 0.5 mg mL^{-1} corresponds to a native Cyt *c* concentration of 13.16 nM.

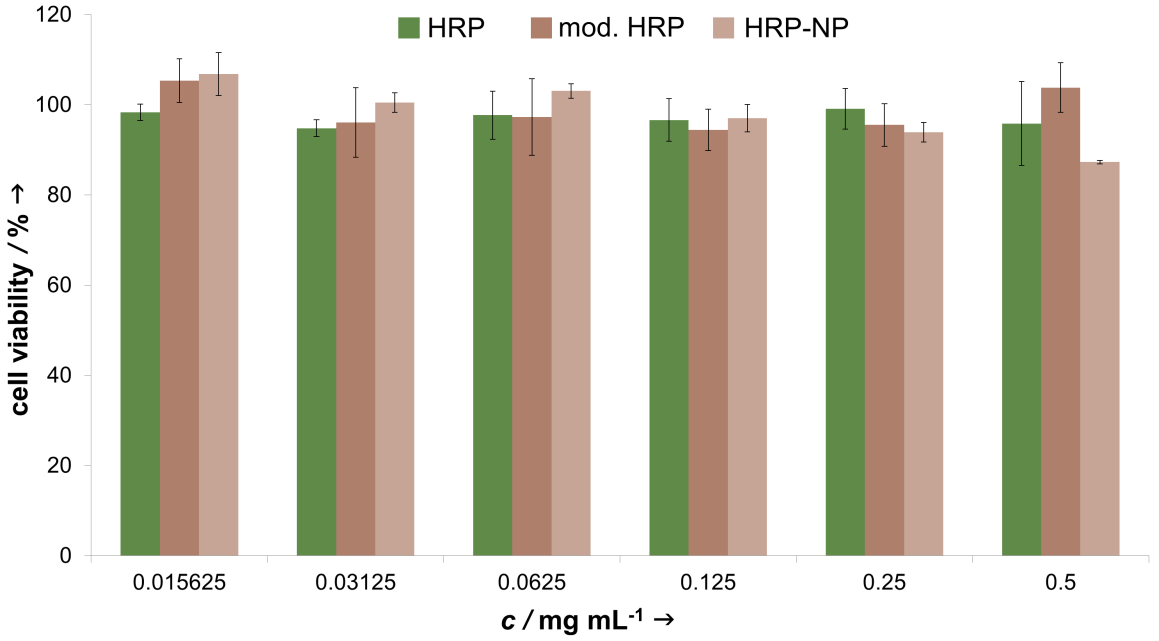

Figure 38: MTT results of HRP samples. The given concentrations refer to the number of nanoparticles in mg mL^{-1}. The highest material concentration of 0.5 mg mL^{-1} corresponds to a native HRP concentration of 18.18 nM.

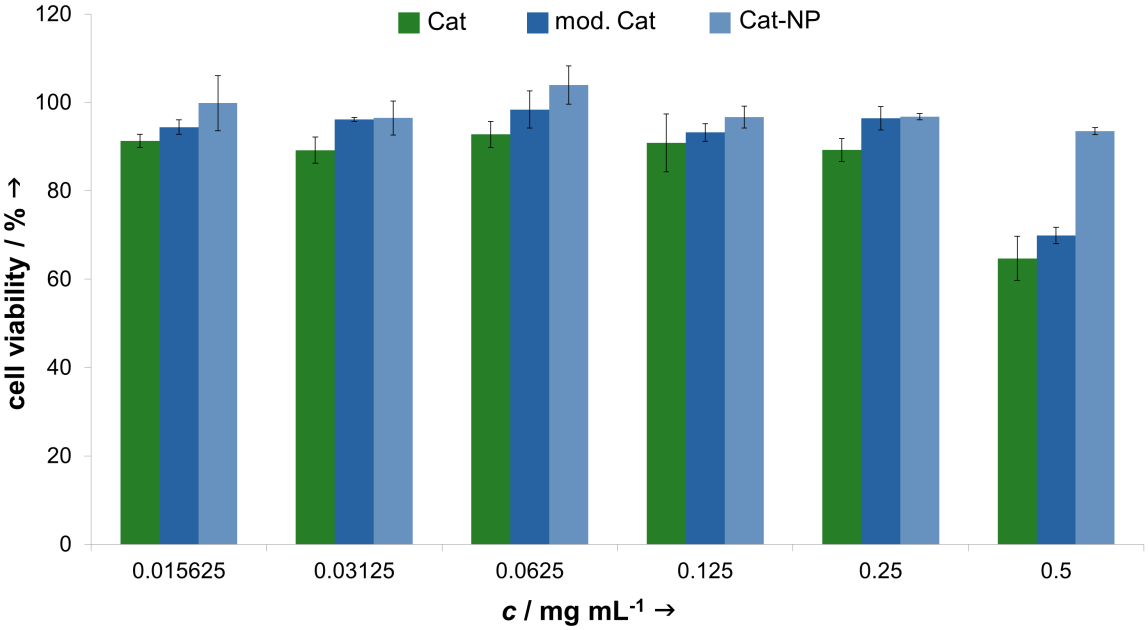

Figure 39: MTT results of Cat samples. The given concentrations refer to the number of nanoparticles in mg mL^{-1}. The highest material concentration of 0.5 mg mL^{-1} corresponds to a native Cat concentration of 0.37 nM.

3.2.3 Catalytic Activity of Peroxidase-based Nanoparticles

In this chapter, the investigation of the enzymatic activity of all prepared materials is presented. After the successful formulation of peroxidase-based nanoparticles, the influence of PEGylation, as well as the NP preparation on the catalytic efficiency of Cyt *c*, HRP and Cat were evaluated.

Determination of the Kinetic Parameters of all Peroxidase Materials

For all Cyt *c* and HRP samples, Michaelis-Menten kinetics were obtained using an ABTS assay with hydrogen peroxide as substrate. To determine the influence of PEGylation and nanoparticle formulation on catalase, an enzyme-specific assay was used, where the consumption of H_2O_2 was investigated spectroscopically at 240 nm.

The intrinsic peroxidase activity of Cyt *c* can be preserved upon PEGylation and NP preparation (Table 8). The analysis of the catalytic parameters confirms a preservation of the catalytic efficiency of PEGylated Cyt *c*. The surface modification results in a K_M value of 0.515 mM (compared to 0.585 mM for native Cyt *c*) which indicates that the PEGylated material has a minimal higher affinity for H_2O_2. The turnover rate (k_{cat}) of the modified Cyt *c* is slightly higher, which points to a marginally faster product conversion. These results are not unexpected since it has been previously described that an altered *a*-helices content can result in an increased peroxidase activity.[115a] A partial protein unfolding or structural change around the heme crevice can lead to an enhanced substrate access, resulting in an improved peroxidase activity.[176] The nanoparticle preparation has also no negative effect on the overall enzymatic activity. Investigations of individual modified enzymes in solution compared to an equivalent amount of assembled ones, show only small differences in catalytic efficiency (K_M = 0.489 mM). This can be most likely contributed to the small substrate, which can easily penetrate within the NPs and achieve the approximately catalytic centers of the individual enzymes.

Table 8: Michaelis-Menten kinetics of native cytochrome *c*, the PEGylated enzyme and the Cyt-NP. Data represent averages, with error bars from three independent experiments performed in triplicate.

sample	Michaelis constant K_M (mM)	turnover rate k_{cat} (s^{-1})	catalytic efficiency k_{cat}/K_M (s^{-1} mM^{-1})
Cyt *c*	0.585 ± 0.076	0.57	0.98
PEGylated Cyt *c*	0.515 ± 0.104	0.71	1.38
Cyt-NP	0.489 ± 0.099	0.79	1.62

The calculated catalytic parameters for the synthesized Cyt *c* samples are comparable with the literature known values. Wang *et al.* investigated the peroxidase activity of native Cyt *c* and after dimerization of this enzyme using the ABTS assay. Turnover rates of 1.77 s^{-1} were determined for the native enzyme, whereby the dimerization leads to an improved peroxidase activity (k_{cat} = 11.3 s^{-1}).[177] Micelles containing native Cyt *c* show turnover rates of 0.311 s^{-1} and 0.25 s^{-1}.[115b, 115c] Duhalt *et al.* showed that a PEGylation of Cyt *c* results in an enhanced peroxidase activity. Measured in 90% tetrahydrofuran they determined a turnover rate of native horse heart Cyt *c* of 0.87 s^{-1}. A surface modification with polyethylene glycol resulted in a turnover rate of 3.5 s^{-1}.[178]

As expected, HRP shows higher peroxidase activity compared to Cyt *c* (Table 9). The PEGylation and the nanoparticle formulation have no negative impact on the catalysis of H_2O_2. Like already seen for the Cyt *c* samples, the surface modification and NP formulation lead to a slightly improved catalytic activity (K_M = 0.032 mM for the PEGylated HRP and K_M = 0.031 mM for the HRP-NPs) compared to native HRP (K_M = 0.034 mM). The increased peroxidase activity can also be explained by the marginally altered *a*-helices amount after PEGylation (an increase of 4%, see Table 6).[179] Considering the error bars of the calculated amounts, the results should be interpreted carefully. Though, it can be summarized that after the chemical modification and the technological treatment the materials retain a certain catalytic activity.

Table 9: Michaelis-Menten kinetics of native HRP, the PEGylated variant and the HRP-NP. Data represent averages, with error bars from three independent experiments performed in triplicate.

sample	Michaelis constant K_M (mM)	turnover rate k_{cat} (s^{-1})	catalytic efficiency k_{cat}/K_M (s^{-1} mM^{-1})
HRP	0.034 ± 0.0034	704.03	20706.79
PEGylated HRP	0.032 ± 0.0104	911.10	28561.09
HRP-NP	0.031 ± 0.0106	717.83	23306.35

Catalase represents one of the most efficient peroxidases and has one of the highest turnover rates of all enzymes. The obtained values for native Cat are not unexpected and can be classified in the literature (Table 10).[180] The PEGylation step shows significant effects on the catalytic activity (K_M value of 50.21 mM compared to 27.42 mM for native Cat). Abuchowski *et al.* had already shown 1977 that the PEGylation of catalase slightly destabilize the structure and leads to a slight decrease in enzymatic activity.[87a] Additionally, this result can be explained by the fact that the heme group is buried in the core of one monomer and approachable via three channels.[181] PEGylations at these sites complicate the access for H_2O_2 which results in decreased turnover rates. The determination of the enzymatic activity of the prepared Cat-NPs was not possible with the selected assay. The decrease of the H_2O_2 concentration at 240 nm could not be tracked spectroscopically when using the Cat-NPs as enzymatic material. Although it is assumed that the small substrate H_2O_2 has access to the catalytic center of the enzyme, the selected assay conditions, especially the short assay duration of 3 minutes, achieve no useful result. Also, a longer contemplation period of 15 min did not lead to the desired results.

In order to exclude that this result can be traced back to the used samples, fresh prepared NPs and hydrogen peroxide solutions were always used. To determine the enzymatic activity of the Cat-NPs a fluorescent-based assay was performed in the following (see next chapter).

Table 10: Michaelis-Menten kinetics of native Cat, the PEGylated enzyme and the Cat-NP. Data represent averages, with error bars from three independent experiments performed in triplicate.

sample	Michaelis constant K_M (mM)	turnover rate k_{cat} (s^{-1})	catalytic efficiency k_{cat}/K_M (s^{-1} mM^{-1})
Cat	27.42	44884.48	1636.92
PEGylated Cat	50.21	50165.02	999.10
Cat-NP	-	-	-

Investigation of the Extracellular H_2O_2 with Peroxidase Material

In first *in vitro* experiments, the extracellular enzymatic activity of the prepared materials was investigated. Cell medium of stressed HeLa cells were used in combination with the different peroxidase samples to determine the hydrogen peroxide content and therefore receive information about the catalytic activity of the prepared peroxidase materials. This investigation can be performed using the Amplex Red assay, a fluorescence method which is based on the oxidation of Amplex Red with H_2O_2 to the highly fluorescent dye resorufin, catalyzed by a peroxidase. To obtain a sufficiently high enough ROS concentration, HeLa cells were stressed with TNF-*a*, a cytokine which promotes the release of these species.[122] Small molecules like hydrogen peroxide can easily diffuse through the cell membrane and can be investigated in the cell medium. For this, native enzymes, PEGylated materials as well as the nanoparticles were incubated with the cell medium for 3 h under shaking. After the addition of the dye solution, the number of fluorescent resorufin molecules was quantified spectrometrically (ex: 563 nm / em: 587 nm). The fluorophore concentration is correlated with the hydrogen peroxide concentration. All calculated amounts for the peroxidase samples were referred to untreated cells.

All Cyt *c* samples successfully reduce the H_2O_2 concentration in the medium (Cyt *c* 48%, PEGylated enzyme 59%, Cyt-NP 57%). The surface-modified enzymes and the NPs show even an increased peroxidase activity compared to native Cyt *c* (Figure 40). This result confirms again the retaining catalytic activity after the surface modification and the nanoparticle preparation.

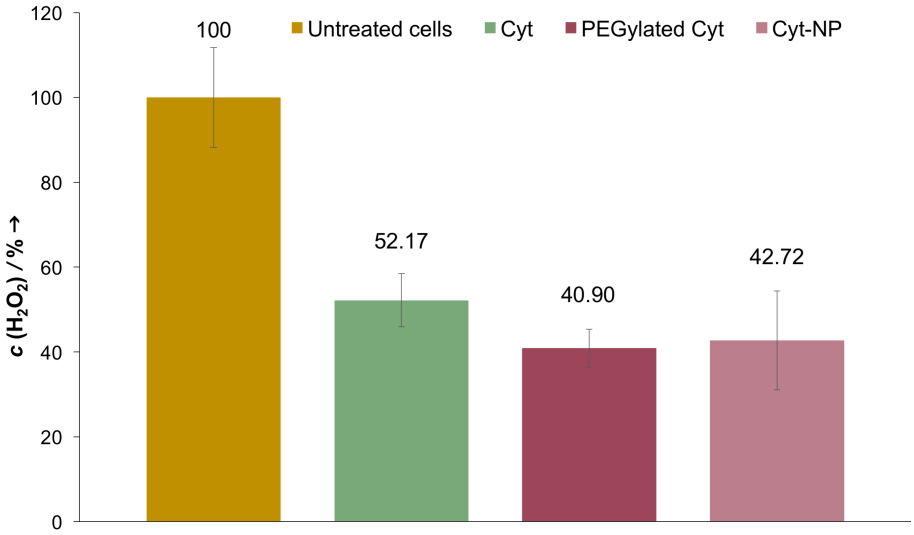

Figure 40: Determination of the extracellular catalytic activity of Cyt *c*, PEGylated enzyme and the nanoparticles using the Amplex red assay. The cell medium of cells which were treated with the Cyt *c* samples contains a reduced hydrogen peroxide quantity compared to untreated cells.

All investigated HRP samples show peroxidase activity and reduce the hydrogen peroxide content in the medium (HRP 53%, PEGylated enzyme 55%, HRP-NP 34%) (Figure 41). The PEGylated enzymes show a slightly higher conversion of the substrate, whereby the large error bars prevent an exact assertion about the catalytic efficiency. According to this assay, the assembly of the PEGylated material into nanoparticles impairs the enzymatic activity by 22%. Nevertheless, the surface modification and nanoparticle formation do not lead to a total loss of the peroxidase activity.

After incubation with the three catalase samples, a reduced H_2O_2 level was determined in the cell medium (Figure 42). But catalase, the most efficient peroxidase among the three selected enzymes, shows only a reduction of 45%, like Cyt *c*. This result disagrees with our calculated catalytic parameters and with values known from the literature (see H_2O_2 assay, Page 67). Nevertheless, the fact that the surface PEGylation leads to a decreased peroxidase activity remains in this assay (reduced by 43%). Additionally, the Cat-NPs show a decreased conversion of hydrogen peroxide (reduced by 15%), seems that the nanoparticle preparation has a greater impact on the enzymatic activity of this enzyme, in comparison to Cyt *c* and HRP. Moreover, the occurring large error bars cannot be underestimated in this assay, so that an exact inference of the catalytic efficiency cannot be made.

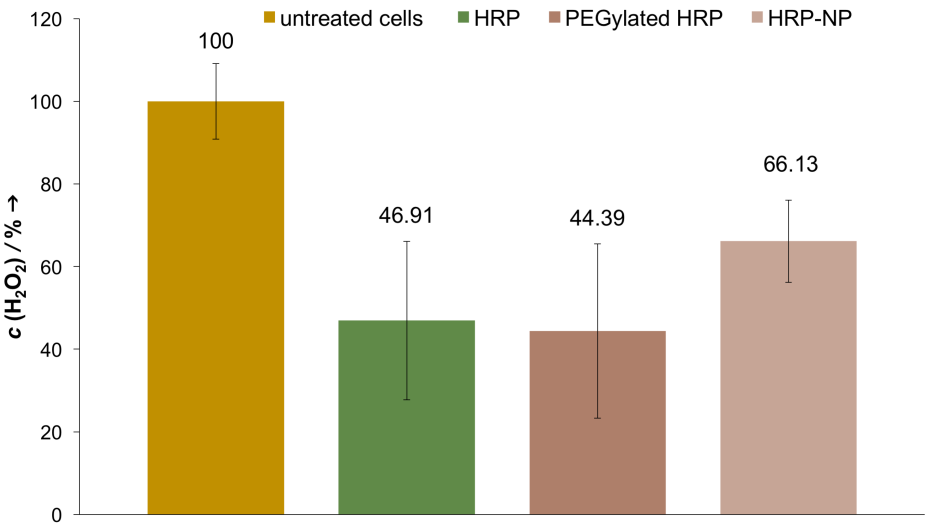

Figure 41: Determination of the extracellular catalytic activity of HRP, PEGylated enzyme and the nanoparticles using the Amplex red assay. The cell medium of cells which were treated with the HRP materials contains a reduced hydrogen peroxide quantity compared to untreated cells. The HRP-NPs show a higher amount of H_2O_2 compared to native HRP and PEGylated one, indicating a decreased catalytic efficiency of the particles.

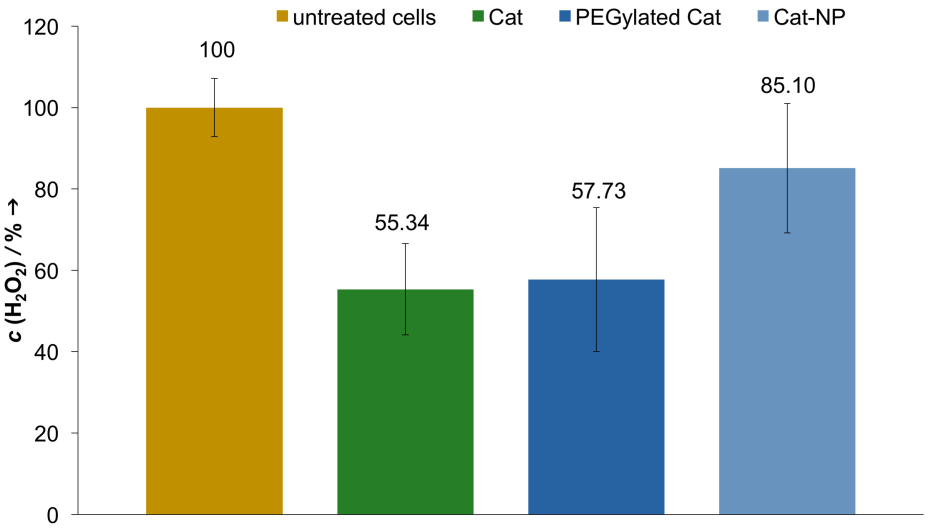

Figure 42: Determination of the extracellular catalytic activity of Cat, PEGylated enzyme and the nanoparticles using the Amplex red assay. The cell medium of cells which were treated with the Cat samples show a reduced hydrogen peroxide quantity compared to untreated cells. The Cat-NP containing solution shows a higher H_2O_2 amount compared to the cell medium containing native Cat and PEGylated Cat. This indicates a decreased catalytic efficiency of the particles.

When performing *in vitro* experiments and using biological samples, it should keep in mind that fluctuations within the triplicate of one sample and the other investigated samples are often present. The exact hydrogen peroxide concentration is unknown and can vary within the wells of one well plate. Moreover, the used Amplex Red assay can lead to errors. Zhao *et al.* showed that Amplex Red itself can be oxidized to the fluorescent dye resorufin after exposure to light in the absence of hydrogen peroxide and a peroxidase.[157] This side reaction can lead to a falsification of the results so that an exact statement about the peroxidase activity cannot be made.

Comparing the results of the three peroxidases with each other, the surface-modified Cyt *c* and the Cyt-NPs show overall the best improved and retained activity. While Cyt *c* has the lowest intrinsic peroxidase activity, other characteristics of this enzyme can lead to this result. The surface modification of Cyt *c* results in the highest structure alteration compared to HRP and Cat. Like already mentioned, the increased number of *a*-helices can result in an increased peroxidase activity. Moreover, this small enzyme shows remarkable characteristics in order to be a good biocatalyst. The containing prosthetic group is covalently linked to the protein scaffold, which prevents or reduces the possibility to lose the heme group while modification, in contrast to HRP and Cat, which bear the prosthetic group (heme *b*) via hydrophilic and hydrophobic interactions. In addition, Cyt *c* is active over a wide pH range (2–11) and at high concentrations of organic solvents. The already existing thermostability can be improved by surface modifications.[178]

Looking at horseradish peroxidase, investigations by other groups confirm the preservation of the enzymatic activity in many organic solvents.[182] However, the dissolution of the PEGylated HRP in dichloromethane and the ultrasonic treatment can lead in our case to a slight decrease of the catalytic activity of this particle system.

The modification of catalase and the NP formation lead to a significant loss of the peroxidase activity in both performed activity assays (H_2O_2 assay and Amplex Red assay). Every subunit of this homotetrameric enzyme contains one NADPH molecule as a cofactor and heme *b* as a prosthetic group, which is responsible for the enzymatic activity. Under physiological conditions, this oxidoreductase catalyzes the dismutation of hydrogen peroxide in an excellent manner. Like already mentioned, the PEGylation can lead to destabilization of the structure. In addition, a dissociation of the multimeric enzyme into subunits can result in a conformational alteration of the three-dimensional structure of the monomer, that cause partial inactivation.[171]

Investigation of the Intracellular H_2O_2 with Peroxidase Particles

Unlike the native enzymes, the developed peroxidase nanoparticles show the benefit to be taken up by cells in a controlled manner. To highlight this advantage of the nanoparticle system, the intracellular catalytic activity was investigated in stressed HeLa cells. Cells were incubated with the three different Cy5-labeled peroxidase particles (Cy5_Cyt-NP, Cy5_HRP-NP, Cy5_Cat-NP) for 24 h and the reduction of the intracellular H_2O_2 concentration was analyzed. For that, the particle-treated cells and untreated ones, which serve as a control, were incubated with a monoboronate-based fluorescent dye (Peroxy Yellow 1 -PY1) for 30 min, which diffuses quickly into the cytosol and reacts there selectively with the remaining H_2O_2 molecules.[183] To achieve a better detection limit of the used fluorescent dye, all HeLa cells were stressed additionally with exogenous hydrogen peroxide (100 μM) for 30 min. Flow cytometry analysis shows that the particles are readily taken up by cells and are able to reduce the intracellular H_2O_2 level (Figure 43).

The treatment with Cyt-NPs leads to a 20% decreased H_2O_2 concentration. Since the Amplex Red assay show double values (Figure 40) compared to this experiment, it should be noted that the intracellular hydrogen peroxide level was measured after 30 min and represent only this considered state of the cell. Moreover, the possible influence of other cell occurring reactions should be kept in mind. Performed investigations in the laboratory cannot always be transferred to living organism. Nevertheless, the nanoparticles show a peroxidase activity in cells and confirm that the formulated system can act as a molecular machinery inside of cells.

Similarly, the HRP-NPs reduce the hydrogen peroxide concentration up to 16%. These nanoparticles are also able to perform catalysis within the cellular environment. This investigation confirms again that the PEGylation and the NP formulation lead to no total loss of the intrinsic peroxidase activity.

After treatment with the Cat-NPs, a 19% reduced intracellular H_2O_2 concentration was measured in HeLa cells. Whereas these NPs show a significantly decreased peroxidase activity in the Amplex Red assay, an intracellular catalytic efficiency was measurable.

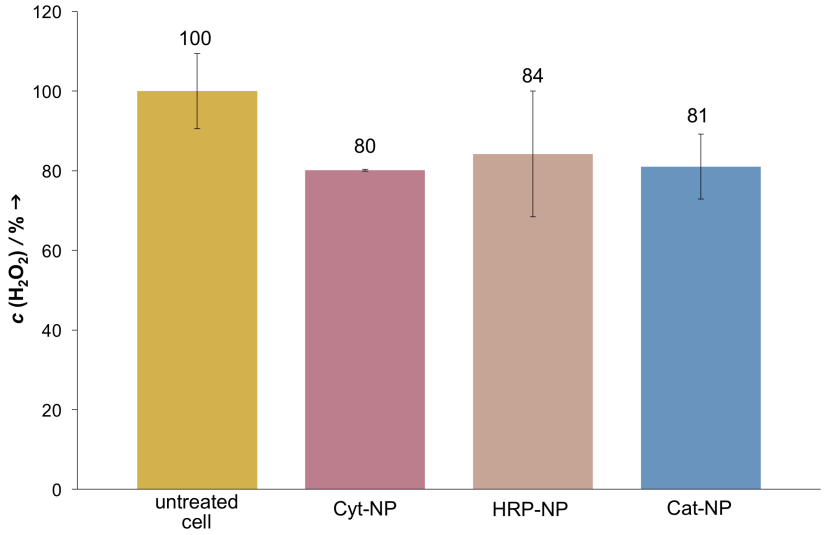

Figure 43: Flow cytometry results of the different peroxidase NPs. HeLa cells which were stressed with hydrogen peroxide and treated subsequently with the developed nanoparticles, show a reduced amount of this harmful species.

These flow cytometry experiments show that it is possible to perform catalysis in cells using the developed enzymatic nanoparticles. The retention of the catalytic activity within the nanoparticle system enables the utilization of the intrinsic peroxidase activity of Cyt *c*, HRP and Cat in order to reduce the amount of the harmful hydrogen peroxide in HeLa cells.

Live-Imaging Microscopy

To verify the findings and to visualize the reduction of the H_2O_2 level within the cells, live-cell imaging microscopy was performed with the Cyt *c* NPs. HeLa cells were incubated with PY1 and treated with exogenous H_2O_2, similarly to the flow cytometry experiments. These images represent a stressed state of the cell with a high amount of toxic hydrogen peroxide (Figure 44A upper row). Within a treatment time of 24 h, the nanoparticles are taken up by cells, probably by endocytosis. We assume that the particles are dissociated into the individual surface-modified enzymes within the endosomes. The subsequent endolysosomal escape of the PEGylated enzymes would lead to a high peroxidase concentration in the cell cytosol, which we expect. At this point, it is important to mention, that we did not investigate this assumed pathway. Previous studies in our group of protein-based nanoparticles, which carried the anti-cancer drug doxorubicin showed cell toxicity, comparable with other doxorubicin delivery systems.

The resulting toxic behavior based on the delivery of the drug to the cell nucleus. This implies the dissociation of the particle system within the cellular environment and includes the endolysosomal escape. Based on this, we expected a similar behavior of the prepared peroxidase NPs.

The Cyt-NPs-treated cells show a 19% weaker average fluorescence signal of PY1, indicating the reduction of hydrogen peroxide within these cells (Figure 44A lower row). Additionally, these *in vitro* results confirm again that the catalytic activity of the nanoparticulate system is preserved in a cellular environment and that these Cyt-NPs can even modulate ROS levels inside of cells.

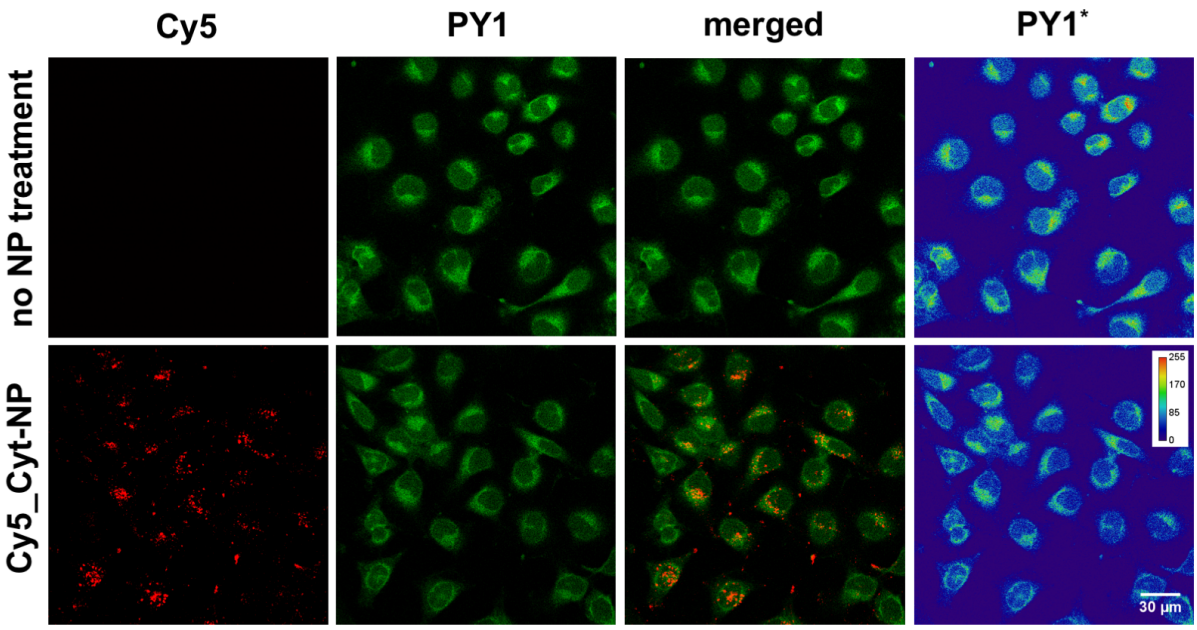

Figure 44: Live-cell imaging of HeLa cells without NP treatment (upper row) and cells incubated with Cy5-labeled Cyt-NPs (lower row; incubation time: 24 h; scale bar for all images: 30 µm). Shown are the images of the individual Cy5 (red) and PY1 (green) channels, as well as the merged images. Cy5-labeled proteins (red dots) accumulate in the cell cytosol. Cells treated with Cyt-NPs show an overall lower green fluorescence signal, which indicates a reduction of intracellular H_2O_2. The PY1* channel focuses on the fluorescence intensity of the PY1 channel. High intensities are represented in red, low intensities in blue. This representation allows a clear illustration of the distinct differences in fluorescence values.

We assume, based on the previously performed flow cytometry experiments with the HRP-NPs and the Cat-NPs, that the catalytic activity of these NPs results in similar cell images, as shown for the Cyt-NPs in this section.

Under physiological conditions, the intracellular hydrogen peroxide concentration is about 0.001-0.01 μM, and in some cases up to approximately 0.1 μM. Higher H_2O_2 concentrations (>0.1 μM) lead to inflammatory responses and damages of biomolecules, denoted as oxidative stress.[184] In summary, the developed NPs demonstrate catalytic activity in the above described simulated situation of an unhealthy state, and lead to the degradation of these toxic species up to 20%.

3.3 Cascade Reactions using Enzyme-based Nanoparticles

In the third project, the obtained knowledge about the enzyme PEGylation and nanoparticle preparation was transferred for the design of a dual-enzyme based particle system. The idea was to create a cascade reaction implementing nanosystem using two different PEGylated enzymes. The primary aim of this study was to investigate whether it is possible to perform coupled enzyme reactions in a single particulate system using the described emulsion-based method.

For this, the two enzymes glucose oxidase (GOx) and horseradish peroxidase (HRP) were co-embedded in a nanoparticle system. GOx oxidizes *β*-D-glucose to D-glucono-*δ*-lactone, which is hydrolyzed to D-gluconic acid in a side reaction, and hydrogen peroxide. In the following step, the generated H_2O_2 can oxidize HRP, which is now able to catalyze the conversion of a chromogenic substrate into a colored product (Figure 45). For this, 2,2'-azinobis-(2-ethylbenzthiazoline-6-sulfonate) (ABTS) and Amplex Red were used to visualize a successful cascade reaction.

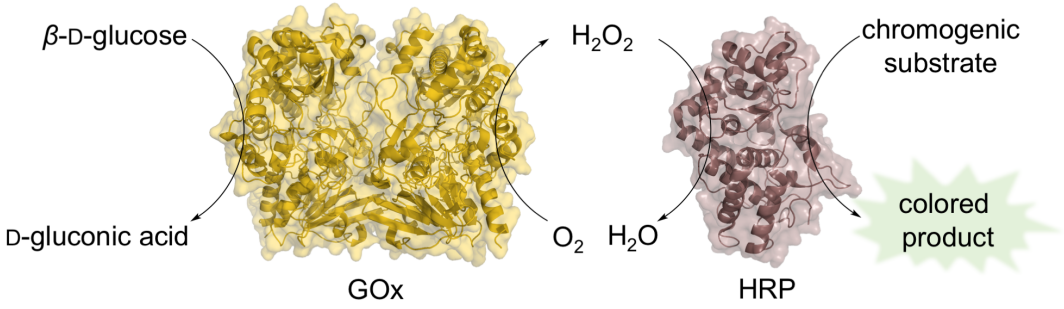

Figure 45: Schematic illustration of the cascade mechanism of GOx and HRP. In a first step, *β*-D-glucose is oxidized by glucose oxidase to D-glucono-*δ*-lactone and hydrogen peroxide, whereby the first one reacts with water to D-gluconic acid. This oxidizing agent H_2O_2 reacts in turn with HRP which oxidizes a chromogenic substrate to a colored product.

To use a single emulsion-based technique and prepare a nanosystem which is solely built-up by these two enzymes, surface modifications with polyethylene glycol were performed. The PEGylation and the nanoparticle preparation, as well as the associated analysis, are presented and discussed in the following sections.

3.3.1 PEGylation of Glucose Oxidase

The modification and analysis of glucose oxidase (GOx) will be described in the following sections. All results for the PEGylation of HRP are found Chapter 3.2.

PEGylation of Glucose Oxidase

To achieve a lipophilic enzyme material, glucose oxidase (GOx) was PEGylated using NHS-mPEG with a molecular weight of 5 kDa ($GOx(mPEG)_{5k}$) and epoxy-mPEG with a molecular weight of 2 kDa ($GOx(mPEG)_{2k}$), respectively. Based on experience acquired for the PEGylation of large enzymes, the high molecular weight polymer was used to modify the surface of GOx, a 160 kDa dimeric enzyme. Utilizing a shorter PEG chain, the epoxy modified polymer was selected due to the high reactivity towards nucleophilic amino acids and additionally the increased stability of this electrophilic group in aqueous solution.[29] Under mild alkaline conditions (pH 8) the modification was performed at 30 °C for 48 h. GOx from *Aspergillus niger* shows a maximal activity in a temperature range of around 40–60 °C.[96] Thus, the slightly increased temperature should not denature or disrupt the enzyme. The PEGylation with both polymers leads to slightly yellow materials that are fully soluble in organic solvents.

Molecular Weight Determination of GOx-Polymer Conjugates by SDS and MALDI-ToF MS

The monomer of the native enzyme shows a defined protein band at around 80 kDa in the SDS polyacrylamide gel electrophoresis (Figure 46, lane 1). The use of $NHS\text{-}mPEG_{5k}$ results in a GOx conjugate with a molecular weight of around 110 to 170 kDa. Because of the broad distributed protein band of this material in the SDS gel, the molecular weight cannot be determined exactly (Figure 46, lane 2). It can be expected that at least four or even more mPEG chains are introduced onto the monomer surface, resulting in at least 8 polymer chains of the overall enzyme. In contrast, the $GOx(mPEG)_{2k}$ material shows a barely detectable increase of the molecular weight in the SDS-PAGE (Figure 46, lane 3). Only a slightly smeared protein band at around 80 kDa is seen.

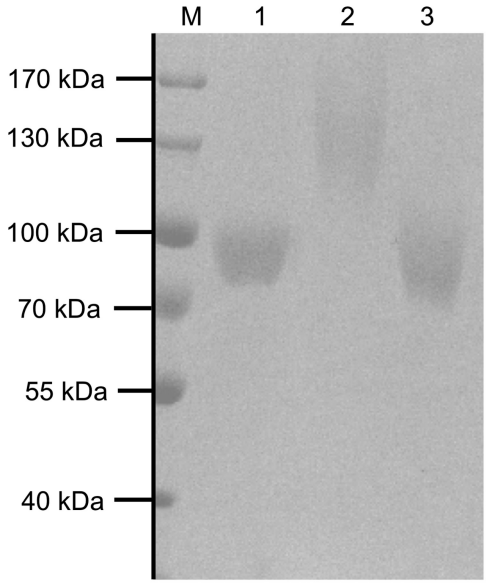

Figure 46: SDS-PAGE (8%) of modified GOx with NHS-mPEG$_{5k}$ (lane 2) and epoxy-mPEG$_{2k}$ (lane 3) in comparison to native enzyme (lane 1).

To investigate the molecular weights more precisely, a MALDI-ToF MS measurement was performed. The monomer of GOx shows a molecular weight of 76.18 kDa. Using NHS-mPEG$_{5k}$ for PEGylation, this leads to products with a molecular weight of 90.14 kDa (Figure 47B). This result is lower than expected from the SDS-PAGE and indicates that only two polymer chains were introduced per monomer. The modification with epoxy-mPEG$_{2k}$ results in a material with a molecular weight of 81.14 kDa, corresponding to two polymer chains per monomer (Figure 47A). This low conjugation rate is not detectable in the SDS-PAGE but is sufficient to prepare a lipophilic enzyme material which is soluble in organic solvents.

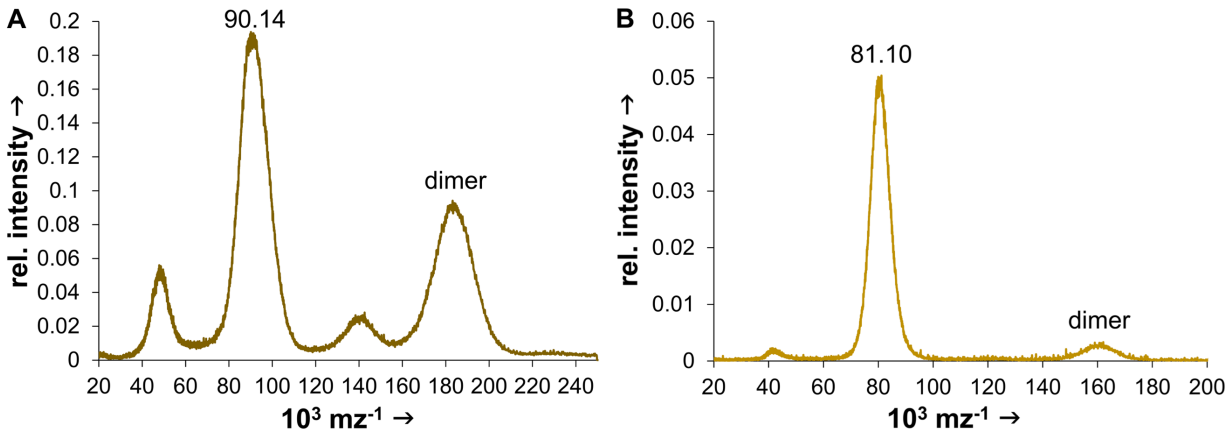

Figure 47: MALDI-ToF MS diagram of modified GOx with NHS-mPEG$_{5k}$ (**A**) and epoxy-mPEG$_{2k}$ (**B**).

Structural Integrity of PEGylated GOx Analyzed by CD

Structural investigations of both PEGylated GOx samples in the far-UV area indicate an overall retention of the secondary structure (Figure 48). A slight decrease of *a*-helices and an increase in unordered structure elements were detected by DICROWEB (Table 11). Looking at enzymes which contain a binding pocket as a catalytic center, structural alterations might have been a higher impact on the enzymatic activity. Thus, the preservation of the secondary structure of the GOx-polymer conjugates is essential.

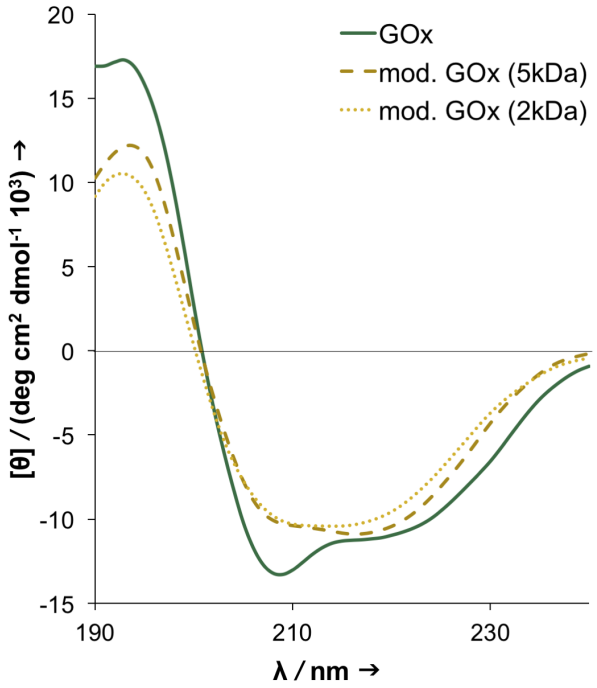

Figure 48: Far-UV CD spectra of the GOx(mPEG)$_{5k}$ material (dark yellow dotted line), GOx(mPEG)$_{2k}$ material (light yellow dotted line) and the native enzyme (green line). The spectra indicates a slight alteration in secondary structure elements of the modified proteins. A detailed analysis can be found in Table 11.

Table 11: Calculated amounts of secondary structure elements for GOx and the PEGylated variant (in %); Results calculated with DICROWEB using the CONTIN-LL method (reference Set 7).

	GOx	**GOx(mPEG)$_{5k}$**	**GOx(mPEG)$_{2k}$**
a-helix	31	23	21.7
β-sheet	22.5	26.5	25.7
turns	19.9	21.1	21.8
unordered	26.6	29.3	30.8

3.3.2 Dual-Enzyme Nanoparticles

General Procedure

As already described in Chapter 3.1.3, a single emulsion-based method was used for the formulation of this dual-enzyme-based nanoparticle system. PEGylated samples of GOx and HRP were dissolved in DCM in different ratios, to obtain overall 2.5 mg modified enzyme material for the particle preparation. The organic phase was covered with PBS (pH 7.4) and the biphasic solution was ultrasonicated for 45 s. The nanoemulsion was stirred in a well-ventilated area and after the evaporation of DCM, a stable nanosuspension was received. The differently composed nanosystems are described in the following section.

Preparation of GOx-HRP Nanoparticles

Nanoparticles with five different ratios of PEGylated GOx and HRP were prepared (Table 12). For this, NHS-mPEG$_{5k}$-modified HRP was used for all approaches (HRP(mPEG)$_{5k}$). Additionally, nanoparticles using only one type of PEGylated enzyme were prepared by the single emulsion technique and were served as controls (GOx(mPEG)$_{5k}$-NP, GOx(mPEG)$_{2k}$-NP, HRP(mPEG)$_{5k}$-NP). In general, the native enzyme quantity in the PEGylated material was determined by an absorption measurement at 280 nm. Thus, the calculated amount of native enzyme in the PEGylated material was used for the individual preparations of the dual-enzyme systems. The used ratios refer to the native enzyme amount in mg, not to the quantity of the PEGylated material.

At the beginning, an excess of HRP referred to GOx molecules (ratio 1:2.5) was used to ensure the rapid and complete conversion of H_2O_2 by HRP. In this ratio, both modified GOx samples (2k and 5k PEG-modified) were combined with PEGylated HRP, respectively.

Furthermore, corresponding to activity results (see Chapter 3.3.3), only the GOx(mPEG)$_{2k}$ material was used for further nanoparticle preparations. Utilizing this material in combination with HRP(mPEG)$_{5k}$, two further particulate systems with different amounts of GOx and HRP were prepared (1:1 and 1:5 ratio).

Based on first *in vitro* results (see Chapter 3.3.2, Page 88) two additional dual-enzyme systems with large excesses of PEGylated HRP were produced (ratio 1:10 and 1:20).

Table 12: Composition of dual-enzyme nanoparticles in different GOx and HRP ratios. All samples were prepared via single emulsion. The used ratios refer to the native enzyme amount in mg, not to the quantity of the PEGylated material.

ratio GOx : HRP	composition of the dual-enzyme NPs
1:1	$GOx(mPEG)_{2k}$ - $HRP(mPEG)_{5k}$
1:2.5	$GOx(mPEG)_{5k}$ - $HRP(mPEG)_{5k}$
1:2.5	$GOx(mPEG)_{2k}$ - $HRP(mPEG)_{5k}$
1:5	$GOx(mPEG)_{2k}$ - $HRP(mPEG)_{5k}$
1:10	$GOx(mPEG)_{2k}$ - $HRP(mPEG)_{5k}$
1:20	$GOx(mPEG)_{2k}$ - $HRP(mPEG)_{5k}$

Size Determination of Dual-Enzyme Nanoparticles by NTA

Size determinations of the combined enzyme nanosystems were performed by nanoparticle tracking analysis (NTA). All nanoparticle suspensions (1 mg mL^{-1}) were diluted in PBS (pH 7.4) to a final concentration of 10 μg mL^{-1}. Concentrations of 20 μg mL^{-1} were used, when the number of nanoparticles was too low for tracking by the NTA software. All particle preparations result in particulate systems.

Figure 49 shows the NTA data of the solely GOx-NPs using two different polymer lengths. Both samples show nanoparticles with a diameter of around 200 nm. In general, compared to the other prepared enzyme-based nanosystems, the use of this protein results in larger nanoparticles. This outcome can probably be explained by the overall negative surface charge of GOx.[95] It is assumed, that the slight shielding effect of only four introduced mPEG chains does not change the overall negative surface charge. Thus, the electrostatic interactions of the individual enzymes within the particle system can lead to a less compact system.

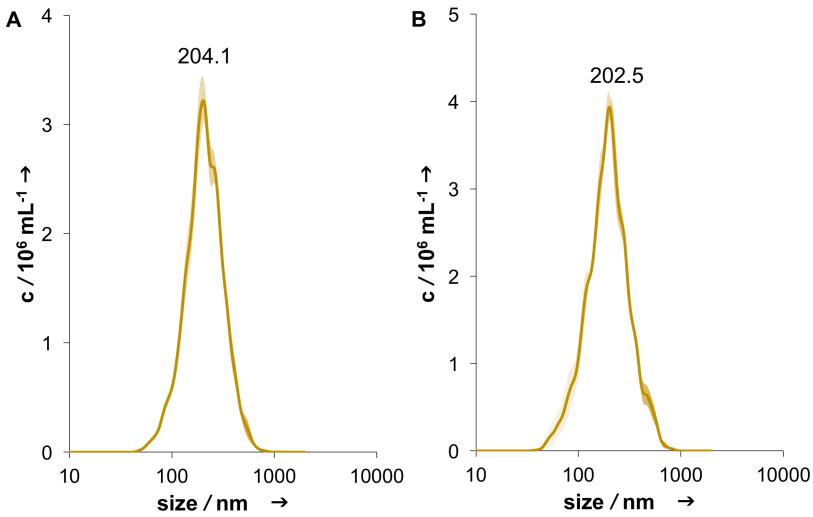

Figure 49: GOx nanoparticles using only the GOx(mPEG)$_{5k}$ (**A**) and the GOx(mPEG)$_{2k}$ material (**B**), respectively. Both materials result in nanoparticles with a diameter of around 200 nm.

The combination of GOx(mPEG)$_{5k}$ with modified HRP in a ratio of 1:2.5, leads to nanoparticles with a diameter of 137.4 nm. In comparison, the use of GOx(mPEG)$_{2k}$ results in slightly smaller nanoparticles with a diameter of 123.3 nm (Figure 50). It seems that the polymer length has to some extent a minimal influence on the particle size. Both systems indicate that the addition of PEGylated HRP results in smaller particles, compared to the GOx-NPs. This can be traced back to the reduced electrostatic interactions within the particle system. Based on the addition of HRP, the negative surface charge of GOx are minimized, leading to a lower repulsion of the individual enzymes and a compacter particle system.

Dual-enzyme systems with either a ratio of 1:5 or equal amounts of both biomacromolecules (ratio 1:1) result in different sized particle materials. A higher amount of PEGylated HRP results in particles with a diameter of 125.2 nm (Figure 51). Again, it seems that higher amounts of PEGylated HRP in the dual-enzyme system lead to more compact particles. The use of a higher GOx(mPEG)$_{2k}$ quantity (ratio 1:1) leads to larger nanoparticles (d = 181.8 nm).

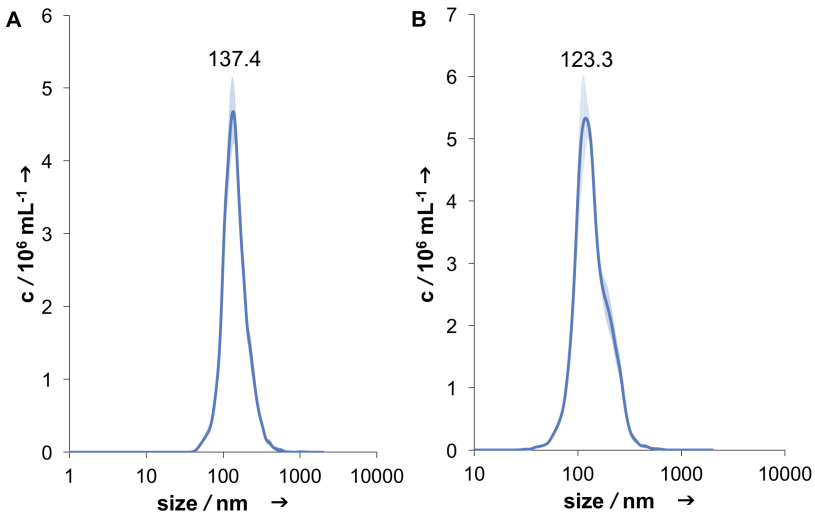

Figure 50: Dual-enzyme NP with a ratio of 1:2.5. The combination of GOx(mPEG)$_{5k}$ with HRP(mPEG)$_{5k}$ leads to nanoparticles with a dimeter of 137.4 nm (**A**), using GOx(mPEG)$_{2k}$ with HRP(mPEG)$_{5k}$ results in a particulate system with a diameter of 123.3 nm (**B**).

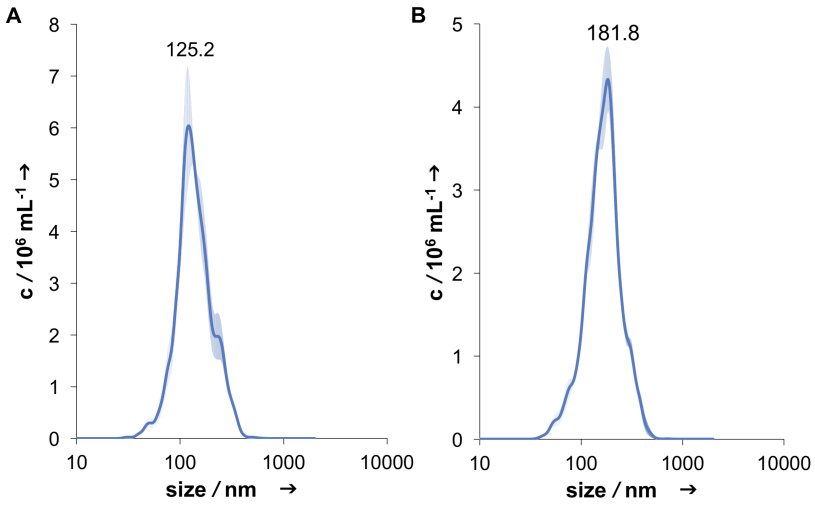

Figure 51: Dual-enzyme system with a higher amount of HRP(mPEG)$_{5k}$ compared to GOx(mPEG)$_{2k}$ in a 1:5 ratio (**A**) and a system with an equal amount of both enzymes (1:1 ratio, **B**). Higher amounts of PEGylated HRP in the dual-enzyme system lead to more compact particles.

Two other combinations were prepared, where the HRP concentration was used in an excess of 10 and 20 compared to GOx. Both sample combinations result in particle systems of around 162 nm and 133 nm in diameter (Figure 52). Comparing these both samples, an increased PEGylated HRP amount leads to smaller nanoparticles.

But in comparison with the other prepared dual-enzyme systems, these samples confirm not the trend, that higher PEGylated HRP amounts lead to overall smaller particles.

In general, NTA data show that all nanosystems which contain both enzymes, tend to be towards small-sized particles compared to the NPs only consisting of GOx (compare with Figure 49). Detailed size values of the investigated dual-enzyme nanoparticles are found in Table 13.

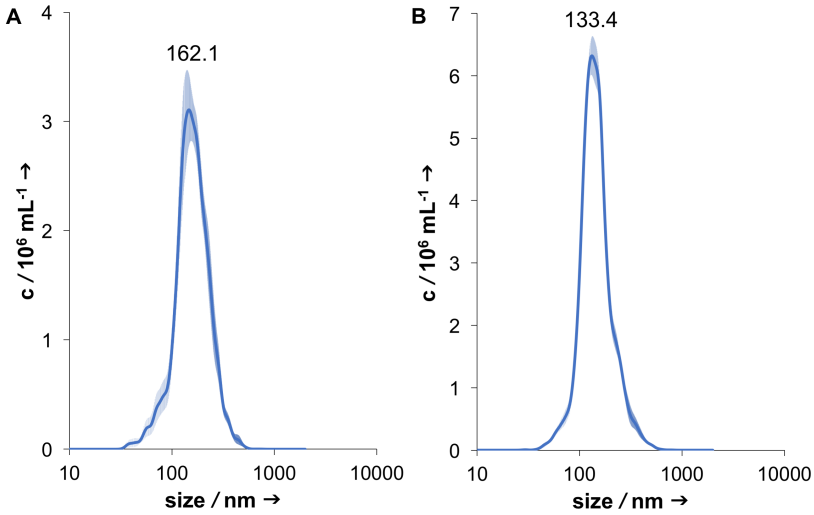

Figure 52: Dual-enzyme systems with high excesses of HRP(mPEG)$_{5k}$ compared to GOx(mPEG)$_{2k}$ in a 1:10 ratio (**A**) and 1:20 ratio (**B**).

Table 13: Detailed size values obtained by NTA measurements of the dual-enzyme nanoparticles. Particle size (diameter) was determined with five individual measurements per sample.

particle	mean / nm	mode / nm	SD / nm
GOx(mPEG)$_{2k}$-NP	268.2 ± 8.7	202.5 ± 7.7	128.8 ± 4.6
GOx(mPEG)$_{5k}$-NP	267.1 ± 4.8	204.1 ± 4.8	113.4 ± 5.3
GOx(mPEG)$_{2k}$-HRP(mPEG)$_{5k}$-NP (1:1)	206.6 ± 2.3	181.8 ± 4.2	81.1 ± 3.6
GOx(mPEG)$_{2k}$-HRP(mPEG)$_{5k}$-NP (1:2.5)	169.2 ± 6.9	123.3 ± 4.1	72.5 ± 6.2
GOx(mPEG)$_{5k}$-HRP(mPEG)$_{5k}$-NP (1:2.5)	179.2 ± 5.6	137.4 ± 4.7	89.9 ± 11.1
GOx(mPEG)$_{2k}$-HRP(mPEG)$_{5k}$-NP (1:5)	174.6 ± 6.5	125.2 ± 6.5	73.5 ± 3.0
GOx(mPEG)$_{2k}$-HRP(mPEG)$_{5k}$-NP (1:10)	193.5 ± 7.4	162.1 ± 16.7	73.0 ± 4.7
GOx(mPEG)$_{2k}$-HRP(mPEG)$_{5k}$-NP (1:20)	181.4 ± 4.0	133.4 ± 3.6	82.5 ± 6.1

Mean size and SD (standard deviation) correspond to the arithmetic calculated values based on the sizes of all particles detected in the NTA measurement. Mode values describe the average size of the main particle population.

TEM Images of GOx-NPs and Dual-Enzyme Nanoparticles

The prepared nanoparticles were visualized by TEM. The images of the GOx nanoparticles show scattered particles in a size range of 150 to 200 nm (Figure 53A and B) and confirm the already shown NTA data. Also, TEM images could be obtained from the prepared dual-enzyme nanoparticle systems (Figure 53C–F). Unlike the low amount of the GOx nanoparticles on the grid, these materials were found widely distributed in high quantities. Looking at the dual-enzyme systems with a ratio of 1:2.5 and 1:1, the TEM images mainly confirm the NTA data and show nanoparticles in a size of approximately 150 nm. NTA data of the dual-enzyme nanoparticles with a 1:5 ratio indicate a narrow size-distributed system. However, TEM images show larger particles with a size of around 200 nm. Because the nanoparticles are presented in a dry stage the resulting size ranges do not always conform to the NTA data, which analyze the particles in solution. Based on the preparation method the particles could be presented in a flattened state. The interpretation of all TEM images should be carried out carefully like mentioned in Chapter 3.1.3, Page 49.

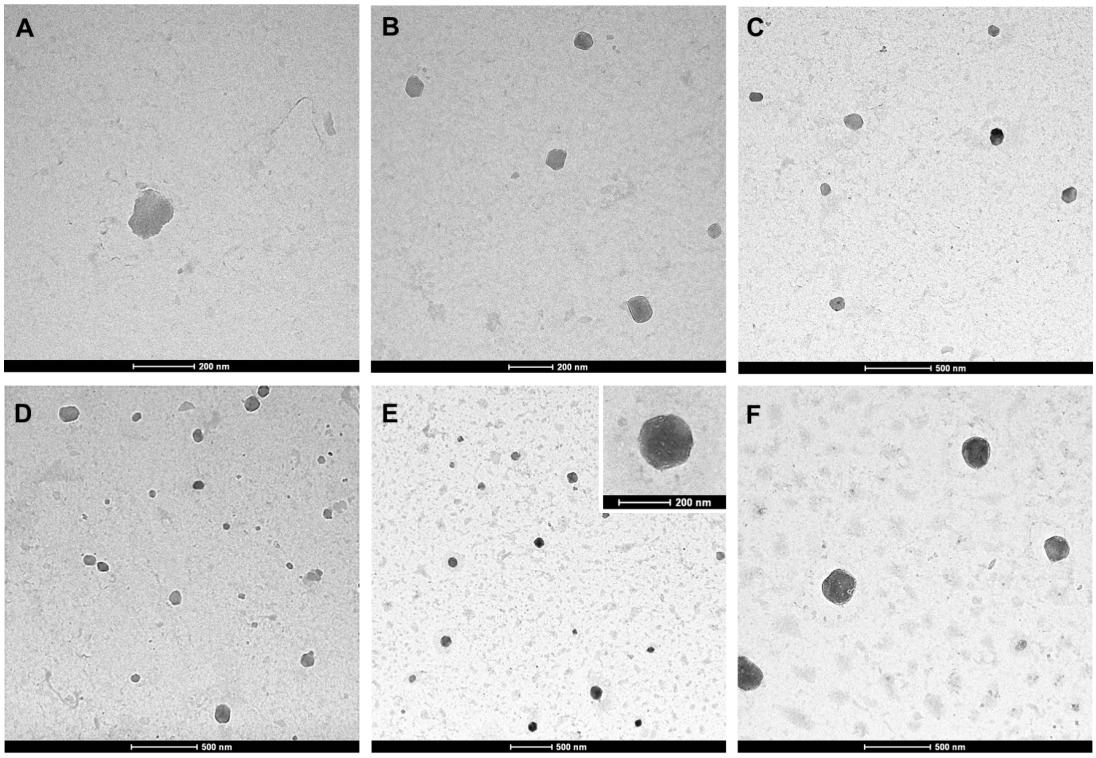

Figure 53: TEM images of GOx nanoparticles and dual-enzyme nanoparticle systems. GOx(mPEG)$_{2k}$-NP (**A**), GOx(mPEG)$_{5k}$-NP (**B**), dual-enzyme systems using GOx(mPEG)$_{2k}$ (**C**) and the GOx(mPEG)$_{5k}$ (**D**) material with PEGylated HRP in a ratio of 1:2.5. The lower row represents the combination of GOx(mPEG)$_{2k}$ with modified HRP in a ratio of 1:1 (**E**) and 1:5 (**F**).

Cell Toxicity of the Dual-Enzyme Nanoparticles

Glucose oxidase causes toxicity to bacteria and cells based on the formation of harmful hydrogen peroxide. The idea was to determine the cascade reaction of the glucose oxidase-horseradish peroxidase system from another point of view using the MTT method. The cell viability should be investigated using HeLa cells which were treated with the dual-enzyme systems.

If the cascade reaction takes place as imagined, the co-embedded horseradish peroxidase intercepts the toxic hydrogen peroxide and the cell viability should not be affected. All prepared GOx containing materials such as PEGylated GOx and GOx-NPs as well as native GOx and HRP-NPs serve as a control. The MTT assay was performed as described in Chapter 5.6.1.

Both individual PEGylated GOx samples were investigated separately, in order to exclude that the polymer length has an influence on the cell viability. The GOx(mPEG)$_{2k}$ material, as well as the corresponding particle system, show a toxicity up to 96%. Native GOx shows similar toxic effects in this concentration range, whereby the HRP-NPs alone are non-toxic (Figure 54).

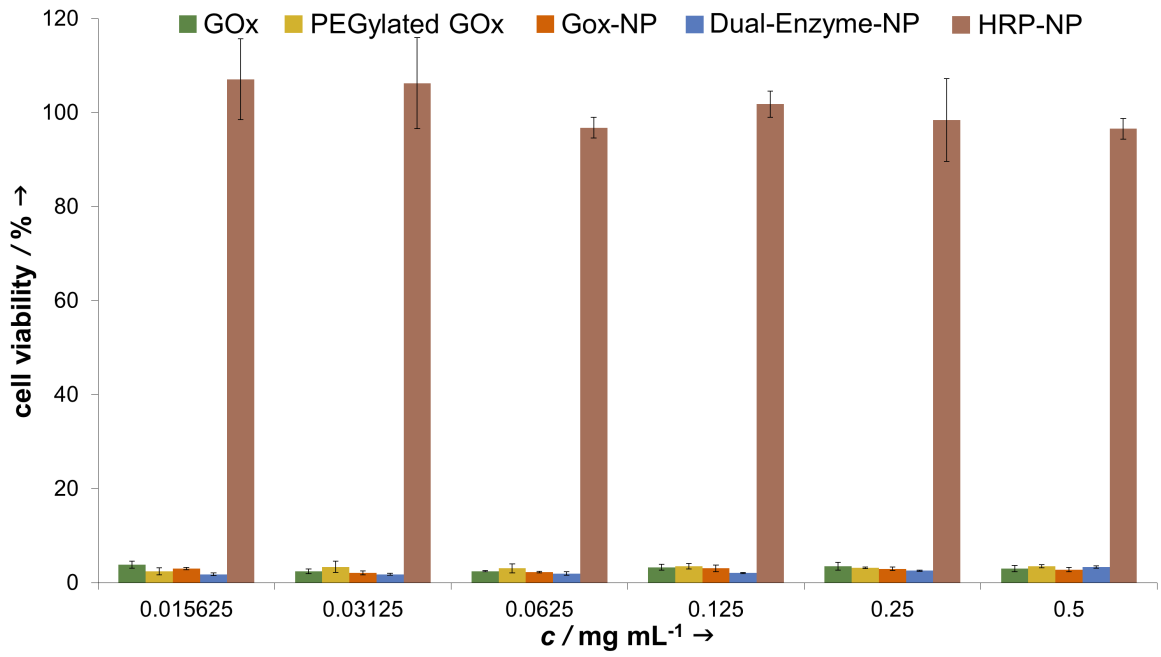

Figure 54: MTT results of native GOx, the GOx(mPEG)$_{2k}$ material, the corresponding GOx-NPs, the dual-enzyme system (ratio 1:2.5) and HRP-NPs. The given concentrations refer to the nanoparticle amount (in mg mL^{-1}) and the enzyme concentrations are orientated towards the dual-enzyme system.

Based on the high amount of H_2O_2 produced by this enzyme, this result was expected. The dual-enzyme system which was formulated in a ratio of 1:2.5, shows a cell viability of around 4%.

Investigations of the GOx(mPEG)$_{5k}$ material and the corresponding nanoparticles, resulting in the same high cell toxicity (Figure 55) as already shown for the previous GOx materials. All GOx samples are toxic on HeLa cells, whereby the HRP-NPs alone, which serve as a control, show no toxicity again.

The available HRP amount in this particle system seems to be not sufficient in order to intercept the formed hydrogen peroxide molecules and thus reduce the cellular toxicity. Based on this result, dual-enzyme nanoparticles with higher HRP amounts were prepared (ratio 1:10 and 1:20, see Figure 56), in order to investigate, if an adequate quantity of HRP can be achieved due to increase the cell viability.

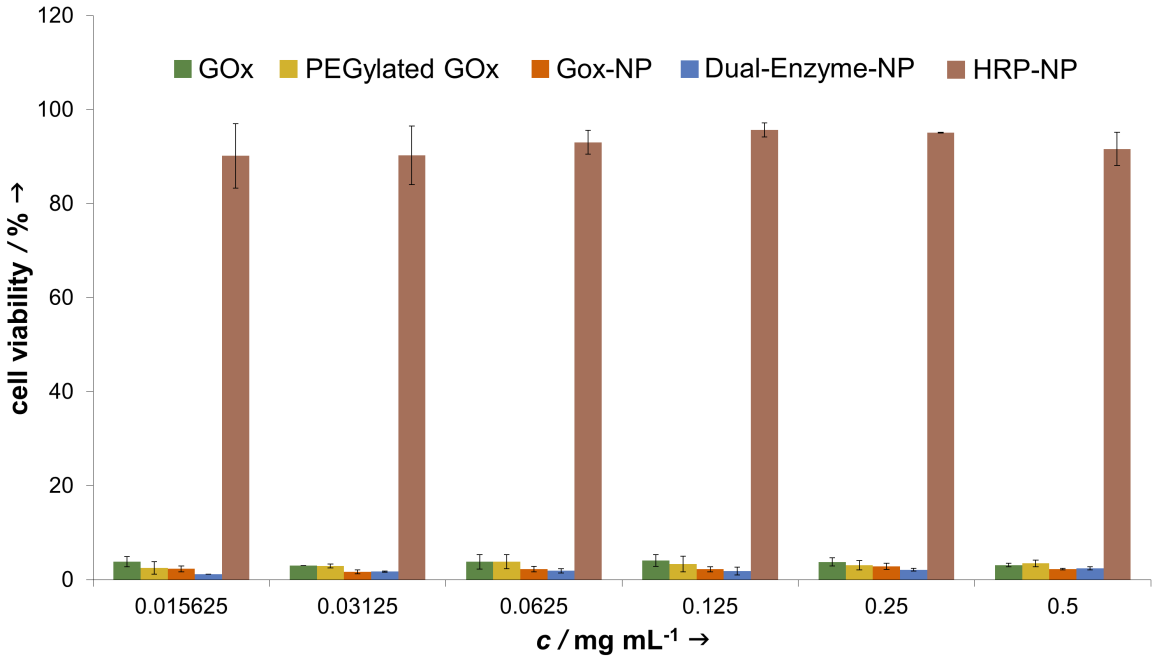

Figure 55: MTT results of native GOx, the GOx(mPEG)$_{5k}$ material, the corresponding GOx-NPs, the dual-enzyme system (ratio 1:2.5) and HRP-NPs. The given concentrations refer to the nanoparticle amount (in mg mL^{-1}) and the enzyme concentrations are orientated towards the dual-enzyme system.

Based on the already mentioned assumption that higher HRP concentrations could lead to an increased cell viability, dual-enzyme particle systems which contain large excesses of PEGylated HRP (ratio 1:5, 1:10 and 1:20) were investigated using the MTT assay. The hypothesis was confirmed, since the 1:10 and 1:20 dual-enzyme systems show enhanced cell viability. At a material concertation of 0.03125 mg, the 1:20 combined nanoparticles show an increased viability up to 25% (Figure 56). Accordingly, the particulate system with a 1:10 ratio shows a cell viability of 25% at the half of the material concentration (0.015625 mg nanoparticles). This result confirms that the toxic hydrogen peroxide produced by glucose oxidase is intercepted by the co-embedded enzyme HRP and the cascade reaction works in this particulate system.

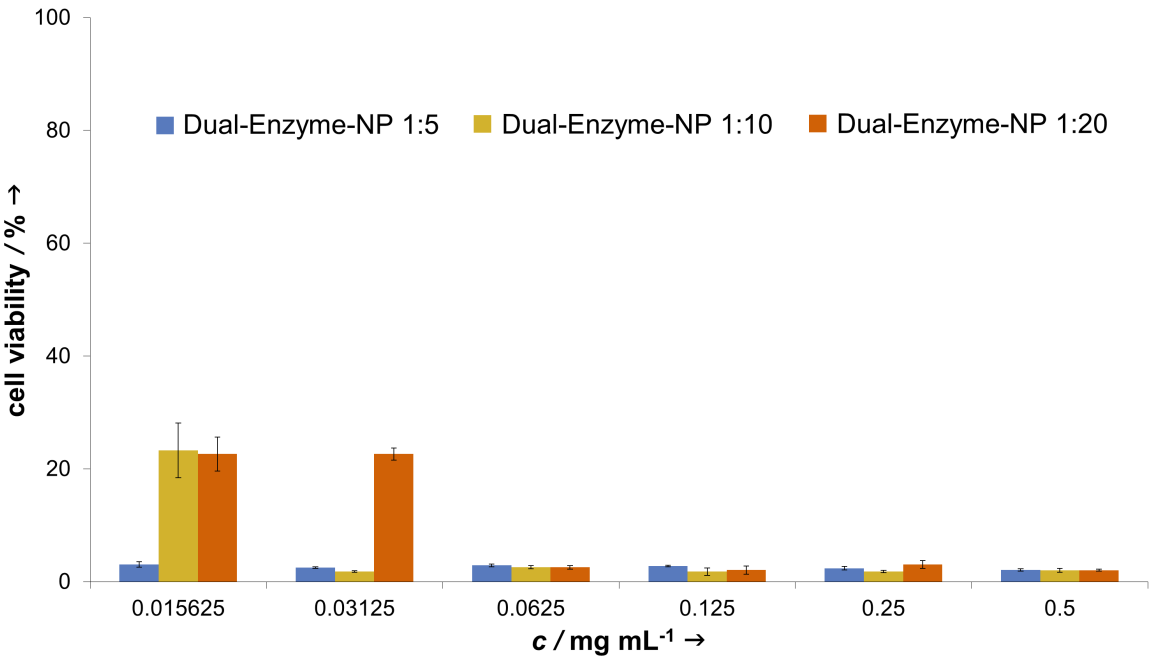

Figure 56: MTT assay of dual-enzyme nanoparticle system with an excess of modified HRP (1:5 blue, 1:10 yellow and 1:20 orange). The given concentrations refer to the nanoparticle amount (in mg mL^{-1}). At a material concertation of 0.03125 mg, the 1:20 combined nanoparticles show an increased viability up to 25%, whereby the 1:10 ratio system shows a cell viability of 25% at the half of the material concentration (0.015625 mg nanoparticles).

UV/Vis Investigations of the Dual-Enzyme Nanoparticles

In order to verify whether both enzymes are co-embedded in the particle system, absorption measurements were carried out. The dual enzyme nanomaterial was compared with the individual single protein-based systems (GOx-NPs and HRP-NPs) by UV/vis spectroscopy (Figure 57). The spectra of the GOx-NPs and HRP-NPs show a slight absorption at 280 nm respectively, which refers to the amide bond. The HRP sample shows additionally an increased absorption at 410 nm caused by the containing heme group. Verifying the dual-enzyme system, the characteristic absorption at 280 nm and an increase at 410 nm are seen, indicating the presence of both enzymes in one particle system.

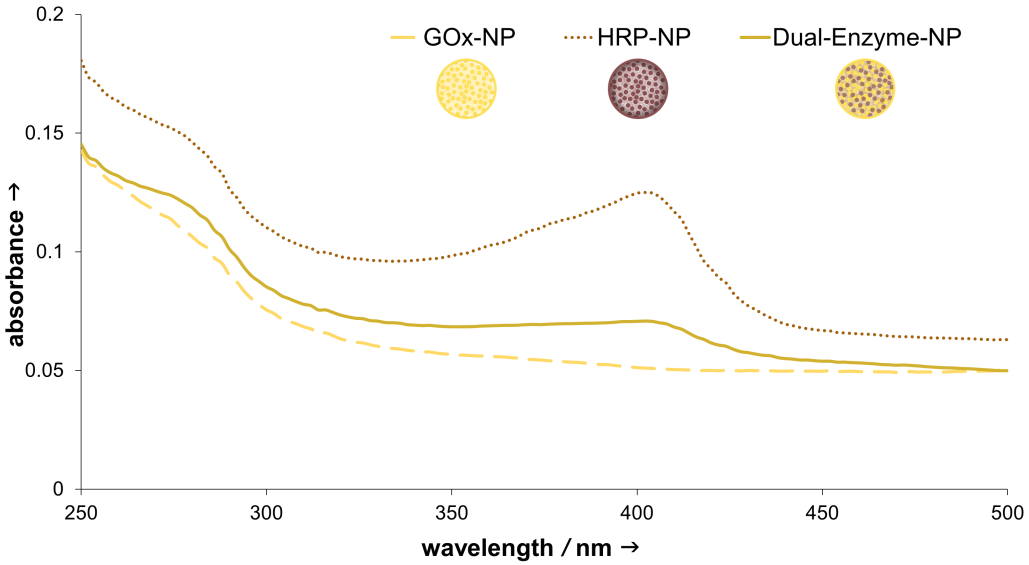

Figure 57: UV/vis spectra of HRP nanoparticles, GOx nanoparticles and the combined system of both enzymes in a ratio of 1:1.

In order to investigate whether the cascade reaction takes place within the particle system, the reaction was detected by UV/vis spectroscopy using ABTS as a chromogenic molecule. This method enables a rapid qualification and visualization of the enzymatic reaction. For this, the dual-enzyme system (ratio 1:1) was combined with *β*-D-glucose and ABTS, and the increase of absorbance of the generated $ABTS^{+\bullet}$ radical was measured between 405–420 nm. Only the dual-enzyme nanoparticle system shows an increase in absorbance at 420 nm (Figure 58).

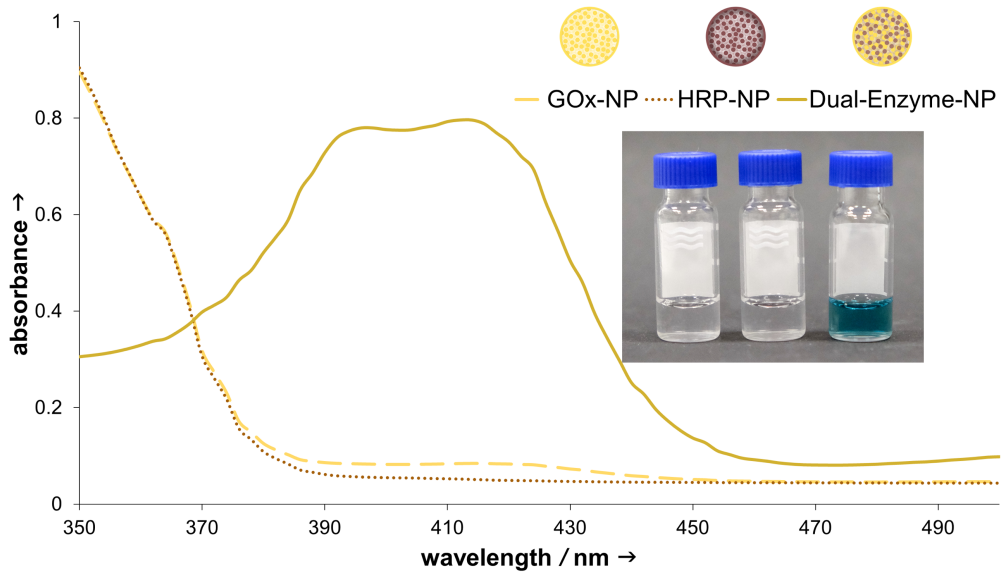

Figure 58: UV/vis spectra of GOx-NPs, HRP-NPs and the dual-enzyme system in the presence of 1 mM glucose and 0.25 mM ABTS. The green colored solution represents the formation of the $ABTS^{+\bullet}$ radical and confirms the successful occurring of the cascade reaction. This generated product can be measured at 405–420 nm. In contrast, the HRP and GOx nanoparticles alone are not able to perform this cascade reaction, which can be visualized by the colorless solution.

This result was assumed, since the co-embedded GOx initiates the cascade reaction by the conversion of β-D-glucose, yielding D-gluconic acid and H_2O_2. The available HRP is oxidized in a following reaction by the generated hydrogen peroxide and reacts with ABTS to a colored product. This result indicates that both enzymes are presented in their active form within the particle system.

3.3.3 Kinetic Investigations of the Dual-Enzyme Cascade Reaction

Investigation of the Catalytic Activity Using the Amplex Red Assay

To investigate the enzymatic activity of the first prepared dual-enzyme nanosystems (ratio 1:2.5), an Amplex Red assay was performed. This fluorescent-based assay is ideally suited for the rapid determination of the GOx-HRP cascade. The reaction starts with the conversion of β-D-glucose by GOx, yielding D-gluconic acid and hydrogen peroxide. Latter one reacts with HRP and the non-fluorescent dye Amplex Red in a three-step peroxidase reaction.

Amplex Red acts as an electron-rich substrate and is oxidized by the oxoferryl porphyrin π-cation radical (compound I) of the heme *b* group to an Amplex Red radical. In a second step, a further dye radical is formed by compound II of the heme *b*. Subsequently, a dismutation of both radicals leads to the formation of the highly fluorescent dye resorufin (Figure 59A). With the resulting slope of the individual fluorescence signals over substrate concentration, an assertion about the enzymatic activity, thus the cascade reaction can be made.

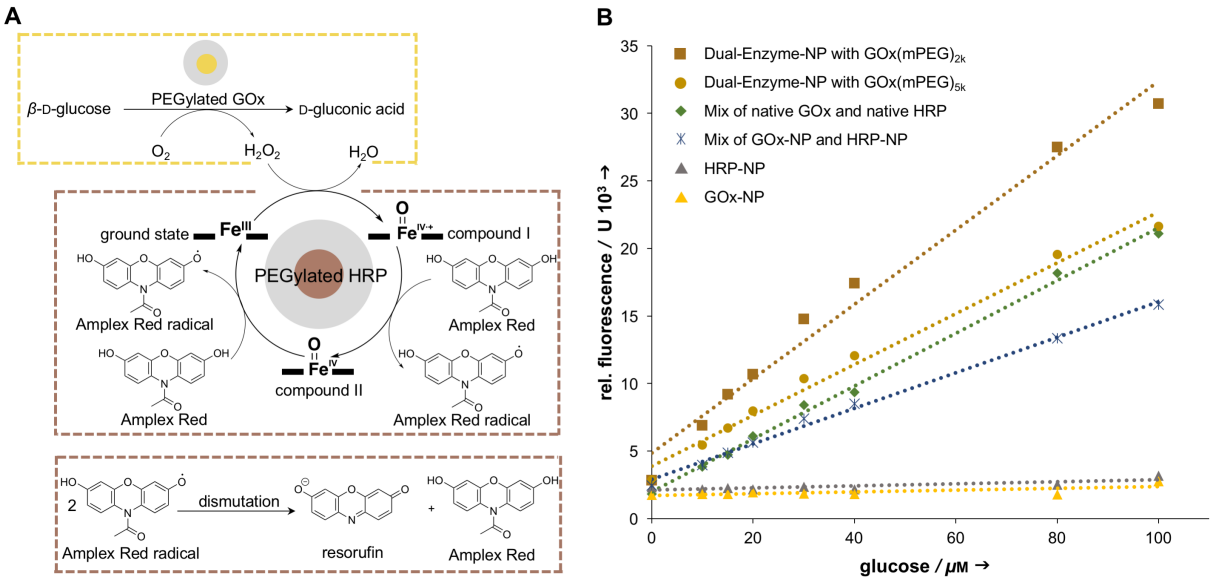

Figure 59: The Amplex Red Assay with the dual-enzyme NPs. The GOx-HRP cascade reaction within the nanoparticle system is shown in detail for the PEGylated variants of both enzymes (yellow and brown points with grey halo): the reaction starts with the conversion of β-D-glucose by PEGylated GOx, yielding D-gluconic acid and H_2O_2 (yellow box). Subsequently, hydrogen peroxide reacts with the HRP in a three steps reaction cycle, yielding two Amplex Red radicals (first brown box). In a dismutation reaction, these both radicals react to the highly fluorescent dye resorufin (second brown box) (**A**). Result of the Amplex Red assay. The different enzyme materials were investigated over a glucose concentration area of 0–100 μM. The resulting slope correlates with the enzymatic activity of the individual samples (**B**).

The main experiment of interest looks at the catalytic activity of the dual-enzyme-NP containing both PEGylated GOx and HRP within one particle system. As control, we also analyzed native (non-PEGylated) GOx and nanoparticles which contain only one type of enzyme (GOx-NP and HRP-NP). The solution of the native GOx contains additionally native HRP (in the same concentration as presented in the dual-enzyme nanoparticle system), in order to compare the catalytic activity of the native enzymes with the modified ones in the dual-enzyme nanoparticle system.

Additionally, a mix of both individual enzyme-based NPs (i.e. mix of "pure" GOx-NP and "pure" HRP-NP) was investigated. Here, the idea was to determine whether the proximity of the individual enzymes in one particle system has an effect on the cascade reaction. Glucose acts as the substrate in this assay and was incubated in different concentrations (0–100 μM) with the corresponding enzyme samples for 3 h. After that, the non-fluorescent dye Amplex Red was added and the solution was shaken for 5 minutes before read out (ex: 563 nm / em: 587 nm).

As expected, no cascade reaction proceeds when only HRP-NPs or GOx-NPs are present. Thus, side reactions from these materials can be excluded. In contrast, both dual-enzyme nanoparticle systems show an increased conversion of β-D-glucose compared to the native non-PEGylated enzymes in solution (Figure 59B). Moreover, the nanoparticle system containing GOx(mPEG)$_{2k}$ material and PEGylated HRP, shows a higher substrate conversion compared to the nanoparticle system containing GOx(mPEG)$_{5k}$. In general, this result confirms that the cascade reaction takes place in both enzyme-dual NP systems. Additionally, the PEGylation step and the nanoparticle preparation seem to have no negative effect on the enzymatic activity of GOx and HRP. A mix (ratio 1:2.5) of both individual enzyme nanoparticles (GOx-NP, HRP-NP) results in lower fluorescence signals, indicating a lower conversion rate of β-D-glucose over time. Thus, the enhanced catalytic activity of the dual-enzyme systems can be credited to the close proximity of both enzymes within one single particle system.

Investigation of the Catalytic Activity Using the ABTS Assay

To investigate the cascade reaction in more detail and to determine all kinetic parameters according to the Michaelis-Menten model, an ABTS assay was performed. Like already shown for the other prepared enzyme materials (see Chapter 3.2.3), this colorimetric method enables a suitable quantification of initial rates of enzymatic reactions and is based on the already mentioned reaction cascade shown in Figure 45.

In the beginning, all used materials such as the PEGylated GOx samples, the PEGylated HRP samples and the corresponding nanoparticles (ratio 1:2.5) were investigated individually. Native (non-PEGylated) GOx and HRP served as control.

β-D-glucose represents again the substrate and was added in different concentrations to a solution of colorless ABTS and the corresponding enzyme samples. The increase in absorbance of the resulting chromogenic ABTS radical was measured over a time of 3 min at 405 nm. In order to detect the ABTS radical, the cascade reaction must proceed. Therefore, every solution contains both enzymes in corresponding amounts and "states" (e.g. as native enzyme, as PEGylated form, or as NP system). The determined parameters and calculated kinetic values are presented in Table 14.

Table 14: Calculated kinetic parameters for all used enzyme materials in a 1:2.5 ratio. The investigations were divided into the use of 2 kDa PEG and 5 kDa PEG for the GOx modification. The HRP modification was performed using NHS-mPEG$_{5k}$.

PEG	**sample**	**substrate**	**Michaelis constant K_M (mM)**	**turnover rate k_{cat} (s^{-1})**	**catalytic efficiency k_{cat}/K_M (s^{-1} mM^{-1})**
	GOx + HRP	glucose	4.30 ± 1.12	3558.40	827.53
2 kDa	GOx(mPEG) + HRP	glucose	30.22 ± 3.16	460.80	15.24
	GOx(mPEG) + HRP(mPEG)		30.85 ± 2.12	640.00	20.74
	Dual-Enzyme-NP		10.69 ± 1.35	1561.60	146.08
	GOx-NP + HRP-NP		13.21 ± 0.28	1126.40	85.27
5 kDa	GOx(mPEG) + HRP	glucose	9.11 ± 3.05	3507.20	384.98
	GOx(mPEG) + HRP(mPEG)		8.91 ± 1.76	2995.20	336.16
	Dual-Enzyme-NP		21.69 ± 1.25	793.60	36.59
	GOx-NP + HRP-NP		29.15 ± 2.04	1664.00	57.08

First, the results containing the PEGylated GOx samples with the shorter mPEG chains (GOx(mPEG)$_{2k}$) will be discussed: The modification of GOx with mPEG$_{2k}$ leads to a significant decrease of the substrate affinity (K_M = 30.22 mM) compared to native GOx, which has a K_M value of 4.30 mM. In these both investigations, native HRP was used as peroxidase in the assay. Adding PEGylated HRP to the PEGylated GOx sample, results in similar K_M values (K_M = 30.85 mM). The PEGylation of HRP seems to have a minimal influence on the cascade reaction. This can be explained by the small size of the substrate H_2O_2 which can easily reach the heme group of HRP, even if the enzyme is highly shielded by PEG.

In addition, separate investigations of HRP samples alone (using H_2O_2 as a substrate) show that the surface modification has no effect on the catalytic activity (K_M = 0.032 mM for modified HRP, 0.034 mM for the native one, see also Table 9). In contrast, looking at the samples containing PEGylated GOx, it seems that the polymer chains on the enzyme surface shield off the active site of GOx and reduce the access for *β*-D-glucose (K_M = 30.22 mM for GOx(mPEG) + HRP, K_M = 4.3 mM for native GOx and HRP). The combination of the two PEGylated enzymes into one dual-enzyme-NP system results in a considerable increase of the enzymatic activity (K_M = 10.69 mM), in comparison to the individual materials. The spatial proximity seems to have a high impact on the catalytic activity and results in faster cascade kinetics. When mixing pure GOx-NPs and HRP-NPs in the same 1:2.5 ratio it results in a K_M value of 13.21 mM. This indicates a slightly lower affinity for *β*-D-glucose compared to the dual-enzyme system and confirms the previous results of the Amplex Red assay. Again, it can be concluded, that the dual-enzyme-NP system, using GOx(mPEG)$_{2k}$ and HRP(mPEG)$_{5k}$ shows an improved catalytic activity.

Next, the results containing the PEGylated GOx samples with the longer mPEG chains (GOx(mPEG)$_{5k}$) will be discussed: The GOx(mPEG)$_{5k}$ material demonstrates higher substrate affinities (K_M = 9.11 mM) compared to the GOx(mPEG)$_{2k}$ material (K_M = 30.22 mM). One reason could be, that the introduced polymers were attached to different amines on the surface of the enzyme, resulting in a changed accessibility of the *β*-D-glucose substrates to the catalytic center of GOx. Similar to the previous results, the use of PEGylated HRP again leads to no change of the overall enzymatic activity (K_M = 8.91 mM). However, looking at the dual-enzyme nanosystem, the substrate affinity decreases with a K_M value of 21.69 mM compared to the GOx(mPEG)$_{2k}$ system with a higher affinity and a K_M value of 10.69 mM. The use of 5 kDa mPEG seems to lead to a higher shielding of the catalytic center of GOx within the particle system and results in a decreased enzymatic activity. Investigating the mix of both individual NP systems (GOx-NPs and HRP-NPs) results again in slightly higher K_M values (K_M = 29.15 mM). Again, the results highlight the advantage of the dual-enzyme system in comparison to the individual NPs.

Looking at the catalytic efficiency of the prepared enzyme materials, all calculated turnover rates do conform to the described substrate affinities. Thus, materials with lower K_M values have high turnover rates, indicating the conversion of a larger number of substrate molecules by one enzyme per second.

Since the GOx(mPEG)$_{2k}$ material combined with PEGylated HRP leads to the best results regarding catalytic activity for the dual-enzyme-NPs, these compounds were used for further NP preparations in different ratios. It was the aim to evaluate, whether the individual enzyme quantities have an influence on the cascade reaction within the particle system. For this, three different amounts of GOx and HRP were chosen (Table 15). The given ratios refer again to the individual enzyme concentrations, not to the used amount of PEGylated material. To the already selected ratio of 1:2.5, a nanoparticle system containing an excess of HRP in proportion to GOx was prepared (ratio 1:5). Additionally, a particulate system with equal amounts of both enzymes was formulated (ratio 1:1). In an independent ABTS assay these three particle systems were investigated.

Table 15: Kinetic Parameters of dual-enzyme nanoparticles in three different ratios. GOx(mPEG)$_{2k}$ and HRP(mPEG)$_{5k}$ were used for the three NP preparations.

ratio	material	substrate	Michaelis constant K_M (mM)	turnover rate k_{cat} (s^{-1})	catalytic efficiency k_{cat}/K_M (s^{-1} mM^{-1})
1:1	GOx(mPEG)$_{2k}$-HRP(mPEG)$_{5k}$-NP	glucose	4.72 ± 0.27	847.75	179.61
1:2.5			11.70 ± 2.22	2327.37	198.92
1:5			14.16 ± 1.78	3005.46	212.25

Kinetic investigations of these three materials show that the 1:1 NP system has the highest substrate affinity (K_M = 4.72 mM). An increase of the HRP amount results in a decreased affinity for β-D-glucose (K_M = 14.16 mM). Comparing the turnover rates of the three nanoparticle systems, it should be noted that this kinetic parameter is lower for the 1:1 system than for the 1:5 nanomaterial even though the 1:1 system has a higher substrate affinity. This result raises the question, why a system which contains a high substrate affinity, shows a lower turnover rate and consequently a lower catalytic efficiency. To explain these values, the GOx-HRP cascade reaction within the particle system should be considered. For illustration, we look inside the particle system which contains equal amounts of both enzymes and imagine exemplary one GOx molecule and one HRP molecule. The glucose oxidase represents the rate-determining step, as the cascade reaction only starts after the formation of H_2O_2 by this enzyme.

A relatively high amount of GOx within the nanoparticle system (in our example 1:1) enables a fast conversion of the added glucose but leads simultaneously to a relatively high amount of hydrogen peroxide. This generated H_2O_2 can now only be oxidized by the available HRP molecules. Consequently, the concentration of generated $ABTS^{+\bullet}$ molecules is lower in the considered period. The chosen experiment setup does not allow a faster conversion of H_2O_2 by HRP, resulting in lower reaction speeds in the NP example with the 1:1 ratio, and subsequently lower turnover ratess and catalytic efficiencies. In contrast, increasing the amount of HRP (in the 1:5 example) can oxidizes more of the generated H_2O_2 per time and leads to an increased cascade turnover rate and an overall improved catalytic efficiency.

To validate the results for the dual-enzyme system with the highest glucose affinity, all used materials were investigated in a ratio of 1:1 (see Table 16; in comparison to the previous detailed assays in a ratio of 1:2.5 which are shown in Table 14). Applying all materials in equal enzyme quantities leads in general to lower K_M values (Table 16). In detail, the PEGylated enzymes in solution show similar affinities (K_M = 2.77 mM) as those calculated for native ones (K_M = 2.73 mM). The formulation of both PEGylated materials in a dual-enzyme particle system leads to a slight loss of the substrate affinity (K_M = 4.1 mM). However, comparing this number with the 1:2.5 NP system (K_M = 10.69 mM, Table 14), an improved binding can be observed. At the chosen conditions, the turnover rates are lower compared to the previously performed reactions containing higher HRP amounts (compare with Table 14 and Table 15). This result confirms the already acquired parameters and the assumption that an increased HRP concentration within the particle system, leads to higher reaction rates. The mix of the two individual particle systems (GOx-NPs and HRP-NPs) results again in a slightly higher K_M value (K_M = 6.3 mM), which in turn confirms the advantage of a dual-enzyme particle system. Also, when comparing the value with the 1:2.5 NP system (K_M = 13.21 mM, Table 14) the binding is improved.

Table 16: Determination of Michaelis-Menten kinetics using the ABTS assay with all samples in an enzyme concentration ratio of 1:1.

sample	substrate	Michaelis constant K_M (mM)	turnover rate k_{cat} (s^{-1})	catalytic efficiency k_{cat}/K_M (s^{-1} mM^{-1})
GOx + HRP	glucose	2.73 ± 0.81	1505.19	551.35
GOx(mPEG) + HRP		4.82 ± 1.27	2128.03	441.50
GOx(mPEG) + HRP(mPEG)		2.77 ± 0.44	1470.59	530.90
Dual-Enzyme-NP		4.1 ± 0.66	899.65	219.42
GOx-NP + HRP-NP		6.3 ± 1.78	1799.31	285.60

In conclusion, the combination of both biomacromolecules in equal amounts (1:1) represents a dual-enzyme nanosystem which exhibits the highest substrate affinity but features at the same time a lower turnover rate and catalytic efficiency, respectively. Looking at application opportunities for the dual-enzyme-NP systems, especially as a glucose sensor, the substrate affinity is more important to obtain a highly sensitive system. In contrast, to achieve a highly efficient system, higher reaction speeds are preferable. Thus, higher HRP concentrations (like 1:5) should be chosen for the particle preparation. These findings present the variability of the developed dual-enzyme particle systems. Depending on the desired application, it is possible to combine the different enzymes in different ratios to obtain the requested sensitivity or speed.

3.3.4 Application of the Dual-Enzyme Nanoparticles

In this section, the dual-enzyme particle system with the highest glucose affinity (ratio 1:1) was investigated in more detail for a specific application as glucose sensor. In literature, both enzymes are described as popular macromolecules for glucose monitoring.[97f] Using this coupled system, the enzymes are often immobilized onto electrodes,[185] attached to magnetic particles[97c] or silica nanoparticles.[97b] All these sensors show a remarkable glucose detection limit of 0.04 to 400 μM.

To verify the sensitivity of our prepared dual-enzyme particle system, a buffered solution which contains glucose concentrations from 0.25–6 mM was investigated using ABTS as a chromogenic indicator. The absorbance measurements indicate the substrate sensitivity down to concentrations of 0.25 mM (Figure 60).

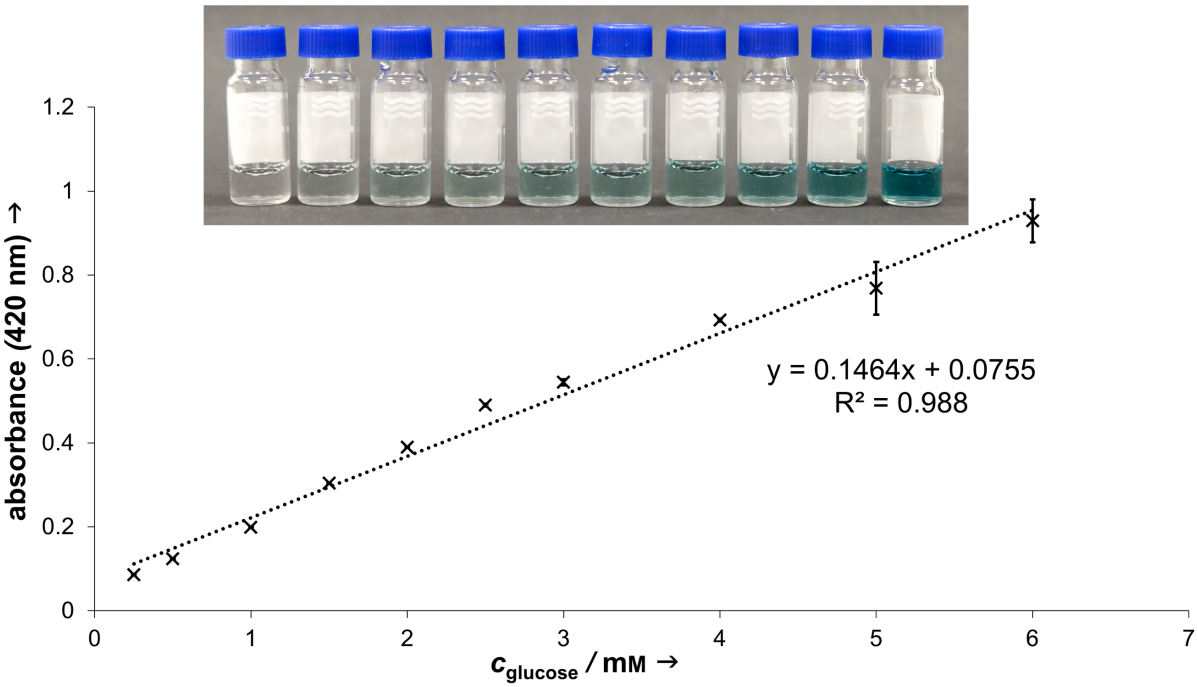

Figure 60: Absorbance measurements of the dual-enzyme particle system with ABTS (0.25 mM) and glucose concentrations of 6–0.25 mM. The sensitivity of the dual-enzyme particle system can be visualized.

However, in comparison to the best literature known sensors, the prepared dual-enzyme nanoparticle system does not reach the same sensitivity. This outcome can be explained with the chosen experiment setup. The investigated 1:1 dual-enzyme particle system has a high substrate affinity for *β*-D-glucose, which is preferable. However, this particle material shows lower turnover rates in the performing ABTS assay in comparison to the developed systems which contain higher amounts of HRP (ratio 1:2.5 and 1:5, compare Table 14–16). Thus, within a considered time, the 1:1 system leads to the formation of less $ABTS^{+\bullet}$ molecules than the 1:2.5 and 1:5 particles. Since we only regard the amount of formed cation radicals at a defined substrate concertation, and not the substrate affinity, only a glucose sensitivity up to a detection limit of this colorimetric assay can be performed.

Hence, a further reduction of the substrate concentration would lead to a lower a $ABTS^{+\bullet}$ formation which results in no detectable absorption values. The combination of these factors leads to the received result. Nevertheless, the prepared system is 10-times more sensitive than usual urine test strip methods. The dual-enzyme nanoparticles would be able to detect very low glucose concentrations in urine, even when a disorder with low glucose levels exists, like in the case of diabetes.

To substantiate our assumption, that the dual-enzyme particles which contain higher amounts of HRP would lead to the formation of more $ABTS^{+\bullet}$ molecules in the considered time, we investigate the glucose sensitivity of the 1:5 system (Figure 61). At same glucose concentrations, the 1:5 system shows higher absorption values than the 1:1 nanoparticle system. A lower glucose detection limit of 0.0625 mM was determined with this system, in comparison to the 1:1 system (0.25 mM). This result can be traced back to the higher turnover rates, thus the higher catalytic efficiency of this system (see Table 15). This presented investigation does not correlate directly with the substrate affinity.

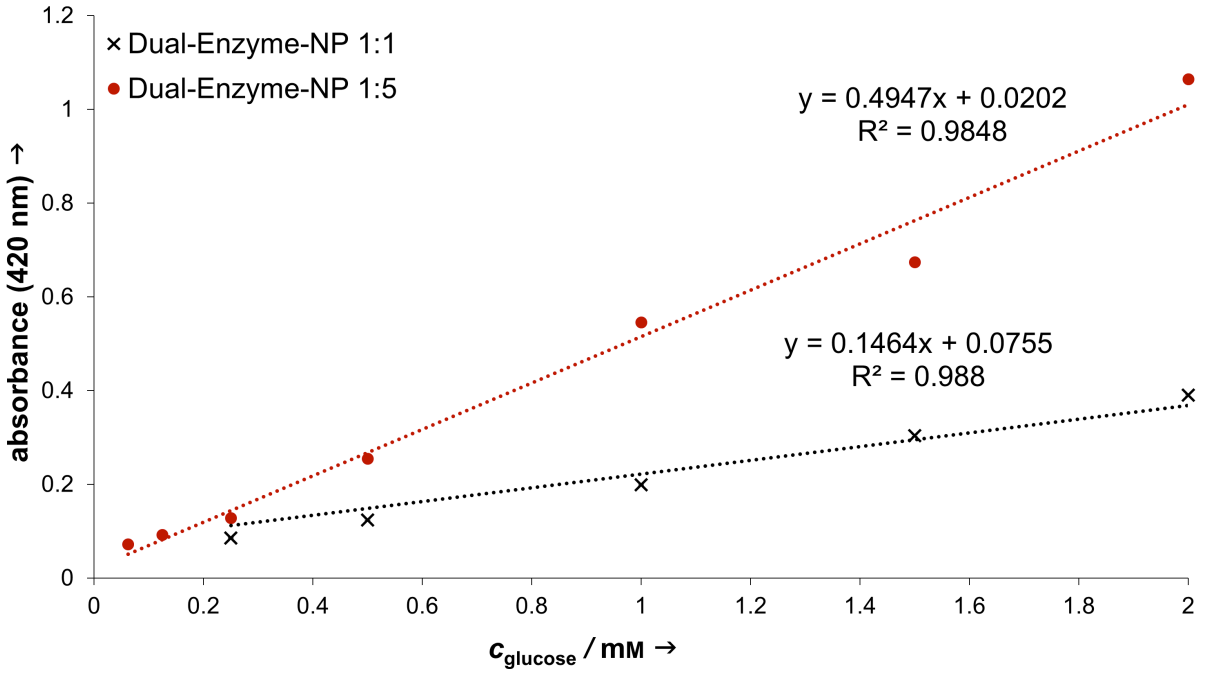

Figure 61: Absorbance measurements of the dual-enzyme particle systems with a ratio of 1:1 (black crosses) and the 1:5 system (red points) in the presence of 0.25 mM ABTS and glucose concentrations of 2–0.0625 mM.

In conclusion, these absorption studies demonstrate the diversity of the developed dual-enzyme systems regarding substrate sensitivity and catalytic efficiency. According to the ABTS assay, the combination of PEGylated GOx and surface-modified HRP in a 1:5 ratio results in highly efficient systems with higher reaction speeds, in comparison to the 1:1 dual-enzyme nanoparticles. This could be confirmed with the presented absorption measurement. The particle system which contains both biomacromolecules in equal amounts (1:1), though showed improved substrate affinities in the ABTS assay. Unfortunately, this characteristic could not be shown in the presented absorption measurement, which considers only the amount of formed $ABTS^{+\bullet}$ molecules at a certain glucose concentration. Nevertheless, it can be stated that it is possible with the presented emulsion technique to combine GOx and HRP in different ratios to obtain the requested sensitivity or speed of a particle system.

4 CONCLUSION AND OUTLOOK

The main focus of this thesis was the development of catalytically active enzyme-based nanosystems. The design of the nanoparticles and the investigation of their catalytic performance revealed new results, leading to the creation of new bio-inspired, catalytic nanomaterials. The following conclusion will recap the most important findings.

4.1 Enzyme Surface PEGylation under Activity Preservation

The first project of this thesis focused on the evaluation of four different PEGylation methods to achieve a high-density surface modification of lysozyme. For this, linear PEG chains were end group activated in order to react with nucleophilic amino acids on the enzyme surface. This modification led to a lipophilic behavior of the biomaterial. The solubility in organic solvents allowed the application of an emulsion-based solvent evaporation method as nanoparticle preparation technique. This led to the formation of stable nanomaterials in the size range of 100–130 nm, without the use of crosslinking or denaturation steps. The resulting nanoparticle characteristics (size, surface potential, particle stability and toxicity) meet important requirements necessary for therapeutic applications.

Four different electrophilic linkers, which differ in their chemical functionality, reactivity and stability were used for the PEG activation. The characteristics of the individual synthesized PEG chains have an effect on the protein conjugation. It has been shown that the efficiency and the extent of enzyme modification significantly vary among the different PEGylation methods. The various reactivities and modification efficiencies are important to consider when differently sized enzymes are modified. In the case of lysozyme, all methods led to the desired enzyme conjugates that are soluble in organic solvents. Therefore, other criteria are gaining importance in the selection of the PEGylation agent. When looking at the initial synthesis of the activated PEG chain, both epoxy and TFP end groups demonstrated the quickest, easiest and cleanest synthesis routes. Since the activation with epichlorohydrin required standard -OH terminated mPEG (in comparison to a carboxylic acid mPEG for TFP reaction) the epoxy activation should be preferred.

When looking at structural alterations and the protein activity, mild and non-destructive surface PEGylations are desirable. Again, the modification with epoxy-mPEG represented the method of choice, due to the relatively minor loss of catalytic activity (20% less compared to native LYZ).

In conclusion, the presented PEGylation methods have the potential to be universally applied for any enzyme of interest in order to increase its lipophilic character. These results extend the current toolkit of possible mildly methods for the high-surface PEGylation of enzymes and can advance the development of new and innovative enzyme-based materials. Furthermore, the developed protein-based nanoparticles represent remarkable delivery systems due to their biocompatibility, biodegradability and non-toxicity. The presented emulsion-based technique enables the entrapment of hydrophobic drugs. Since the successful encapsulation of the anti-cancer drug doxorubicin was already presented in our group, these carriers can be applied to the delivery of other poorly water-soluble drugs.

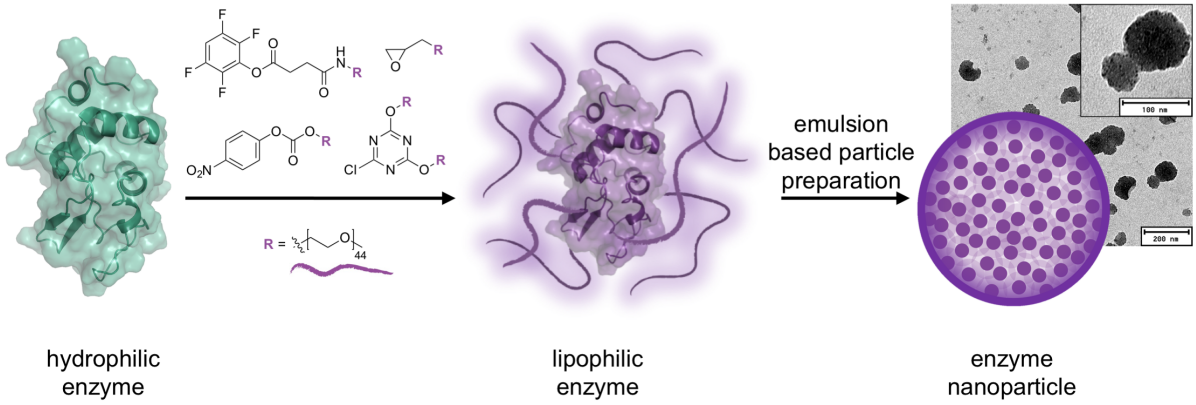

Figure 62: The LYZ surface PEGylation was performed using four different activated PEG chains. This results in a lipophilic enzyme material, which can be used for the preparation of enzyme-based nanoparticles by an emulsion-based technique. The performed method lead to spherical enzyme-based nanomaterials.

4.2 Design of Catalytically Active Enzyme Nanoparticles

The main goal of this PhD thesis was the development of catalytically active enzyme-based nanosystems. In the second project, this idea was implemented using three peroxidases Cyt *c*, HRP and Cat. Non-toxic, enzymatically active biopolymer-based nanosystems (115–145 nm) were developed, using the single emulsification method.

Looking at the PEGylation step, it has been shown that the first experiences of the lysozyme surface modification cannot be easily transferred to the conjugation of the peroxidases. Based on the different reactivity behaviors of enzymes, the most commonly used and highly reactive NHS-mPEG acylating agent had to be utilized. Moreover, the use of high molecular weight PEGs (5 kDa) was necessary for the surface PEGylation of large enzymes such as HRP and Cat in order to achieve a lipophilic enzyme material.

The investigation of the catalytic efficiency of the designed enzyme nanomaterials represented the main analysis of the second project. Looking at the initial enzyme PEGylation, the surface modification of Cyt *c* and HRP led to enzyme-polymer conjugates with a slightly enhanced catalytic efficiency. The PEGylation of Cat resulted in a significant decrease of the peroxidase activity. Based on enzyme characteristics such as structural composition, physicochemical stability as well as the integrity of the catalytic center, the surface alteration had different effects on the enzymatic activity. The following sonication treatment during the particle preparation showed again no influence on the catalytic activity of Cyt *c* and HRP, whereas the processing of the Cat-PEG conjugates led to a decreased peroxidase efficiency. Nevertheless, the prepared nanoparticles retained a sufficiently catalytic activity and presented artificial nanomolecular machines which can be used for the modulation of cellular pathways. This was demonstrated in independently enzymatic activity assays where the nanosystems act as a redox-active biomaterial and degrade both extra- and intracellular H_2O_2. The kinetic results of the developed enzyme materials correlated with the intrinsic catalytic differences of the used peroxidases. As expected, native catalase showed the highest turnover rates for H_2O_2 in comparison to native Cyt *c* and HRP. But looking at the processing of the individual enzymes, the utilization of Cyt *c* and HRP resulted in nanomaterials with the best retained catalytic activity. Since PEGylated Cyt *c* and the resulting Cyt-NPs showed an enhanced extra- and intracellular catalysis compared to the HRP materials, Cyt *c* should be preferred as biomacromolecule.

In conclusion, an engineered peroxidase-based nanosystem, which performs catalysis inside of cells was successfully developed. As demonstrated here, the particle preparation can be universally applied to other different sized enzymes. Thus, this method offers the possibility to be transferred to a wide range of enzymes in order to modulate various cellular processes. To get a better insight of the intervention of the enzyme-based materials within the cellular environment, uptake mechanisms of the particles should be considered more detailed in future. For this, the assumed endocytosis pathway can be tracked by using, for example, various fluorescent markers known from the literature. With the knowledge that the developed nanoparticles are able to reach certain cellular compartments, more specifically and more efficient enzyme-based systems can be created. Since the designed enzymatically active NPs can also be considered as classical drug delivery carriers, combined therapeutic approaches might be possible for treatment of various diseases.

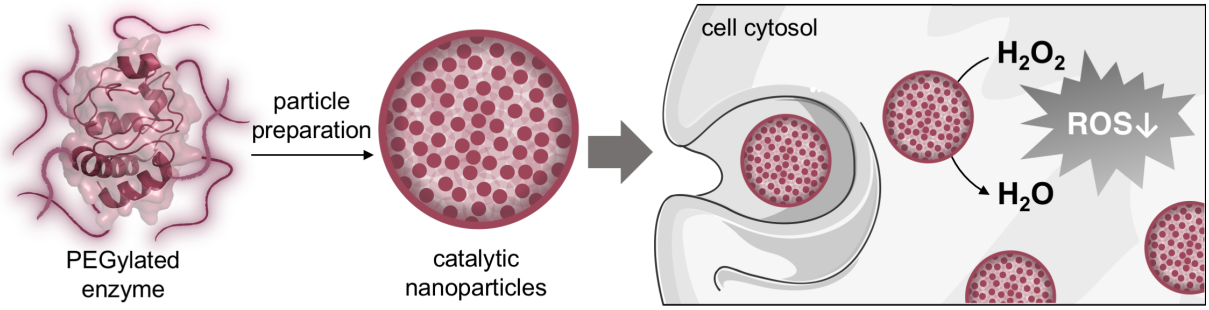

Figure 63: The enzyme PEGylation and the emulsion-based nanoparticle preparation lead to the design of catalytically active enzyme-based nanomaterials. After the cellular uptake, these particles are able to perform catalysis within the cell and to reduce harmful H_2O_2 concentration.

4.3 Cascade Reactions in Enzyme-based Nanoparticles

The third project of this PhD thesis focused on the development of a dual-enzyme system, which are able to perform a cascade reaction. Utilizing PEGylated GOx and HRP respectively, resulted in fully active nanoparticle systems in a size range of 120–180 nm.

Starting again with the surface modification, GOx was fully soluble in organic solvents after the introduction of PEG chains using either the epoxy-mPEG$_{2k}$ or the NHS-mPEG$_{5k}$ derivatives.

Since the PEGylation with epoxy-mPEG$_{2k}$ led to the formation of a more reactive GOx-polymer conjugate within the dual-enzyme particle system, compared to the resulting GOx material when using the higher molecular weight PEG, this PEGylation agent should be preferred for the modification of GOx. This result demonstrated again the different behavior of enzymes towards PEGylation methods and indicates how important it is to consider the individual characteristics of enzymes in the selection of their PEGylation agent.

Focusing on the cascade reaction and the resulting kinetic parameters of the dual-enzyme particle systems, promising results regarding reaction kinetic and substrate affinity were determined. The use of both enzymes in a 1:1 ratio for the particle preparation, resulted in nanoparticles with the highest substrate affinity. The combination of PEGylated GOx with an excess of modified HRP led to dual-enzyme systems with higher turnover rates. This result demonstrates the diversity of the used preparation method. Depending on the desired application, it is possible to combine the different enzymes in different ratios to obtain the requested sensitivity or speed.

Looking at possible applications, the created 1:1 system represents a suitable biosensor for glucose monitoring. The presented variability of the dual-enzyme system offers the potential to be generally applied for other cascade coupled enzyme systems. Inspired by the developed nanoreactors by Stephen Mann and co-workers, the designed dual-enzyme nanoparticle systems could represent a catalytically active material within a created compartment, which could undertake a task in order to imitate catalysis of cells.

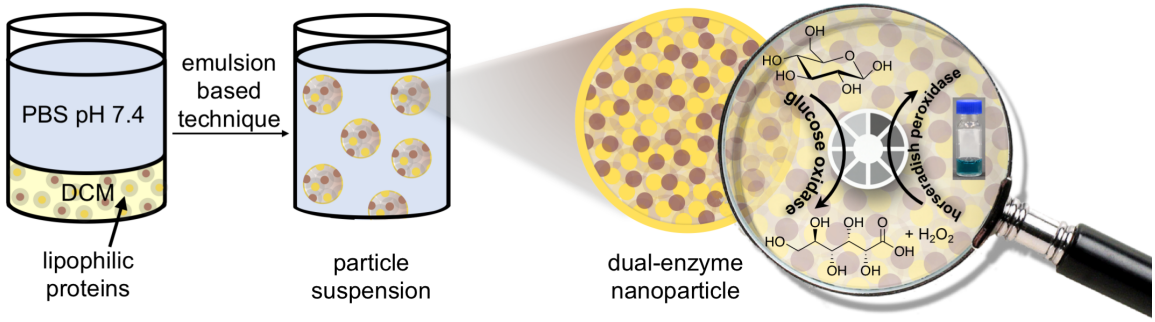

Figure 64: The combination of two PEGylated enzymes in a single emulsion-based technique leads to a catalytically active dual-enzyme nanomaterial. The co-embedded enzymes are able to perform a cascade reaction within the particles system, yielding the green $ABTS^{+\bullet}$ molecules, which was utilized as a chromogenic indicator.

5 EXPERIMENTAL PART

5.1 Materials

5.1.1 Reagents and Solvents

Chemical	Supplier	CAS
Acetic acid	Sigma Aldrich	64-19-7
ABTS	Alfa Aesar	30931-67-0
Aceton	Sigma Aldrich	67-64-1
Ammoniumperoxodisulfat	Carl Roth	7727-54-0
Benzene	Carl Roth	71-43-2
Catalase from bovine liver 11000 U/mg	Serva Electrophoresis	9001-05-2
Catalase from bovine liver 2000-5000 U/mg	Sigma-Aldrich	9001-05-2
Chloroform-*d*	Deutero	865-49-6
Cytochrome *c* from horse heart	Serva Electrophoresis	9007-43-6
Dichloromethane anhydrous, ≥99.8%, contains	Sigma-Aldrich	75-09-2
Diethyl ether	Carl Roth	69-29-7
DMEM GlutaMAX™	Sigma-Aldrich	
Epichlorohydrin	TCI	106-89-8
Fetal Calf Serum (FCS)	Life Technologies	
Fluorescein	Fluka	2321-07-5
D-(+)-Glucose	Sigma-Aldrich	50-99-7
Glucose Oxidase from *Aspergillus niger*	Sigma-Aldrich	9001-37-0
Glycine	Sigma Aldrich	56-40-6
n-Hexylamine	Sigma Aldrich	111-26-2
Horseradish peroxidase	Alfa-Aesar	9003-99-0
Hydrochloric acid 37%	Carl Roth	7647-01-0
Hydrogen peroxide solution 30%	Sigma Aldrich	7722-84-1
Lysozyme from chicken egg white	Sigma Aldrich	12650-88-3
4-Methylumbelliferyl β-D-*N*,*N*',*N*''	Sigma Aldrich	53643-13-3
p-nitrophenyl chloroformate	TCI	7693-46-1

PageRuler Prestained Protein Ladder (SM0671)	Thermo Scientific	
Penicillin-streptomycin (5,000 U/mL) Gibco™	Thermo Scientific	
Petroleum ether		
Phosphate buffered saline (10x concentrate)	Sigma Aldrich	
Polyethylenglycol (2000) monomethylether	Sigma Aldrich	9004-74-4
Polyethylenglycol (5000) monomethylether	Sigma Aldrich	9004-74-4
Polyethylenglycol (2000) *a*-methoxy-*ω*-carboxy	Rapp Polymere	
Polyethylenglycol (2000) *a*-methoxy-*ω*-NHS	Rapp Polymere	
Roti®-Histofix 4% acid free (pH 7)	Carl Roth	
Rotiload	Carl Roth	
Rotiphoresegel Gel30	Carl Roth	
Sodium chloride	Carl Roth	7647-14-5
Sodium dihydrogen phosphate	Amresco	7558-80-7
Sodium dodecyl sulfate	Carl Roth	151-21-3
Sodium hydroxide	Carl Roth	1310-73-2
Sulfo-Cyanine 5 NHS-Ester (Cy5-NHS)	Lumiprobe	
Tetrafluorophenol	Alfa Aesar	769-39-1
Tetrahydrofuran	Carl Roth	109-99-9
Thiazolyl blue tetrazolium bromide (MTT)	Sigma Aldrich	298-93-1
Toluene (anhydrous)	Sigma Aldrich	108-88-3
Trichloro-*s*-triazine	Sigma Aldrich	108-77-0
Triethylamine	Carl Roth	121-44-8
Trypsin from bovine pancreas	Sigma Aldrich	9002-07-7
Zinc oxide		1314-13-2

HeLa Cells

The carcinoma cell line was derived from a cervical cancer tissue sample of Henrietta Lacks (February 8 in 1951). Cells with passage numbers of 15–25 were used for all investigations.

5.1.2 Buffers and Media

All buffers and media were prepared using purified water (Direct-Q®) and filtered through a sterile syringe filter with a pore size of 0.22 μm (CME membrane, Rotilabo®). Aqueous buffers were stored at 4 °C to prevent contamination.

Borate Buffer (0.1 M, pH 7)

6.18 g boric acid (M_W 61.83 g mol^{-1}) were dissolved in water (1 L) and adjusted with NaOH to pH 7.

Borate Buffer (0.1 M, pH 10)

6.18 g boric acid (M_W 61.83 g mol^{-1}) were dissolved in water (1 L) and adjusted with NaOH to pH 10.

Carbonate Buffer (0.1 M, pH 8)

10.60 g sodium carbonate (M_W 105.99 g mol^{-1}) were dissolved in water and the pH was adjusted with NaOH to pH 8.

CD Buffer (10 mM K_3PO_4, 50 mM Na_2SO_4 pH 7)

2.12 g potassium phosphate (M_W 212.27 g mol^{-1}) and 7.10 g sodium sulfate (M_W 142.04 g mol^{-1}) were dissolved in water (1 L) and the pH was adjusted with NaOH to pH 7.

Coomassie Staining Solution

250 mg Coomassie Brillant Blue R-250 were dissolved in a mixture of water (45 mL), acetic acid (10 mL) and ethanol (45 mL).

Destaining Solution for Coomassie Stained Gels

A mixture of water (450 mL), ethanol (450 mL) and acetic acid (100 mL) was used.

DMEM for HeLa cells

DMEM GlutaMAX™ with phenol red was mixed with 10% FCS, 1% pyruvate and 1% penicillin-streptomycin.

Glycine Buffer (0.5 M, pH 12.0)

37.5 g glycine (M_W 75.07 g mol^{-1}) and 5.84 g sodium chloride (M_W 58.44 g mol^{-1}) were dissolved in water (1 L) and adjusted with NaOH to pH 12.0.

Phosphate Buffer (0.1 M, pH 5.2)

12 g sodium dihydrogen phosphate (M_W 119.98 g mol^{-1}) were dissolved in water and the pH was adjusted with NaOH to pH 5.2.

Phosphate Buffer (0.1 M, pH 6)

12 g sodium dihydrogen phosphate (M_W 119.98 g mol^{-1}) were dissolved in water and the pH was adjusted with NaOH to pH 6.

Phosphate Buffer (0.1 M, pH 8)

12 g sodium dihydrogen phosphate (M_W 119.98 g mol^{-1}) were dissolved in water and the pH was adjusted with NaOH to pH 8.

Phosphate Buffer (0.1 M, pH 8.5)

12 g sodium dihydrogen phosphate (M_W 119.98 g mol^{-1}) were dissolved in water and the pH was adjusted with NaOH to pH 8.5.

Phosphate Buffer (250 mM, pH 6)

30 g sodium dihydrogen phosphate (M_W 119.98 g mol^{-1}) were dissolved in water and the pH was adjusted with NaOH to pH 6.

Phosphate Buffer (0.05 M, pH 7)

6 mg sodium dihydrogen phosphate (M_W 119.98 g mol^{-1}) were dissolved in 1 mL water and the pH was adjusted with NaOH to pH 7.

Phosphate Buffer (10 mM, pH 7.4)

1.2 g sodium dihydrogen phosphate (M_W 119.98 g mol^{-1}) were dissolved in water and the pH was adjusted with NaOH to pH 7.4.

Running Buffer for Gel Electrophoresis (5x concentrated)

15.1 g Tris and 94 g glycine and a solution of SDS in water (20%, 25 mL) were dissolved with water to final volume of 1 L.

SDS 20% in water

20 g sodium dodecyl sulfate were dissolved in water to a final volume of 100 mL.

5.1.3 Disposables

Consumables	Supplier
Amicon® Ultra 15 mL, MWCO 30 kDa, 100 kDa	Merck Millipore
CELLSTAR® cell culture flasks 175 cm^2, 25 cm^2, 75 cm^2	Greiner Bio One
Disposable cuvettes, polystyrene	Carl Roth
Disposable hypodermic needles (size: 21 G)	B. Braun
Disposable pipettes 2 mL, 5 mL, 10 mL, 20 mL	Sarstedt
Disposable syringes 1 mL, 2 mL, 5 mL, 10 mL, 20 mL	B. Braun
Filtropur S 0.2 (sterile, non-pyrogenic)	Sarstedt
Microplate 12-well, flat bottom, clear, sterile	Greiner Bio-One
Microplate 96-well, flat bottom, clear, sterile	Greiner Bio-One
Microplate 96-well, flat bottom, clear	Sarstedt
Microplate 96-well, flat bottom, clear, UV-Star®	Greiner Bio-One
Microplate 96-well, flat bottom, black	Greiner Bio-One
Microsep™ Advance Centrifugal Devices (MWCO 30 kDa)	PALL
Pipette tips 2 μL, 250 μL, 1000 μL	Sarstedt
Slide-A-Lyzer™ Dialysis Cassettes (MWCO 10 kDa, 20 kDa)	ThermoFischer
μ-Slide 8 well plate	ibidi GmbH
Tubes 13 mL, 100×16 mm, polypropylene	Sarstedt
Tubes 15 mL, 120×17 mm, polypropylene	Sarstedt
Tubes 50 mL, 114×28 mm, polypropylene	Sarstedt

5.2 Equipment

Absorption and Fluorescence Measurements

Equipment: Infinite® Pro M200 Plate Reader, Tecan Group Ltd., Switzerland. Analysis was carried out using i-control 1.7 software and Microsoft Excel.

Absorption measurements were performed with clear 96-well microplates (flat bottom). Absorption measurements to determine protein concentrations (λ = 280 nm) were performed with 96-well UV-Star plates. Fluorescence measurements were performed with black 96-well microplates (flat bottom).

Atomic Force Microscopy

Equipment: Bruker Dimension Icon FastScan AFM, Bruker Corporation, Massachusetts, USA. Analysis was carried out using the software *Gwyddion* 2.38 and *NanoScopeAnalysis* 1.50.

Bath Sonicator

Equipment: Sonorex RK 102 H, Bandelin electronic GmbH & Co. KG, Berlin, Germany.

Biological Safety Cabinet

Equipment: Herasafe™, Kendro Laboratory Products, Langenselbold, Germany.

All cell culture experiments were performed in a sterile environment using a biological safety cabinet.

Centrifuge

Equipment: Heraeus™ Multifuge™ X3R, Thermo Scientific, Waltham, Massachusetts, USA.
Heraeus™ Megafuge™ 8 R, Thermo Scientific, Waltham, Massachusetts, USA.

Circular Dichroism (CD)

Equipment: J-815 Circular Dichroism Spectrometer, JASCO International co., LTD., Hachioji, Tokyo, Japan.
Analysis was carried out using the software Spectra Manager 2.12 00.

Measurements were performed at 20 °C in 1 mm and 5 mm path length quartz cuvettes (Hellma Analytics).

Dialysis

Equipment: Slide-A-Lyzer™ Dialysis Cassettes, MWCO 10 kDa / 20 kDa, ThermoFischer Scientific, Waltham, Massachusetts, USA.

Flow Cytometry

Equipment: BD LSRFortessa, BD Bioscience, USA.
Data processing was performed with FlowJo (Version 10.2.).

FT-IR

Equipment: Nicolet Avatar 330-IR ATR-Einheit, Thermo Electron Corporation.

All compounds were measured without further preparation on the diamond crystal surface of the device.

Gel Permeation Chromatography

Equipment: Agilent 1100 Series, Agilent Technologies, Santa Clara, USA.

Polymer Standards Service was used as external standard. A HEMA 300/100/40 column (l: 95.0 cm; d: 0.8 cm) was used with a flow rate of 1 mL/min at 50.0 °C. A refractive index detector (Agilent G1362A) and an UV detector (Agilent G1314A) were used for detection and the results were obtained with the Fa. PSS WinGPC Unity software.

Incubator

Equipment: Heraeus® BB15 FUNCTION Line, Thermo Scientific, Waltham, Massachusetts, USA.

Cell incubations were performed in a humidified incubator at 37 °C with 5% CO_2 atmosphere.

Inert Gas

Equipment: Argon gas bomb in 99.998% purity N46, Air Liquide Deutschland GmbH.

Argon was used as inert gas to flood flasks and reaction containers.

Lyophilizer

Equipment: ALPHA 1-4 LSC, Martin Christ Gefriertrocknungsanlagen GmbH.

Mass Spectroscopy (MALDI-ToF MS)

Equipment: Shimadzu Axima CFR MALDI-ToF mass spectrometer, Columbia, Maryland, USA.

Sinapinic acid was used as matrix. The samples were measured in positive ion and in linear mode of the spectrometer.

Microscopy

Equipment: Leica TCS SP5 Microscope (water immersion objective lens HCX PL APO CS 40.0x/1.10 WATER UV and an incubator for temperature and CO_2 control), Leica Mikrosysteme Vertrieb GmbH Mikroskopie und Histologie, Wetzlar, Germany.

Nanoparticle Tracking Analysis (NTA)

Equipment: NanoSight LM 14, NanoSight Ltd., Amesbury, Wiltshire, United Kingdom. Analysis was carried out using Nanosight NTA 3.1 software.

Nuclear Magnetic Resonance (NMR)

Equipment: Bruker Topspin Fourier 300 MHz.

For standard analytical purpose ^{1}H-NMR spectra were recorded at 300 MHz. The experiments were performed at room temperature using the indicated solvents. The chemical shifts were reported in ppm against the solvent signal of TMS. For the description of the signals the following abbreviations were used: s = singlet, d = doublet, t = triplet, q = quartet, m = multiplet, br = broad signal. Integrals were calculated by using MestReNova Software.

Particle Sonicator

Equipment: Bandelin Ultrasonic Homogenisator Sonoplus UW 70 (v220-240w), microtip MS 73 SH70G Stufenhorn 20 kHz, BANDELIN electronic GmbH & CO. KG, Berlin, Germany.

Sonication of all samples was carried out on an ice bath (Settings: power 75%, cycle 70% MS 72/D) for 45 s.

pH Measurement

Equipment: SevenCompact™ pH/Ion S220 with a InLab® Micro special electrode, Mettler Toledo, Mettler-Toledo Ltd., Beaumont Leys, Leicester, United Kingdom.

The pH-meter was calibrated with commercial available buffer standards (pH 4.00, pH 7.00, and pH 11.00).

Rotary Evaporation

Equipment: IKA RV06-ML Janke-Kunkel rotavapor; IKA HB4 basic water bath; Vacuubrand CVC24 vacuum controller; Vacuubrand 1715550193 Membrane pump.

Sample Incubation

Equipment: Thermomixer pro, CellMedia, Elsteraue, Germany.

Scales

Equipment: Mettler Toledo Excellence Plus. Sartorius™ M-Prove™ Scales AY303, Sartorius, Göttingen, Germany.

SDS Gel Electrophoresis

Equipment: Mini Vertical Electrophoresis Unit Hoefer SE260, Hoefer Inc., Holliston, Massachusetts, USA.
GelDoc XR$^+$ with Image LabTM Software, Bio-Rad Laboratories Inc., Hercules, California, USA.

The stacking gel was running for 45 min at 90 V, whereby the running gel was running for 45 min at 200 V.

Table 17. Composition of the stacking gel with a total volume of 2 mL for SDS-PAGE.

H_2O/ mL	Rotiphorese® 30/ mL	1 M Tris (pH 6.8)/ mL	20% SDS/ mL	10% APS/ mL	TEMED/ mL
1.37	0.34	0.26	0.01	0.02	0.002

Table 18. Composition of running gels with a total volume of 5 mL for SDS-PAGE.

PA Content/ %	H_2O/ mL	Rotiphorese® 30/ mL	1.5 M Tris (pH 8.8)/ mL	20% SDS/ mL	10% APS/ mL	TEMED/ mL
8	2.325	1.3	1.3	0.025	0.05	0.003
15	1.125	2.5	1.3	0.025	0.05	0.002

Transmission Electron Microscopy (TEM)

Equipment: Tecnai T12 (FEI, acceleration voltage: 120 keV, electron source: LaB6 BIO-TWIN cathode, TVIPS-F416 Camera), Hillsboro, Oregon, USA.

300-mesh copper carbon grids from Plano GmbH were used for sample preparation.

Water

Equipment: Direct-Q® 5 UV Remote Water Purification System, Merck Millipore, Germany.

Water (*dd*-H_2O) for buffers was purified by a Direct-Q® 5 UV Remote Water Purification System.

Zeta Potential

Equipment: Malvern Zetasizer Nano ZS, Malvern Instruments GmbH, Herrenberg, Germany.

5.3 Enzyme PEGylation

5.3.1 Activation of mPEG

mPEG Activation with Tetrafluorophenol (TFP-mPEG)

mPEG was activated according to Zhang *et al.*[161] DCC (24.8 mg, 0.12 mmol) was added at room temperature to a solution of *a*-methoxy-*ω*-carboxy PEG 2000 (200 mg, 0.1 mmol) and tetrafluorophenol (18.3 mg, 0.1 mmol) in dichloromethane (DCM) (15 mL). After being stirred for 24 h, the mixture was diluted with acetone (50 mL) and filtered. The solvent was removed under reduced pressure and the product was dried *in vacuo* (61.43%).

^{1}H NMR (300 MHz, $CDCl_3$, Me_4Si) δ(ppm) = 7.05–6.95 (m, 1H), 6.60–6.52 (m, 1H), 3.64 (s, 184H), 3.38 (s, 3H), 3.04 (t, J = 7.0 Hz, 2H), 2.64 (t, J = 7.2 Hz, 2H)

^{13}C NMR (600 MHz, $CDCl_3$, Me_4Si) δ(ppm) = 103.32, 70.69, 39.55, 30.54, 28.92

IR $\tilde{\nu}$ (max/cm^{-1}) = 2882vs (CH_3), 1651s (CO)

mPEG Activation with Epichlorohydrin (epoxy-mPEG$_{2k}$)

The activation of mPEG (2 kDa) with epichlorohydrin was synthesized according to Park *et al.*[162] Sodium hydride (137 mg, 5.7 mmol) and epichlorohydrin (531 mg, 5.7 mmol) were added to 20 mL of dry tetrahydrofuran (THF) under argon atmosphere. mPEG (1 g, 0.5 mmol) was added at 40 °C and stirred for 2 h. After the reaction, the mixture was filtered and poured into 200 mL of cold diethyl ether. The light-yellow solid was filtered, dissolved in THF and precipitated again with diethyl ether and dried *in vacuo* (92%).

^{1}H NMR (300 MHz, D_2O, Me_4Si) δ(ppm) = 3.98–3.90 (m, 2H), 3.69 (s, 163H), 3.37 (s, 3H), 3.36–3.30 (m, 1H), 2.95 (t, J = 4.3 Hz, 1H), 2.78–2.74 (m, 1H)

^{13}C NMR (300 MHz, DMSO, Me_4Si) δ(ppm) = 42.57, 49.96, 69.96

IR $\tilde{\nu}$ (max/cm^{-1}) = 2882vs (CH_3), 1466br (CO)

mPEG Activation with Epichlorohydrin (epoxy-mPEG$_{5k}$)

The activation of mPEG (5 kDa) with epichlorohydrin was synthesized according to the synthesis using the low molecular weight mPEG (2 kDa). Sodium hydride (115.15 mg, 4.8 mmol) and epichlorohydrin (444.14 mg, 4.8 mmol) were added to 40 mL of dry tetrahydrofuran (THF) under argon atmosphere. mPEG (2 g, 0.4 mmol) was added at 40 °C and stirred for 2 h. After the reaction, the mixture was filtered and poured into 400 mL of cold diethyl ether. The light-yellow solid was filtered, dissolved in THF and precipitated again with diethyl ether and dried *in vacuo* (85%).

^{1}H NMR (300 MHz, D_2O, Me_4Si) δ(ppm) = 3.70 (s, 474 H), 3.37 (s, 3H), 3.36–3.31 (m, 1H), 2.95 (t, J = 4.3 Hz, 1H), 2.78–2.74 (m, 1H)

mPEG Activation with *p*-nitrophenyl chloroformate (carbonate-mPEG)

Methoxypolyethylene glycol was activated according to Qi *et al.*[163] mPEG 2000 (1 g, 0.5 mmol) was dissolved in 100 mL of dry tetrahydrofuran (THF) at room temperature. *p*-nitrophenyl chloroformate (300 mg, 1.5 mmol) and triethylamine (150 mg, 1.5 mmol) were added, followed by stirring for 48 h at room temperature. The obtained carbonate mPEG mixture was purified by recrystallization of the product from diethyl ether and dried *in vacuo* (70%).

^{1}H NMR (300 MHz, $CDCl_3$, Me_4Si) δ(ppm) = 8.28 (d, J = 9.2 Hz, 2H), 7.40 (d, J = 9.2 Hz, 2H), 4.51–4.37 (m, 2H), 3.64 (s, 178H), 3.38 (s, 3H)

^{13}C NMR (300 MHz, $CDCl_3$, Me_4Si) δ(ppm) = 70.90, 121.74, 125.25

IR $\tilde{\nu}$ (max/cm^{-1}) = 2882vs (CH_3), 1766s (CO), 1616vw and 1594vw (NO)

mPEG Activation with TsT (TsT-mPEG)

TsT-activated mPEG 2000 was synthesized according to Inada *et al.*[164] *a*-Methoxy-*ω*-hydroxy polyethylene glycol (mPEG) (1 g, 0.5 mmol), molecular sieve (4 Å, 1 g), zinc oxide (1.14 g, 14 mmol) and 2,4,6-trichloro-1,3,5-triazine (TsT) (46.1 mg, 0.25 mmol) were added to 3 mL of anhydrous benzene and stirred at 80 °C for 72 h. The mixture was centrifuged (15000 g, 15 min.) and zinc oxide was separated. The supernatant was added drop wise with vigorous stirring to petroleum ether (30 mL). The product was isolated by centrifugation (15000 g, 15 min). The resulting pellet was redissolved in benzene and precipitated in petroleum ether (30 mL) again. The washing step was repeated for five times. The white solid was dried under reduced pressure and stored under argon atmosphere at –20 °C (74.28%).
Elemental analysis was performed to determine the nitrogen content (Found: C, 52.17; H, 10.88; N, 0.9. $C_{181}H_{358}N_3Cl$ requires C, 52.87; H, 8.71; N, 1.02%), indicates a modification of 88% of TsT with two mPEG chains per molecule.

^{13}C NMR (300 MHz, DMSO, Me_4Si) δ(ppm) = 68.77

IR $\tilde{\nu}$ (max/cm^{-1}) = 2882vs (CH_3), 1729s (CO), 759w (CCl)

Size Exclusion Chromatography (SEC)

The activated mPEGs were analyzed by size-exclusion chromatography (SEC). The measurements were performed in DMF containing 1 g L^{-1} lithium bromide (LiBr) with a sample concentration of 1-3 mg mL^{-1} on an Agilent 1100 Series, using PSS (Polymer Standards Service) as standard. A HEMA 300/100/40 column (*l*: 95.0 cm; *d*: 0.8 cm) was used with a flow rate of 1 mL min^{-1} at 50.0 °C (Agilent G1316A). A refractive index detector (Agilent G1362A) and an UV detector (Agilent G1314A) was used for detection and the results were obtained with the Fa. PSS WinGPC Unity software. The measurement was performed by Monika Schmelzer of the working group of Prof. Dr. H. Frey (JGU Mainz, Germany).

5.3.2 Fluorescence Labeling of Cyt *c*, HRP and Cat

The enzymes were respectively dissolved in 1 mL of 0.1 M borate buffer pH 7 and combined with sulfo-cyanin 5 NHS ester (used amount see Table 19). The mixture was stirred for 1 h at room temperature and shielded from light. The modified protein was purified by column chromatography (NAP™-25 Columns Sephadex™ G-25 DNA Grade, buffer: *dd*-H_2O). After lyophilization a fluffy blue product was obtained.

Table 19: Used amounts of Cyt *c*, HRP, Cat and the corresponding Cy5 concentrations.

enzyme	m / mg	n / μmol	m_{Cy5} / mg	n_{Cy5} / μmol
Cyt *c*	5	0.40	0.31	0.40
HRP	5	0.11	0.09	0.11
Cat	10	0.02	0.02	0.02

The fluorescent labelling was quantified by measuring the fluorescence (ex: 605 nm; em: 675 nm) of the modified protein in comparison to free Cy5 in triplets of 100 μL, using an Infinite® 200 PRO plate reader. The Cy5 standard was prepared in 0.1 M borate buffer pH 7. Cy5-labeled enzymes were dissolved in the same buffer and diluted to a corresponding concentration (see Table 20).

Table 20: Cy5 content of labeled enzymes.

enzyme	c / μM	M / kDa	Cy5:protein ratio	content of Cy5-labeled enzymes
Cyt *c*	38.57	12.96	0.0168:1	59
HRP	11.32	44.73	0.1968:1	5
Cat	2.08	240.56	0.3103:1	3

5.3.3 Enzyme PEGylation

Lysozyme PEGylation with TFP-mPEG, epoxy-mPEG and carbonate-mPEG

Lysozyme [EC 3.2.1.17] (15.0 mg, 1.0 μmol) was dissolved in 3 mL of 0.1 M carbonate buffer pH 8 and combined respectively with TFP-mPEG (48.4 mg, 22.0 μmol), epoxy-mPEG (44.0 mg, 22.0 μmol) or carbonate-mPEG (44.0 mg, 22.0 μmol). The mixture was stirred at room temperature for 48 h. The product was purified by dialysis (Slide-A-Lyzer® Dialysis Cassettes, 10000 MWCO) against water for 3–7 days and was then lyophilized.

Lysozyme PEGylation with TsT-mPEG

Lysozyme [EC 3.2.1.17] (5.0 mg, 0.3 μmol) was dissolved in 1 mL of 0.1 M borate buffer pH 10 and combined with activated TsT-mPEG (195.7 mg, 48.9 μmol). After 2 h at 40 °C the reaction was stopped with 2 mL 0.1 M phosphate buffer pH 6. The excess of mPEG was removed with Microsep™ centrifugal devices (MWCO 30 kDa) and the resulting solution was lyophilized.

Cytochrome *c* PEGylation with NHS-mPEG$_{2k}$

Cyt *c* [EC 232-700-9] or fluorescent labeled Cy5_Cyt (5.0 mg, 0.4 μmol) was dissolved in 1 mL of 0.1 M phosphate buffer pH 8.5 and combined with NHS-mPEG (2 kDa, 12.1 mg, 6 μmol). The mixture was stirred overnight at 4 °C. The reaction mixture was separated by column chromatography (NAP™-25 Columns Sephadex™ G-25 DNA Grade, buffer: *dd*-H_2O), yielding the modified enzyme in the first fraction. The product was lyophilized subsequently.

Horseradish Peroxidase PEGylation with NHS-mPEG$_{5k}$

Horseradish peroxidase [EC 1.11.1.7] or fluorescent labeled Cy5_HRP (5.0 mg, 0.11 μmol) was dissolved in 1 mL of 0.1 M phosphate buffer pH 8.5 and combined with NHS-mPEG (5 kDa, 68.68 mg, 13.6 μmol). The mixture was stirred 48 h at 4 °C. The reaction mixture was purified by centrifugal filter (Amicon Ultra centrifugal filter units, MWCO 30 kDa) for four times with water. The product was lyophilized subsequently.

Catalase PEGylation with NHS-mPEG$_{5k}$

Catalase [EC 1.11.1.6] or fluorescent labeled Cy5_Cat (5.0 mg, 0.02 μmol) was dissolved in 1 mL of 0.1 M phosphate buffer pH 8.5 and combined with NHS-mPEG (5 kDa, 56 mg, 11.2 μmol). The mixture was stirred 48 h at 4 °C. The reaction mixture was purified by centrifugal filter (Amicon Ultra centrifugal filter units, MWCO 100 kDa) for four times with water. The product was lyophilized subsequently.

Glucose Oxidase PEGylation with NHS-mPEG$_{5k}$ and epoxy-mPEG$_{2k}$

Glucose oxidase [EC 232-601-0] (2.5 mg, 0.015625 μmol) was diluted in 0.5 mL of 0.1 M phosphate buffer pH 8 and combined with either NHS-mPEG (5 kDa, 23.43 mg, 4.68 μmol) or epoxy-mPEG (2 kDa, 18.75 mg, 9.375 μmol). The mixture was stirred for 48 h at 30 °C. The reaction mixture was purified with a NAP-25 column (buffer: *dd*-H_2O). The product was lyophilized subsequently.

5.3.4 Analysis of Protein-Polymer Conjugates

SDS Gel Electrophoresis

SDS-PAGE was performed as described elsewhere[186] using 15% polyacrylamide gel (Rotiphorese® 30 gel mix) for low-molar weight enzymes (LYZ, Cyt *c*) and 8% polyacrylamide gel (Rotiphorese® 30 gel mix) for high-molecular weight proteins (HRP, Cat, GOx) with a thickness of 0.75 mm (T Spacer, Hoefer, USA). The gel was stained with Coomassie Brilliant Blue G. 5 μL of PageRuler Pre-Stained Protein Ladder (10–170 kDa) were used as marker. Samples of native enzymes (1 mg mL^{-1}) and PEGylated ones (4 mg mL^{-1}) were dissolved in water. The proteins were denaturized by adding 5 μL of Roti®-Load 1 (Carl Roth) to 15 μL protein solution and heating in a boiling water bath for 10 min. 20 μL was loaded on each bag. Images of SDS-PAGE gels were taken with the GelDoc™ XR+ (Bio-Rad Laboratories Inc.) and processed with the Image Lab™ Software (camera filter 1).

MALDI-ToF MS Measurement

MALDI-ToF MS measurements were obtained with a Shimadzu Axima CFR MALDI-ToF mass spectrometer, equipped with a nitrogen laser delivering 3 ns laser pulses at 337 nm. Samples were prepared by dissolving the sample in CH_3CN/TFA 0.1% at a concentration of ~ 1 mg mL^{-1}. 1 μL of this mixture was applied to a multistage target to evaporate and create a thin analyte film. Sinapinic acid was used as matrix and applied in the target before adding the sample. The samples were measured in positive ion and in linear mode of the spectrometer.

Fluorescamine Assay of Native LYZ and PEGylated Variants

A protocol for quantification of primary amines on the protein surface, based on fluorescence, was carried out. All samples were dissolved in PBS pH 7.4 at a concentration of 2 mg mL^{-1} and native lysozyme at a concentration of 0.2 mg mL^{-1}. Hexylamine was used as external standard in a concentration range of 19–40 μg mL^{-1} and was prepared similar. 125 μL PBS pH 7.4 was pipetted into each well of a black 96-well-microplate (flat bottom).

25 μL sample dispersion or 25 μL PBS (blank) or 25 μL standard were added in triplets to each well. Finally, 50 μL of 0.3 mg mL^{-1} fluorescamine solution (in acetone) was added, mixed and measured immediately. The emission was measured with a Tecan Plate Reader. For all measurements, the excitation was set to 380 nm, the emission was set to 460 nm.

Circular Dichroism (CD)

CD spectra were recorded on a J-815 (JASCO) using the software Spectra Manager 2.12.00. Far-UV CD spectra (240–190 nm) were recorded at 20 °C with a total concentration of 0.1 mg mL^{-1} in 10 mM K_3PO_4/50 mM Na_2SO_4 pH 7 buffer using quartz cells with a path length of 1 mm. Near-UV CD spectra (320–260 nm) and Soret band spectra (350–450 nm) were recorded at 20 °C with a total enzyme concentration of 0.32 mg mL^{-1} using the same buffer and a quartz cell with a path length of 5 mm. All spectra were corrected by subtraction from the background (buffer). Data points were collected at a resolution of 1 nm. Secondary structure contents were predicted with DICHROWEB using the CONTIN-LL method (reference set 7).[172] The Soret CD spectra was smoothed using the Spectra Manager (Version 2.12.00) means-movement with a convolution width 13.

5.4 Nanoparticle Preparation

5.4.1 Single Emulsion-Based Nanoparticle Preparation

Enzyme-based nanoparticles were prepared using a single emulsion method.[11, 29] If not mentioned separately, the PEGylated enzyme (2.5 mg) was dissolved in ice cold dichloromethane (DCM, 0.5 mL) and added to 2.5 mL of ice cold PBS buffer pH 7.4. The mixture was sonicated for 45 s on ice, using an ultrasonicator (Bandelin Ultrasonic Homogenisator Sonoplus UW 70, microtip MS 73 SH70G Stufenhorn 20 kHz). The emulsion was stirred in a well-ventilated hood overnight for the evaporation of DCM.

5.4.2 Nanoparticle Analysis

Nanoparticle Tracking Analysis (NTA)

Nanoparticle Tracking Analysis (NTA) was performed on a NanoSight LM 14 equipped with a green laser (532 nm) and a marlin charged coupled device (CCD) camera. Samples (NP stock solution 1 mg mL^{-1} in PBS) were diluted in a ratio of 1:100 or 1:50 in PBS and loaded into the measurement cell. Movements of particles in the samples were recorded as videos for 30 seconds at 25 °C. The videos were analyzed with the NanoSight NTA 3.1 software showing the mean values of five individual measurement.

Transmission Electron Microscopy (TEM)

The nanoparticle suspension (1 mg mL^{-1}) was drop-casted on a 300-mesh copper carbon grid from Plano GmbH for TEM measurements (5 μL). The image acquisition was done with a transmission electron microscope Tecnai T12 equipped with a TVIPS-F416 camera.

Atomic Force Microscopy (AFM)

A freshly prepared NP solution (1 mg mL^{-1} in PBS) was diluted with ultrapure water to 200 μg mL^{-1}. 40 μL of this NP solution was spotted on a freshly cleaved mica and was incubated overnight. To remove undesired buffer salts, the mica was rinsed three times with 100 μL ultrapure water. After drying overnight, the sample was measured on a Bruker Dimension Icon FastScan AFM in tapping-in-air mode. Several AFM images were acquired at different areas of the mica surface to ensure the reproducibility of the results. The obtained data was processed and analyzed by using the software *Gwyddion* 2.38 and *NanoScopeAnalysis* 1.50.

5.5 Enzyme Activity Assays

5.5.1 Enzymatic Activity of Lysozyme

PEGylated LYZ was dissolved in 0.1 M phosphate buffer pH 5.2 and diluted to a final protein concentration of 2 μM. A solution of 4-methylumbelliferyl-β-D-N,N',N'' triacetylchitotrioside ($(GlcNAc)_3MeU$) (20 μM in the same buffer) was preheated to 42 °C for 5 min. 200 μL of each solution were combined and further incubated at 42 °C. Every 30 min 50 μL of each sample was transferred to 300 μL 0.5 M glycine buffer pH 12 to stop the catalytic activity of the protein and enhance the fluorescence intensity of methylumbelliferone. The fluorescence of the samples was determined with a Tecan Plate Reader (ex. 380 nm; em. 460 nm). A solution of native lysozyme (2 μM), treated under the same conditions, was used as a reference. The remaining activity of the PEGylated protein was calculated in comparison to native lysozyme.

5.5.2 Enzymatic Activity of PEGylated Peroxidases and Peroxidase-NPs

Kinetic Parameters of Cyt(mPEG) and Cyt-NPs by ABTS Assay

The peroxidase activity of Cyt *c,* the PEGylated Cyt *c* and the NP were measured by using 2,2'-azinobis-(2-ethylbenzthiazoline-6-sulfonate) (ABTS, final concentration in well: 1 mM). 10 mM potassium phosphate buffer pH 7.4 were used as buffer. 100 μL of ABTS solution and 50 μL of each sample (native enzyme, the PEGylated sample or the NP, final concentration in well: 6.45 μM of Cyt *c*) were pipetted in a 96-well-microplate (flat bottom). The reaction was initiated by addition of 50 μL H_2O_2 (final concentration in well: 0.1–2 mM). The increase in absorbance at 405 nm was measured with a Tecan Plate Reader. All measurements were performed for 3 minutes. Michaelis-Menten kinetics were calculated with GraFit (Version 7.0.3).

Kinetic Parameters of HRP(mPEG) and HRP-NPs by ABTS Assay

The peroxidase activity of HRP, PEGylated HRP and the NP were measured by using 2,2'-azinobis-(2-ethylbenzthiazoline-6-sulfonate) (ABTS, 0.25 mM). The assay mixture contained 250 mM potassium phosphate buffer pH 6, hydrogen peroxide (0.025–1 mM), the native enzyme, the PEGylated sample and the nanoparticles (7.244 nM of enzyme) and ABTS in a total volume of 200 μL. The reaction was initiated by addition of H_2O_2. The assay was performed in a 96-well-microplate (flat bottom) and the increase in absorbance at 405 nm was measured with a Tecan Plate Reader. All measurements were investigated for 3 minutes. Michaelis-Menten kinetics were calculated uisng GraFit Version 7.0.3.

Kinetic Parameters of Cat(mPEG) by H_2O_2 Assay

The peroxidase activity of the catalase samples was determined using an enzyme-specific assay according to Shangari *et al.*[158] Native catalase or the PEGylated sample was diluted in 0.05 M phosphate buffer pH 7 to a final enzyme concentration of 100 U mL^{-1}. 145 μL of the enzyme sample were combined with 5 μL of H_2O_2 (0.0625–200 mM) in 96-well UV-Star plates and the decrease in absorption was investigated at 240 nm with a Tecan Plate Reader for 3 minutes. Michaelis-Menten kinetics were calculated using GraFit Version 7.0.3.

Extracellular Activity of Peroxidase Materials by Amplex Red Assay

HeLa cells were seeded at a density of $2 \cdot 10^5$ cells per well, in a 12-well plate and allowed to attach overnight. The cells were washed with PBS and then stimulated with TNF-*a* (10 ng mL^{-1}) diluted in phenol red-free DMEM medium for 16 h to generate ROS. The ROS-containing medium was removed from the cells and used for investigations. Cyt *c,* PEGylated Cyt *c* and the Cyt-NP (500 μL, 0.32 mg Cyt *c* mL^{-1}), HRP, PEGylated HRP and HRP-NP (500 μL, 0.17 mg HRP mL^{-1}) or Cat, PEGylated Cat and Cat-NP (500 μL, 0.28 mg Cat mL^{-1}) were respectively incubated with the ROS-containing cell medium (1 mL) in microcentrifuge tubes for 3 h under shaking. The extracellular hydrogen peroxide concentration was measured using Amplex Red.

For this 50 μL of the cell medium-sample mixture was combined with 50 μL Amplex Red working solution, containing 100 μM Amplex Red and 0.4 U mL^{-1} HRP, and read out directly. The emission was measured with a Tecan Plate Reader. For all measurement, the excitation was set to 563 nm, the emission was set to 587 nm.

Flow Cytometry of Peroxidase-NPs

HeLa cells were seeded at a density of $6 \cdot 10^4$ cells per well in a 12-well-plate (Greiner Bio-One) and allowed to attach overnight. The cells were washed with PBS and incubated with either cell medium (control) or the Cy5_labeled enzyme-NPs (Cy5_Cyt-NP, Cy5_HRP-NP, Cy5_Cat-NP) (0.25 mg particles mL^{-1}) for 24 h. The cells were detached with trypsin, quenched with DMEM medium and collected by centrifugation. The cell pellet was dissolved in 1 mL of 10 μM PY1 (from 5 mM stock solution in DMSO) in PBS with $CaCl_2$ and $MgCl_2$ (100 mg L^{-1}) and incubated for 30 min at 37 °C, 5% CO_2. The cell solution was divided into two portions, one for ROS treatment and one for control conditions. For ROS treatment, H_2O_2 with a final concentration of 100 μM was added to the cell suspension and incubated for 30 min (37 °C, 5% CO_2). The other cell suspension remained untreated. Each cell solution was analyzed by flow cytometry (BD LSRFortessa) using excitation by a 488-nm laser and collection by a 530/30-nm band pass filter for the boronate-based dye (PY1) and an excitation by a 640-nm laser and collection using a 670/30-nm band pass filter for Cy5. Data processing was performed with FlowJo (Version 10.2.).

Live-cell Microscopy of Cyt-NP

All steps were carried out at 37 °C and 5% CO_2. HeLa cells were seeded at a density of $6 \cdot 10^4$ cells per well in μ-Slide 8 well plate (ibidi GmbH) and allowed to attach overnight. The cells were treated for 24 h with 0.25 mg mL^{-1} Cy5_Cyt-NP diluted in 200 μL cell culture medium. The control cells remained untreated. Cells were washed with PBS before staining for 30 min with 10 μM PY1 (from 5 mM stock solution in DMSO) in PBS with $CaCl_2$ and $MgCl_2$ (100 mg L^{-1}). Subsequently, H_2O_2 in a final concentration of 100 μM was added to the cell solution and incubated for 30 min.

Live-cell imaging was performed with a Leica TCS SP5 Microscope, equipped with a water immersion objective lens HCX PL APO CS 40.0x/1.10 WATER UV and an incubator for temperature and CO_2 control. PY1-loaded cells were excited at 488 nm with an Argon laser and emission was collected between 498 and 571 nm using a HyD detector. The Cy5 was excited with a 633 nm HeNe laser, while the emission was collected between 649 and 774 nm using a PMT detector. Image analysis was performed with Fiji software (Version 1.51q). The fluorescence intensity of raw images was determined via a binary mask, created automatically through thresholding (isodata algorithm). The mean grey value (sum of the gray values of all the pixels in the selection divided by the number of pixels) of CY5_Cyt-NP treated cells (n = 203) was compared to untreated cells (n = 183).

5.5.3 Enzymatic Activity of Dual-Enzyme NPs

Dual-Enzyme-Nanoparticle Activity by Amplex Red Assay

HeLa cells were seeded at a density of $2 \cdot 10^5$ cells per well, in a 12-well plate and allowed to attach overnight. The cells were washed with PBS and then stimulated with TNF-*a* (10 ng mL^{-1}) diluted in phenol red-free DMEM medium for 16 h to generate ROS. The ROS-containing medium was removed from the cells and used for further investigations. Native GOx with native HRP, dual-enzyme NPs (using $GOx(mPEG)_{2k}$, 500 μL, 0.152 mg GOx mL^{-1}, 0.41 mg HRP mL^{-1}), dual-enzyme NPs (using $GOx(mPEG)_{5k}$, 500 μL, 0.161 mg GOx mL^{-1}, 0.41 mg HRP mL^{-1}), HRP-NPs (diluted to the same concentration as in the dual-enzyme particle system), GOx-NPs (diluted to the same concentration as in the dual-enzyme particle system) and a mix of both individual NP systems (mix HRP-NP and GOx-NP) were respectively incubated with the ROS-containing cell medium (1 mL) in microcentrifuge tubes for 3 h under shaking. The extracellular hydrogen peroxide concentration was measured using Amplex Red. For this 50 μL of the cell medium-sample mixture was combined with 50 μL Amplex Red (100 μM Amplex Red), and read out directly. The emission was measured with a Tecan Plate Reader. For all measurement, the excitation was set to 563 nm, the emission was set to 587 nm.

Kinetic Parameters of Dual-Enzyme NPs by ABTS Assay

The enzymatic activity of all samples was measured by using 2,2'-azinobis-(2-ethylbenzthiazoline-6-sulfonate) (ABTS, final concentration in well: 0.25 mM). The catalytic activity of all HRP samples was determined like mentioned in section 5.5.2. All GOx samples and the dual-enzyme NPs were treated as follows. 250 mM potassium phosphate buffer pH 6 were used as buffer. 100 μL ABTS solution and 50 μL of each sample (native enzymes, PEGylated samples or the NPs) were pipetted in a 96-well-microplate (flat bottom). The reaction was initiated by addition of 50 μL glucose (final concentration in well: 1–200 mM). The increase in absorbance at 405 nm was measured with a Tecan Plate Reader. All measurements were performed for 3 minutes and Michaelis-Menten kinetics were calculated using GraFit (Version 7.0.3).

5.6 Cell Toxicity of PEGylated Materials and NPs

HeLa cell lines were grown in Dulbecco's Modified Eagle Medium (DMEM) supplemented with 10% (v/v) fetal calf serum (FCS), 1% pyruvate and 1% penicillin/streptomycin. Cell incubations were performed in a humidified incubator at 37 °C with 5% CO_2 atmosphere. All used buffers were either autoclaved, sterile filtered or already sterile when supplied and were preheated to 37 °C. Cells were grown in 175 cm^2, 75 cm^2 or 25 cm^2 standard cell culture flasks.

5.6.1 Cell Viability

The cell viability of human HeLa cells in presence of native enzymes, PEGylated ones and all prepared NP was determined using the MTT method. Cells were seeded in 96-well plates with a density of $1.5 \cdot 10^4$ cells per well and allowed to attach overnight. 100 μL of different dilutions of the samples in culture media were added as triplets to the well plate. After an incubation time of 48 h (37 °C, 5% CO_2) a solution of 3-(4,5-dimethyl-2-thiazolyl)-2,5-diphen-yl-2H-tetrazolium bromide (MTT) in medium (40 μL, 3.0 mg mL^{-1}) was added directly to each well and the plate was incubated for additional 20 min. The medium was then replaced and a mixture of DMSO (200 μL/well) and 0.1 M glycine buffer (25 μL/well, pH 10) was added. 50 μL/well of purple DMSO solution was added to another clear-bottom 96-well assay plate (Greiner Bio-One) containing a mixture of glycine buffer (17 μL/well, pH 10) and DMSO (133 μL/well).

The absorbance at 570 nm was measured using an Infinite® 200 PRO Tecan plate reader. The absorbance at 690 nm was subtracted as background. Cell viability was normalized to the absorbance measured from untreated cells.

6 APPENDIX

6.1 List of Abbreviations

ABTS	2,2'-azinobis-(2-ethylbenzthiazoline-6-sulfonate)
AFM	atomic force microscopy
ATRP	atom-transfer radical-polymerization
BLG	*β*-lactoglobulin
BSA	bovine serum albumin
Cat	catalase
Cat-NP	catalase nanoparticles
Cy5_Cat-NP	Cy5-labeled catalase nanoparticles
CCD	marlin charged coupled device
CD	circular dichroism
CNS	central nervous system
Cyt *c*	cytochrome *c*
Cyt-NP	cytochrome *c* nanoparticles
Cy5_Cyt-NP	Cy5-labeled cytochrome *c* nanoparticles
dd	double distilled
Da	dalton (1 Da equals 1 g mol^{-1})
DCM	dichloromethane
DMSO	dimethyl sulfoxide
e.g.	exempli gratia
em.	emission
eq.	equation
et al.	et alii
ex.	excitation
EtOH	ethanol
FAD	flavin adenine dinucleotide
FCS	fetal calf serum
FDA	food and drug administration

GlcNAc	*N*-acetylglucosamine
GOx	glucose oxidase
GOx-NP	glucose oxidase nanoparticles
$GOx(mPEG)_{2k}$	glucose oxidase modified with epoxy-$mPEG_{2k}$
$GOx(mPEG)_{5k}$	glucose oxidase modified with NHS-$mPEG_{5k}$
$GOx(mPEG)_{2k}$ - $HRP(mPEG)_{5k}$	dual-enzyme system of these materials
$GOx(mPEG)_{5k}$ - $HRP(mPEG)_{5k}$	dual-enzyme system of these materials
GSH	glutathione
h	hour(s)
HSA	human serum albumin
HRP	horseradish peroxidase
HRP-NP	horseradish peroxidase nanoparticles
$HRP(NHS\text{-}mPEG)_{5k}$	HRP modified with NHS-mPEG (5 kDa)
Cy5_HRP-NP	Cy5-labeled horseradish peroxidase nanoparticles
k_{cat}	turnover rate
K_M	Michaelis constant
λ	wavelength
LYZ	lysozyme
LYZ(carbonate-mPEG)	lysozyme modified with carbonate-mPEG (2 kDa)
LYZ(epoxy-mPEG)	lysozyme modified with epoxy-mPEG (2 kDa)
LYZ(TFP-mPEG)	lysozyme modified with TFP-mPEG (2 kDa)
LYZ(TsT-mPEG)	lysozyme modified with TsT-mPEG (2 kDa)
m	mass
M	molar (1 M equals 1 mol L^{-1})
MALDI ToF MS	matrix-assisted laser desorption/ionization time of flight
min.	minute(s)
mPEG	monomethoxy poly(ethylene glycol)
$mPEG_{2k}$	monomethoxy poly(ethylene glycol), 2000 g mol^{-1}
$mPEG_{5k}$	monomethoxy poly(ethylene glycol), 5000 g mol^{-1}
MS	mass spectroscopy
MTT	3-(4,5-dimethylthiazol-2-yl)-2,5-diphenyl-tetrazoliumbromide

MWCO	molecular weight cut-off
NADP	Nicotinamide adenine dinucleotide phosphate
NHS	*N*-hydroxysuccinimide
NHS-mPEG$_{2k}$	NHS activated mPEG (2 kDa)
NHS-mPEG$_{5k}$	NHS activated mPEG (5 kDa)
NP	nanoparticle
NTA	nanoparticle tracking analysis
OVA	ovalbumin
PBS	phosphate buffered saline
pdb	protein data bank
PEG	poly(ethylene glycol)
PEG-pAsp-(DET)	PEG-poly[*N*-{*N*'-2-aminoethyl}-aspartamide]
PLGA	poly(lactid-co-glycolid)
PNIPAAm	poly(*N*-isoporpylacrylamide)
RAFT	reversible addition-fragmentation chain transfer
rel.	relative
rt.	room temperature
SD	standard deviation
SDS-PAGE	sodium dodecyl sulfate polyacrylamide gel electrophoresis
SEC	size exclusion chromatography
SOD	superoxide dismutase
SPARC	secreted protein acid rich in cysteine
TAT	trans-activator of transcription
TEM	transmission electron microscopy
TEMED	tetramethylethylenediamine
TsT	trichloro-*s*-triazine
U	units
UV	ultra violet
V	volume
v_{max}	maximal rate

6.2 Literature

[1] B. Leader, Q. J. Baca, D. E. Golan, *Nat. Rev. Drug Discovery* **2008**, *7*, 21-39.
[2] a) A. D. Bangham, *Chem. Phys. Lipids* **1993**, *64*, 275-285; b) A. D. Bangham, *BioEssays* **1995**, *17*, 1081-1088.
[3] R. A. Petros, J. M. DeSimone, *Nat. Rev. Drug Discovery* **2010**, *9*, 615-627.
[4] M. Rother, M. G. Nussbaumer, K. Renggli, N. Bruns, *Chem. Soc. Rev.* **2016**, *45*, 6213-6249.
[5] G. Chen, I. Roy, C. Yang, P. N. Prasad, *Chem. Rev.* **2016**, *116*, 2826-2885.
[6] a) T. Sun, Y. S. Zhang, B. Pang, D. C. Hyun, M. Yang, Y. Xia, *Angew. Chem. Int. Ed.* **2014**, *53*, 12320-12364; b) M. E. Davis, Z. Chen, D. M. Shin, *Nat. Rev. Drug Discovery* **2008**, *7*, 771-782.
[7] M. Nazıroğlu, S. Muhamad, L. Pecze, *Expert Rev. Clin. Pharmacol.* **2017**, *10*, 773-782.
[8] P. Fonte, F. Araujo, C. Silva, C. Pereira, S. Reis, H. A. Santos, B. Sarmento, *Biotechnol. Adv.* **2015**, *33*, 1342-1354.
[9] a) G. Chen, H. Qiu, P. N. Prasad, X. Chen, *Chem. Rev.* **2014**, *114*, 5161-5214; b) A. Louie, *Chem. Rev.* **2010**, *110*, 3146-3195.
[10] Y. Jiang, S. Wong, F. Chen, T. Chang, H. Lu, M. H. Stenzel, *Bioconjugate Chem.* **2017**, *28*, 979-985.
[11] M. Fach, L. Radi, P. R. Wich, *J. Am. Chem. Soc.* **2016**, *138*, 14820-14823.
[12] H. Hao, Q. Ma, C. Huang, F. He, P. Yao, *Int. J. Pharm.* **2013**, *444*, 77-84.
[13] Z. Shen, M.-P. Nieh, Y. Li, *Polymers* **2016**, *8*, 83.
[14] K. Cho, X. Wang, S. Nie, Z. G. Chen, D. M. Shin, *Clin. Cancer Res.* **2008**, *14*, 1310-1316.
[15] A. D. Smith, **2013**.
[16] Y. Barenholz, *J. Controlled Release* **2012**, *160*, 117-134.
[17] P. Yingchoncharoen, D. S. Kalinowski, D. R. Richardson, *Pharmacol. Rev.* **2016**, *68*, 701-787.
[18] Q. Lin, J. Chen, Z. Zhang, G. Zheng, *Nanomedicine (London, U. K.)* **2014**, *9*, 105-120.
[19] J. Lu, S. C. Owen, M. S. Shoichet, *Macromolecules* **2011**, *44*, 6002-6008.
[20] P. Kesharwani, K. Jain, N. K. Jain, *Prog. Polym. Sci.* **2014**, *39*, 268-307.
[21] S. M. Kuiper, M. Nallani, D. M. Vriezema, J. J. Cornelissen, J. C. van Hest, R. J. Nolte, A. E. Rowan, *Org. Biomol. Chem.* **2008**, *6*, 4315-4318.
[22] Y. Liu, K. Li, J. Pan, B. Liu, S.-S. Feng, *Biomaterials* **2010**, *31*, 330-338.
[23] R. H. Prabhu, V. B. Patravale, M. D. Joshi, *Int. J. Nanomed.* **2015**, *10*, 1001-1018.
[24] N. Kamaly, B. Yameen, J. Wu, O. C. Farokhzad, *Chem. Rev.* **2016**, *116*, 2602-2663.
[25] R. Liang, M. Wei, D. G. Evans, X. Duan, *Chem. Commun. (Cambridge, U. K.)* **2014**, *50*, 14071-14081.
[26] C. Buzea, Pacheco, II, K. Robbie, *Biointerphases* **2007**, *2*, MR17-71.
[27] a) F. Foerster, D. Bamberger, J. Schupp, M. Weilbacher, L. Kaps, S. Strobl, L. Radi, M. Diken, D. Strand, A. Tuettenberg, P. R. Wich, D. Schuppan, *Nanomedicine (London, U. K.)* **2016**, *11*, 2663-2677; b) D. Bamberger, D. Hobernik, M. Konhauser, M. Bros, P. R. Wich, *Mol. Pharmaceutics* **2017**, *14*, 4403-4416.
[28] J. Li, L. Mo, C.-H. Lu, T. Fu, H.-H. Yang, W. Tan, *Chem. Soc. Rev.* **2016**, *45*, 1410-1431.
[29] L. Radi, M. Fach, M. Montigny, E. Berger-Nicoletti, W. Tremel, P. R. Wich, *Med. Chem. Commun.* **2016**, *7*, 1738-1744.
[30] M. J. Hawkins, P. Soon-Shiong, N. Desai, *Adv. Drug Delivery Rev.* **2008**, *60*, 876-885.
[31] T. Sun, Y. S. Zhang, B. Pang, D. C. Hyun, M. Yang, Y. Xia, *Angew. Chem. Int. Ed.* **2014**, *53*, 12320-12364.

[32] S. Schubert, J. J. T. Delaney, U. S. Schubert, *Soft Matter* **2011**, *7*, 1581-1588.
[33] A. O. Elzoghby, W. M. Samy, N. A. Elgindy, *J. Controlled Release* **2012**, *157*, 168-182.
[34] B. B. Breitenbach, I. Schmid, P. R. Wich, *Biomacromolecules* **2017**.
[35] B. von Storp, A. Engel, A. Boeker, M. Ploeger, K. Langer, *J. Microencapsulation* **2012**, *29*, 138-146.
[36] A. W. Martinez, J. M. Caves, S. Ravi, W. Li, E. L. Chaikof, *Acta Biomater.* **2014**, *10*, 26-33.
[37] M. Martins, A. Loureiro, N. G. Azoia, C. Silva, A. Cavaco-Paulo, *Trends Biotechnol.* **2016**, *34*, 496-505.
[38] E. M. Bachelder, T. T. Beaudette, K. E. Broaders, J. Dashe, J. M. Frechet, *J. Am. Chem. Soc.* **2008**, *130*, 10494-10495.
[39] S. Tenzer, D. Docter, J. Kuharev, A. Musyanovych, V. Fetz, R. Hecht, F. Schlenk, D. Fischer, K. Kiouptsi, C. Reinhardt, K. Landfester, H. Schild, M. Maskos, S. K. Knauer, R. H. Stauber, *Nat. Nanotechnol.* **2013**, *8*, 772.
[40] D. Maiolo, P. Del Pino, P. Metrangolo, W. J. Parak, F. Baldelli Bombelli, *Nanomedicine (London, U. K.)* **2015**, *10*, 3231-3247.
[41] S. Schöttler, G. Becker, S. Winzen, T. Steinbach, K. Mohr, K. Landfester, V. Mailänder, F. R. Wurm, *Nat. Nanotechnol.* **2016**, *11*, 372.
[42] Y. Matsumura, H. Maeda, *Cancer Res.* **1986**, *46*, 6387.
[43] a) S. D. Li, L. Huang, *Mol. Pharmaceutics* **2008**, *5*, 496-504; b) R. Toy, P. M. Peiris, K. B. Ghaghada, E. Karathanasis, *Nanomedicine (London, U. K.)* **2014**, *9*, 121-134.
[44] J. Shi, P. W. Kantoff, R. Wooster, O. C. Farokhzad, *Nat. Rev. Cancer* **2017**, *17*, 20-37.
[45] E. Blanco, H. Shen, M. Ferrari, *Nat. Biotechnol.* **2015**, *33*, 941-951.
[46] X. Xu, W. Ho, X. Zhang, N. Bertrand, O. Farokhzad, *Trends Mol. Med.* **2015**, *21*, 223-232.
[47] H. Herd, N. Daum, A. T. Jones, H. Huwer, H. Ghandehari, C. M. Lehr, *ACS Nano* **2013**, *7*, 1961-1973.
[48] J. P. Lim, P. A. Gleeson, *Immunol. Cell Biol.* **2011**, *89*, 836-843.
[49] Z. G. Qu, X. C. He, M. Lin, B. Y. Sha, X. H. Shi, T. J. Lu, F. Xu, *Nanomedicine (London, U. K.)* **2013**, *8*, 995-1011.
[50] a) Y. W. Yang, W. H. Luo, *J. Controlled Release* **2016**, *227*, 82-93; b) N. Hoshyar, S. Gray, H. Han, G. Bao, *Nanomedicine* **2016**, *11*, 673-692.
[51] M. S. Cartiera, K. M. Johnson, V. Rajendran, M. J. Caplan, W. M. Saltzman, *Biomaterials* **2009**, *30*, 2790-2798.
[52] G. Ruan, A. Agrawal, A. I. Marcus, S. Nie, *J. Am. Chem. Soc.* **2007**, *129*, 14759-14766.
[53] Z. Gu, A. Biswas, M. Zhao, Y. Tang, *Chem. Soc. Rev.* **2011**, *40*, 3638-3655.
[54] N. Murthy, M. Xu, S. Schuck, J. Kunisawa, N. Shastri, J. M. Frechet, *Proc. Natl. Acad. Sci. U. S. A.* **2003**, *100*, 4995-5000.
[55] Y. Lee, T. Ishii, H. Cabral, H. J. Kim, J. H. Seo, N. Nishiyama, H. Oshima, K. Osada, K. Kataoka, *Angew. Chem. Int. Ed.* **2009**, *48*, 5309-5312.
[56] a) O. G. Jones, D. J. McClements, *Compr. Rev. Food Sci. Food Saf.* **2010**, *9*, 374-397; b) I. J. Joye, D. J. McClements, *Curr. Opin. Colloid Interface Sci.* **2014**, *19*, 417-427.
[57] B. S. Zolnik, A. Gonzalez-Fernandez, N. Sadrieh, M. A. Dobrovolskaia, *Endocrinology* **2010**, *151*, 458-465.
[58] W. Lohcharoenkal, L. Wang, Y. C. Chen, Y. Rojanasakul, *BioMed Res. Int.* **2014**, *2014*, 180549-180512.
[59] a) F. P. Seib, G. T. Jones, J. Rnjak-Kovacina, Y. Lin, D. L. Kaplan, *Adv. Healthcare Mater.* **2013**, *2*, 1606-1611; b) T. Wongpinyochit, P. Uhlmann, A. J. Urquhart, F. P. Seib, *Biomacromolecules* **2015**, *16*, 3712-3722.

[60] M. Papi, V. Palmieri, G. Maulucci, G. Arcovito, E. Greco, G. Quintiliani, M. Fraziano, M. De Spirito, *J. Nanopart. Res.* **2011**, *13*, 6141-6147.
[61] M. Santoro, A. M. Tatara, A. G. Mikos, *J. Controlled Release* **2014**, *190*, 210-218.
[62] W. F. Daamen, J. H. Veerkamp, J. C. M. van Hest, T. H. van Kuppevelt, *Biomaterials* **2007**, *28*, 4378-4398.
[63] a) S. Nitta, K. Numata, *Int. J. Mol. Sci.* **2013**, *14*, 1629-1654; b) R. L. DiMarco, S. C. Heilshorn, *Adv. Mater.* **2012**, *24*, 3923-3940; c) F. Mottaghitalab, M. Farokhi, M. A. Shokrgozar, F. Atyabi, H. Hosseinkhani, *J. Controlled Release* **2015**, *206*, 161-176; d) S. Perteghella, B. Crivelli, L. Catenacci, M. Sorrenti, G. Bruni, V. Necchi, B. Vigani, M. Sorlini, M. L. Torre, T. Chlapanidas, *Int. J. Pharm.* **2017**, *520*, 86-97; e) W. Friess, *Eur. J. Pharm. Biopharm.* **1998**, *45*, 113-136.
[64] M. Tarhini, H. Greige-Gerges, A. Elaissari, *Int. J. Pharm.* **2017**, *522*, 172-197.
[65] a) Q. Li, C. Liu, X. Zhao, Y. Zu, Y. Wang, B. Zhang, D. Zhao, Q. Zhao, L. Su, Y. Gao, B. Sun, *Int. J. Nanomed.* **2011**, *6*, 397-405; b) S. Jiang, X. Gong, X. Zhao, Y. Zu, *Drug Deliv* **2015**, *22*, 206-213.
[66] H. B. Wijayanti, N. Bansal, H. C. Deeth, *Compr. Rev. Food Sci. Food Saf.* **2014**, *13*, 1235-1251.
[67] S. Yu, P. Yao, M. Jiang, G. Zhang, *Biopolymers* **2006**, *83*, 148-158.
[68] K. Piradashvili, M. Fichter, K. Mohr, S. Gehring, F. R. Wurm, K. Landfester, *Biomacromolecules* **2015**, *16*, 815-821.
[69] a) C. Boyer, X. Huang, M. R. Whittaker, V. Bulmus, T. P. Davis, *Soft Matter* **2011**, *7*, 1599-1614; b) R. M. Broyer, G. N. Grover, H. D. Maynard, *Chem. Commun.* **2011**, *47*, 2212-2226.
[70] a) Y. Wu, D. Y. Ng, S. L. Kuan, T. Weil, *Biomater. Sci.* **2015**, *3*, 214-230; b) D. Y. W. Ng, Y. Wu, S. L. Kuan, T. Weil, *Acc. Chem. Res.* **2014**, *47*, 3471-3480.
[71] a) C. Werner, Y. Wu, T. Wang, D. Y. W. Ng, T. Weil, *Macromol. Rapid Commun.* **2012**, *33*, 1474–1481; b) S. L. Kuan, Y. Wu, T. Weil, *Macromol. Rapid Commun.* **2013**, *34*, 380-392.
[72] Y. Wu, E. K. Shih, A. Ramanathan, S. Vasudevan, T. Weil, *Biointerphases* **2012**, *7*, 1–10.
[73] a) W. J. Gradishar, *Expert Opin. Pharmacother.* **2006**, *7*, 1041-1053; b) M. R. Green, *Annals of Oncology* **2006**, *17*, 1263-1268; c) E. Miele, G. P. Spinelli, E. Miele, F. Tomao, S. Tomao, *Int. J. Nanomed.* **2009**, *4*, 99-105.
[74] a) C. Zhang, Y. Zhu, R. Zhang, Y. Xie, K. Wang, X. Liu, *RSC Adv.* **2015**, *5*, 90651-90658; b) Z. Li, Y. Wang, Y. Pei, W. Xiong, C. Zhang, W. Xu, S. Liu, B. Li, *Food Res. Int.* **2015**, *75*, 98-105.
[75] R. S. Shukla, W. Tai, R. Mahato, W. Jin, K. Cheng, *Mol. Pharmaceutics* **2013**, *10*, 4534-4545.
[76] a) R. Khandelia, A. Jaiswal, S. S. Ghosh, A. Chattopadhyay, *Small* **2013**, *9*, 3494-3505; b) A. G. Tkachenko, H. Xie, D. Coleman, W. Glomm, J. Ryan, M. F. Anderson, S. Franzen, D. L. Feldheim, *J. Am. Chem. Soc.* **2003**, *125*, 4700-4701.
[77] O. Boutureira, G. J. Bernardes, *Chem. Rev.* **2015**, *115*, 2174-2195.
[78] G. N. Grover, H. D. Maynard, *Curr. Opin. Chem. Biol.* **2010**, *14*, 818-827.
[79] E. M. Pelegri-O'Day, H. D. Maynard, *Acc. Chem. Res.* **2016**, *49*, 1777-1785.
[80] E. M. Pelegri-O'Day, E. W. Lin, H. D. Maynard, *J. Am. Chem. Soc.* **2014**, *136*, 14323-14332.
[81] a) M. J. Roberts, M. D. Bentley, J. M. Harris, *Adv. Drug Delivery Rev.* **2002**, *54*, 459–476; b) G. Pasut, F. M. Veronese, *J. Controlled Release* **2012**, *161*, 461-472.
[82] J. Herzberger, K. Niederer, H. Pohlit, J. Seiwert, M. Worm, F. R. Wurm, H. Frey, *Chem. Rev.* **2016**, *116*, 2170-2243.
[83] K. Knop, R. Hoogenboom, D. Fischer, U. S. Schubert, *Angew. Chem. Int. Ed.* **2010**, *49*, 6288-6308.
[84] a) J. K. Dozier, M. D. Distefano, *Int. J. Mol. Sci.* **2015**, *16*, 25831-25864; b) N. Nischan, C. P. Hackenberger, *J. Org. Chem.* **2014**, *79*, 10727-10733.

[85] a) M. Gao, Y. Tong, X. Gao, W. Yao, *Drug Dev. Res.* **2013**, *74*, 186-193; b) H. Qiu, E. Boudanova, A. Park, J. J. Bird, D. M. Honey, C. Zarazinski, B. Greene, J. S. Kingsbury, S. Boucher, J. Pollock, J. M. McPherson, C. Q. Pan, *Bioconjugate Chem.* **2013**, *24*, 408-418; c) M. H. Stenzel, *ACS Macro Letters* **2013**, *2*, 14-18.

[86] S. Shaunak, A. Godwin, J. W. Choi, S. Balan, E. Pedone, D. Vijayarangam, S. Heidelberger, I. Teo, M. Zloh, S. Brocchini, *Nat. Chem. Biol.* **2006**, *2*, 312-313.

[87] a) J. R. M. A. Abuchowski, N. C. Palczuk, T. van Es, F. F. Davis, *J. Biol. Chem.* **1977**, 3582–3586; b) A. Abuchowski, T. van Es, N. C. Palczuk, F. F. Davis, *J. Biol. Chem.* **1977**, *252*, 3578-3581; c) R. H. L. Chen, A. Abuchowski, T. Van Es, N. C. Palczuk, F. F. Davis, *Biochim. Biophys. Acta* **1981**, *660*, 293-298; d) K. V. Savoca, A. Abuchowski, T. van Es, F. F. Davis, N. C. Palczuk, *Biochim. Biophys. Acta* **1979**, *578*, 47-53.

[88] S. Jevsevar, M. Kunstelj, V. G. Porekar, *Biotechnol. J.* **2010**, *5*, 113-128.

[89] M. J. Roberts, M. D. Bentley, J. M. Harris, *Adv. Drug Delivery Rev.* **2012**, *64*, 116-127.

[90] A. Kozlowski, J. M. Harris, *J. Controlled Release* **2001**, *72*, 217-224.

[91] S. N. S. Alconcel, A. S. Baas, H. D. Maynard, *Polym. Chem.* **2011**, *2*, 1442-1448.

[92] a) R. Xu, M. Fisher, R. L. Juliano, *Bioconjugate Chem.* **2011**, *22*, 870–878; b) J. Zhang, Y. Lei, A. Dhaliwal, Q. K. T. Ng, J. Du, M. Yan, Y. Lu, T. Segura, *Biomacromolecules* **2011**, *12*, 1006-1014; c) J. D. Brodin, A. J. Sprangers, J. R. McMillan, C. A. Mirkin, *J. Am. Chem. Soc.* **2015**, *137*, 14838-14841.

[93] X. Huang, M. Li, D. C. Green, D. S. Williams, A. J. Patil, S. Mann, *Nat. Commun.* **2013**, *4*.

[94] N. Vanparijs, R. De Coen, D. Laplace, B. Louage, S. Maji, L. Lybaert, R. Hoogenboom, B. G. De Geest, *Chem. Commun.* **2015**, *51*, 13972-13975.

[95] H. J. Hecht, D. Schomburg, H. Kalisz, R. D. Schmid, *Biosens. Bioelectron.* **1993**, *8*, 197-203.

[96] S. B. Bankar, M. V. Bule, R. S. Singhal, L. Ananthanarayan, *Biotechnol. Adv.* **2009**, *27*, 489-501.

[97] a) L. Zhao, L. Wang, Y. Zhang, S. Xiao, F. Bi, J. Zhao, G. Gai, J. Ding, *Polymers* **2017**, *9*, 255; b) Y. Zhao, Y. Wang, X. Zhang, R. Kong, L. Xia, F. Qu, *Talanta* **2016**, *155*, 265-271; c) M. J. Chaichi, M. Ehsani, *Sensors and Actuators B: Chemical* **2016**, *223*, 713-722; d) M. E. Welch, T. Doublet, C. Bernard, G. G. Malliaras, C. K. Ober, *J. Polym. Sci., Part A: Polym. Chem.* **2015**, *53*, 372-377; e) M. Khan, S. Y. Park, *J. Colloid Interface Sci.* **2015**, *457*, 281-288; f) A. L. Galant, R. C. Kaufman, J. D. Wilson, *Food Chem.* **2015**, *188*, 149-160.

[98] J. Cheng, Q. Liu, A. J. Shuhendler, A. M. Rauth, X. Y. Wu, *Colloids and Surfaces B: Biointerfaces* **2015**, *130*, 164-172.

[99] W. Zhao, J. Hu, W. Gao, *ACS Appl. Mater. Interfaces* **2017**, *9*, 23528-23535.

[100] a) X. Gu, H. Wang, Z. D. Schultz, J. P. Camden, *Anal. Chem.* **2016**, *88*, 7191-7197; b) D. Liu, J. Yang, H. F. Wang, Z. Wang, X. Huang, Z. Wang, G. Niu, A. R. Hight Walker, X. Chen, *Anal. Chem.* **2014**, *86*, 5800-5806.

[101] C. M. Wong, K. H. Wong, X. D. Chen, *Appl. Microbiol. Biotechnol.* **2008**, *78*, 927-938.

[102] K. Opwis, D. Knittel, E. Schollmeyer, P. Hoferichter, A. Cordes, *Eng. Life Sci.* **2008**, *8*, 175-178.

[103] T. L. Poulos, *Chem. Rev.* **2014**, *114*, 3919-3962.

[104] a) S. E. J. Bowman, K. L. Bren, *Nat. Prod. Rep.* **2008**, *25*, 1118-1130; b) R. Fiammengo, K. Wojclechowski, M. Crego-Calama, P. Timmerman, A. Figoli, M. Wessling, D. N. Reinhoudt, *Org. Lett.* **2003**, *5*, 3367-3370.

[105] I. S. Isaac, J. H. Dawson, *Essays Biochem.* **1999**, *34*, 51-69.

[106] a) F. W. Krainer, A. Glieder, *Appl. Microbiol. Biotechnol.* **2015**, *99*, 1611-1625; b) G. Battistuzzi, M. Bellei, C. A. Bortolotti, M. Sola, *Arch. Biochem. Biophys.* **2010**, *500*, 21-36.

[107] K. Chattopadhyay, S. Mazumdar, *Biochemistry* **2000**, *39*, 263-270.

[108] N. C. Veitch, *Phytochemistry* **2004**, *65*, 249-259.
[109] Z. Qu, H. Xu, P. Xu, K. Chen, R. Mu, J. Fu, H. Gu, *Anal. Chem.* **2014**, *86*, 9367-9371.
[110] X. Cao, C. Chen, H. Yu, P. Wang, *Biotechnol. Lett* **2015**, *37*, 81-88.
[111] Y. P. Ow, D. R. Green, Z. Hao, T. W. Mak, *Nat. Rev. Mol. Cell Biol.* **2008**, *9*, 532-542.
[112] J. G. Kleingardner, K. L. Bren, *Acc. Chem. Res.* **2015**, *48*, 1845-1852.
[113] M. Fedurco, *Coord. Chem. Rev.* **2000**, *209*, 263-331.
[114] a) C. Garrido, L. Galluzzi, M. Brunet, P. E. Puig, C. Didelot, G. Kroemer, *Cell Death Differ.* **2006**, *13*, 1423-1433; b) Y. Zhao, Z. B. Wang, J. X. Xu, *J. Biol. Chem.* **2003**, *278*, 2356-2360.
[115] a) J. B. Essner, R. N. McCay, C. J. Smith Ii, S. M. Cobb, C. H. Laber, G. A. Baker, *J. Mater. Chem. B* **2016**, *4*, 2163-2170; b) T. Yang, Y. S. Zhang, X. L. Yang, F. Y. Geng, B. L. Xiao, M. M. Xu, D. Li, J. Hong, A. A. Moosavi-Movahedi, *Bio-Med. Mater. Eng.* **2015**, *26 Suppl 1*, S73-79; c) F. Farivar, A. A. Moosavi-Movahedi, Y. Sefidbakht, K. Nazari, J. Hong, N. Sheibani, *Biochem. Eng. J.* **2010**, *49*, 89-94; d) N. H. Kim, M. S. Jeong, S. Y. Choi, J. H. Kang, *Bull. Korean Chem. Soc.* **2004**, *25*, 1889-1892.
[116] P. Nicholls, *Arch. Biochem. Biophys.* **2012**, *525*, 95-101.
[117] M. M. Goyal, A. Basak, *Protein Cell* **2010**, *1*, 888-897.
[118] a) S. Rashtbari, G. Dehghan, R. Yekta, A. Jouyban, M. Iranshahi, *Adv. Pharm. Bull.* **2017**, *7*, 349-357; b) E. V. Batrakova, S. Li, A. D. Reynolds, R. L. Mosley, T. K. Bronich, A. V. Kabanov, H. E. Gendelman, *Bioconjugate Chem.* **2007**, *18*, 1498-1506.
[119] J. E. A., L. A. E., *Antimicrobials in food*, 3rd ed., **2005**.
[120] K. Brieger, S. Schiavone, F. J. Miller, Jr., K. H. Krause, *Swiss Med. Wkly.* **2012**, *142*, w13659.
[121] J. P. Fruehauf, F. L. Meyskens, Jr., *Clin. Cancer Res.* **2007**, *13*, 789-794.
[122] R. Fischer, O. Maier, *Oxid. Med. Cell. Longevity* **2015**, *2015*, 610813.
[123] F. L. Heppner, R. M. Ransohoff, B. Becher, *Nat. Rev. Neurosci.* **2015**, *16*, 358-372.
[124] S. S. Sabharwal, P. T. Schumacker, *Nat. Rev. Cancer* **2014**, *14*, 709-721.
[125] C. Lennicke, J. Rahn, R. Lichtenfels, L. A. Wessjohann, B. Seliger, *Cell Commun. Signaling* **2015**, *13*, 39.
[126] C. Glorieux, M. Zamocky, J. M. Sandoval, J. Verrax, P. B. Calderon, *Free Radical Biol. Med.* **2015**, *87*, 84-97.
[127] M. O. Pereverzev, T. V. Vygodina, A. A. Konstantinov, V. P. Skulachev, *Biochem. Soc. Trans.* **2003**, *31*, 1312-1315.
[128] a) B. Poljsak, D. Suput, I. Milisav, *Oxid. Med. Cell. Longevity* **2013**, *2013*, 956792; b) A. M. Pisoschi, A. Pop, *Eur. J. Med. Chem.* **2015**, *97*, 55-74.
[129] Y. Liu, J. Li, Y. Lu, *Adv. Drug Delivery Rev.* **2015**, *90*, 24-39.
[130] P. A. Dinndorf, J. Gootenberg, M. H. Cohen, P. Keegan, R. Pazdur, *Oncologist* **2007**, *12*, 991-998.
[131] N. Schlesinger, U. Yasothan, P. Kirkpatrick, *Nat. Rev. Drug Discovery* **2011**, *10*, 17-18.
[132] a) D. S. Pisal, M. P. Kosloski, S. V. Balu-Iyer, *J Pharm Sci* **2010**, *99*, 2557-2575; b) Y. Lu, W. Sun, Z. Gu, *J. Controlled Release* **2014**, *194*, 1-19.
[133] a) S. Santra, C. Kaittanis, J. M. Perez, *Mol. Pharmaceutics* **2010**, *7*, 1209-1222; b) C. G. C. M. Netto, H. E. Toma, L. H. Andrade, *J. Mol. Catal. B: Enzym.* **2013**, *85-86*, 71-92; c) Z. Gu, A. A. Aimetti, Q. Wang, T. T. Dang, Y. Zhang, O. Veiseh, H. Cheng, R. S. Langer, D. G. Anderson, *ACS Nano* **2013**, *7*, 4194-4201; d) Z. Zhao, J. Fu, S. Dhakal, A. Johnson-Buck, M. Liu, T. Zhang, N. W. Woodbury, Y. Liu, N. G. Walter, H. Yan, *Nat. Commun.* **2016**, *7*, 10619.
[134] a) G. Cheng, S. Y. Zheng, *Sci. Rep.* **2014**, *4*, 6947; b) C. Mukai, L. Gao, J. L. Nelson, J. P. Lata, R. Cohen, L. Wu, M. M. Hinchman, M. Bergkvist, R. W. Sherwood, S. Zhang, A. J. Travis, *Angew. Chem.* **2017**, *129*, 241-244.

[135] J. Mendez, M. Morales Cruz, Y. Delgado, C. M. Figueroa, E. A. Orellano, M. Morales, A. Monteagudo, K. Griebenow, *Mol. Pharmaceutics* **2014**, *11*, 102-111.
[136] Z. Y. Zhao, J. Liu, M. Hahn, S. Qiao, A. P. J. Middelberg, L. He, *RSC Adv.* **2013**, *3*, 22008–22013.
[137] N. Miletic, V. Abetz, K. Ebert, K. Loos, *Macromol. Rapid Commun.* **2010**, *31*, 71-74.
[138] A. M. Brynskikh, Y. Zhao, R. L. Mosley, S. Li, M. D. Boska, N. L. Klyachko, A. V. Kabanov, H. E. Gendelman, E. V. Batrakova, *Nanomedicine (London, U. K.)* **2010**, *5*, 379-396.
[139] S. B. P. E. Timmermans, J. C. M. van Hest, *Curr. Opin. Colloid Interface Sci.* **2018**, *35*, 26-35.
[140] a) L. Schoonen, R. J. Nolte, J. C. van Hest, *Nanoscale* **2016**, *8*, 14467-14472; b) L. Schoonen, J. C. M. van Hest, *Nanoscale* **2014**, *6*, 7124-7141.
[141] B. C. Buddingh, J. C. M. van Hest, *Acc. Chem. Res.* **2017**, *50*, 769-777.
[142] W. F. Daamen, P. J. Geutjes, H. T. B. van Moerkerk, S. T. M. Nillesen, R. G. Wismans, T. Hafmans, L. P. W. J. van den Heuvel, A. M. A. Pistorius, J. H. Veerkamp, J. C. M. van Hest, T. H. van Kuppevelt, *Adv. Mater.* **2007**, *19*, 673-677.
[143] a) Y. Lin, J. Ren, X. Qu, *Acc. Chem. Res.* **2014**, *47*, 1097-1105; b) H. Wei, E. Wang, *Chem. Soc. Rev.* **2013**, *42*, 6060-6093; c) M. Raynal, P. Ballester, A. Vidal-Ferran, P. W. van Leeuwen, *Chem. Soc. Rev.* **2014**, *43*, 1734-1787.
[144] a) J. Chen, S. Patil, S. Seal, J. F. McGinnis, *Nat. Nanotechnol.* **2006**, *1*, 142-150; b) G. A. Silva, *Nat. Nanotechnol.* **2006**, *1*, 92-94.
[145] a) C. Korsvik, S. Patil, S. Seal, W. T. Self, *Chem. Commun.* **2007**, 1056-1058; b) E. G. Heckert, A. S. Karakoti, S. Seal, W. T. Self, *Biomaterials* **2008**, *29*, 2705-2709.
[146] T. Pirmohamed, J. M. Dowding, S. Singh, B. Wasserman, E. Heckert, A. S. Karakoti, J. E. S. King, S. Seal, W. T. Self, *Chem. Commun.* **2010**, *46*, 2736-2738.
[147] a) A. Asati, C. Kaittanis, S. Santra, J. M. Perez, *Anal. Chem.* **2011**, *83*, 2547-2553; b) A. Asati, S. Santra, C. Kaittanis, S. Nath, J. M. Perez, *Angew. Chem., Int. Ed.* **2009**, *48*, 2308-2312.
[148] F. Tan, Y. Zhang, J. Wang, J. Wei, Y. Cai, X. Qian, *J. Mass Spectrom.* **2008**, *43*, 628-632.
[149] a) J. M. Perez, *Nat. Nanotechnol.* **2007**, *2*, 535-536; b) N. V. S. Vallabani, A. S. Karakoti, S. Singh, *Colloids Surf., B* **2017**, *153*, 52-60; c) H. Wei, E. Wang, *Anal. Chem.* **2008**, *80*, 2250-2254.
[150] L. Gao, J. Zhuang, L. Nie, J. Zhang, Y. Zhang, N. Gu, T. Wang, J. Feng, D. Yang, S. Perrett, X. Yan, *Nat. Nanotechnol.* **2007**, *2*, 577-583.
[151] a) Y. Lin, J. Ren, X. Qu, *Adv. Mater.* **2014**, *26*, 4200-4217; b) Y. Jv, B. Li, R. Cao, *Chem. Commun.* **2010**, *46*, 8017-8019.
[152] Y. Lin, Z. Li, Z. Chen, J. Ren, X. Qu, *Biomaterials* **2013**, *34*, 2600-2610.
[153] a) A. M. Schrand, M. F. Rahman, S. M. Hussain, J. J. Schlager, D. A. Smith, A. F. Syed, *Wiley Interdiscip. Rev.: Nanomed. Nanobiotechnol.* **2010**, *2*, 544-568; b) S. Hussain, F. Al-Nsour, A. B. Rice, J. Marshburn, B. Yingling, Z. Ji, J. I. Zink, N. J. Walker, S. Garantziotis, *ACS Nano* **2012**, *6*, 5820-5829.
[154] a) S. Hünig, *Justus Liebigs Ann. Chem.* **1964**, *676*, 32-35; b) S. Hünig, H. Balli, H. Conrad, A. Schott, *Justus Liebigs Ann. Chem.* **1964**, *676*, 52-65; c) S. Hünig, H. Balli, H. Conrad, A. Schott, *Justus Liebigs Ann. Chem.* **1964**, *676*, 36-51.
[155] a) T. Farrugia, A. W. Perriman, K. P. Sharma, S. Mann, *Chem. Commun. (Cambridge, U. K.)* **2017**, *53*, 2094-2097; b) H. Cai, X. Liu, J. Zou, J. Xiao, B. Yuan, F. Li, Q. Cheng, *Chemosphere* **2018**, *193*, 833-839.
[156] E. N. Kadnikova, N. M. Kostić, *J. Mol. Catal. B: Enzym.* **2002**, *18*, 39-48.
[157] B. Zhao, F. A. Summers, R. P. Mason, *Free Radical Biol. Med.* **2012**, *53*, 1080-1087.
[158] N. Shangari, P. J. O'Brien, *Current Protocols in Toxicology* **2006**, *Chapter 7*, Unit 7 7 1-15.

[159] a) D. Pfister, M. Morbidelli, *J. Controlled Release* **2014**, *180*, 134-149; b) C. J. Fee, J. M. Van Alstine, *Chem. Eng. Sci.* **2006**, *61*, 924-939.
[160] a) K. R. Gee, E. A. Archer, H. C. Kang, *Tetrahedron Lett.* **1999**, *40*, 1471-1474; b) M. R. Lockett, M. F. Phillips, J. L. Jarecki, D. Peelen, L. M. Smith, *Langmuir* **2008**, *24*, 69-75.
[161] L. Zhang, C. R. Robertson, B. R. Green, T. H. Pruess, H. S. White, G. Bulaj, *J. Med. Chem.* **2009**, *52*, 1310-1316.
[162] S.-J. Sung, S. H. Min, K. Y. Cho, S. Lee, Y.-J. Min, Y. I. Yeom, J.-K. Park, *Biol. Pharm. Bull.* **2003**, *26*, 492-500.
[163] R. Qi, Y. Gao, Y. Tang, R.-R. He, T.-L. Liu, Y. He, S. Sun, B.-Y. Li, Y.-B. Li, G. Liu, *AAPS J.* **2009**, *11*, 395-405.
[164] K. Ono, Y. Kai, H. Maeda, F. Samizo, K. Sakurai, H. Nishimura, Y. Inada, *J. Biomater. Sci., Polym. Ed.* **1991**, *2*, 61-65.
[165] K. Huthmacher, D. Most, in *Ullmann's Encyclopedia of Industrial Chemistry*, Wiley-VCH Verlag GmbH & Co. KGaA, **2000**.
[166] C. Zheng, G. Ma, Z. Su, *Electrophoresis* **2007**, *28*, 2801-2807.
[167] N. J. Greenfield, *Nat. Protocols* **2007**, *1*, 2876-2890.
[168] V. Filipe, A. Hawe, W. Jiskoot, *Pharm. Res.* **2010**, *27*, 796–810.
[169] L. E. Franken, E. J. Boekema, M. C. A. Stuart, *Adv. Sci. (Weinheim, Ger.)* **2017**, *4*, 1600476.
[170] S. Das, A. Chaudhury, *AAPS PharmSciTech* **2011**, *12*, 62-76.
[171] L. Betancor, A. Hidalgo, G. Fernández-Lorente, C. Mateo, R. Fernández-Lafuente, J. M. Guisan, *Biotechnol. Prog.* **2003**, *19*, 763-767.
[172] S. M. Kelly, T. J. Jess, N. C. Price, *Biochimica et Biophysica Acta (BBA) - Proteins and Proteomics* **2005**, *1751*, 119-139.
[173] H. García-Arellano, B. Valderrama, G. Saab-Rincón, R. Vazquez-Duhalt, *Bioconjugate Chem.* **2002**, *13*, 1336-1344.
[174] a) C. M. Hoo, N. Starostin, P. West, M. L. Mecartney, *J. Nanopart. Res.* **2008**, *10*, 89-96; b) A. Rao, M. Schoenenberger, E. Gnecco, T. Glatzel, E. Meyer, D. Brändlin, L. Scandella, *J. Phys.: Conf. Ser.* **2007**, *61*, 971-976.
[175] M. P. Barnes, W. C. Shen, *Int. J. Pharm.* **2009**, *369*, 79-84.
[176] R. E. Diederix, M. Fittipaldi, J. A. Worrall, M. Huber, M. Ubbink, G. W. Canters, *Inorg. Chem.* **2003**, *42*, 7249-7257.
[177] Z. Wang, T. Matsuo, S. Nagao, S. Hirota, *Org. Biomol. Chem.* **2011**, *9*, 4766-4769.
[178] R. Vazquez-Duhalt, *Journal of Molecular Catalysis B-Enzymatic* **1999**, *7*, 241-249.
[179] S. Debnath, D. Das, P. K. Das, *Biochem. Biophys. Res. Commun.* **2007**, *356*, 163-168.
[180] Preety, V. Hooda, *Appl. Biochem. Biotechnol.* **2014**, *172*, 115-130.
[181] B. Koohshekan, A. Divsalar, M. Saiedifar, A. A. Saboury, B. Ghalandari, A. Gholamian, A. Seyedarabi, *J. Mol. Liq.* **2016**, *218*, 8-15.
[182] Y.-P. Hsieh, S.-C. Lin, *Process Biochem.* **2015**, *50*, 1372-1378.
[183] B. C. Dickinson, C. Huynh, C. J. Chang, *J. Am. Chem. Soc.* **2010**, *132*, 5906-5915.
[184] H. Sies, *Redox Biol.* **2017**, *11*, 613-619.
[185] S. Xu, H. Qi, S. Zhou, X. Zhang, C. Zhang, *Microchim. Acta* **2014**, *181*, 535-541.
[186] U. K. Laemmli, *Nature* **1970**, *227*, 680-685.

6.3 Supplemental Data

6.3.1 Data of the First Project

IR Data of Activated PEG

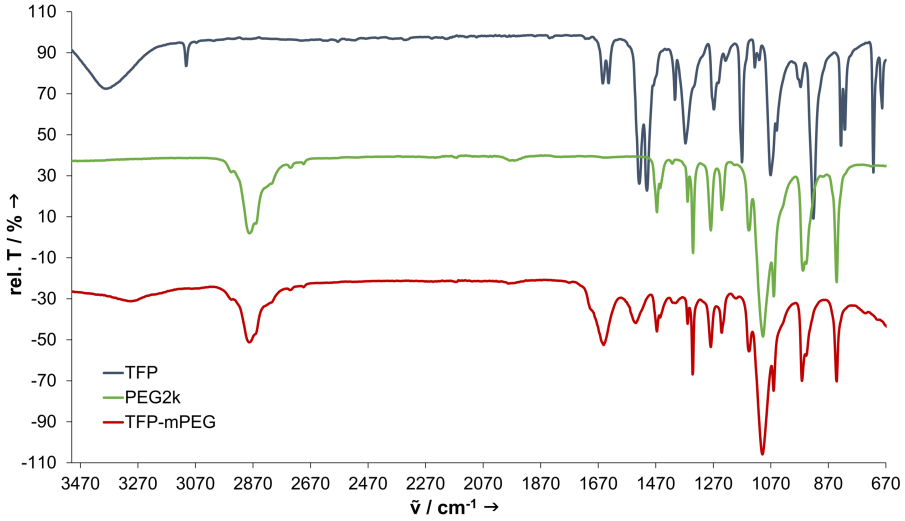

Figure 65: IR diagram of tetrafluorophenol (TFP, blue), mPEG 2000 (green) and TFP-mPEG (red). The activated mPEG shows one peak that can be assigned to TFP (1651 cm^{-1}).

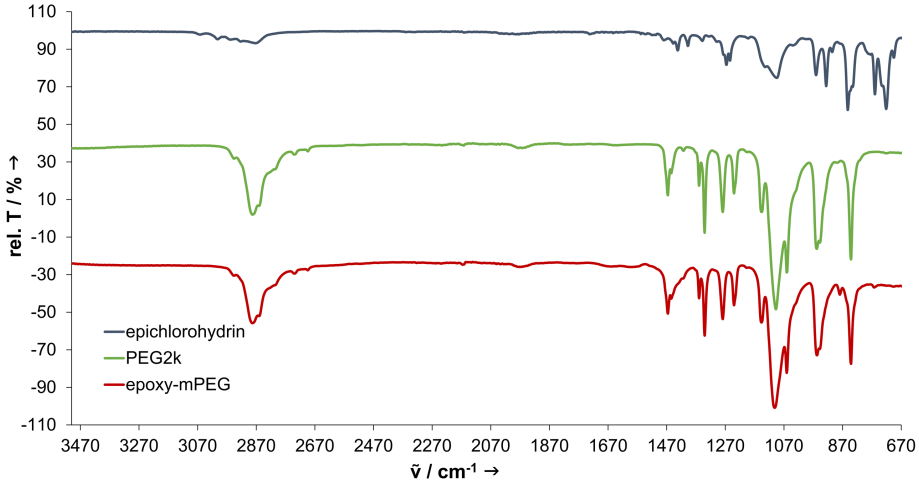

Figure 66: IR diagram of epichlorohydrin (blue), mPEG 2000 (green) and epoxy-mPEG (red). The activated mPEG shows one peak that can be assigned to epichlorohydrin (1466 cm^{-1}).

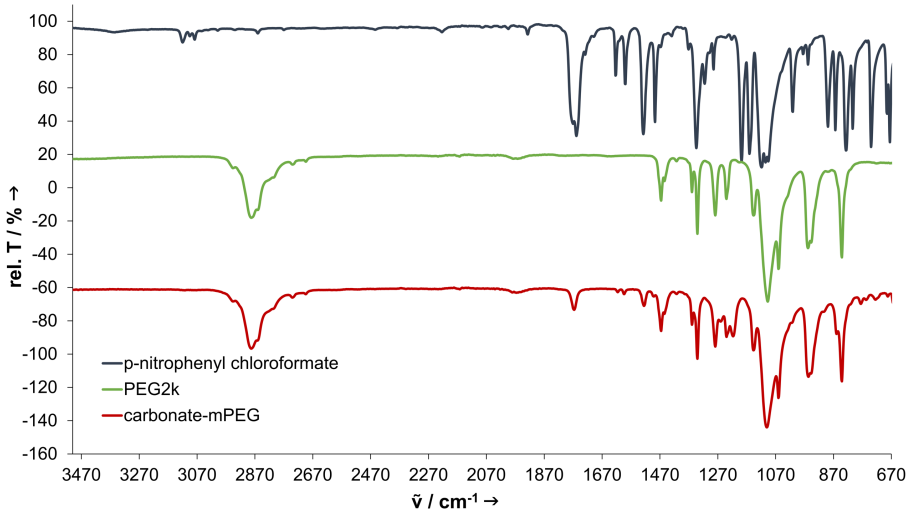

Figure 67: IR diagram of *p*-nitrophenyl chloroformate (blue), mPEG 2000 (green) and the activated mPEG with *p*-nitrophenyl chloroformate (carbonate-mPEG, red). Three peaks can be assigned to *p*-nitrophenyl chloroformate (1766, 1616, 1594 cm^{-1}).

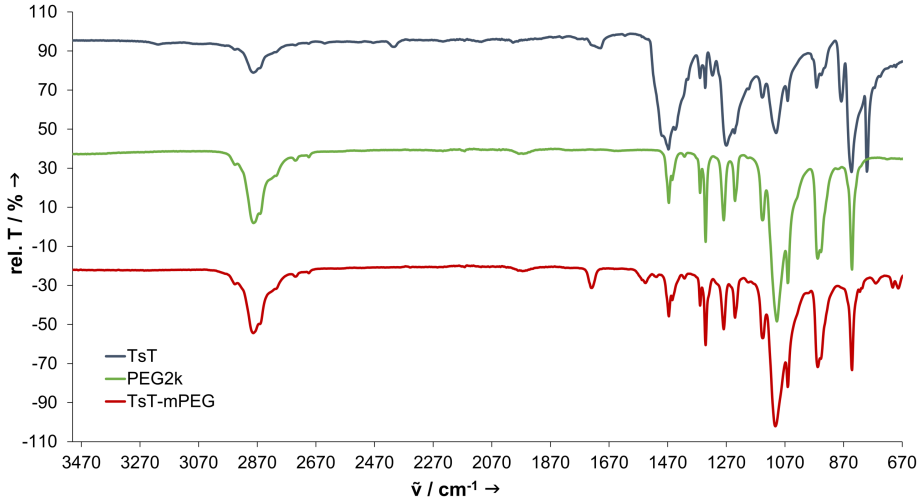

Figure 68: IR diagram of 2,4,6-trichloro-1,3,5-triazine (TsT, blue), mPEG 2000 (green) and TsT-mPEG (red). The activated mPEG shows two peaks that can be assigned to TsT (1729, 759 cm^{-1}).

SEC of Activated PEG

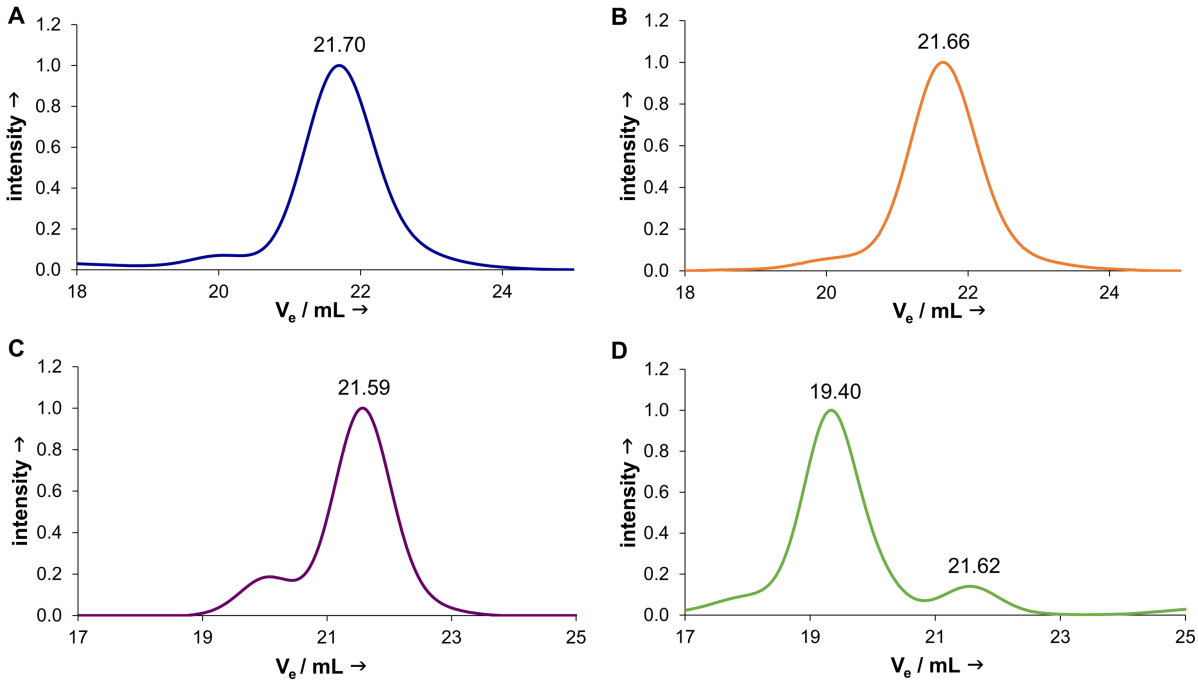

Figure 69: SEC diagrams of activated mPEG. Diagram of TFP-mPEG indicates that TFP is modified with one mPEG chain (V_e = 21.70 mL) (A). SEC diagram of epoxy-mPEG show that epoxy-mPEG present one mPEG chain (V_e = 21.66 mL) (B). SEC diagram of carbonate-mPEG. The diagram indicates that carbonate-mPEG present one mPEG chain (V_e = 21.59 mL). At V_e = 20.00 mL a small "barrow" is present which can be ascribe to mPEG itself (see other SEC diagrams) (C). SEC diagram of TsT-mPEG. This diagram shows, that most TsT molecules are modified with two mPEG chains (V_e = 19.40 mL; compare elementary analysis). As byproduct, TsT with one mPEG chain exists (V_e = 21.62 mL) (D). mPEG itself produces a RI signal at 21.65 mL and no UV-signal and show a small "barrow" at V_e = 20.00 mL.

NMR Data of Activated PEG

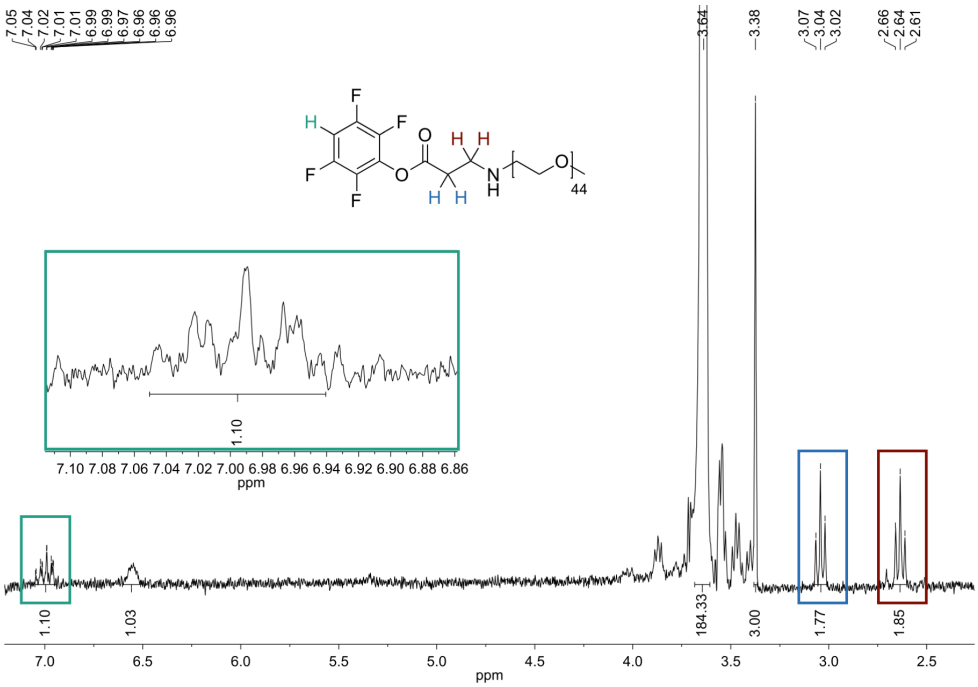

Figure 70: ^{1H}NMR of TFP-mPEG.

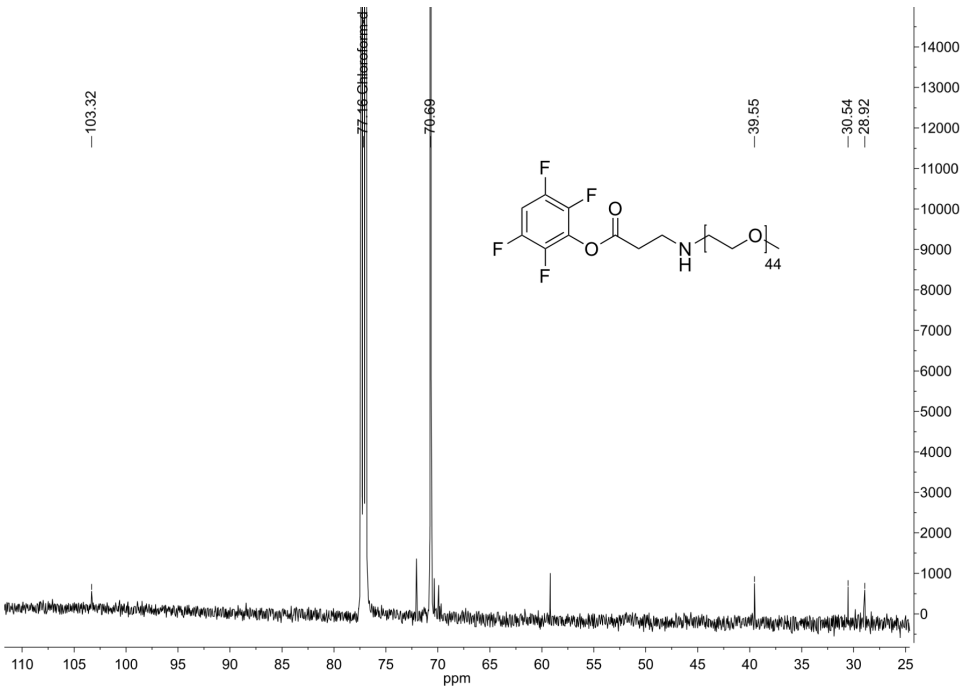

Figure 71: ^{13C}NMR of TFP-mPEG.

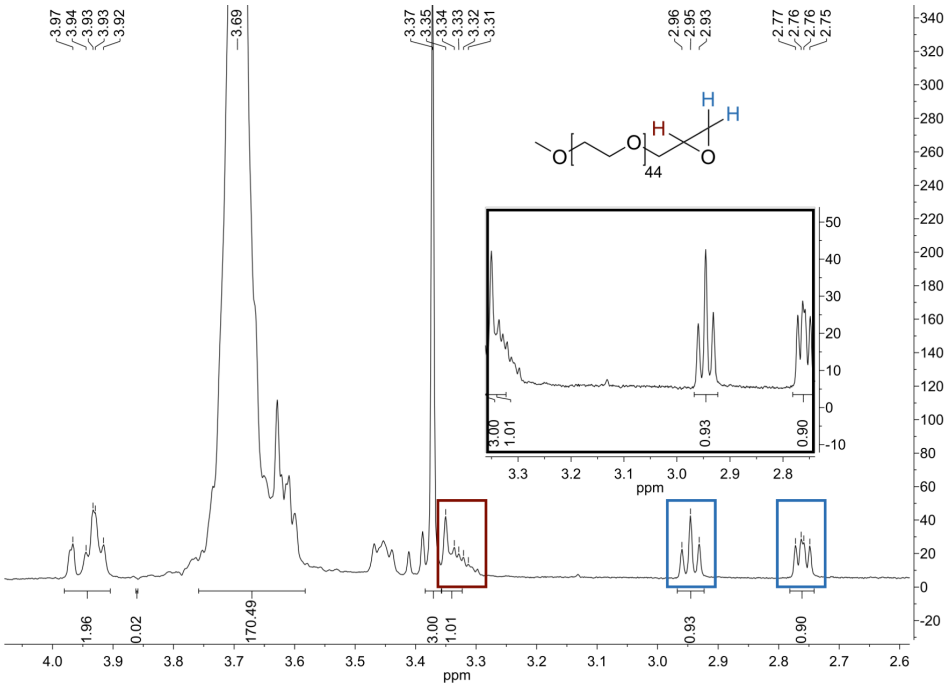

Figure 72: ^{1H}NMR of epoxy-mPEG$_{2k}$.

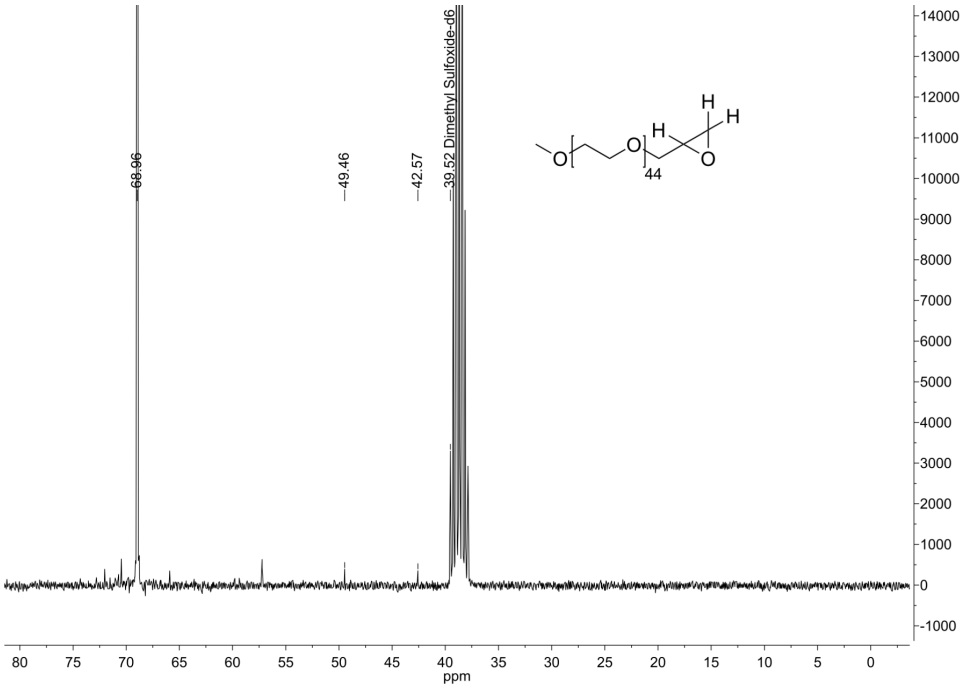

Figure 73: ^{13C}NMR of epoxy-mPEG$_{2k}$.

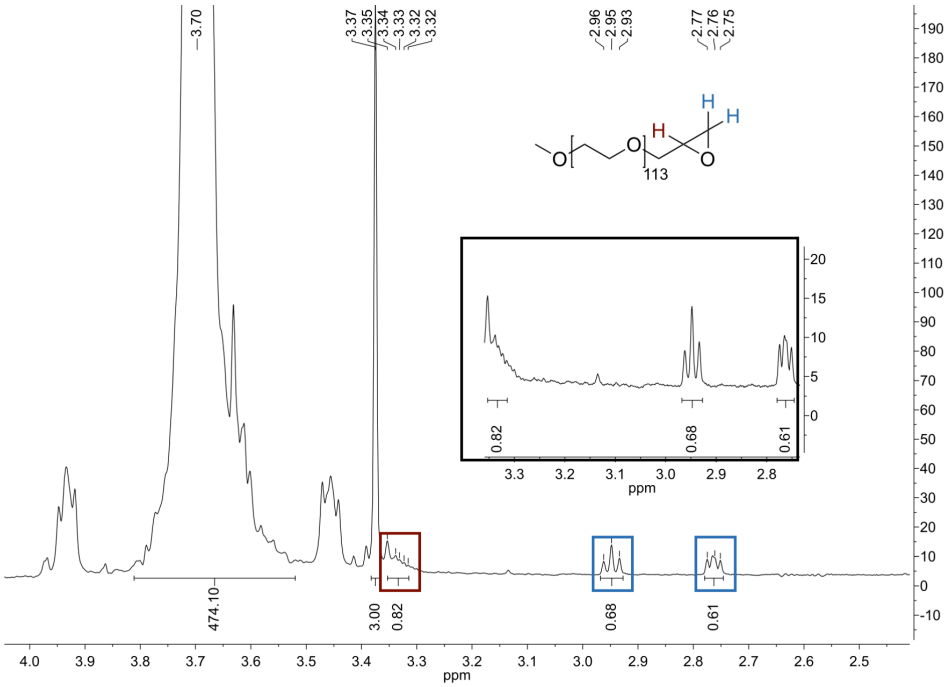

Figure 74: ^{1H}NMR of epoxy-mPEG$_{5k}$.

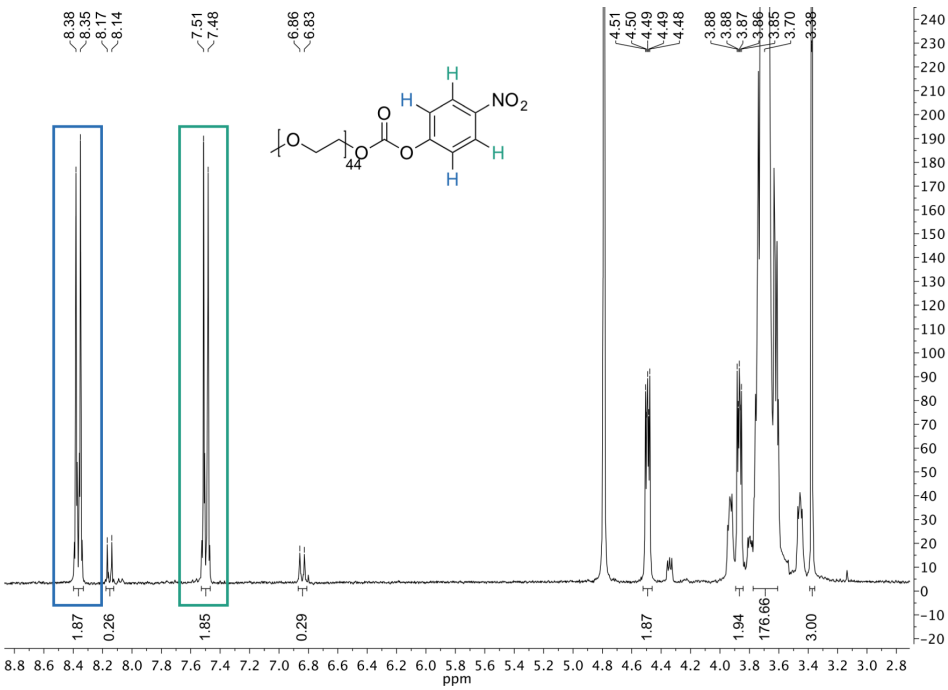

Figure 75: ^{1H}NMR carbonate-mPEG.

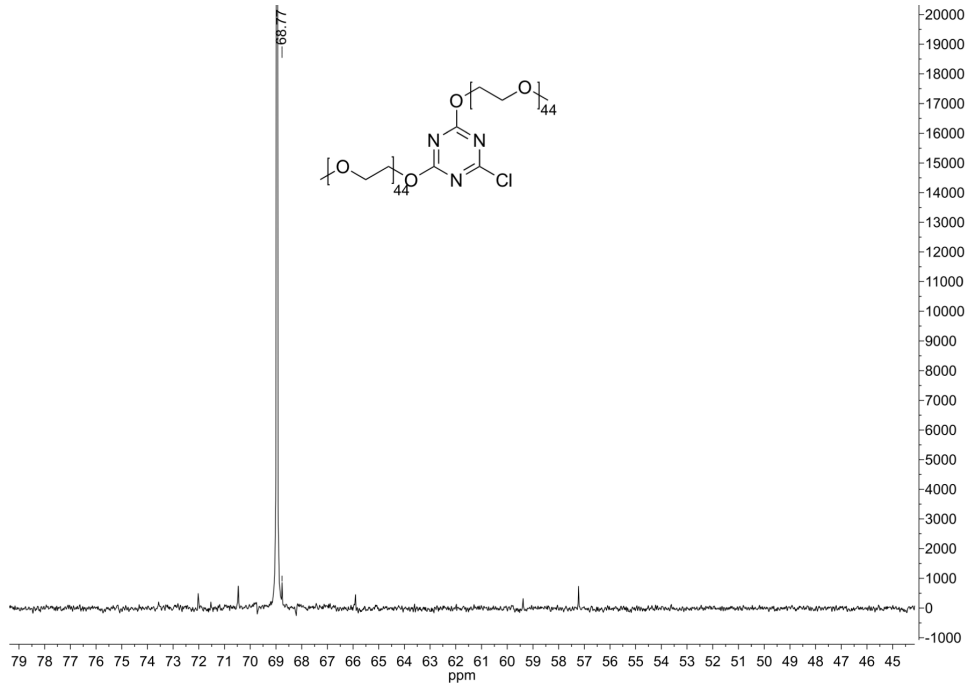

Figure 76: ^{13C}NMR TsT-mPEG.

Fluorescamine Assay of LYZ-PEG Conjugates

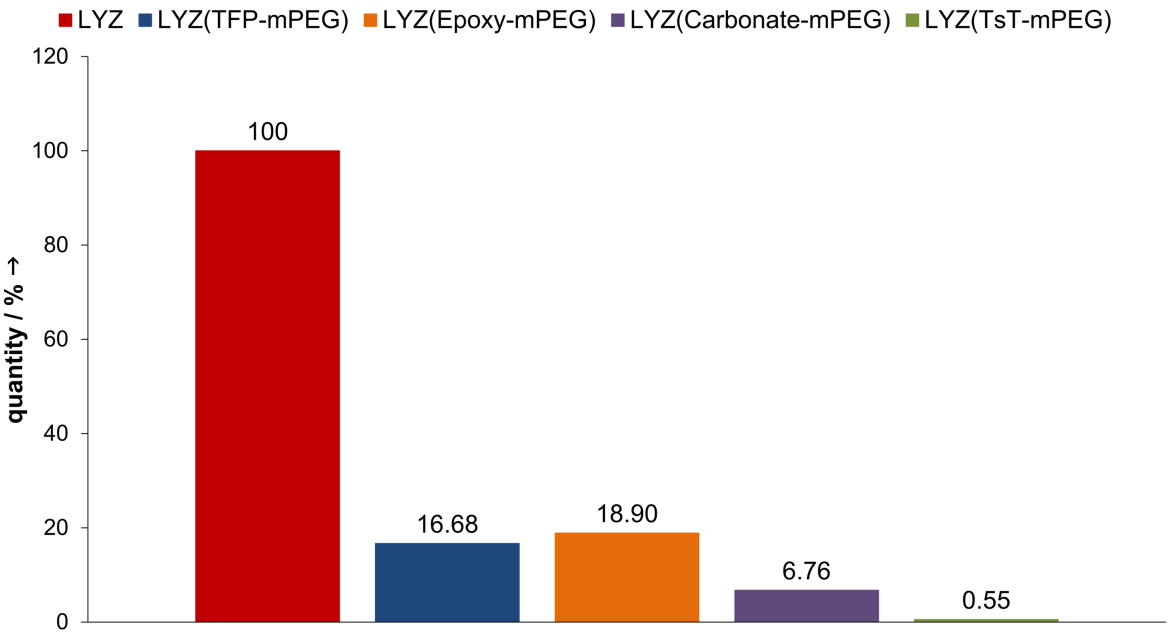

Figure 77: Fluorescamine assay of the PEGylated LYZ samples. For the LYZ sample modified with TFP-mPEG and epoxy-mPEG only one free amine was measured. For LYZ(carbonate-mPEG) only 0.5 free amines were calculated in average. No amines can be detected in the LYZ(TsT-mPEG) sample. Unmodified lysozyme contains 7 free amines on its surface (red bar on the left).

6.3.2 Data of the Second Project

Michaelis-Menten Diagrams of Peroxidase Materials

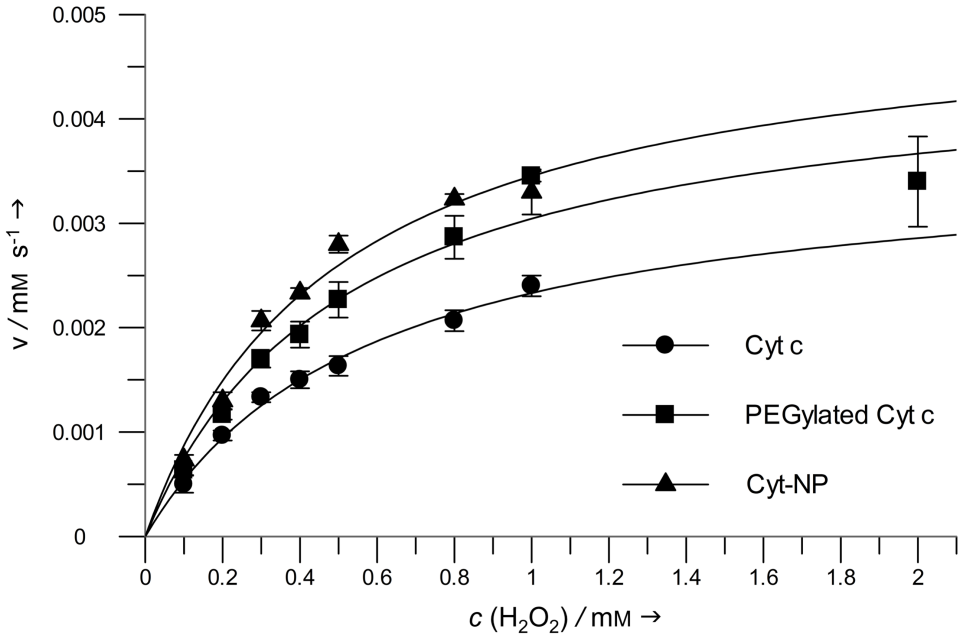

Figure 78: Michaelis-Menten kinetic of the Cyt *c* materials calculated by GraFit.

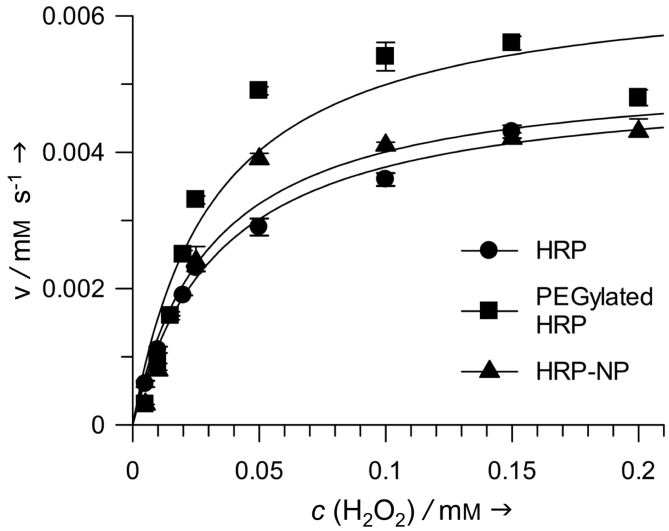

Figure 79: Michaelis-Menten kinetic of the HRP materials calculated by GraFit.

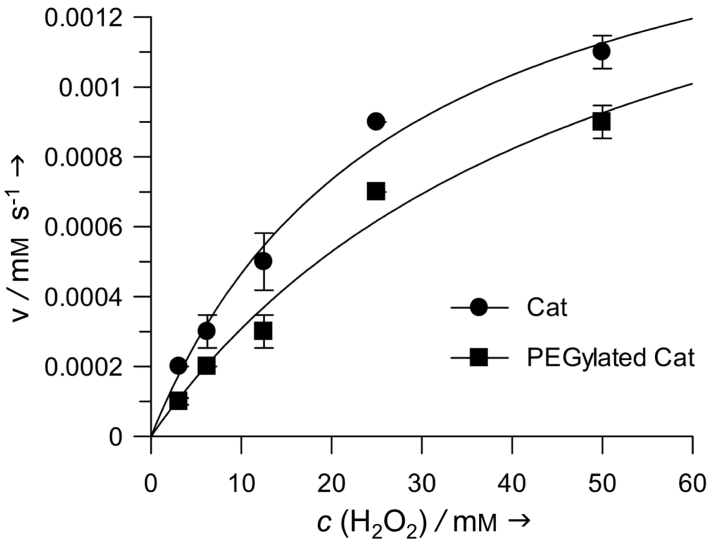

Figure 80: Michaelis-Menten kinetic of native Cat and the PEGylated material calculated by GraFit.

6.3.3 Data of the Third Project

Michaelis-Menten Diagrams of GOx-HRP Materials

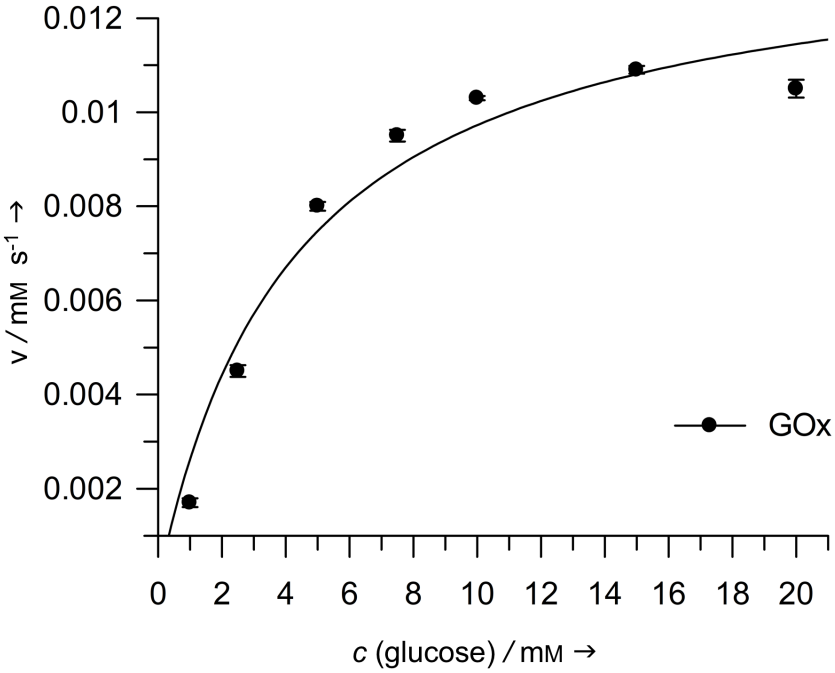

Figure 81: Michaelis-Menten kinetic of native GOx calculated by GraFit.

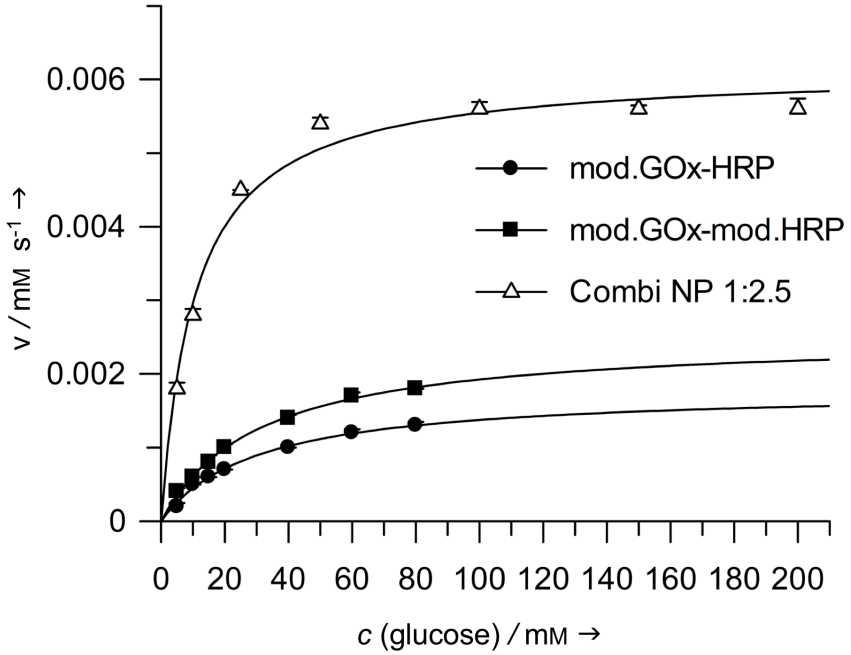

Figure 82: Michaelis-Menten kinetic of GOx(mPEG)$_{2k}$ material with the native HRP, HRP(mPEG)$_{5k}$ and the corresponding dual-enzyme system (ratio 1:2.5) calculated by GraFit. Enzyme materials were used in a ratio of 1:2.5.

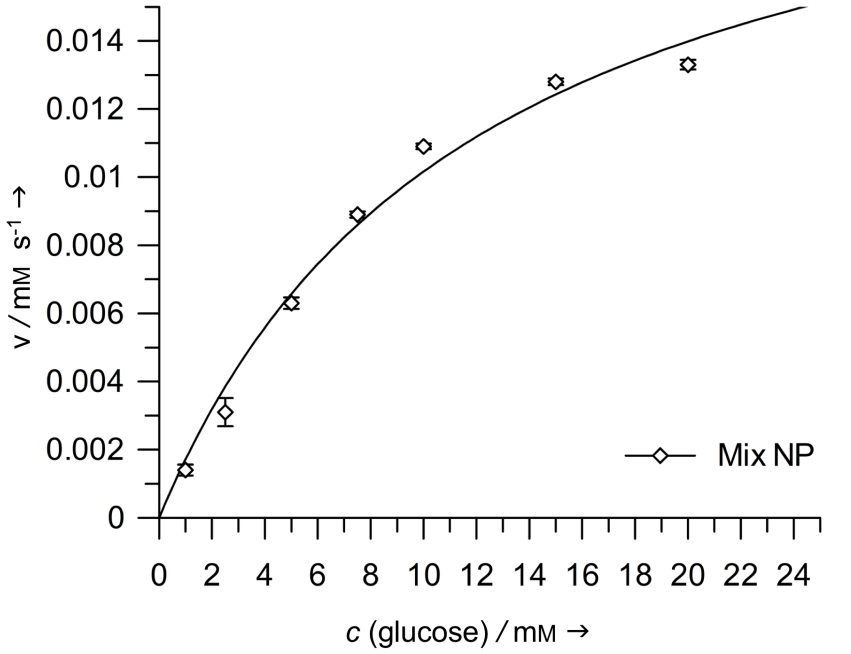

Figure 83: Michaelis-Menten kinetic of GOx-NPs (using GOx(mPEG)$_{2k}$) mixed with HRP-NPs calculated by GraFit. Enzyme materials were used in a ratio of 1:2.5.

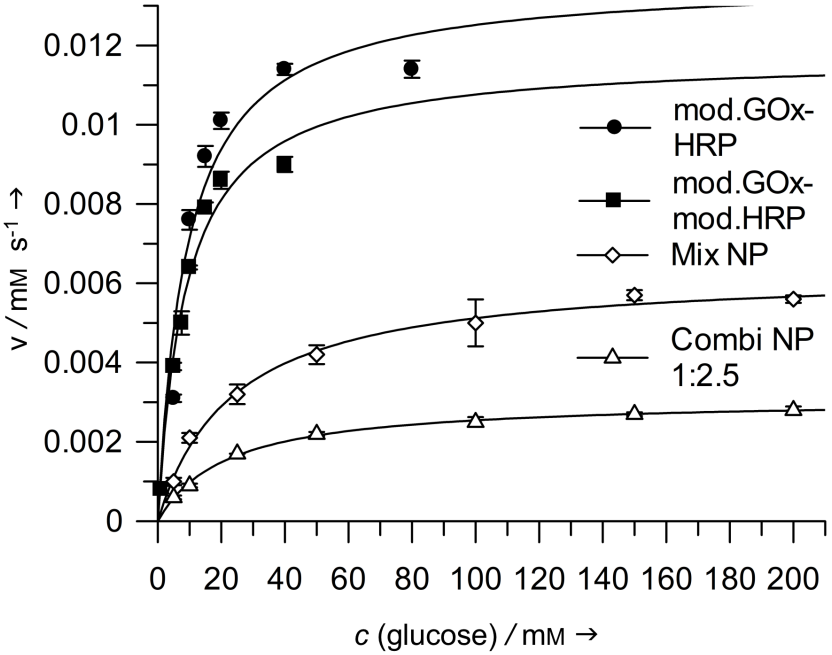

Figure 84: Michaelis-Menten kinetic of GOx(mPEG)$_{5k}$ material with the native HRP, HRP(mPEG)$_{5k}$, HRP-NPs and the corresponding dual-enzyme system (ratio 1:2.5) calculated by GraFit. Enzyme materials were used in a ratio of 1:2.5.

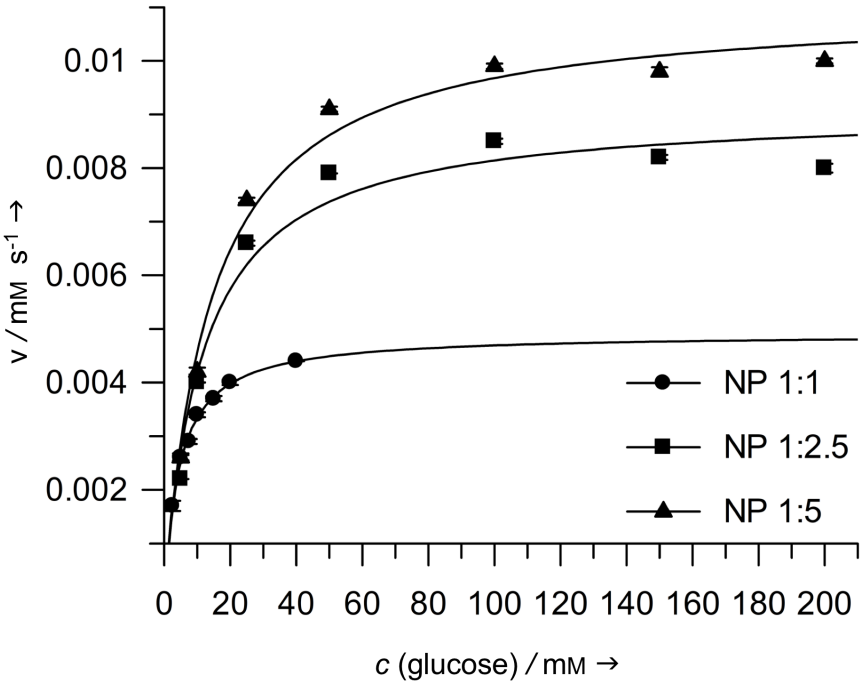

Figure 85: Michaelis-Menten kinetic of dual-enzyme systems in different ratios calculated by GraFit.

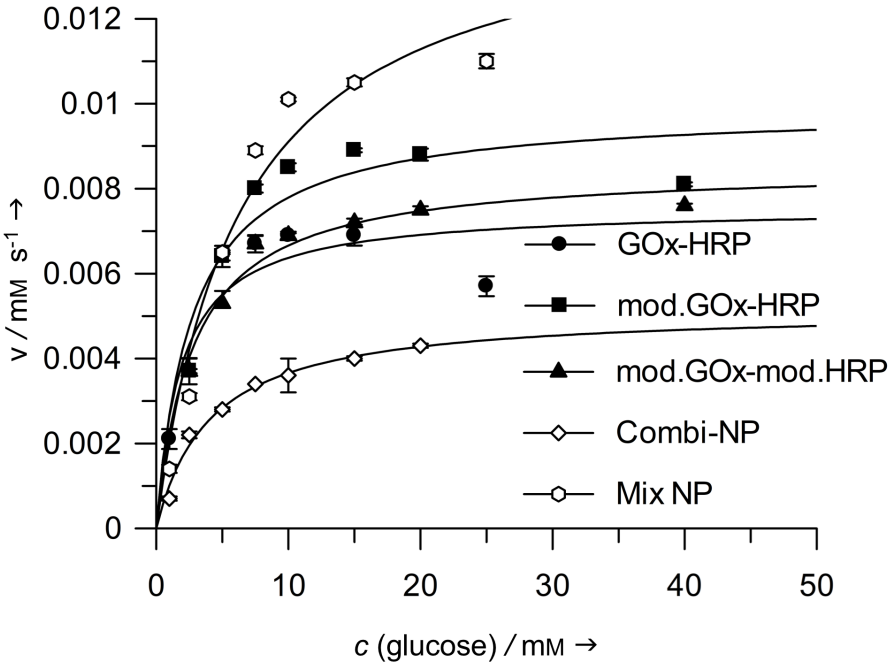

Figure 86: Michaelis-Menten kinetic of $GOx(mPEG)_{2k}$ material with the native HRP, $HRP(mPEG)_{5k}$, HRP-NPs and the corresponding dual-enzyme system (ratio 1:1) calculated by GraFit. Enzyme materials were used in a ratio of 1:1.

CURRICULUM VITAE

LIST OF PUBLICATIONS

1. L. Radi, M. Fach, M. Montigny, E. Berger-Nicoletti, W. Tremel, P. R. Wich, *Med. Chem. Commun.* **2016**, *7*, 1738-1744.

   "Methods of protein surface PEGylation under structure preservation for the emulsion-based formation of stable nanoparticles"

2. M. Fach, L. Radi, P. R. Wich, *J. Am. Chem. Soc.* **2016**, *138*, 14820-14823.

   "Nanoparticle Assembly of Surface-Modified Proteins"

3. F. Foerster, D. Bamberger, J. Schupp, M. Weilbacher, L. Kaps, S. Strobl, L. Radi, M. Diken, D. Strand, A. Tuettenberg, P. R. Wich, D. Schuppan, *Nanomedicine (London, U. K.)* **2016**, *11*, 2663-2677.

   "Dextran-based therapeutic nanoparticles for hepatic drug delivery"

4. A. Beyer, L. Radi, H. Grohganz, K. Löbmann, T. Rades, C. S. Leopold, *Eur. J. Pharm. Biopharm.* **2016**, *104*, 72-81.

   "Preparation and recrystallization behavior of spray-dried co-amorphous naproxen–indomethacin"

5. L. Radi, E. Steiert, C. Seidler, T. Weil, P. R. Wich, **2018**, *submitted.*

   "Catalytically Active Nanoparticles for the Intracellular Modulation of Redox Processes"

6. E. Steiert, L. Radi, M. Fach, P. R. Wich, *Macromol. Rapid Commun.* **2018**, *accepted.*

   "Protein-based Nanoparticles for the Delivery of Enzymes with Antibacterial Activity"

7. L. Radi, E. Steiert, M. Fach, P. R. Wich, **2018**, *in preparation.*

   "Proteins as Natural Materials for Nanoparticles"